



UNIVERSITÀ DEGLI STUDI DI NAPOLI "FEDERICO II"

DIPARTIMENTO DI FARMACIA

PhD Thesis in Pharmaceutical Sciences

XXX cycle

By

Alessia CASO

Date of defense: 26/06/2018

Novel bioactive metabolites from marine sources: isolation, structural elucidation and synthetic studies.

Tutor: Prof. COSTANTINO Valeria

Co-Tutor: Prof. PICCIALLI Vincenzo

*“Non chi comincia
ma quel che persevera”*

CONTENTS

ABSTRACT	I
INTRODUCTION	1
<i>References</i>	8
CHAPTER 1	9
STRUCTURAL ELUCIDATION TECHNIQUES	9
1.1 Nuclear Magnetic Resonance.....	9
1.1.1 One-dimensional NMR experiments	12
1.1.2 Two-dimensional NMR experiments	13
1.2. Methods for the determination of relative/absolute configurations	15
1.3 Mass spectrometry	17
1.4. Infrared Spectroscopy	20
1.5. Circular Dichroism.....	21
1.6. Marfey's Method.....	22
1.7 Conclusion.....	25
<i>References</i>	26

PART 1 - Total synthesis of new hybrid PKS/NRPS compounds, in the frame of the anticancer drug discovery	27
CHAPTER 2	28
TOTAL SYNTHESIS OF 16- <i>EPI</i> - AND <i>ENT</i> -SMENAMIDE A, TWO ANALOGUES OF THE CYTOTOXIC SMENAMIDE A	28
2.1 Cancer and bioactive natural products	28
2.2 Smenamides A and B, two cytotoxic secondary metabolites from the marine sponge <i>Smenospongia aurea</i>	33
2.3. Towards the synthesis of smenamide A: total synthesis of 16- <i>epi</i> - and <i>ent</i> -smenamide A.....	35
2.4 Previous stereochemical studies on smenamide A.....	35
2.5. Synthetic strategy	40
2.5.1 Retrosynthetic analysis	40
2.5.2 Synthesis of the polyketide moiety.....	42
2.5.3 Preparation of the peptide moiety and final coupling	47
2.6. Conclusions	51
2.7. Experimental section.....	51
2.7.1 Generals.....	51
2.7.2 Experimental procedures	52
Determination of the absolute configuration at C-8 of smenamide A by using Marfey's method.	52
2.8 Supplementary spectroscopic data	78

<i>References</i>	106
CHAPTER 3	108
SYNTHESIS AND BIOLOGICAL ACTIVITY OF EIGHT SMENAMIDE A-FUNCTIONAL ANALOGUES	108
3.1 Synthesis of eight smenamide A-analogues of the 16- <i>epi</i> - series and their biological activity	108
3.2. In vitro evaluation of the antiproliferative activity	112
3.3 Conclusions	112
3.4. Experimental section	113
3.4.1 Generals	113
3.4.2 Experimental procedures	113
3.6 Supplementary spectroscopic data	121
<i>References</i>	129

PART 2 - Isolation and structural determination of new bioactive metabolites from marine sources

CHAPTER 4

CONULOTHIAZOLES A AND B, TWO CHLORINATED PEPTIDE/POLYKETIDE METABOLITES FROM THE MARINE SPONGE *SMENOSPONGIA CONULOSA*

4.1 Isolation of conulothiazoles A and B	134
4.2 Structural determination of compound 5 and 6	135

4.3 Stereostructural determination of the two double bonds of conulothiazole A and B	140
4.4 Determination of the absolute configuration of the amino acid residues of conulothiazoles A and B	141
4.5 Biogenetic studies	143
4.6 Conclusions.....	146
4.7 Experimental section.....	147
4.7.1 Collection	147
4.7.2 Extraction and Isolation.....	147
4.7.3 Conulothiazole A (5)	148
4.7.4 Conulothiazole B (6)	148
4.7.5 Ozonolysis and Hydrolysis.....	149
4.7.6 Marfey's Derivatization with D- and L-FDAA.....	149
4.7.7 High-resolution LC-MS Analysis of Marfey's derivatives.....	149
4.8 Supplementary spectroscopic data	151
<i>References</i>	159
CHAPTER 5	161
EVALUATION OF THE ANTIPROLIFERATIVE ACTIVITY OF THE ORGANIC EXTRACT OF <i>GEODIA CYDONIUM</i>	161
5.1 Bioguided fractionation of <i>G. cydonium</i> extracts	162
5.2 Combined use of LC-HRMS, LC-HRMS/MS and molecular networking as a novel dereplication strategy.....	163

5.3 Biological studies	167
5.4 Conclusions	173
5.5 Experimental section	174
5.5.1 Collection, extraction, and separation	174
5.5.2 LC-HRMS and LC-HRMS/MS and Molecular Networking Analyses	175
5.5.3 Cell culture	176
5.5.4 Cell treatment and cell proliferation assay	177
5.5.5 Apoptosis evaluation	178
5.5.6 Cell cycle assay	178
5.5.7 Extraction of the polar fractions in untreated and treated cancer cells	179
5.5.8 ¹ H-NMR Metabolomic Analysis of the cellular polar fractions	179
5.5.9 Statistical and Pathway Analysis	180
5.5.10 Bio-Plex Assay	180
<i>References</i>	182
CONCLUSION	184
<i>References</i>	186

List of Figures

CHAPTER 1	9
Figure 1.1. Scheme of a NMR spectrometer.....	10
Figure 1.2. A spinning charged particule generate a magnetic field.	11
Figure 1.3. Spin energy states.	11
Figure 1.4. ESI mass spectrometry	18
Figure 1.5. Ion trajectories in an Orbitrap mass spectrometer.....	20
Figure 1.6. L-FDAA structure.	23
Figure 1.7. Plausible conformations of the L- and D-amminoacids derivatives during separation by Marfey's method.	24
CHAPTER 2	28
Figure 2.1 Structures of smenamamide A (1) and B (2).....	33
Figure 2.2. MTT assay of smenamides A and B. Evaluation by MTT assay of Calu- 1 cell viability after 72 h of treatment with (A) compound 1 and (B) compound 2.....	34
Figure 2.3. Evaluation of pro-apoptotic activity of smenamides using the Annexin- V FITC/PI assay.	34
Figura 2.4. High-resolution ESI mass spectrum of smenamamide A.	36
Figura 2.5. ¹ H NMR spectrum of smenamamide A (1) (CD ₃ OD, 700 MHz).	36
Figure 2.6. 2D ROESY spectrum of smenamamide A (CD ₃ OD, 700 MHz).	37

Figure 2.7. Main correlation peaks provided ROESY 2D NMR spectrum of smenamide A allowing the assignment of the configuration of the two double bonds of the molecule.	38
Figure 2.8. Ozonolysis, hydrolysis and derivatisation of smenamide A with L-FDAA.....	39
Figure 2.9. High resolution LC-MS analysis of Marfey's derivative from smenamide A. Extracted-ion chromatograms at m/z 418.1357 of authentic 1-fluoro-2,4-dinitrophenyl-5-alanine amide L-phenilalanine (L-FDAA-L-Phe), authentic D-FDAA-L-Phe and L-FDAA-Phe from smenamide A.....	40
Figure 2.10. Retrosynthetic analysis of smenamide A	41
Figure 2.11 Preparation of the fully protected triol 5	43
Figure 2.12 Installation of the N-methylacetamido function.....	45
Figure 2.13. Installation of the chlorovinyl moiety.	46
Figure 2.14. Preparation of the α,β -unsaturated ester 24.	47
Figure 2.15. Synthesis of the pyrrolidinone unit 24.....	48
Figure 2.16. Final coupling.	49
Figure 2.17. ^1H NMR spectra of 16- <i>epi</i> -smenamide A and natural smenamide A.	49
Figure 2.18. Synthesis of <i>ent</i> -smenamide A.	50
Figure 2.19. ^1H NMR spectra of <i>ent</i> -smenamide A and natural smenamide A....	50
Figure 2.20. Ozonolysis, hydrolysis and derivatization of smenamide A with l-enantiomer of Marfey's reagent.	52
Figure 2.21. HR-ESI-MS-HPLC analysis of Marfey's derivative from smenamide A. Extracted-ion chromatograms at m/z 418.1357 of authentic 1-fluoro-2,4-	

dinitrophenyl-5-alanine amide L-phenilalanine (L-FDAA-L-Phe), authentic D-FDAA-L-Phe and L-FDAA-Phe from smenamide A.	54
Figure 2.22. ¹ H NMR spectrum of compound 30 (CDCl ₃ , 400 MHz)	78
Figure 2.23. ¹³ C NMR spectrum of compound 30 (CDCl ₃ , 100 MHz)	78
Figure 2.24. ¹ H NMR spectrum of compound 8 (CDCl ₃ , 400 MHz)	79
Figure 2.25. ¹³ C NMR spectrum of compound 8 (CDCl ₃ , 100 MHz)	79
Figure 2.26. ¹ H NMR spectrum of compound 31 (CDCl ₃ , 400 MHz)	80
Figure 2.27. ¹³ C NMR spectrum of compound 31 (CDCl ₃ , 100 MHz)	80
Figure 2.28. ¹ H NMR spectrum of compound 33 (CDCl ₃ , 400 MHz)	81
Figure 2.29. ¹³ C NMR spectrum of compound 33 (CDCl ₃ , 100 MHz)	81
Figure 2.30. ¹ H NMR spectrum of compound 9 (CDCl ₃ , 400 MHz)	82
Figure 2.31. ¹³ C NMR spectrum of compound 9 (CDCl ₃ , 100 MHz)	82
Figure 2.32. ¹ H NMR spectrum of compound 34 (CDCl ₃ , 400 MHz)	83
Figure 2.33. ¹³ C NMR spectrum of compound 34 (CDCl ₃ , 100 MHz)	83
Figure 2.34. ¹ H NMR spectrum of compound 10 (CDCl ₃ , 400 MHz)	84
Figure 2.35. ¹ H NMR spectrum of compound 12 (CDCl ₃ , 400 MHz)	85
Figure 2.36. ¹³ C NMR spectrum of compound 12 (CDCl ₃ , 100 MHz)	85
Figure 2.37. ¹ H NMR spectrum of compound 5 (CDCl ₃ , 400 MHz)	86
Figure 2.38. ¹³ C NMR spectrum of compound 5 (CDCl ₃ , 100 MHz)	86
Figure 2.39. ¹ H NMR spectrum of compound 35 (CDCl ₃ , 400 MHz)	87
Figure 2.40. ¹³ C NMR spectrum of compound 35 (CDCl ₃ , 100 MHz)	87
Figure 2.41. ¹ H NMR spectrum of compound 36 (CDCl ₃ , 400 MHz)	88
Figure 2.42. ¹³ C NMR spectrum of compound 36 (CDCl ₃ , 100 MHz)	88
Figure 2.43. ¹ H NMR spectrum of compound 13 (CDCl ₃ , 400 MHz)	89
Figure 2.44. ¹³ C NMR spectrum of compound 13 (CDCl ₃ , 100 MHz)	89

Figure 2.45. ^1H NMR spectrum of compound 14 (CDCl_3 , 400 MHz)	90
Figure 2.46. ^{13}C NMR spectrum of compound 14 (CDCl_3 , 100 MHz)	90
Figure 2.47. ^1H NMR spectrum of compound 37 (CDCl_3 , 400 MHz)	91
Figure 2.48. ^{13}C NMR spectrum of compound 37 (CDCl_3 , 100 MHz)	91
Figure 2.49. ^1H NMR spectrum of compound 15 (CDCl_3 , 400 MHz)	92
Figure 2.50. ^{13}C NMR spectrum of compound 15 (CDCl_3 , 100 MHz)	92
Figure 2.51. ^1H NMR spectrum of compound 16 (CDCl_3 , 400 MHz)	93
Figure 2.52. ^{13}C NMR spectrum of compound 16 (CDCl_3 , 100 MHz)	93
Figure 2.53. ^1H NMR spectrum of compound 17 (DMSO, 400 MHz)	94
Figure 2.54. ^{13}C NMR spectrum of compound 17 (DMSO, 100 MHz)	94
Figure 2.55. ^1H NMR spectrum of compound 18 (CDCl_3 , 400 MHz)	95
Figure 2.56. ^1H NMR spectrum of compound 20 (CDCl_3 , 400 MHz)	96
Figure 2.57. ^{13}C NMR spectrum of compound 20 (CDCl_3 , 100 MHz)	96
Figure 2.58. ^1H NMR spectrum of compound 21 (CDCl_3 , 400 MHz)	97
Figure 2.59. ^{13}C NMR spectrum of compound 21 (CDCl_3 , 100 MHz)	97
Figure 2.60. ^1H NMR spectrum of compound 22 (CDCl_3 , 400 MHz)	98
Figure 2.61. ^{13}C NMR spectrum of compound 22 (CDCl_3 , 100 MHz)	98
Figure 2.62. ^1H NMR spectrum of compound 24 (CDCl_3 , 400 MHz)	99
Figure 2.63. ^{13}C NMR spectrum of compound 24 (CDCl_3 , 100 MHz)	99
Figure 2.64. ^1H NMR spectrum of compound 3 (CDCl_3 , 400 MHz)	100
Figure 2.65. ^1H NMR spectrum of compound 26 (CDCl_3 , 400 MHz)	100
Figure 2.66. ^1H NMR spectrum of compound 4 (CDCl_3 , 400 MHz)	101
Figure 2.67. ^{13}C NMR spectrum of compound 4 (CDCl_3 , 100 MHz)	101
Figure 2.68. ^1H NMR spectrum of compound 27 (CD_3OD , 500 MHz)	102
Figure 2.69. ^{13}C NMR spectrum of compound 27 (CD_3OD , 125 MHz)	102

Figure 2.70. ^1H NMR spectrum of compound 29 (CD_3OD , 700 MHz)	103
Figure 2.71. ^{13}C NMR spectrum of compound 29 (CD_3OD , 175 MHz)	103
Figure 2.72. ECD spectra of natural smenamide A (solid red line) and <i>ent</i> -smenamide A (29) (dashed blue line).	104
CHAPTER 3	108
Figure 3.1. Structures of compounds 7-15	109
Figure 3.2. Preparation of dolapyrrolidinone derivative 8	110
Figure 3.3. Ketone 9 as a versatile intermediate.	110
Figure 3.4. Preparation of compounds 9-13	111
Figure 3.5. Preparation of compounds 14 and 15	112
Figure 3.6. ^1H NMR spectrum of compound 16 (CDCl_3 , 400 MHz)	121
Figure 3.7. ^1H NMR spectrum of compound 8 (CDCl_3 , 400 MHz)	122
Figure 3.8. ^{13}C NMR spectrum of compound 8 (CDCl_3 , 100 MHz)	122
Figure 3.9. ^1H NMR spectrum of compound 10 (CDCl_3 , 400 MHz)	123
Figure 3.10. ^{13}C NMR spectrum of compound 10 (CDCl_3 , 100 MHz)	123
Figure 3.11. ^1H NMR spectrum of compound 11 (CDCl_3 , 400 MHz)	124
Figure 3.12. ^{13}C NMR spectrum of compound 11 (CDCl_3 , 100 MHz)	124
Figure 3.13. ^1H NMR spectrum of compound 12 (CDCl_3 , 400 MHz)	125
Figure 3.14. ^{13}C NMR spectrum of compound 12 (CDCl_3 , 100 MHz)	125
Figure 3.15. ^1H NMR spectrum of compound 22 (CDCl_3 , 400 MHz)	126
Figure 3.16. ^{13}C NMR spectrum of compound 22 (CDCl_3 , 100 MHz)	126
Figure 3.17. ^1H NMR spectrum of compound 14 (CDCl_3 , 400 MHz)	127
Figure 3.18. ^{13}C NMR spectrum of compound 14 (CDCl_3 , 100 MHz)	127
Figure 3.19. ^1H NMR spectrum of compound 15 (CDCl_3 , 400 MHz)	128

Figure 3.20. ^{13}C NMR spectrum of compound 15 (CDCl_3 , 100 MHz).....	128
CHAPTER 4	133
Figure 4.1. <i>Smenospongia aurea</i> and <i>conulosa</i> sponges, respectively.	133
Figure 4.2. Structures of smenamide A (1) and B (2), and smenothiazole A (3) and B (4).	134
Figure 4.3. Structures of conulothiazoles A (5) and B (6).....	135
Figure 4.4. Positive ion mode high-resolution ESI MS spectrum of compound 5.	136
Figure 4.5. Positive ion mode high-resolution ESI MS spectrum of compound 6.	139
Figure 4.6. The most significant correlations provided by the COSY, HMBC, and NOESY/ROESY 2D NMR spectra of conulothiazoles A (5) and B (6).....	141
Figure 4.7. Ozonolysis, hydrolysis and derivatization of conulothiazole A (5) with L-enantiomer of Marfey's reagent.	142
Figure 4.8. HR-ESI-MS-HPLC analysis of Marfey's derivatives from conulothiazole A (5) and B (6).....	142
Figure 4.9. Structural analogies of <i>Smenospongia</i> metabolites with cyanobacteria metabolites.	143
Figure 4.10. ^1H NMR spectrum of conulothiazole A (5) (CD_3OD , 700MHz)...	151
Figure 4.11. COSY spectrum of conulothiazole A (5) (CD_3OD , 700MHz).....	151
Figure 4.12. NOESY spectrum of conulothiazole A (5) (CD_3OD , 700MHz). ...	152
Figure 4.13. HSQC spectrum of conulothiazole A (5) (CD_3OD , 700MHz).....	153
Figure 4.14. HMBC spectrum of conulothiazole A (5) (CD_3OD , 700MHz).....	154
Figure 4.15. ^1H NMR spectrum of conulothiazole B (6) (CD_3OD , 700MHz)...	155

Figure 4.16. COSY spectrum of conulothiazole B (6) (CD ₃ OD, 700MHz).....	155
Figure 4.17. ROESY spectrum of conulothiazole B (6) (CD ₃ OD, 700MHz).....	156
Figure 4.18. HSQC spectrum of conulothiazole B (6) (CD ₃ OD, 700MHz).....	157
Figure 4.19. HMBC spectrum of conulothiazole B (6) (CD ₃ OD, 700MHz).....	158
CHAPTER 5	161
Figure 5.1. A specimen of the Mediterranean sponge <i>Geodia cydonium</i>	161
Figure 5.2. Two-dimensional molecular network of the active fraction from the sponge <i>Geodia cydonium</i>	164
Figure 5.3. Cell proliferation. Cell viability rate (CR) related to breast cancer cells: (a) MCF-7; (b) MDA-MB231; and (c) MDA-MB468, after treatment with fraction 3 for 24 (blue line) and 48 (red line) hours.....	168
Figure 5.4. RT-qPCR analysis: mRNA fold changes were evaluated as ratios between the expression levels of five genes in three breast cancer cell lines, MCF-7, MDA-MB231 and MDA-MB468, after treatment with the active fraction compared to the control (untreated cells).....	170
Figure 5.5. OPLS-DA plot. (a) OPLS-DA and variable importance in projection (VIP) analysis where the metabolites increased or decreased in the endo-metabolome of (b) MCF-7, (c) MDA-MB231 and (d) MDA-MB468 cells after treatment with the active fraction from the sponge <i>Geodia cydonium</i> , compared to untreated cells.	172
Figure 5.6. Cytokine levels in breast cancer cells. Scheme reporting the cytokines modulated by the active fraction obtained from the sponge <i>Geodia cydonium</i>	173

List of Tables

CHAPTER 2	28
Table 2.1. NMR data of natural smenamide A and ent-smenamide A.	105
CHAPTER 4	133
Table 4.1. NMR data of conulothiazole A (5) (700 MHz, CD ₃ OD).	138
Table 4.2. NMR data of conulothiazole B (6) (700 MHz, CD ₃ OD).	140
CHAPTER 5	161
Table 5.1. Apoptosis. Percentage of live, apoptotic and dead cells expressed as mean ± standard deviation by the Muse Annexin V and Dead Cell assay in MCF-7, MDA-MB231 and MDA-MB468 cells at IC ₅₀ concentration after 48h of treatment. Untreated cells were used as the control.....	169
Table 5.2. Cell percentages in the different cell cycle phases (G ₀ /G ₁ , S, G ₂ and M) expressed as mean ± standard deviation after Muse Cell cycle assay in MCF-7, MDA-MB231 and MDA-MB468 cells at IC ₅₀ concentration after 48h of treatment. Untreated cells were used as the control.....	170

Abstract

Among marine organism, Porifera have proven to be a rich source of new metabolites. Sponges are sessile organisms, therefore lacking any physical defence against predators. To make up to this lack, they produce species-specific molecules, known as secondary metabolites, which may play a key role in interspecific competition, defense against predators and reproduction processes. Secondary metabolites of marine origins are interesting molecules, often characterised by complex and unusual structures, which have shown to have a broad spectrum of pharmacological activities, such as anti-inflammatory, antiviral, antibiotic and anticancer. These compounds are hence considered promising lead compounds in drug discovery. Recently, many marine natural products have been approved, and others are in clinical trials. Due to the small amount isolated from the marine source, the evaluation of the biological activity of these compounds is often limited. Many alternatives have been considered to solve this issue. The total or semi-synthesis of these compounds represents a valid alternative to provide greater amounts of the metabolites of interest, allowing to gain a better insight in their biological activity. Currently, the number of synthetic or semi-synthetic drugs is indeed strongly increasing.

This research field forms the backdrop to my PhD work, aimed to the identification and structural elucidation of new bioactive marine natural products and to the synthesis of analogues with improved biological activities. The main topic of my research activity was the total synthesis of hybrid peptide/polyketide compounds of marine origins. Simultaneously, I was involved in the analysis of the chemical

content of the Caribbean sponge *Smenospongia conulosa* and the Mediterranean sponge *Geodia cydonium*.

The analysis of the lipophilic extract of the Caribbean sponge *S. aurea* led to the isolation, in 2013, of two hybrid peptide/polyketide compounds: smenamide A and B. Although both compounds possess a cytotoxic activity at nanomolar levels, smenamide A resulted more active blocking the cell proliferation through a pro-apoptotic mechanism. Therefore the total synthesis of smenamide A and its analogues was undertaken in order to provide greater amount of the compounds needed to confirm the structure of the compound, determine the absolute configuration at C-16, that remained undetermined until the end of the synthetic project, and to further investigate the cytotoxic activity. The total synthesis resulted in the preparation of 16-*epi*- and *ent*-smenamide A, two synthetic analogues of smenamide A.

In order to investigate the role of the structural determining-features of smenamides family, eight shorter-chain analogues of the synthetic 16-*epi*-smenamide A have been designed and prepared. The evaluation of the antiproliferative activity of 16-*epi*-smenamide A, together with its analogues, is now in progress.

On the other hand, the analysis of the organic extracts of the Caribbean sponge *Smenospongia conulosa* and the Mediterranean sponge *Geodia cydonium* led to the identification of two new hybrid peptide/polyketide compounds, conulothiazole A and B, and an active fraction, respectively.

The evaluation of the biological activity of conulothiazoles could not be carried out because of the low amount isolated from the marine source.

As for *G. cydonium* active fraction, it showed an antiproliferative activity on three human cancer breast cell lines (MCF-7, MDA-MB-231 and MDA-MB-468). The

use of LC-HRMS, LC-HRMS/MS coupled with a bioinformatic techniques, e.g. Molecular Networking, as a novel dereplication strategy allowed to identify most of the metabolites contained in this fraction. In addition, the evaluation of the metabolomic profiling and the cytokine levels of the three cancer cell lines after treatment with the active fraction showed that the latter participates in the modulation of several metabolites in pro- or anti-tumor processes. Further studies are necessary in order to understand the mechanism of action of each compound contained in this fraction, as well as the evaluation of the possible synergistic effect of a pool of compounds.

INTRODUCTION

Since the dawn of time natural products have been used as a remedy to relieve their pains. The first humans nourished themselves not only with meat, but also roots, berries, herbs and wild fruits. By eating them, they accidentally discovered their healing benefits. Ancient apothecaries learned several techniques in order to prepare, store and make use of medicinal herbs. They used them as a *panacea*, only basing their uses on empirical evidences.

Extremely relevant is the example of aloe species, widely described by the Greek physician Dioscoride, in his play *De materia medica*. Among the remarkable benefits of these plants, it is possible to cite: healing of plagues and wounds, protection and relief towards burns, itching and cutaneous inflammation. In addition, it is worth to mention nettle, also known as "green gold", which is a potent anti-inflammatory, stimulator of microcirculation, with antiseptic and elasticising properties especially when used in combination with olive oil.

However, it is only in eighteenth century that, through the manipulation of the organic extracts from natural sources, scientists isolated the first chemical pure compounds. With the introduction of new isolation and purification techniques an increasing number of these compounds have been identified, prompting researchers to study cells and organisms from which they derive from, identifying similarities and differences.

Primary metabolism is the ensemble of chemical reactions by which some substances, known as primary metabolites, are produced. Carbohydrates, amino acids, nucleic acids and fatty acids are primary metabolites. They are essential for cell survival. Secondary metabolites, on the other hand, regulate other functions and

they vary from species to species. They are part of specialised characteristics of a cell, and participate in interspecific competition, defense against predators and promotion of reproduction processes.

Secondary metabolites are characterised by peculiar and complex structure, which brings about several different biological activities.

Currently, about 42% of compounds used in therapy are natural substances or their derivatives. Among them, it is worth to cite some molecules with anti-inflammatory (*e.g.* acetylsalicylic acid), bronchodilator (*e.g.* ephedrine), cardiotoxic (*e.g.* digoxin and digitoxin) and anticancer (*e.g.* vincristine, vinblastine, taxol) activities. Therefore, modern pharmaceutical discovery programs owe much to natural products. Pharmaceutical companies are always looking for new drugs for the treatment of life-threatening diseases, in particular cancer. Despite the cancer death rate has significantly dropped since 1991,¹ cancer still is the leading cause of death in 21 States. In particular, because of the increasing of drug resistance against common anticancer therapies, new chemotherapeutic agents are urgently required. Moreover, the incidence of new types of cancer, such as glioblastoma, increases rapidly². In the latest 50 years, thanks to advances in technologies (in particular scuba diving) researchers have quickly turned their attention to the marine environment, thus beginning the "blue chemistry Age". Marine natural products (MNPs)³ are interesting molecules characterised by complex and unusual molecular skeletons, as well as a great structural diversity. Due to the greater genetic heterogeneity of marine organisms, this structural variability results in a variety of biological activities.

As reported recently,³ a wide range of molecules with cytotoxic, antimicrobial and antiviral activities have been isolated. Therefore, MNPs are largely recognized as one of the most prolific source of therapeutics.

From a practical point of view, there are many problems concerning the isolation of new MNPs. The main difficulty of developing drugs from a marine source resides in the sustainable supply from the natural source.⁴

For instance, Porifera and Tunicates, source of many bioactive compounds, are sessile organisms, the collection of which can only be performed by hand using scuba diving or with the aid of submarines equipped with robotic arms. In addition, the chemical composition of organic extracts can deeply vary within samples of the same species when collected in different places or at different moments. Moreover, due to the exiguous amounts of these compounds isolated from the marine source, the study of their biological activity is more complicated. Nevertheless, the interest for this kind of molecules remains high, pushing the researchers to find solutions for the supply. Among the alternatives, of great importance are aquaculture (massive growth of the organisms in a controlled area) and production of metabolites of interest through cell cultures. Recent studies have shown that secondary metabolites are often produced by the microbial symbionts of the sponges.⁵ Since the microbial fauna is largely unculturable, chemical synthesis represents a valid alternative.

Organic synthesists aim to the construction of natural or designed molecules whose primary element is carbon with the purpose of synthesising in the laboratory natural products occurring from the living world.⁶ Organic synthesis sinks its roots in 1828, when German chemist Friedrich Wöhler performed the serendipitous synthesis of urea from ammonium isocyanate.⁷

Chemical synthesis is fundamental to provide larger quantities of the desired natural compound needed to further investigate its biological activity. Several to hundred grams are instead required for preclinical and clinical development of a drug. Synthesis is also extremely useful to determine the absolute stereochemistry of stereogenic centers when this cannot be achieved by spectroscopical tools or derivatization methods such as Marfey's method.⁸ Moreover, synthetic analogues can be prepared in order to perform SAR (structure–activity relationship) studies aiming to improve the bioactivity and reduce the toxic side effects.

Although most of the drugs currently approved are natural products, the number of synthetic or semi-synthetic drugs is increasing thanks to their production cost, time effectiveness and easy quality control.

Among drugs of marine origins currently produced *via* synthesis, it is worth to mention Trabectedin (Yondelis[®]), a tetrahydroisoquinoline alkaloid isolated from the Caribbean tunicate *Ecteinascidia turbinata*.⁹ It has been approved as anti-neoplastic drug for the treatment of soft tissue sarcoma and, in combination with pegylated liposomal doxorubicin, for patients with platinum-refractory ovarian cancer. Trabectedin is now produced synthetically.

Ziconotide (Prialt[®]) is a synthetic non-opioid analgesic drug, equivalent of the 25-amino acid peptide ω -conotoxin MVIIA, originally isolated from the venom of the marine snail *Conus magus*.¹⁰ It is used in symptomatic management of severe chronic pain in patients with cancer or AIDS, for whom intrathecal (IT) therapy is warranted, and who are intolerant of or refractory to treatment with morphine and systemic analgesics.

Brentuximab vedotin (ADCETRIS[®])¹¹ is a cysteine-linked antibody-drug conjugate (ADC) in which the chimeric monoclonal anti-CD30 antibody (obtained by

recombinant DNA technology), is covalently linked to the monomethylauristatin E (MMAE). The latter is a semi-synthetic analogue of the marine cytotoxic peptide dolastatin-10, isolated from the mollusk *Dolabella auricularia*. ADCETRIS® is actually used in the treatment of Hodgkin's lymphoma (HL) and systemic anaplastic large cell lymphoma (ALCL).

The present research project is focused on the study of Caribbean and Mediterranean marine sponges in order to discover novel anticancer lead molecules and to design and prepare their synthetic or semi-synthetic analogues.

More precisely, during my PhD I was involved in the study of the chemical composition of the organic extracts of the Caribbean sponges *Smenospongia aurea* and *conulosa* and the Mediterranean sponge *Geodia cydonium*.

Four hybrid polyketide/peptide (PKS/NRPS) compounds have been previously isolated by our group from the organic extract of *S. aurea*.^{12,13} Among these compounds, smenamide A showed a potent cytotoxic activity at nanomolar concentrations on a non-small-cell lung cancer (NSCLC) cell line, known as Calu-1. As part of my PhD project, a strategy to prepare synthetic derivatives has been set up. The stereoselective total synthesis resulted in the preparation of two analogues of smenamide A: 16-*epi*- and *ent*-smenamide A.¹⁴

A different approach was instead used for the study of the chemical content of the Mediterranean sponge *G. cydonium*. A bioguided fractionation of the cytotoxic organic extract of the sponge was performed. This procedure allowed the identification of one antiproliferative fraction acting with an apoptotic mechanism against MCF-7, MDA-MB231, and MDA-MB468 breast cancer cell lines.¹⁵ Interestingly, no activity was observed on the normal breast cell line (MCF-10A)

used as control. Such a result opens up the possibility of using this fraction for therapeutic purposes.

The results obtained during my PhD have been divided in two sections:

- The main project of my research activity, which resulted in the total synthesis of 16-*epi*- and *ent*-smenamide A, two new hybrid PKS/NRPS compounds.
- Simultaneously, I analysed the chemical composition of two marine sponges, *S. conulosa* and *G. cydonium*.

The results achieved during my Ph.D. have been reported in four publications on peer-reviewed journals.

1. A. Caso, A. Mangoni, G. Piccialli, V. Costantino, and V. Piccialli, Studies toward the Synthesis of Smenamide A, an Antiproliferative Metabolite from *Smenospongia aurea*: Total Synthesis of ent-Smenamide A and 16-epi-Smenamide A, *ACS Omega*, **2017**, 2(4), 1477–1488. Impact Factor: *
2. G. Esposito, G. Della Sala, R. Teta, A. Caso, M.L. Bouguet-Kondracki, J.R. Pawlik, A. Mangoni, V. Costantino, Chlorinated thiazole containing polyketide-peptides from the Caribbean sponge *Smenospongia conulosa*: structure elucidation on microgram scale. *Eur. J. Org. Chem.* **2016**, 16, 2871–2875. Impact Factor: 2.834 (2016).
3. S. Costantini, E. Guerriero, R. Teta, F. Capone, Caso, A. Sorice, G. Romano, A. Ianora, N. Ruocco, A. Budillon, V. Costantino, M. Costantini, Evaluating the effects of an organic extract from the mediterranean sponge *Geodia cydonium* on human breast cancer cell lines, *Int J Mol Sci.*, **2017**, 18(10). pii: E2112. Impact Factor: 3.226 (2016).
4. A. Caso, I. Laurenzana, D. Lamorte, S. Trino, G. Esposito, V. Piccialli, and V. Costantino, Smenamide-A-analogues: a case-example of the application of the functional-analogues strategy to design and study complex natural lead compounds, *Mar. Drugs*, **2018**, accepted. Impact Factor: 3.503 (2016).

* The first volume of this paper was published in December 2015. The value of its impact factor has not yet been disclosed.

References

- ¹ R. L. Siegel, K. D. Miller, A. Jemal, *CA Cancer J Clin*, **2016**, 66 (1), 7-30.
- ² J. W. Blunt, B.R. Copp, R. A. Keyzers, M. H. G. Munro, M.R. Prinsep, *Nat. Prod. Rep.*, **2016**, 33, 382-431.
- ³ K. von Schwarzenberg and A.M. Vollmar, *Cancer Letters*, **2013**, 332, 295–303.
- ⁴ T. F. Molinski, D. S. Dalisay, S. L. Lievens and J. P. Saludes, *Nature Reviews Drug Discovery*, **2009**, 8, 69-85.
- ⁵ (a) Unson, M. D.; Holland, N. D.; Faulkner, D. *J. Mar. Biol.* **1994**, 119, 1-11. (b) Hentschel, U.; Hopke, J.; Horn, M.; Friedrich, A.B.; Wagner, M., Moore, B.S. *Appl. Environ. Microbiol.* **2002**, 68, 4431-4440.
- ⁶ K. C. Nicolaou, *Proc. R. Soc.*, **2014**, A 470: 20130690.
- ⁷ F. Wöhler, *Poggendorff's Ann, Phys. Chem*, **1828**, 12, 253.
- ⁸ P. Marfey, *Carlsberg Res. Commun.* **1984**, 49, 591–596.
- ⁹ (a) K.L. Rinehart et al., *J. Org. Chem.*, **1991**, 56, 1676; (b) A. E. Wright et al., *J. Org. Chem.* **1990**, 55, 4508–4512.
- ¹⁰ B. M. Olivera, *Drugs from the Sea* (Fusetani, N., ed.), Basel, Karger, **2000**, pp 74-85.
- ¹¹ L. N. Tumey, Han, Sean, *Current Topics in Medicinal Chemistry*, **2017**, 17, 32, 3444-3462.
- ¹² R. Teta, E. Irollo, G. Della Sala, G. Pirozzi, A. Mangoni, V. Costantino, *Marine Drugs*, **2013**, 11 (11), 4451-4463.
- ¹³ Esposito G., Teta R., Miceli R., Ceccarelli L., Della Sala G., Camerlingo R., Irollo E., Mangoni A., Pirozzi G., Costantino V., *Mar. Drugs* **2015**, 13, 444-459.
- ¹⁴ A. Caso, A. Mangoni, G. Piccialli, V. Costantino, V. Piccialli, *ACS Omega*, **2017**, 2, 1477–1488.
- ¹⁵ S. Costantini, E. Guerriero, R. Teta, F. Capone, A. Caso, A. Sorice, G. Romano, A. Ianora, N. Ruocco, A. Budillon, V. Costantino, M. Costantini, *Int J Mol Sci.*, **2017**, 18(10). pii: E2112.

Chapter 1

Structural elucidation techniques

Before the introduction of spectroscopy, structural determination of new chemical compounds was carried out through degradative methods and/or derivatisation of functional groups. The main problem of degradative techniques is the total loss of the sample. As regards derivatisation methods, these can change sample composition, may not be quantitative or give by-products, and reduce amount of the analyte. Considering that natural products are often isolated in very exiguous amounts, these techniques are evidently unsuitable for structural elucidation of micrograms of compounds.

The introduction of highly sensitive and non-degradative methodologies marks a turning point in the field of structural determination, allowing the elucidation of submilligram samples.

Structural elucidation of each molecule described in thesis has been accomplished through spectroscopic techniques, mostly NMR spectroscopy and mass spectrometry (MS), but also IR and CD spectroscopy. The absolute stereochemistry of amino acids has been established by using Marfey's method. The specific rotation of each chiral compound has been determined by measuring the optical rotation at the sodium D line (589 nm).

1.1 Nuclear Magnetic Resonance

Nuclear Magnetic Resonance (NMR) spectroscopy is a powerful, high sensitive and non-destructive analytical tool used for the identification of the carbon-

hydrogen framework of an organic compound. It allows structure elucidation, qualitative and quantitative analysis of single molecules or mixtures of compounds. NMR experiments involve the nuclei of atoms: the chemical environment of a specific nucleus is determined getting information about that nucleus. When the sample is placed in a magnetic field, it is excited by radio waves. Therefore, the nuclei get into nuclear magnetic resonance, and it is detected with sensitive detectors (Figure 1).

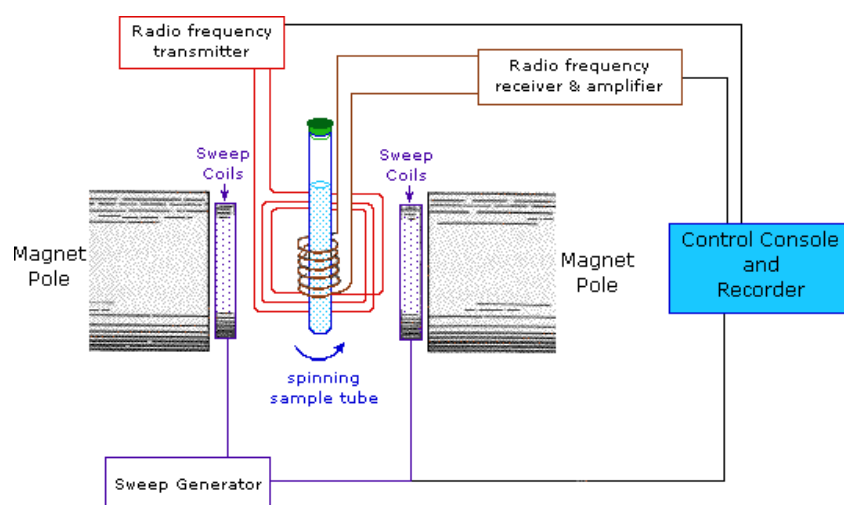


Figure 1.1. Scheme of a NMR spectrometer.

Subatomic particles (protons, neutrons and electrons) can be imagined as spinning around their axes. In some cases, these spins are paired against each other and the nucleus of the atom has no overall spin. However, in some atoms (such as ^1H and ^{13}C) the nucleus has an overall spin.

The rules for determining the net spin of a nucleus are the following:

1. If the number of neutrons **and** the number of protons are both even, then the nucleus has **NO** spin.
2. If the number of neutrons **plus** the number of protons is odd, then the nucleus has a half-integer spin (i.e. $1/2$, $3/2$, $5/2$)

3. If the number of neutrons **and** the number of protons are both odd, then the nucleus has an integer spin (i.e. 1, 2, 3)

Therefore, what is important is the overall spin, I . Particularly useful isotopes are ^1H , ^{13}C , ^{19}F and ^{31}P , all of which have spin $I = 1/2$.

A spinning charge generates a magnetic field (Figure 2). The resulting spin-magnet has a magnetic moment (μ) proportional to the spin.



Figure 1.2. A spinning charged particle generate a magnetic field.

Since spin I has have $2I + 1$ possible orientations, a nucleus with spin $1/2$ will have 2 possible orientations. In the absence of an external magnetic field, these orientations are of equal energy. When a magnetic field is applied, these nuclei align themselves with or against the magnetic field (B_0) and the energy levels split. Each level is characterized by a *magnetic quantum number*, m (Figure 1.3).

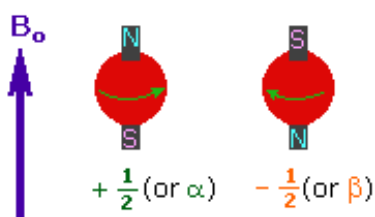


Figure 1.3. Spin energy states.

In particular, irradiation with electromagnetic radiation allow the low energy state to flip over to the high-energy state. The difference in energy between the two spin states is dependent on the external magnetic field strength, and is always very small. The stronger is the magnetic field (B_0), the larger is the difference in energy

of the two energy states. For nuclei with spin 1/2 the energy difference between the two spin states at a given magnetic field strength is proportional to their magnetic moments.

When the radiation ceases, a free induction decay (FID) is produced because of the nuclei relaxation. The FID is transformed through the Fourier transform to give the peaks of the NMR spectrum. The Fourier transform is a mathematic transformation that allows to write a time-dependent function in the frequency domain.

The use of mono and two-dimensional NMR experiments represented a fundamental tool for the structural determination of each compound described in this thesis.

1.1.1 One-dimensional NMR experiments

A single nucleus is analysed in a one-dimensional NMR experiment. In a 1D NMR spectrum the intensity is expressed as a function of the frequency. It is a two-dimensional chart but it is defined as one-dimensional because it involves only one dimension "frequency".

The most common one-dimensional NMR experiments concern ^1H and ^{13}C .

As for ^1H spectra, since protons all have the same magnetic moment we might expect no difference in their resonance signals. Fortunately, they behave differently in the NMR experiment. This phenomenon can be explained by electrons shielding. Electrons are indeed charged particles, hence they respond to the external magnetic field (B_0) generating a secondary field. The latter, opposing to B_0 , shields the nucleus from the applied magnetic field. Therefore, to achieve resonance and then absorption of rf energy, B_0 must be increased.

Based on its chemical environment, each proton resonates at a specific chemical shift (expressed in parts per million, ppm). This means that it is differently located in the proton spectrum.

Although the ^1H NMR spectroscopy is a powerful tool in the field of structural determination, it can not provide information for those molecules composed by big portions lacking carbon-hydrogen bonds.

^{13}C NMR experiments can provide the missing information. It is worth noting that ^{13}C isotope is only 1.1% abundant and the nucleus is fifty-fold less sensitive than a proton in a NMR experiment. For these reasons high concentrated samples are required. Moreover, the spectra are complicated by the large one-bond coupling between and ^1H . Protons bonded to a ^{13}C atom split its NMR signals from 130 to 270 Hz, further complicating the spectrum. The issue has been solved thanks to the use of the high-field pulse technology in combination with broadband heteronuclear decoupling of all protons. Several acquisitions are accumulated in each experiment in order to provide a stronger signal. Also, thanks to the decoupling irradiation the sensitivity of carbon nuclei bonded to protons is enhanced.

1.1.2 Two-dimensional NMR experiments

In addition to 1D experiments, two-dimensional experiments have been recorded and analysed in order to complete the resonance assignment of each molecule.

A two-dimensional NMR spectrum is a three-dimensional chart in which two frequencies are expressed as function of the intensity.

Considering that, in a NMR experiment, frequencies derive from the Fourier transformation of a time-dependent function, the simultaneous acquisition of two temporal functions is required to obtain a 2D spectrum.

Although the nuclei resonate in crowded regions of the spectra, a remarkably easier interpretation characterises 2D spectra (signals' superimposition is much less frequent in two dimensions than in one). Their easier interpretation and shorter acquisition times make 2D experiments superior than the one-dimensionals.

Two kinds of two-dimensional experiments can be mentioned: homonuclear and heteronuclear experiments. A 2D experiment is defined as homonuclear if the two frequencies refer to the same nucleus. Vice versa, in a heteronuclear experiment the correlation peaks between two different nuclei are observed.

The COSY (Correlation SpettroscopY) experiment was the first two-dimensional NMR experiment invented. It is simple and still widely used today in its various versions (COSY, DQF-COSY, COSY-b, COSY-90). The analysis of a COSY spectrum provides information about homonuclear correlations of protons between them to 2 or 3 bonds (scalar spin-spin coupling).

The HSQC (Heteronuclear Single Quantum Coherence)¹ experiment is a 2D heteronuclear correlation experiment detecting correlation peaks between ^{13}C and ^1H nuclei directly bonded each other through the direct coupling constant $1J_{\text{C-H}}$.

The HMBC (Heteronuclear Multiple Bond Correlation)² experiment is a long-range heteronuclear experiment acquired in reverse detection. In a HMBC spectrum correlations between ^1H and ^{13}C through two ($^2J_{\text{CH}}$) or three bonds ($^3J_{\text{CH}}$) are visible. This experiment allows the identification of the correlations between quaternary carbons (not visible in the HSQC spectrum) with protons close to them.

However, not all of the correlation peaks expected from the structure of a molecule are present in many HMBC spectra. Since $^{2,3}J_{CH}$ can vary differently to each other, the optimization of the experiment for each type of coupling is required.

1.2. Methods for the determination of relative/absolute configurations

Since most of the natural compounds have one or more chiral centers, the determination of their relative and absolute configuration is fundamental for their structural characterization. The knowledge of the stereochemistry of a molecule allows to trace back to its three-dimensional structure and its role in the interaction with the biological systems, e.g. the SAR studies of synthetic molecules which are designed and prepared in order to improve the drug-receptor interaction and, then, their biological activity in comparison with the natural lead compounds.

The determination of the relative configuration of the chiral centers can be achieved evaluating NMR data such as the values of chemical shifts (δ), coupling constants (J) and NOE effects.

The chemical environment of a proton influences its chemical shift, hence protons of two diastereomers show different values.

Many information about the relative stereochemistry of an organic molecule can be obtained studying the coupling constants values (J_{H-H}). The application of Karplus law The application of Karplus law allows to calculate both homonuclear, $^3J_{H-H}$, and heteronuclear, $^3J_{C-H}$ constants values. These values depend on the dihedral angle θ between the coupled atoms.³ When θ is approximately 90° , the $^3J_{H-H}$ values are very small, about 0-1.5 Hz, whereas the values increase considerably when θ is between 0° or 180° . In addition, the axial-axial relationship between two protons of a six terms cycle ($^3J_{a-a} \sim 9-13$ Hz) can be distinguished in comparison with the axial-

equatorial (${}^3J_{a-e} \sim 5-8$ Hz) and the equatorial-equatorial (${}^3J_{e-e} \sim 2.5$ Hz). As a consequence, the *cis-trans* relationship between the protons of a double bond (${}^3J_{cis} \sim 6-12$ Hz, ${}^3J_{trans} \sim 14-20$ Hz) can be determined.

Moreover, the study of homonuclear couplings between neighboring protons (dipolar couplings) can provide further information about the relative configuration of a chiral center. Dipolar coupling involves nuclei which are close in space, and not coupled through bonds, as in scalar coupling.

Exploiting the dipolar coupling, the spatial relationship between the substituents of a molecule can be established through the evaluation of the NOE effect (Nuclear Overhauser Enhancements)⁴.

When a proton H_A , nearby located to another, H_B , undergo irradiation, a variation of the signal intensity of H_B can be observed. This phenomenon is known as NOE effect. Generally, an increasing of the signal intensity (positive NOE) is observed for small organic molecules, while a decreasing is observed for macromolecules (negative NOE). Since the increase in intensity is small, normally the NOE is measured using the difference spectra (NOE difference): two spectra are recorded with and without irradiation. In the difference spectrum, deriving from the two original spectra, only the protons showing NOE effect, can be detected.

Since this experiment involves a pair of protons at a time, nowadays it is often replaced by a single two-dimensional experiment, called NOESY (Nuclear Overhauser Effect Spectroscopy). The latter is a 2D NMR homonuclear correlation experiment which is able to provide information about dipolar couplings of each of the pairs of protons of the molecule at the same time. It shows the presence of a NOE effect between two protons, suggesting hence that they are close in space.

In addition to NOESY, the ROESY (Rotating-frame Overhauser Spectroscopy) experiment can be performed: it detects the ROE effect. Since the latter is related to dipolar coupling between nuclei, and depends on the geometric distance between the nuclei, it is similar to NOE. But while NOE effect can be positive or negative, depending on the size of the molecules, ROE effect is always positive. For this reason, the ROESY experiment is particularly useful in the analysis of medium-sized molecules, which would show a NOE effect close to zero.

1.3 Mass spectrometry

Mass spectrometry (MS) is a powerful analytical technique used to identify unknown compounds, elucidate their structure and chemical properties, and also to quantify known materials within a sample.

The principle underlying a MS experiment is the conversion of a sample into gaseous ions, each of which is characterised by a specific mass-to-charge ratio (m/z ratio) and relative abundance. The ions that arise from the ionisation process are then separated on the basis of their m/z ratio and revealed by a detector.

A molecule is converted in ions losing an electron: a radical cation is formed (molecule ion). The latter is subjected to fragmentation giving in part molecules and/or neutral radicals (not detected by the instrument), and in part cations and/or cations radicals (fragment ions).

The ionisation of the sample is then the key step of the whole experiment. The sample, which can be solid, liquid or gaseous, is introduced into a vacuum chamber through an appropriate introduction system. The molecules may already exist in solution as ions, or they can undergo ionization *in situ* after volatilization or by other methods in the ion source. According to their m/z ratio, the gaseous ions

obtained are separated in the analyzer and collected by the detector. An electrical signal, proportional to the number of ions present, is generated. It is recorded as a function of the m/z ratio by the data processing system records and converted into the mass spectrum.

As result of the experiment a graph, named as mass spectrum, is obtained in which is the representation of the relative abundance of the ions according to their m/z ratio.

Mass spectrometry is a high sensitive tool allowing the determination of the molecular mass of compound and its molecular formula, even if only sub-milligrams of the molecule are available.

A mass spectrometer is composed by an ion source, (in which the sample is ionized), a mass analyser (where ions are separated on the basis of their m/z ratio) and a detector. Many types of ion sources, mass analysers and detectors exist.

Hereinafter only the methods used for the realisation of this thesis work will be described.

Each molecule described in this thesis have been analyzed by ESI (*Electrospray Ionization*) mass spectrometry (Figure 1.4) through an *Orbitrap* system.

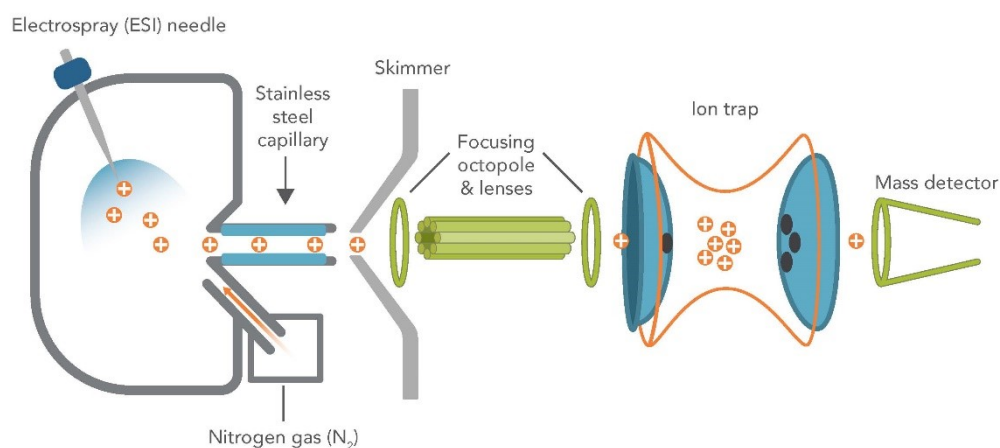


Figure 1.4. ESI mass spectrometry.

A solution of the sample, dissolved in a polar and volatile solvent such as H₂O, CH₃OH and CH₃CN, is nebulized at atmospheric pressure inside the ionization chamber through a needle held at high electrical potential.

Therefore, a spray of droplets is formed. The droplets are positively charged because of the presence of an electric field. Once the ions are created, it is the role of the “ion lens” (which consists of a capillary maintained under vacuum and in a negative potential) to extract ions from the source efficiently and focus them as they pass through the mass spectrometer accelerating them towards the analyser.

It is worth to mention a kind of mass spectrometry known as tandem mass (MS/MS) spectrometry. During or after ionization, the molecules may indeed undergo fragmentation. If the fragmentation does not occur spontaneously, this can be induced letting the ions to collide with gas molecules. Since each molecule has a specific fragmentation pattern, the analysis of the fragments provides information about its the structure. In this case, a second analyzer is used to measure the mass of the fragments.

In some cases, the formation of multiple-charged ions can be observed. This happens for molecules with high molecular weight such as proteins. The formation of multiple-charged ions facilitates the analysis of this kind of molecules because the m/z ratio of the ions is reduced, and therefore easier to measure.

The mass spectrometer used for the experiments performed in this project was equipped with an Orbitrap analyzer, a new type of mass analyzer introduced by Makarov.⁵ The LTQ Orbitrap XL™ Hybrid Ion Trap-Orbitrap Mass Spectrometer is a Fourier Transform Mass Spectrometer (FTMS) in which the most advanced Ion Trap and Fourier Transform technologies are combined.

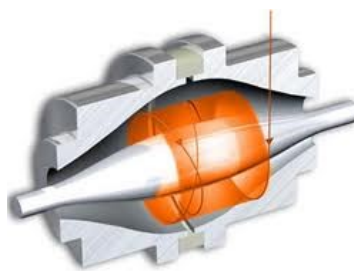


Figure 1.5. Ion trajectories in an Orbitrap mass spectrometer.

In a Orbitrap analyzer (Figure 1.5) a central electrode, and a pair of bell-shaped external electrodes which surrounded it, generate electric fields in order to capture and confine the ions. The ions orbit around the central electrode and oscillate back and forth down the center axis with periodic motion. Through a Fast Fourier Transformation (FFT), the device receives the frequencies of these axial oscillations and, therefore, the m/z relations of the ions.

1.4. Infrared Spectroscopy

Infrared spectroscopy is a conservative analytical technique based on the interaction between the matter and the infrared light. The most interesting region of IR radiations have a wavelength range from 4000 and 400 cm^{-1} . However, near (14290-4000 cm^{-1}) and far (700-200 cm^{-1}) infrared regions are also considered suitable to contribute to the determination of the structure of a molecule.

As a consequence of the hitting of a molecule by IR radiations, an absorption of energy, converted in vibrational energy, is observed. Therefore, such a technique can be defined as a vibrational spectroscopy.

Molecular vibrations can be classified in fundamental and non-fundamental. Two kinds of fundamental vibration can essentially be observed in a molecule: stretching and bending vibrations. The stretching vibration involves the continuous change, in terms of interatomic distance, along the axis of the bond between two atoms. The bending vibration concerns indeed the variation of the angle between two bonds. Stretching vibrations can be symmetric and asymmetric, whereas four different bending vibrations can be observed: scissoring and rocking (in-plane bendings), wagging and twisting (out of the plane bendings).

Non-fundamental vibrations appears as a consequence of fundamental vibrations.

Generally, IR spectroscopy is not sufficient to reveal the structure of a molecule, but it can provide useful information to be used in combination with other spectroscopic data. Although the IR spectrum is characteristic of each molecule, certain functional groups show typical bands in specific regions of the spectrum, independently from the whole structure of the molecule.

The infrared spectrum is a graph in which the absorption bands of the functional groups are represented as a function of the wavelength.

1.5. Circular Dichroism

Circular dichroism (CD) is the physical phenomenon whereby a chiral molecule can differently absorb both components, left- and right-handed, of circularly polarised light at a given wavelength. Circular dichroism ΔA is then the difference in terms of absorbance of the left (A_L) and right (A_R) circularly polarised light:

$$\Delta A = A_L - A_R$$

CD spectroscopy is a spectroscopic technique, which measures the CD of the molecules over a range of wavelengths. It is widely used to determine the three-

dimensional structure of chiral organic molecules of all types and sizes, but mostly of macromolecules such as proteins. Such a technique can provide information about absolute configurations, conformations, reaction mechanisms, etc.

The presence of at least one chromophore in the structure of the molecule is required to observe a *differential* absorbance. If the molecule does not have a chromophore, this can be introduced through derivatisation methods.

A CD spectrum is a graph in which circular dichroism (ΔA) is represented as a function of wavelength. A circular dichroism signal can be positive or negative.

Since asymmetric electromagnetic radiations are used, CD spectroscopy can distinguish between enantiomers. The CD of pure enantiomers differs in sign, but not in magnitude. Any relation between the absolute configuration of an enantiomer and the sign of its electronic circular dichroism (ECD) can be established: CD depends on details of the electronic and geometric molecular structure. However, nowadays the ECD can be predicted through electronic structure calculations allowing the assignment of the absolute configuration by simply comparison of experimental and computed CD spectra.

1.6. Marfey's Method

Marfey's method⁶ is one of the most used analytical approaches for determining the regiochemistry of enantiomeric amino acid residues in natural products. This is a derivative method, whereby the natural compound undergoes acid hydrolysis to deliver the amino acid residues, the configuration of which is undetermined. The amino acid residues are then derivatised with a chiral reagent, the 1-fluoro-2,4-dinitrophenyl-5-L-alaninamide (L-FDAA) (Figure 1.6) and analysed by LC-MS analysis. The LC-MS retention times of the derivatised amino acids deriving from

the peptide are compared with retention times of the corresponding standards D and L amino acid derivatised with the same reagent.

When the standard amino acids are commercially available, the analysis is quite easy and consists of the following steps:

- Hydrolysis of the peptide with 6N HCl
- Derivatization of hydrolysed amino acids with L-FDAA
- Derivatization of both D and L standards amino acids with L-FDAA. If the steric D series standard is not commercially available, or is too expensive, the L-aminoacid under study can be derivatised with L and D-FDAA.
- LC/MS analysis of derivatised samples and comparison of respective retention times.

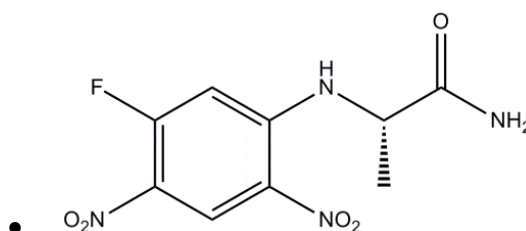


Figure 1.6. L-FDAA structure.

For non-proteinogenic amino acids, for which the corresponding commercially standards are not available, a modified Marfey's method, known as "Method of Marfey Advanced", has been set up.⁷

This method, based on the elution order of the L-FDAA-amino acids, was tested on a series of proteinogenic and non-proteinogenic amino acids showing that the L-FDAA-L-amino acid is almost invariably eluted through a C18 column before its corresponding L-FDAA-D-enantiomer.

Several NMR and UV measurements allowed to understand the mechanism of elution of the L-FDAA-derivatised amino acids of L and D steric series through a C18 column.

The more hydrophobic substituents present at the α -carbon of non-proteinogenic amino acids were observed to form *cis* or *trans* rearrangements with the substituent at the α -carbon of L-FDAA. For D-(amino acid)-L-FDAA stereoisomers essentially *cis* rearrangements have been observed. This makes them more hydrophobic and then strongly retained by the C18 phase. They show indeed greater retention times compared to the less hydrophobic L-(aminoacid)-L-FDAA stereoisomers, which are preferentially involved in *trans* type rearrangements (Figure 1.7).

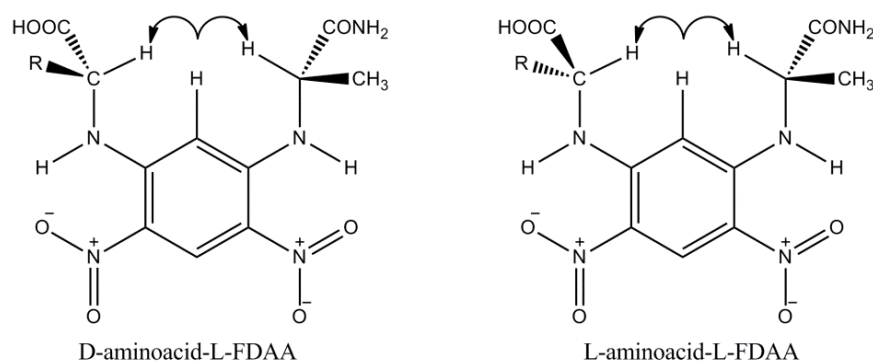


Figure 1.7. Plausible conformations of the L- and D-aminoacids derivatives during separation by Marfey's method.

This method, overcoming the limits of Marfey's method, allowed to establish the configuration at α -carbon of unconventional amino acids.

In conclusion, the configuration of a non-proteinogenic amino acid can be determined as described below:

- An aliquot of amino acid is derivatised with L-FDAA
- An aliquot of amino acid is derivatised with D-FDAA
- Analysis of the LC/MS retention times.

1.7 Conclusion

In this chapter, the main techniques used for the structural determination of the molecules described in my thesis have been discussed.

Among the spectroscopic techniques, NMR and MS provided valuable data about the isolated and synthesised compounds.

The determination of absolute configuration of amino acids in PK/NRP compounds was carried out by using Marfey's method.

References

- ¹ Palmer III, A. G.; Cavanagh, J.; Wright, P. E.; Rance, M.; *J. Magn. Reson.* **1991**, 151-170.
- ² Bax, A.; Summers, M. F. *J. Am. Chem. Soc.* **1986**, 2093.
- ³ Karplus, M.; *J. Chem. Phys.* **1959**, 11.
- ⁴ Sanders, J. K. M.; Mersh, J. D. *Prog. NMR Spectrosc.* **1982**, 353.
- ⁵ Hu, Q.; Noll, R. J.; Li, H.; Makarov, A.; Hardmanand, M.; Cooks, R. G.; *J. Mass Spectrom.*, **2005**, 40, 430-443.
- ⁶ Marfey, P. *Carlsberg Res. Commun.* **1984**, 49, 591-596.
- ⁷ Fujii, K.; Ikai, Y.; Oka, H.; Suzuki, M.; Harada, K. *Anal. Chem.* **1997**, 69, 3346-3352.

PART 1

**Total synthesis of new hybrid PKS/NRPS
compounds, in the frame of the anticancer
drug discovery**

Chapter 2

Total synthesis of 16-*epi*- and *ent*-smenamide A, two analogues of the cytotoxic smenamide A

2.1 Cancer and bioactive natural products

Cancer is a generic term to define a group of diseases involving abnormal cell growth. Such a disease, also known as malignant tumour or neoplasm, arises without obvious causes from pre-existing body cells. It has no purposeful function, and it has the tendency to independent and uncontrolled growth.

Compared with benign tumours, in which the mass of abnormal tissue remains confined to its original location, a malignant tumour invades adjoining parts of the body and spreads to other organs, through the cardiovascular system and other channels. The latter process is known as metastasizing.

Cancer cells are defined as abnormal because they have undergone one or more of the following alterations:

- hypertrophy: the increase in size of individual cells;
- hyperplasia: the increase in number of the cells;
- anaplasia: the regression of the cells towards a more primitive or undifferentiated type.

Neoplasms arise from the transformation of normal cells into cancer cells through a multistage process which, starting as a pre-cancerous lesion, leads to a malignant tumour. Only in 5–10% of cases the development of tumours can be attributed to genetic defects,¹ whereas the remaining 90–95% sink their roots in external causes, such as the environmental factors and lifestyle. Environmental factors do not only

include pollution, but every causative factor which is not genetically inherited.² Three categories of external factor can be cited: physical carcinogens (e.g. ultraviolet and ionizing radiation), chemical carcinogens [e.g. asbestos, components of tobacco, aflatoxin (a food contaminant), and arsenic (a drinking water contaminant)] and biological carcinogens (e.g. infections caused by viruses, bacteria, or parasites).

In normal tissues, there is a delicate balance between the cell growth and proliferation and the replacing of dead or damaged cells. The body must continually regulate this balance to support own proper development and maintain healthy homeostasis of mature tissues.

In malignant tumours the regulation of the balance is compromised: a continuous proliferation of cells occurs, whereas apoptosis processes fail. This phenomenon can be traced back to the occurrence of genetic alterations. The incidence of several genetic mutations causes the accumulation of many errors which can give birth to a cancerogenic process. Some of these mutations are hereditary, while others are caused by external factors.

The genetic events underlying these mutations are essentially two:

- activation of proto-oncogenes into oncogenes. Proto-oncogenes positively control the cell cycle through the regulation of cell division, apoptosis and differentiation. When they become oncogenes, normal cell division is disrupted and malignant changes occurs.
- inactivation of tumour suppressor genes. In normal conditions, cells possess genes which have the ability to suppress malignant alterations (tumor suppressor). Mutations in these genes can trigger the carcinogenic process.

As for therapeutical approaches, many treatments are used in the fight against cancer. The choice of a specific treatment depends on the type of cancer and its stage of development. Among the most common anti-cancer approaches it is worth to cite surgery, chemotherapy, and radiotherapy. The surgery is a medical procedure by which a surgeon removes and/or examines the tumor mass. Radiation therapy is a treatment in which high doses of radiation are used in order to kill cancer cells and shrink tumours. Chemotherapy is indeed a treatment involving the use of drugs to kill the cancer. Some patients with cancer undergo only one treatment, but most patients have a combination of treatments such as surgery with chemotherapy and/or radiation therapy.

The efficacy of chemotherapy depends on the selectivity of the drug against cancer cells. The greater the biological differences between healthy and tumor cells are, the more the effectiveness of the treatment is. As these differences are minimal, there is no anticancer drug which does not cause serious toxic side effects. Therefore, the anticancer chemotherapy is severely limited by the drugs toxicity.

One of the most daunting features of cancer is its biological diversity which occurs not only in different types of tumours but also in the same population. Moreover, cancer cells develop very fast cells resistance against common anticancer therapies. Despite this seemingly catastrophic scenario, the chances of cancer survival have significantly increased in the last decade thanks to the early diagnosis and the efficiency of the therapies currently available.

Since cancer is a constantly evolving disease, the research of safe and effective chemotherapeutic agents is a formidable challenge.

In the frame of the constant anticancer research, natural products, with their unusual and often complex structures, have shown a broad spectrum of pharmacological activities.

Among natural anticancer molecules it is worth to mention vinca alkaloids derived from the periwinkle plant *Catharanthus roseus*, also known as *Vinca Rosea*. The cytotoxic effect of this class of compounds is due to their capability to bind to tubulin.³ Tubulin is a cytoplasmic protein which plays a key role during cell division: its polymerised form constitutes the “spindle fibers”, also called microtubules. The formation of microtubules is a crucial step during cellular mitosis, because it provides cells with both the structure and flexibility needed for division and replication. Without microtubules, cells cannot divide. The vinca alkaloids mechanism exert their mechanism by blocking tubulin polymerisation and then the assembly of microtubules. Since the mitotic spindle can not be created, the cell consequently stops in metaphase during mitosis.

The taxanes represent another class of anticancer natural products. Compared with vinca alkaloids, they show the opposite mechanism of action: they prevent from the disassembly of the microtubules and the mitotic spindle. Paclitaxel, the progenitor of taxanes family, was isolated for the first time from the bark of *Taxus brevifolia*⁴. It is a promoter of tubulin polymerisation. In particular, it bonds the tubulin which constitutes the microtubules, stabilising them and preventing them from disassembly. Therefore, a morphological alteration is created that leads the tumor cell to undergo apoptosis (programmed cell death mechanism). Docetaxel, the semi-synthetic analogue of Paclitaxel, was shown to have a slightly different mechanism of action. It binds to tubulin, giving rise to different-size microtubules in comparison with those induced by Paclitaxel. Moreover, it shows a much longer

residence time in the cell. Cabazitaxel is another antineoplastic drug belonging to taxanes family, the action of which is based on the breaking of the microtubular network. It binds to tubulin and facilitates its polymerisation, stabilizing at the same time the microtubules. This process leads to the inhibition of their disassembly, and consequentially to the block of both mitosis and interphase cellular functions.

Although plants are still the main source of bioactive compounds, marine organisms and their symbiont microorganisms represent a new prolific source of new bioactive molecules.

In 2007 trabectedin has been approved the first marine anticancer drug with the name of Yondelis[®]. Three years later, auristatin E, a semi-synthetic derivative of the cytotoxic marine depsipeptide dolastatin-10, was approved, in combination with a monoclonal antibody, for the treatment of Hodgkin's lymphoma.^{5,6}

Among marine organisms it is worth to cite marine sponges, from which the most part of the MNPs have been isolated. An example is the nucleoside analogue Ara-C, approved since 1969 as anticancer drugs. The latter is a synthetic derivative of a compound isolated from the Caribbean sponge *Cryptotethia crypta*. Recently, Eribuline mesylate, a synthetic analogue of halichondrin B (isolated from the Japanese sponge *Halichondria okadai*), has been approved for the treatment of metastatic breast cancer.

My thesis work perfectly matches with this wide research line aiming to the isolation and structural determination of new molecules to be used as lead compounds in the anticancer drug discovery. Several new hybrid peptide/polyketide compounds isolated by my research group.^{7,8,9} In addition, many synthetic analogues have been designed and prepared in order to detect the

pharmacophore of this class of compound and further investigate their biological activity.^{10,11}

2.2 Smenamides A and B, two cytotoxic secondary metabolites from the marine sponge *Smenospongia aurea*

Marine sponges are considered one of the most productive sources of novel scaffolds to be used as leads in the anticancer drug research. The analysis of the organic extract of the Caribbean sponge *S. aurea* (order Dictyoceratida, family Thorectidae) led to the isolation of two new hybrid peptide/polyketide compounds, namely smenamide A and B (Figure 2.1).⁷

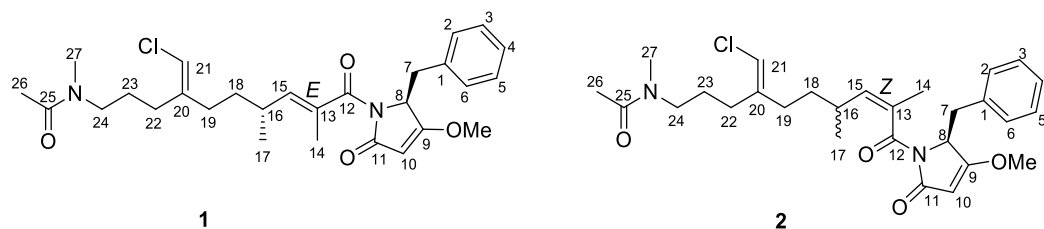


Figure 2.1. Structures of smenamide A (1) and B (2).

Although smenamides have no structural analogues in the field of marine natural products, they share some structural features with several compounds of cyanobacterial origin. The unusual N-methylacetamido function and the dolapyrrolidone terminus are typical of dolastatins-15,¹² while the chlorovinyl moiety is common in some cyanobacterial metabolites, such as jamaicamides, isolated from *Lyngbia majuscula*.¹³

Smenamides only differ in the configuration of the C-13 double bond, which was determined as E in smenamide A. Both compounds were shown to have a potent cytotoxic activity at nanomolar concentrations on the Calu-1 lung cancer cell line (Figure 2.2).

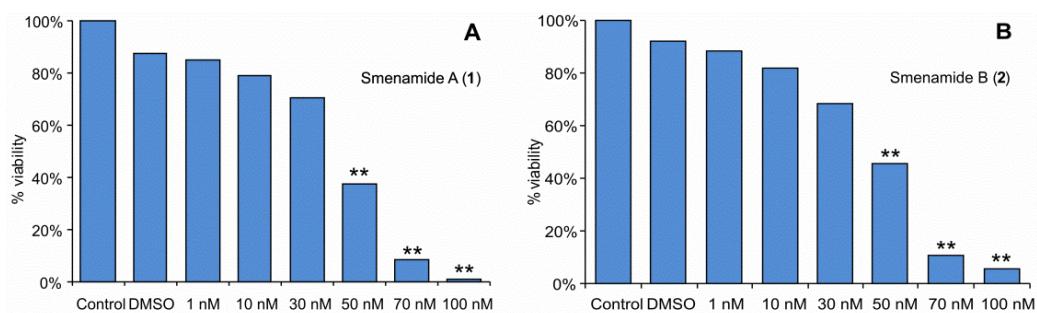


Figure 2.2. MTT assay of smenamides A and B. Evaluation by MTT assay of Calu-1 cell viability after 72 h of treatment with (A) compound 1 and (B) compound 2. ** $P < 0.0005$.

In particular, smenamide A exerts its cytotoxic activity through a clear pro-apoptotic mechanism in a dose-dependent way (Figure 2.3).

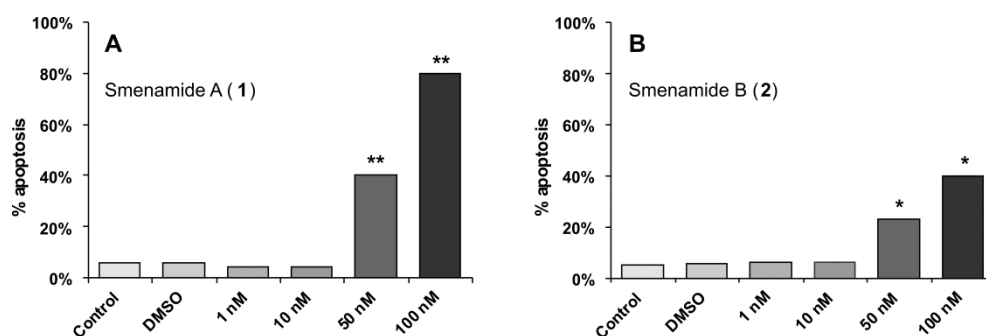


Figure 2.3. Evaluation of pro-apoptotic activity of smenamides using the Annexin-V FITC/PI assay. (A) The percentage of apoptosis for cells treated for 72 h with compound 1 at 1, 10, 50, and 100 nM was, respectively, 4%, 4%, 40%, and 80%; the remaining cells remained viable. (B) The percentage of apoptosis for cells treated for 72 h with compound 2 at 1, 10, 50, and 100 nM was, respectively, 6%, 6%, 23%, 40%; the remaining cells remained viable except at concentration of 100 nM, where 47% of cells were necrotic. ** $P < 0.0005$, * $P < 0.001$.

In lights of the promising biological activity of smenamide A, a flexible synthetic route was planned in order to prepare synthetic analogues aiming to confirm its structure, determine the configuration at C-16 -which was undetermined before the synthetic project was carried out- and further investigate the cytotoxic activity.

2.3. Towards the synthesis of smenamide A: total synthesis of 16-*epi*- and *ent*-smenamide A

Smenamides are two intriguing molecules belonging to the class of hybrid peptide/polyketide compounds. The latter are mixed biogenesis molecules, biosynthetically derived from amino acids and short carboxylic acids, showing many biological activities (antibiotic, immunosuppressive, antifungal and cytotoxic). The skeleton of this class of molecules consists of two main building blocks: a peptide and a polyketide moiety. Once the disconnection between the two moieties has been identified, the asymmetric total synthesis of these compounds can be achieved through the parallel synthesis of the two fragments and their final coupling.

The total synthesis of 16-*epi*- and *ent*-smenamide A is a case-example of the synthetic approach to this class of compounds.

2.4 Previous stereochemical studies on smenamide A

Despite the small amount of smenamide A isolated from the natural source, it was nevertheless possible to determine its structure using spectrometric and one- and two-dimensional spectroscopic techniques. The chemical shifts of the carbon nuclei were obtained from the two-dimensional NMR spectra, therefore the one-dimensional ^{13}C NMR spectra were not recorded.

The positive ion mode high-resolution ESI mass spectrum of smenamide A (Figure 2.4) showed the presence of the $[\text{M} + \text{H}]^+$ and $[\text{M} + \text{Na}]^+$ pseudomolecular ion peaks at m/z 501.2508 and 523.2326, respectively. Both ions show an isotopic peak $\text{M} + 2$, whose intensity is about 32%, suggesting the presence in the molecule of a

chlorine atom, then confirmed by the peak at m/z 487.2557 corresponding to $[M-HCl+Na]^+$ ion peak.

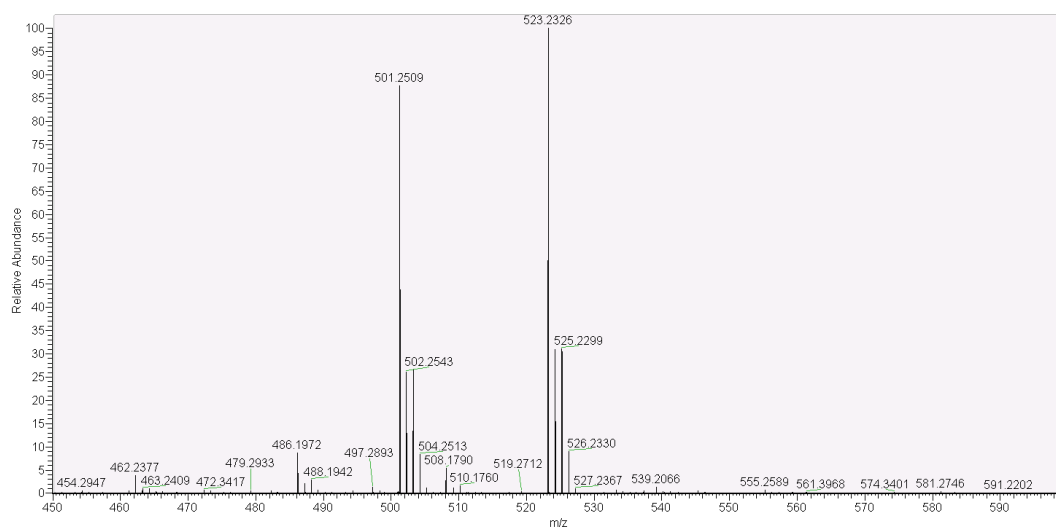


Figure 2.4. High-resolution ESI mass spectrum of smenamamide A.

The molecular formula $C_{28}H_{37}ClN_2O_4$ is in perfect agreement with these data.

The analysis of the proton spectrum (Figure 2.5) showed the presence of five aromatic protons (belonging to a mono-substituted benzene), three olefinic protons, an amino acidic α -proton and five methyl signals (one *O*-methyl, one *N*-methyl, one acetyl methyl, one olefinic methyl, and one aliphatic methyl).

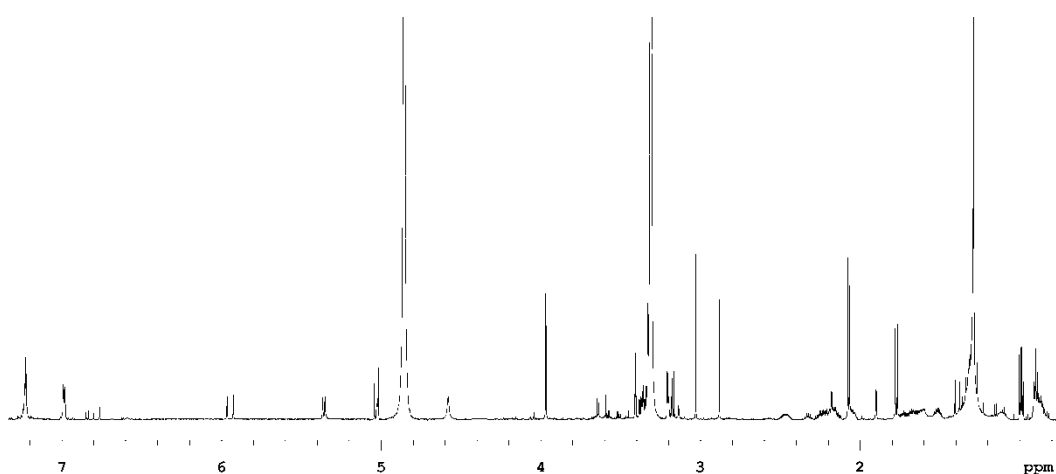


Figure 2.5. 1H NMR spectrum of smenamamide A (1) (CD_3OD , 700 MHz).

Smenamide A possess two double bonds, whose configurations have been determined through the analysis of the ROESY spectrum (Figure 2.6).

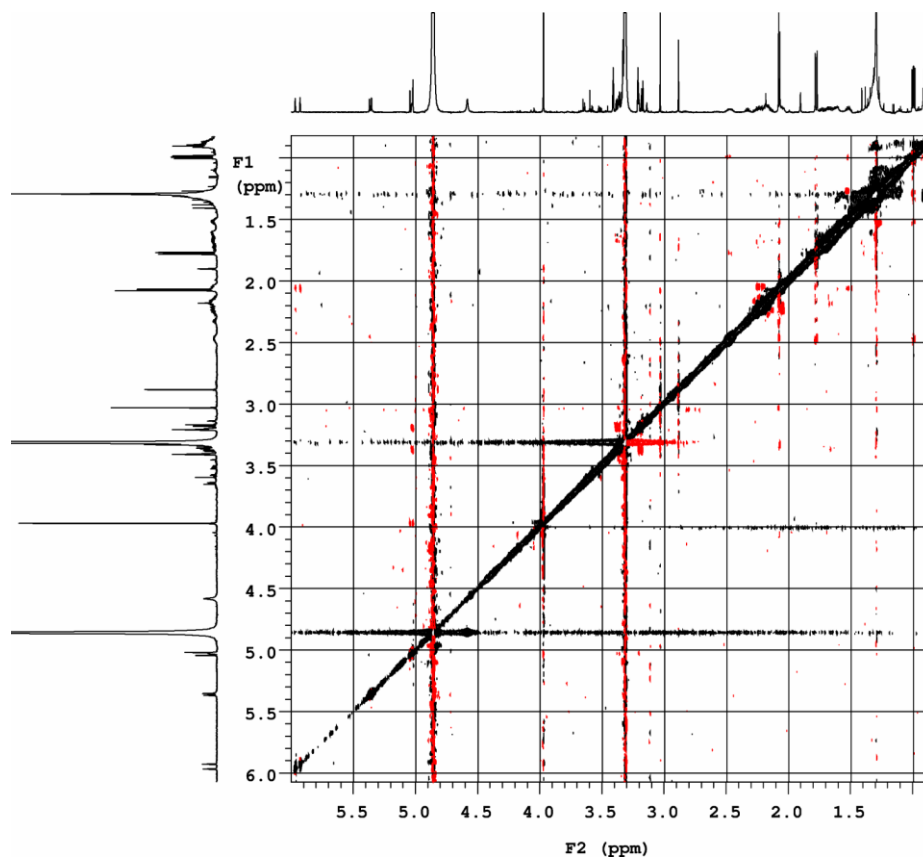


Figure 2.6. 2D ROESY spectrum of smenamamide A (CD_3OD , 700 MHz).

The presence of the correlation peak between protons $\text{H}_3\text{-14}$ and H-16 , and the absence of a correlation peak between $\text{H}_3\text{-14}$ and H-15 , showed the E configuration of the double bond between C-13 and C-15 (Figure 2.7). At the same time, the presence of the correlation peak between the protons H-21 and H-19_a and the absence of a correlation peak between H-21 and $\text{H}_2\text{-22}$ allowed to determine as Z the configuration of the double bond between C-20 and C-21.

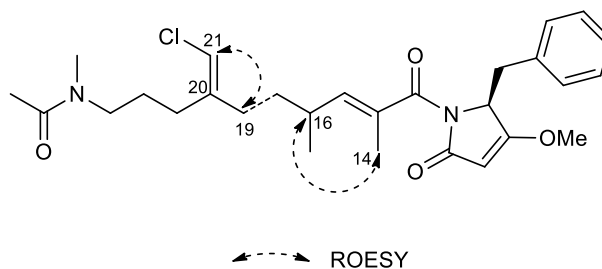


Figure 2.7. Main correlation peaks provided ROESY 2D NMR spectrum of smenamamide A allowing the assignment of the configuration of the two double bonds of the molecule.

Smenamide A contains two chiral centers, at C-8 and C-16. The absolute configuration of C-8 carbon was determined by using Marfey's method (Figure 2.8).¹⁴ A small amount of smenamamide A (5 μg) was suspended in 300 μL of ozone-saturated CH_3OH at -78°C for 5 minutes.

The sample was dried under N_2 stream to remove ozone, then treated with 6N HCl and heated in a sealed glass tube at 180°C for 2 hours. The residual HCl fumes were removed under vacuum. The hydrolysate was then dissolved in $(\text{CH}_3\text{CH}_2)_3\text{N}$ /acetone (2: 3, 100 μL) and the solution was treated with 100 μL of 1% 1-fluoro-2,4-dinitrophenyl-5-L-alaninamide (L-FDAA) in CH_3CN /acetone (1: 2). The vial was heated to 50°C for 1 hour. The mixture was dried, and the resulting L-FDAA-Phe derivative was re-dissolved in $\text{CH}_3\text{CN}/\text{H}_2\text{O}$ (5:95, 500 μL) for LC-MS analysis. An authentic L-Phe standard was treated with L-FDAA and D-FDAA, as described above, to give respectively the L-FDAA-L-Phe and D-FDAA-L-Phe standards used in the subsequent LC-MS analysis.

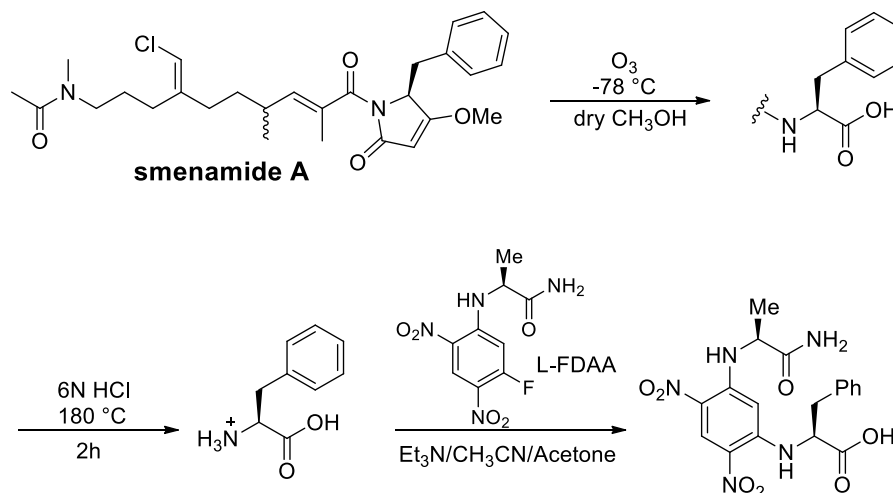


Figure 2.8. Ozonolysis, hydrolysis and detivatisation of smenamamide A with L-FDAA.

Marfey's derivatives were analyzed by high-resolution LC-MS. A $5\text{ }\mu\text{m}$ Kinetex C18 column ($50 \times 2.10\text{ mm}$), maintained at $25\text{ }^\circ\text{C}$, was eluted at $200\text{ }\mu\text{L min}^{-1}$ with H_2O and CH_3CN , using the following elution gradient: CH_3CN 5% for 3 minutes, from 5 to 60% CH_3CN over 20 minutes and CH_3CN 90% 5 minutes. The retention times of the L-FDAA-L-Phe and D-FDAA-L-Phe standards were determined as 17.32 and 18.60 minutes, respectively, on the basis of the extracted-ion chromatograms at m/z 418.1357. The retention time (17.36 min), measured in the same way, of L-FDAA-Phe sample deriving from smenamamide A, allowed to determine as L the absolute configuration of the phenylalanine residue of smenamamide A (figure 2.9).

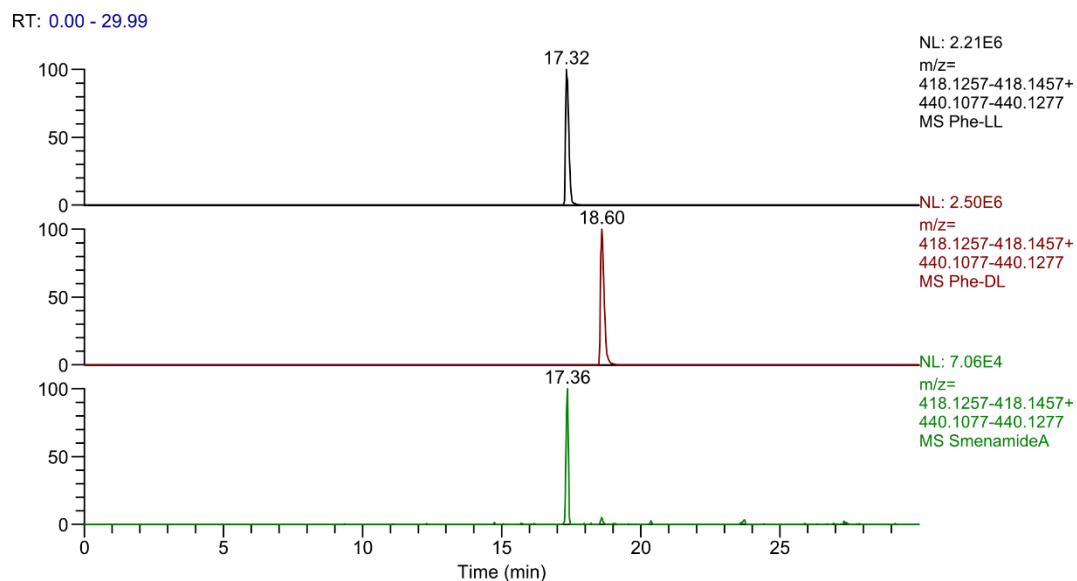


Figure 2.9. High resolution LC-MS analysis of Marfey's derivative from smenamamide A. Extracted ion chromatograms at m/z 418.1357 of authentic 1-fluoro-2,4-dinitrophenyl-5-alanine amide L-phenylalanine (L-FDAA-L-Phe), authentic D-FDAA-L-Phe and L-FDAA-Phe from smenamamide A.

As for the absolute configuration at the C-16, the spectrometric and spectroscopic tools available were not sufficient to determine it. Therefore, this configuration remained undetermined until the end of the synthetic project.

In conclusion, the total synthesis of smenamamide A was planned to solve the problem of the scarce amount of natural product isolated from *S. aurea*, with the aim of deepening the knowledge about its mechanism of action, the pharmacological activity, the structure-activity relationships and the stereochemistry.

2.5. Synthetic strategy

2.5.1 Retrosynthetic analysis

Smenamide A is a small but densely functionalised molecule in which a N-methylacetamido western terminus, a chlorovinyl moiety and a pyrrolinone subunit are present.

From a retrosynthetic point of view, the molecule can be disconnected in two building blocks: the acid (**3**) and the pyrrolinone moiety (**4**), corresponding to the polyketide and to the peptide portions of the molecule, respectively (Figure 2.10).

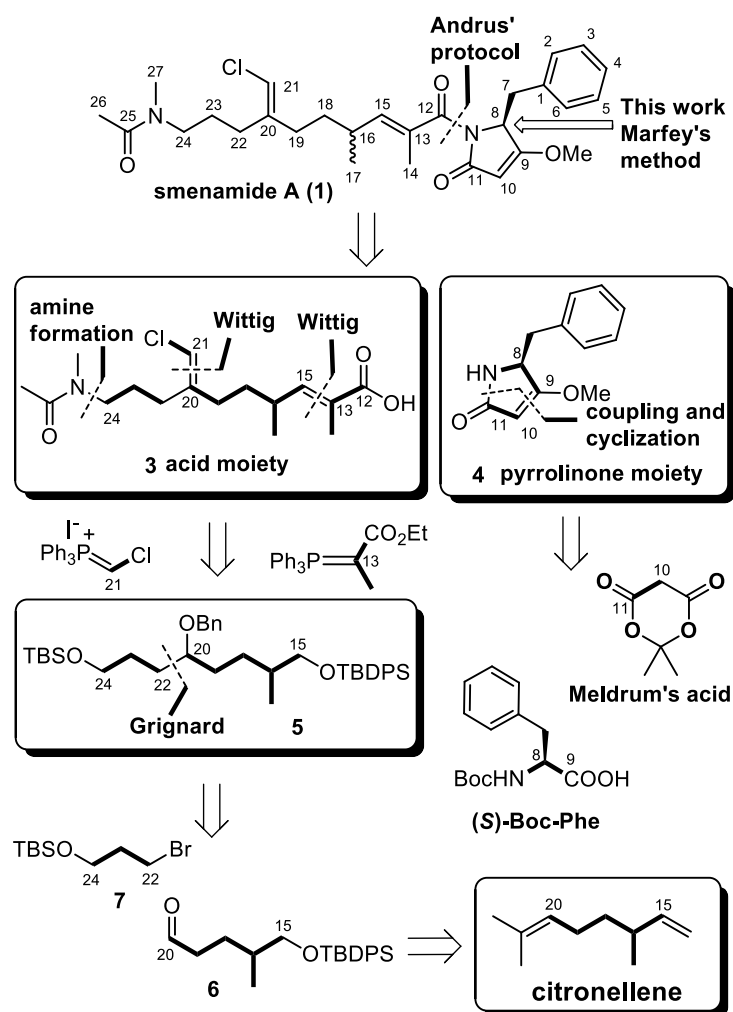


Figure 2.10. Retrosynthetic analysis of smenamamide A

Fragment **3** can be further simplified by the cleavage of the two carbon-carbon double bonds and the C-24/N bond, leading to the fully protected triol **5** (C-15/C-24). The protecting groups were chosen so as that the timing of their removal coincided with that of the introduction of the three main functionalities of the molecule. The presence, in compound **5**, of a methyl at position 16 suggests a

further disconnection between the C-20 and the C-22, revealing the aldehyde **6** (C-15/C-20) which can be easily traced back to citronellene. As the configuration at C-16 was unknown, the *S* enantiomer of citronellene was arbitrarily chosen. The protected bromalcohol **7** was recognized as the functionalized form of the remaining C-22/C-24 structural fragment. The entire carbon backbone of the polyketidic moiety **3** was eventually build up through two Wittig reactions, one of which is *E*-selective (generating the *E* C-13/C-15 double bond), and a Grignard reaction (generating the C-20/C-21 bond).

As for the synthesis of the dolapyrrolidinone unit, a racemisation free approach was used in order to avoid the racemisation at C-8.¹⁵ It is indeed known that this stereogenic center is prone to racemisation.¹⁶ Fragment **4** was synthesised from Meldrum acid and Boc-*L*-phenylalanine acid. The final coupling was accomplished *via* activation of **3** as pentafluorophenyl ester (Andrus' protocol) and its coupling with fragment **4**.

2.5.2 Synthesis of the polyketide moiety

The *S* enantiomer of the commercially available citronellene, was selected as the chiral precursor for the synthesis of the polyketide moiety (**3**). *S*-citronellene, suitably degraded and functionalised, provided the C15/C20 portion of the molecule.

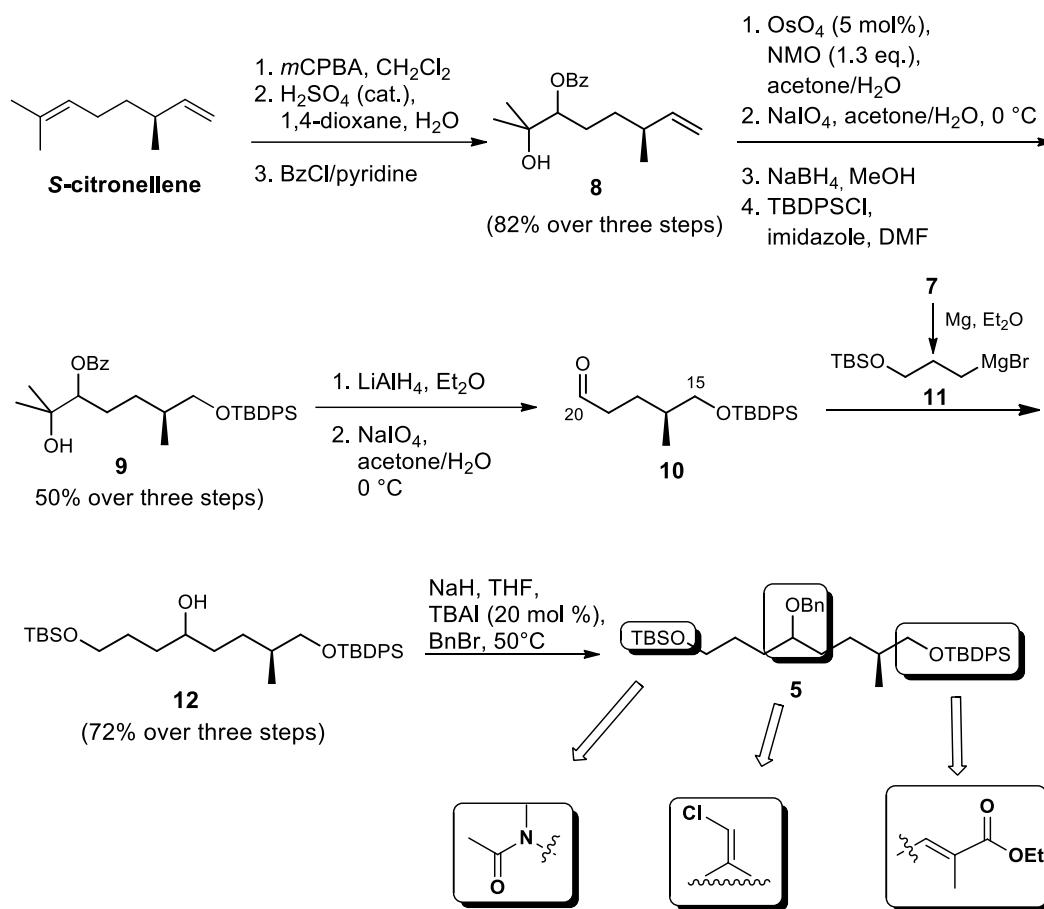


Figure 2.11. Preparation of the fully protected triol **5**.

The chemoselective epoxidation of the tri-substituted double bond, followed by an acid-catalyzed opening of the resulting epoxide and the subsequent benzylation of the secondary alcohol function afforded benzoate **8**, as a 1: 1 mixture of two diastereomers (82 % over three steps). The terminal double bond underwent dihydroxylation with OsO₄ (cat.)/NMO,¹⁷ and the resulting diol was cleaved with sodium periodate to give the C-15 aldehyde. The latter was reduced with sodium borohydride and the corresponding primary alcohol was protected with the TBDPS group¹⁸ affording silylether **9** (50% over four steps). Aldehyde **10** was prepared through removal of the benzoate under reductive conditions with lithium aluminum hydride and cleavage of the resulting diol. Aldehyde **10** was then reacted with Grignard reagent **11**, previously prepared from the commercially available

bromoalcohol **7**, affording secondary alcohol **12** as a mixture of two diastereomers in a 1:1 ratio (72% over three steps). The latter allowed the extension of the skeleton of the molecule from C-20 to C-24 the extension of the skeleton of the molecule from C-20 to C-24. The conversion of alcohol **12** into the corresponding benzyl ether, using sodium hydride, benzyl bromide and tetrabutylammonium iodide (TBAI) as the catalyst, resulted in the fully protected triol **5** (Figure 2.11).

The choice of protecting groups required particular attention. A protecting group is introduced into a molecule to mask a functionality in order to make it inactive in the subsequent reactions. In this case it was necessary to choose orthogonal protecting groups, which can be installed or removed under different conditions, without interfering with each other. The selected groups are benzoyl (Bz), benzyl (Bn), *tert*-butyldimethylsilyl (TBS) and *tert*-butyldiphenylsilyl (TBDPS).

The introduction of the *N*-methylacetamido function was carried out in three steps (Figure 2.12). The removal of the TBS group with CH₃COOH/THF/H₂O (3: 1: 1), followed by tosylation of the delivered alcohol with TsCl and treatment of tosyl derivative with an excess of methylamine (40% solution in water)¹⁹ afforded secondary amine **13**. The latter was left to react with AcCl/triethylamine giving the desired amide (**14**) as a 1: 1 mixture of two rotamers (53% over four steps). The hydrogenolysis of the benzylether **14** (H₂/Pd(OH)), followed by oxidation of the secondary alcohol with the TPAP(cat.)/NMO system, according to Ley's method,²⁰ provided ketone **15** required for the following Wittig olefination (79% over two steps).

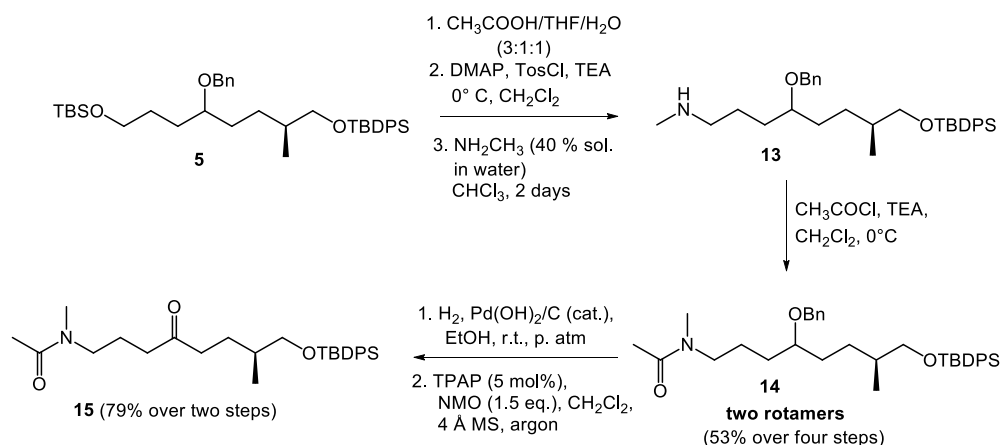


Figure 2.12 Installation of the *N*-methylacetamido function.

A crucial issue of the whole synthetic plan was the installation of the *Z*-chlorovinyl function. Some synthetic procedures have been reported for the construction of that function in related substances,²¹ but relatively few methods have been described for the stereoselective preparation of chloroolefins. Paige et al.²² exploited the palladium-mediated regio- and stereospecific silylstannation of a terminal alkyne²³ to ensure the stereoselectivity of the process. Unfortunately, this strategy, although very elegant, resulted in a moderate yield (42%), and similar results were obtained by others (45–51% yields).²⁴ Therefore, we envisioned that this approach could neither provide any advantage in terms of the overall efficiency of the synthesis nor reduce the necessity of chromatographic purifications. The Wittig olefination, on the other hand, has been reported as a good, easy, and efficient method to generate a chlorovinyl function.^{21a}

Therefore, the Wittig reaction was first tested on the model compound **16** (Figure 2.13) obtained from the catalytic oxidation of alcohol **12** under Ley's conditions (90%). The phosphonium salt **17** was prepared by reaction of iodochloromethane and triphenylphosphine.^{21a}

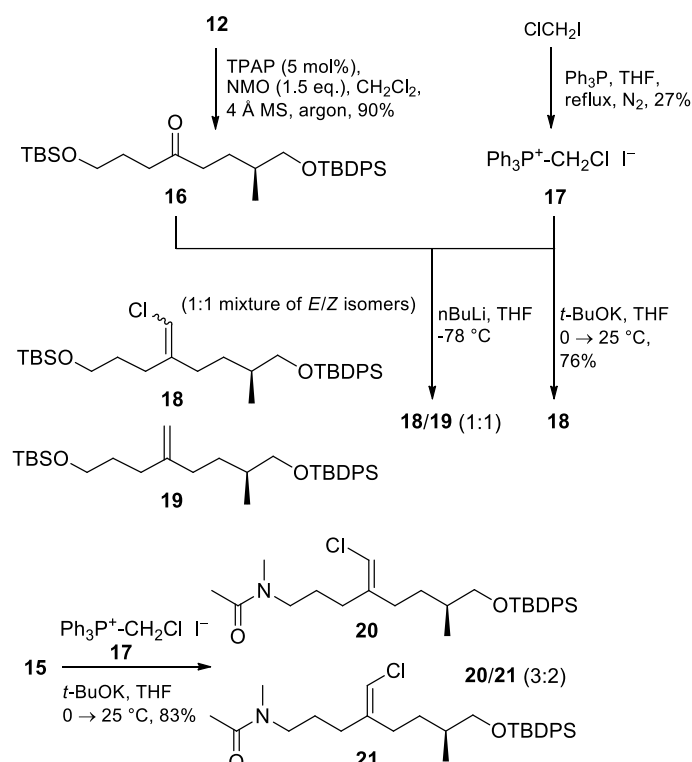


Figure 2.13. Installation of the chlorovinyl moiety.

As reported in literature, the Wittig olefination was conducted with *n*BuLi as the base in THF at -78 °C.^{21c,d} Despite the mass recovery was satisfactory, in addition to the expected chlorovinyl derivatives **18** (1: 1 mixture of geometric isomers), this process also afforded a large amount of product **19**, with a methylene function instead of the chlorovinyl moiety (Figure 2.13). The use of a slightly modified procedure, involving the use of potassium tert-butoxide as the base,^{21a} in a range of temperature between 0 and 25 °C, led to the desired products both in the reaction on the model ketone **16** (**18**, 76%), and the intermediate **15** (**20** and **21**, in a 3: 2 ratio in favor of the desired *Z* isomer, 83%). It is worth highlighting that only traces of the by-product with the methylene function are obtained with this procedure. Compounds **20** and **21** were easily separated by column chromatography. The analysis of the data provided by the ROESY spectrum allowed the assignment of configuration of the double bond in each isomer.

Finally, the introduction of the α,β -unsaturated acid function was addressed (Figure 2.14). The removal of the TBDPS group in compound **20** with tetrabutylammonium fluoride (TBAF) in THF, followed by the oxidation of alcohol **22** with TPAP_(cat.)/NMO, afforded aldehyde **23**, which was applied for the subsequent *E*-selective Wittig olefination without further purification. Thus, aldehyde **23** was reacted with $\text{Ph}_3\text{P}=\text{CH}(\text{Me})\text{CO}_2\text{Et}$ leading to the synthesis of the α,β -unsaturated ester **24**, which was eventually hydrolyzed to acid **3** by treatment with hydrated lithium hydroxide (53% over four steps).

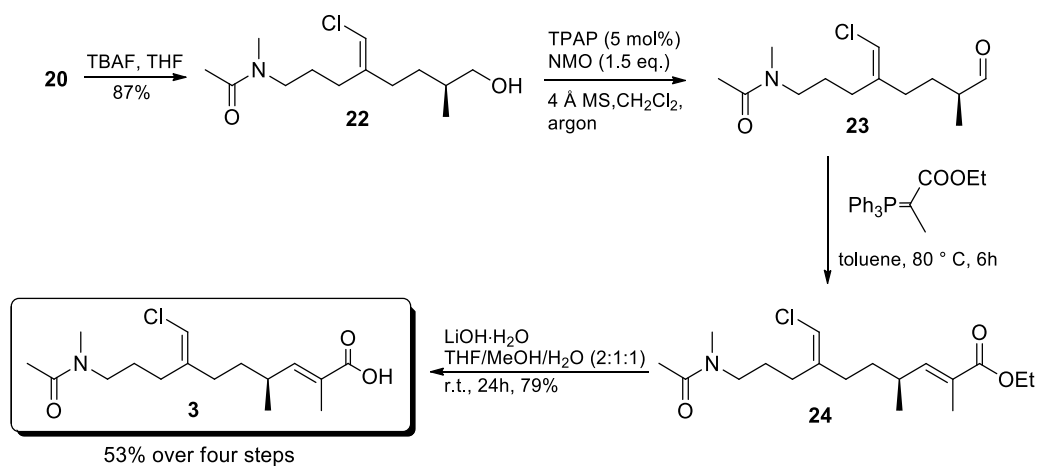


Figure 2.14. Preparation of the α,β -unsaturated ester **24**.

2.5.3 Preparation of the peptide moiety and final coupling

The synthesis of the pyrrolidinone portion **4** (57% overall yield) is depicted in Figure 2.15. The reaction of (*S*)-Boc-Phenylalanine with Meldrum acid, followed by reflux of the crude in ethyl acetate over 30 minutes, gave the Boc-protected tetramic acid **25**. The latter was methylated according to Mitsunobu conditions,²⁵ and the removal of the protecting group Boc gave the desired compound **4**.

The optical rotation measured for this product is in perfect agreement with the value reported in the literature ($[\alpha]_D = -62.3$; lit. -63);²⁶ this confirmed its high enantiomeric purity.

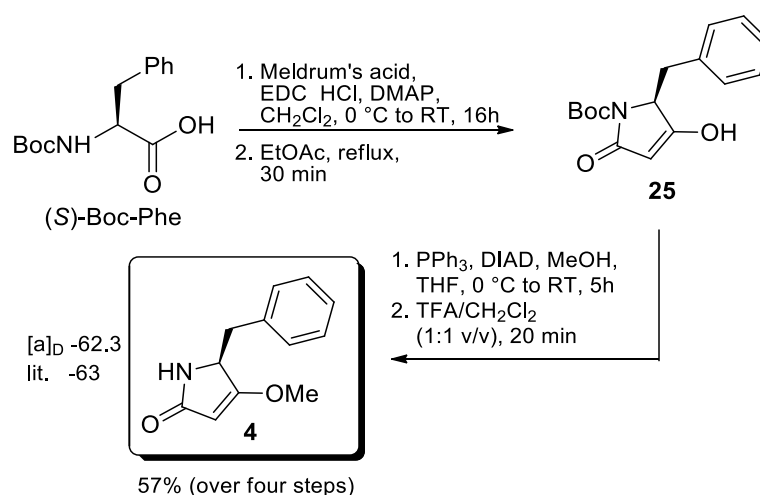


Figure 2.15. Synthesis of the pyrrolidinone unit 24.

Finally, the two building blocks **3** and **4** were coupled by using Andrus protocol²⁷ (Figure 20). The acid portion **3** was activated as pentafluorophenyl ester **26** by reaction with $\text{C}_6\text{F}_5\text{OH}/\text{DCC}$ (82%). Intermediate **26** was coupled with an excess of the lithium imidate, deriving by reaction from pyrrolinone **4** with $n\text{BuLi}$. The reaction proceeded smoothly, affording product **27** in 91% yield.

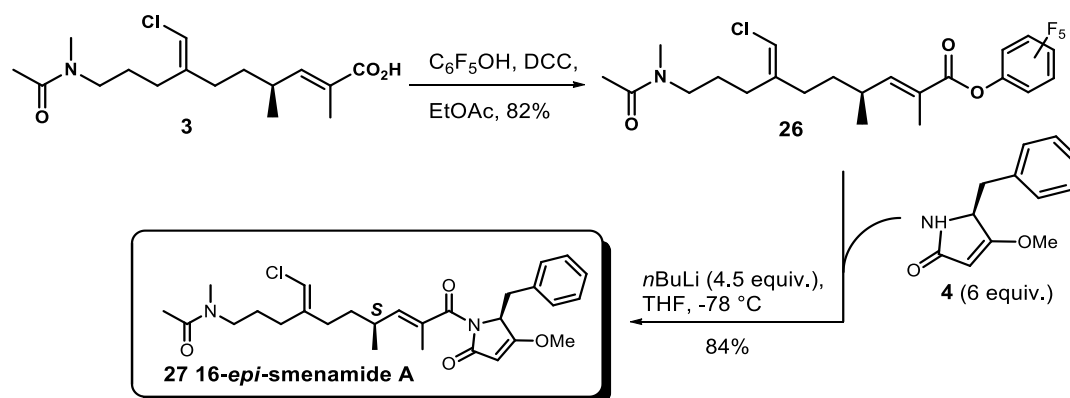


Figure 2.16. Final coupling.

Unfortunately, the proton spectrum of **27** did not match that of natural smenamamide A. In particular, the shape and value of the chemical shifts of H-15 vinyl proton signals, adjacent to the C-16 stereogenic center, were different (Figure 2.16). This suggested that compound **27** was the epimer at C-16 of smenamamide A and, consequently, the natural smenamamide A should possess the R configuration at C-16.

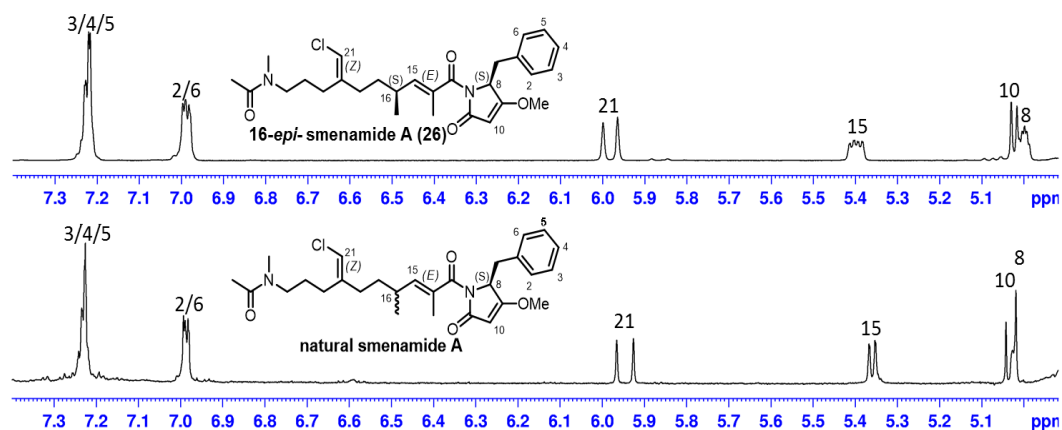


Figure 2.17. ^1H NMR spectra of **16-epi-smenamamide A** and natural smenamamide A.

At this point, in order to confirm the structure of smenamamide A the synthesis of the *ent*-smenamamide A was carried out (figure 2.17). Two enantiomers show the same NMR spectrum, therefore the proton spectra of **29** and natural smenamamide A should

perfectly match. Starting from (*R*)-Boc-phenylalanine, (*R*)-pirrolinone **28** (47%) was obtained. The latter was coupled, following the Andrus method, with pentafluorophenylester **26** to give *ent*-smenamide A **29** (88%).

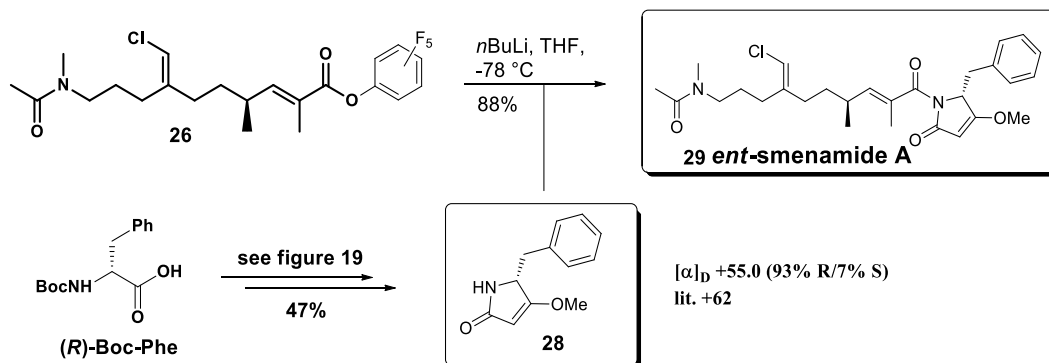


Figure 2.18. Synthesis of *ent*-smenamide A.

The comparison between the proton spectra of both compounds, which perfectly match, confirmed the R absolute configuration at C-16 (Figure 2.18). Furthermore, as expected, natural smenamide A and *ent*-smenamide A show specular CD spectra (for more details see Experimental section).

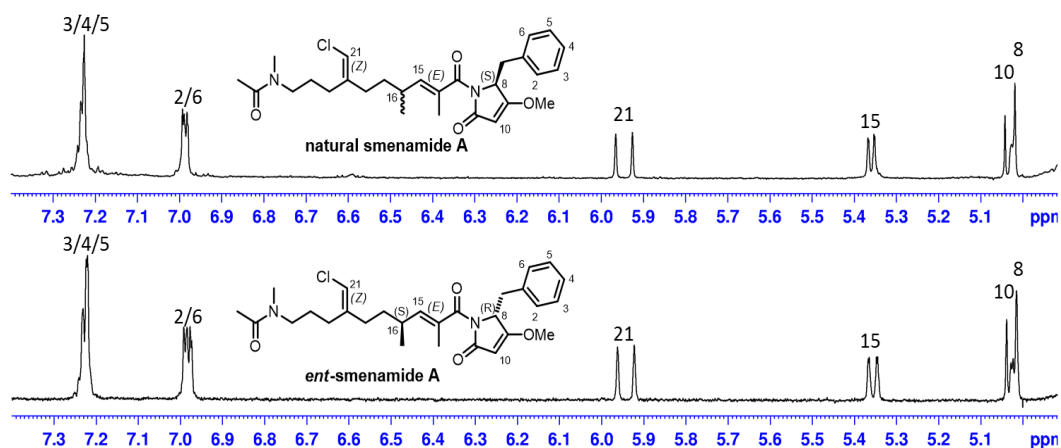


Figure 2.19. ^1H NMR spectra of *ent*-smenamide A and natural smenamide A.

2.6. Conclusions

The total syntheses of *ent*- and 16-*epi*-smenamamide A was accomplished with a 2.6% and 2.5% overall yield, respectively, in 23 steps. The total synthesis of these two compounds confirmed the structure of natural smenamamide A, and the assignment of the *R* absolute configuration to the C-16 carbon, which remained undetermined before the synthetic project was carried out. The evaluation of the antiproliferative activity of *ent*- and 16-*epi*-smenamamide A is in progress in collaboration with the IRCCS CROB (Scientific Institute of Hospitalization and Care- Basilicata Oncological Center) of Rionero in Vulture (PZ).

2.7. Experimental section

2.7.1 Generals

All reagents and anhydrous solvents were purchased (Aldrich and Fluka) at the highest commercial quality and used without further purification. Where necessary, flame-dried and argon-charged glassware was used. Reactions were monitored by thin-layer chromatography carried out on precoated silica gel plates (Merck 60, F254, 0.25 mm thick). Merck silica gel (Kieselgel 40, particle size 0.063-0.200 mm) was used for column chromatography. MgSO₄ was used as a drying agent for aqueous work-up. NMR experiments were performed on a Varian Unity Inova spectrometers at 400, 500 and 700 MHz spectrometers in CDCl₃. Proton chemical shifts were referenced to the residual CHCl₃ signal (7.26 ppm). ¹³C-NMR chemical shifts were referenced to the solvent (77.0 ppm). Abbreviations for signal coupling are as follows: s=singlet, d=doublet, t=triplet, q=quartet, m=multiplet, b=broad. IR spectra were recorded neat on Perkin Elmer spectrum 100R spectrophotometer and are reported in cm⁻¹. Optical rotations were measured using a Jasco P-2000

polarimeter at the sodium D line. ECD spectra were recorded using a Jasco J-710 spectropolarimeter. HRMS spectra were recorded by infusion on Thermo LTQ Orbitrap XL mass spectrometer equipped with an Electrospray source in the positive mode using MeOH as the solvent.

2.7.2 Experimental procedures

Determination of the absolute configuration at C-8 of smenamide A by using Marfey's method.

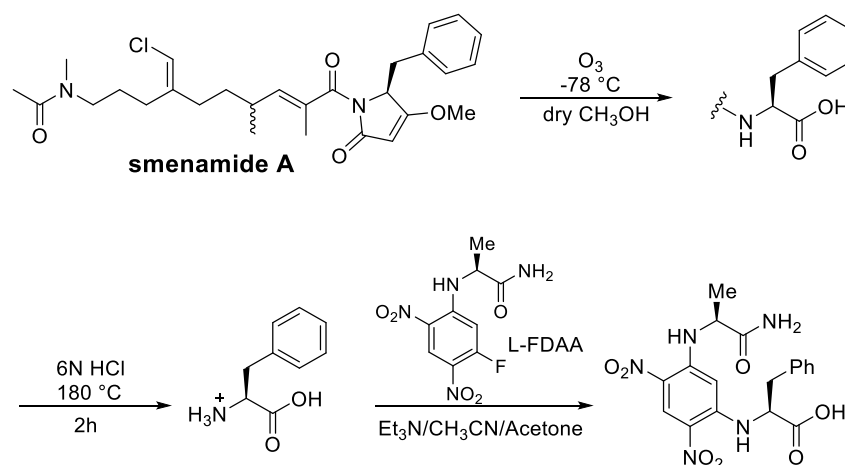


Figure 2.20. Ozonolysis, hydrolysis and derivatization of smenamide A with l-enantiomer of Marfey's reagent.

A small amount of smenamide A (5 µg) was suspended in ozone-saturated MeOH (300 µL) at -78 °C for 5 min (Figure 2.20). The sample was dried under a N₂ stream to remove ozone, then treated with 6N HCl and heated in a sealed glass tube at 180 °C for 2 h. The residual HCl fumes were removed *in vacuo*.

The hydrolysate was dissolved in Et₃N/acetone (2:3, 100 µL) and the solution was treated with 100 µL of 1% 1-fluoro-2,4-dinitrophenyl-5-l-alaninamide (L-FDAA) in CH₃CN/acetone (1:2). The vial was heated at 50 °C for 1 h. The mixture was

dried, and the resulting L-FDAA-Phe derivative was redissolved in CH₃CN/H₂O (5:95, 500 μL) for LC-MS analysis. An authentic L-Phe standard was treated with L-FDAA and D-FDAA as described above to give, respectively, the L-FDAA-L-Phe and D-FDAA-L-Phe standards used in the subsequent LC-MS analysis.

Marfey's derivatives were analyzed by LC-HRESIMS. A 5 μm Kinetex C18 column (50 × 2.10 mm), maintained at 25 °C, was eluted at 200 μL min⁻¹ with H₂O and CH₃CN, using a gradient elution. The gradient program was as follows: 5% CH₃CN 3 min, 5-60% CH₃CN over 20 min, 90% CH₃CN 5 min. Mass spectra were acquired in positive ion detection mode and the data were analyzed using the suite of programs Xcalibur. The retention times of L-FDAA-L-Phe and D-FDAA-L-Phe standards were determined as 17.32 min and 18.60 min, respectively, on the basis of the extracted-ion chromatograms at *m/z* 418.1357. The retention time, measured in the same way for the L-FDAA-Phe sample obtained from smenamide A, was 17.36 min, and was indicative of the L configuration of Phe residue in smenamide A (Figure 2.21).

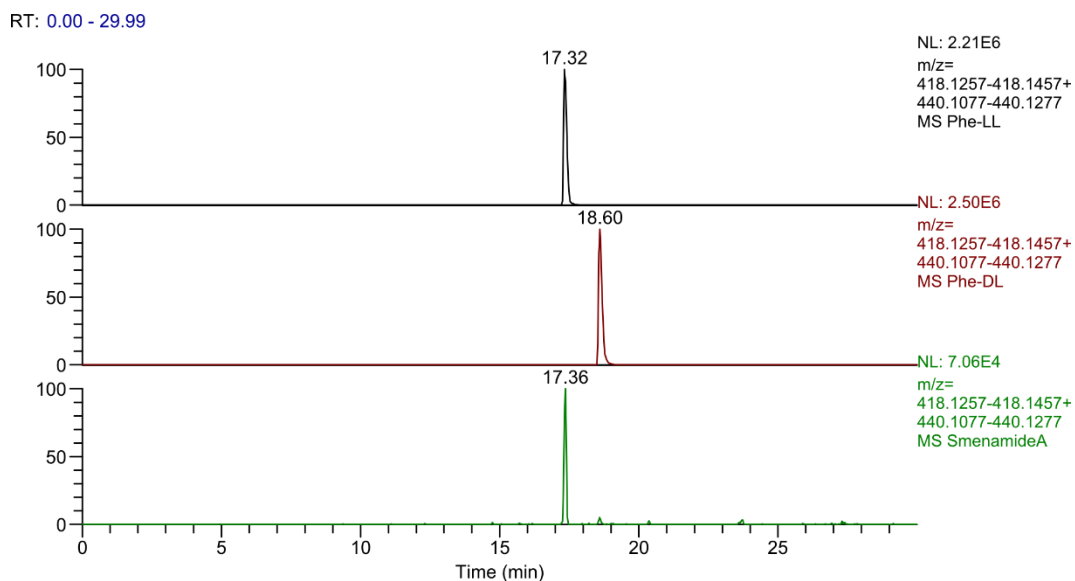
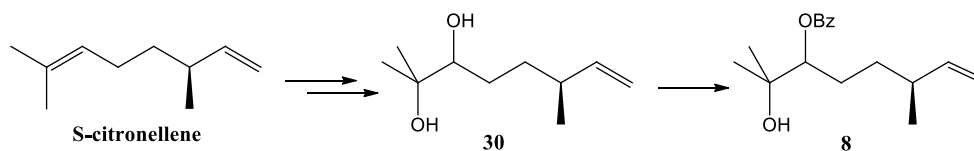


Figure 2.21. HR-ESI-MS-HPLC analysis of Marfey's derivative from smenamide A. Extracted-ion chromatograms at m/z 418.1357 of authentic 1-fluoro-2,4-dinitrophenyl-5-alanine amide L-phenylalanine (L-FDAA-L-Phe), authentic D-FDAA-L-Phe and L-FDAA-Phe from smenamide A.

Benzoate **8**

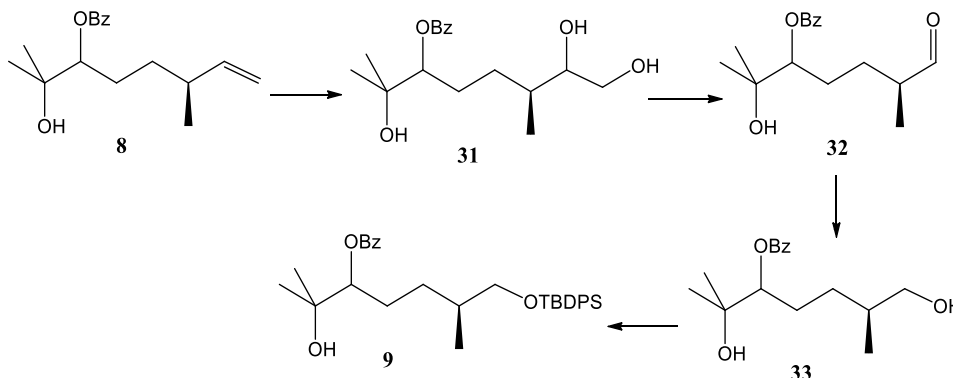


According to a literature procedure,²⁸ commercially available (Sigma Aldrich, e.e. ≥ 98.5 %) β -citronellene (10 mL, 7.6 g, 54.9 mmol) was converted into the corresponding 6,7-epoxide (8.44 g, 100%), a smelling colourless oil. To a flask containing the crude epoxide in 1,4-dioxane-H₂O (34 mL, 2:1), conc. H₂SO₄ (3 drops) was added. After 1h solid NaHCO₃ was added portionwise until the effervescence ceased. The mixture was concentrated in vacuo and partitioned between water and EtOAc (3 x 20 mL). The organic phase was dried and evaporated in vacuo to give diol **30** (8.22 g, 87%) as a colourless oil. An analytically pure sample of this compound was obtained by chromatography over silica gel

(hexane/EtOAc, 7:3) for characterization. Mixture of two diastereomers, IR (neat) ν_{\max} : 3410, 2957, 2927, 2858, 1699, 1640, 1454, 1378, 1271, 1167, 1069, 995, 911, 713 cm^{-1} ; $^1\text{H-NMR}$ (400 MHz, CDCl_3): δ 5.76-5.61 (2H, m, 2 x H-15), 4.97 (2H, bd, $J=18.0$, vinyl proton), 4.93, (2H, bd, $J=11.0$, vinyl proton), 3.35 (2H, bt, $J=9.2$, 2 x H-20), 2.14 (2H, m, 2 x H-16), 1.89 (bs, 2 x OH), 1.204, 1.203, 1.153, 1.147 (3H each, all s, 2 x $\text{C}(\text{CH}_3)_2$), 1.02, 1.01 (3H each, both d, $J=6.7$, 2 x H₃-17); $^{13}\text{C-NMR}$ (100 MHz, CDCl_3): δ 144.5, 144.3, 113.0, 112.8, 78.9, 78.5, 73.4, 73.3, 38.0, 37.8, 33.7, 33.4, 29.4, 29.2, 26.5, 23.1, 20.6, 20.2; HRMS (ESI) m/z calcd for $\text{C}_{10}\text{H}_{20}\text{NaO}_2$ $[\text{M}+\text{Na}]^+$ 195.1361, found 195.1348.

To a stirred solution of diol **30** (7.34 g, 42.6 mmol) in pyridine (20 mL), benzoyl chloride (0.052, 6 mL) was added. After 2.5 h water (8 mL) was added and the mixture stirred for 15 min in a water bath and then taken to dryness. The residue was taken up in CHCl_3 (50 mL) and washed with a satd. aq. NaHCO_3 solution and water. The organic phase was dried, filtered and evaporated in vacuo. Purification over silica gel (hexane/EtOAc, 9:1) gave benzoate **8** (11.0 g, 94%), mixture of two diastereomers. IR (neat) ν_{\max} : 3482, 2974, 2929, 1718, 1704, 1452, 1275, 1177, 1113, 1070, 1027, 711 cm^{-1} ; $^1\text{H-NMR}$: (400 MHz, CDCl_3): δ 8.07 (4H, d, $J=7.1$, ArH), 7.57 (2H, t, $J=7.5$, ArH), 7.46 (4H, t, $J=7.6$, ArH), 5.71-5.55 (2H, m, 2xH-15), 5.12-5.02 (2H, m), 5.01-4.87 (4H, m), 2.22-2.04 (2H, m), 1.94 (2H, bs, 2xOH), 1.85-1.58 (4H, m), 1.43-1.29 (4H, m), 1.26 (12H, s, 2 x $\text{C}(\text{CH}_3)_2$), 0.96 (6H, d, $J=6.9$, H₃-17); $^{13}\text{C-NMR}$ (100 MHz, CDCl_3): δ 166.63, 166.60, 144.2, 144.0, 133.0, 130.1, 129.6, 128.4, 113.2, 112.9, 80.7, 80.3, 72.7, 37.8, 37.6, 33.0, 32.7, 27.4, 27.2, 26.5, 25.1, 20.6, 20.0; HRMS (ESI) m/z calcd for $\text{C}_{17}\text{H}_{25}\text{O}_3$ $[\text{M}+\text{H}]^+$ 277.1798, found 277.1788.

Silylether **9**



To a stirred solution of benzoate **8** (7.93 g, 28.7 mmol) in acetone/water (120 mL, 5:1) OsO₄ (369 mg, 14.5 mmol, 5 mol%) was added. After 2 hours the reaction was quenched by addition of solid Na₂S₂O₅ (720 mg, 2.9 mmol) and the reaction mixture was stirred for further 30 min. Acetone was evaporated under reduced pressure and the resulting aqueous suspension was extracted with EtOAc (3 x 50 mL). The organic phase was dried and evaporated in vacuo to give diol **31** (8.71 g) as a colourless oil. An analytically pure sample of this compound was obtained by chromatography over silica gel (CHCl₃/CH₃OH, 9:1) for characterization. Mixture of four diastereomers, IR (neat) ν_{max} : 3400, 2971, 2932, 1716, 1701, 1452, 1278, 1177, 1115, 1071, 1017, 712 cm⁻¹; ¹H-NMR: (400 MHz, CDCl₃): δ 8.05 (4H, d, J=7.5, ArH), 7.57 (2H, t, J=7.8, ArH), 7.44 (4H, t, J=7.6, ArH), 5.05 (2H, m, 2xH-20), 3.77-3.37 (6H, overlapped m's), 2.55 (bs, OH's), 1.26, 1.25 (6H each, both s, 2x C(CH₃)₂), 0.89, 0.88, 0.863, 0.858 (3H each, d's, J=6.7, 4 x H3-17); ¹³C-NMR (100 MHz, CDCl₃): δ 167.0, 166.9, 166.76, 166.73, 133.2, 133.1, 130.02, 129.99, 129.94, 129.91, 129.68, 129.67, 128.48, 128.47, 80.8, 80.5, 80.3, 80.2, 76.0, 75.6, 75.3, 74.9, 72.65, 72.62, 72.5, 65.0, 64.6, 64.50, 64.46, 35.7, 35.4, 35.3, 35.1, 29.7, 29.3, 29.2, 28.6, 27.0, 26.9, 26.8, 26.7, 26.0, 25.95, 25.88, 25.84, 25.73, 25.66,

25.62, 25.57, 15.5, 15.3, 14.6, 14.5; HRMS (ESI) m/z calcd for $C_{17}H_{26}NaO_5$ $[M+Na]^+$ 333.1678, found 333.1663.

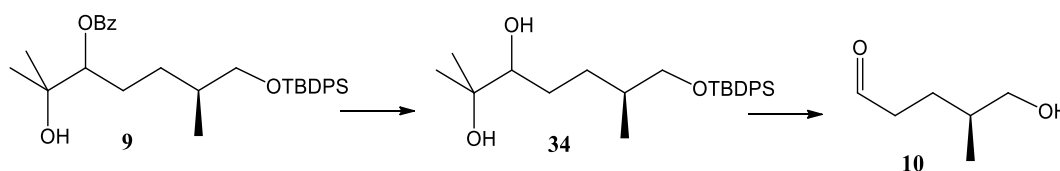
To a stirred solution of diol **31** (8.69 g, 29.0 mmol) in acetone/water (180 mL, 5:1) at 0°C, sodium periodate (12.35 g, 58.0 mmol) was added. After a few minutes a large amount of a white solid precipitated. After 4 h the reaction mixture was filtered under vacuum and the precipitate was carefully washed with acetone. The solvent was evaporated in vacuo and the aqueous suspension was extracted with EtOAc (3 x 30 mL). The organic layer was dried and concentrated in vacuo to give aldehyde **32** as a colourless oil (5.54 g) that was applied to next step without further purification.

To a stirred solution of aldehyde **32** (5.52 g, 20.0 mmol) in methanol (70 mL) at 0°C, $NaBH_4$ (376 mg, 9.9 mmol) was added in portions. After 1h the reaction was quenched by dropwise addition of CH_3COOH (3.5 mL). Then, the reaction mixture was concentrated in vacuo, treated with a satd. aq. solution of $NaHCO_3$ (30 mL) and extracted with EtOAc (3 x 30 mL). The organic phase was dried and evaporated under reduced pressure to give crude **33** (5.29 g). An analytically pure sample of this compound was obtained by chromatography over silica gel ($CHCl_3/CH_3OH$, 9:1) for characterization. Mixture of two diastereomers, IR (neat) ν_{max} : 3400, 2972, 2930, 1716, 1699, 1451, 1277, 1177, 1113, 1070, 1027, 711 cm^{-1} ; 1H -NMR: (400 MHz, $CDCl_3$): δ 8.07 (4H, d, $J=7.1$, ArH), 7.57 (2H, t, $J=7.5$, ArH), 7.46 (4H, t, $J=7.6$, ArH), 5.11-5.04 (2H, m, 2xH-20), 3.53-3.36 (4H, m, 2 x H₂-15), 1.91-1.11 (10H, m), 1.28 (12H, s, 2 x $C(CH_3)_2$), 0.92, 0.90 (3H each, both d, $J=6.9$, 2 x H₃-17); ^{13}C -NMR (100 MHz, $CDCl_3$): δ 166.8, 166.7, 133.06, 133.08, 130.0, 129.6, 128.4, 80.7, 80.4, 72.64, 72.57, 67.9, 67.6, 35.43, 35.39, 29.7, 29.4, 26.9, 26.1,

25.43, 25.39, 16.7, 16.3; HRMS (ESI) m/z calcd for $C_{16}H_{24}NaO_4$ $[M+Na]^+$ 303.1572, found 303.1561.

To a stirred solution of alcohol **33** (5.29 g, 19.0 mmol) in DMF (19 mL) were sequentially added imidazole (1.56 g, 23 mmol) and *tert*-butyldiphenylsilyl chloride (6.32 g, 5.88 mL, 23 mmol), at rt. After 40 min, DMF was evaporated in vacuo and the residue was taken up in $CHCl_3$ and washed with brine. The organic phase was dried, concentrated in vacuo and purified by chromatography over silica gel (hexane/EtOAc, 95:5) to give TBDPS ether **9** (7.54 g, 50% over four steps). Mixture two diastereomers, IR (neat) ν_{max} : 3485, 2960, 2931, 2858, 1715, 1602, 1588, 1472, 1452, 1428, 1275, 1112, 1071, 824, 806, 741, 703 cm^{-1} ; 1H -NMR: (400 MHz, $CDCl_3$): δ 8.07 (4H, d, $J=7.1$, ArH), 7.67-7.29 (26H, overlapped m's, ArH), 5.07 (2H, d, $J=8.7$, 2 x H-20), 3.44 (4H, m, 2 x H₂-15), 2.00-1.46 (10H, m), 1.27, 1.26 (6H each, both s, 2 x C(CH₃)₂), 1.00, 0.97 (9H each, both s, 2 x C(CH₃)₃), 0.91 (6H, d, $J=6.5$, 2 x H₃-17); ^{13}C -NMR (100 MHz, $CDCl_3$): δ 166.6, 135.6, 133.9, 133.0, 130.1, 129.7, 129.5, 128.4, 127.5, 80.8, 80.6, 72.7, 68.7, 68.4, 35.7, 35.5, 29.8, 29.6, 27.3, 27.0, 26.8, 26.7, 26.6, 26.5, 25.16, 25.11, 19.23, 19.18, 17.0, 16.6; HRMS (ESI) m/z calcd for $C_{32}H_{42}NaO_4Si$ $[M+Na]^+$ 541.2750, found 541.2733.

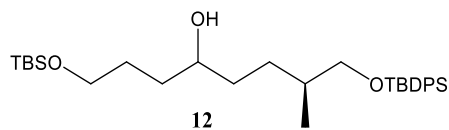
Aldehyde **10**



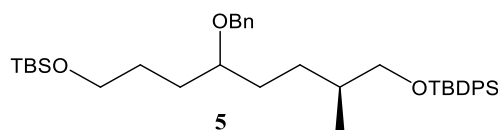
To a stirred solution of silyl ether **9** (7.54 g, 14.5 mmol) in dry Et_2O (50 mL) at $0^\circ C$, $LiAlH_4$ (762 mg, 20.1 mmol) was added in portions. The mixture was allowed to warm to room temperature over 1h and then quenched by dropwise addition of wet

ethyl ether and then water. After all inorganic materials were precipitated, the solid was filtered and washed with EtOAc (3 x 20 mL). The organic phase was dried, concentrated in vacuo and purified by chromatography on silica gel (hexane/EtOAc, 85/15) to give diol **34** (5.71 g, 95%) as a colourless oil. Mixture of two diastereomers, IR (neat) ν_{\max} : 3412, 2958, 2931, 2858, 1472, 1461, 1428, 1388, 1112, 1075, 702 cm^{-1} ; $^1\text{H-NMR}$: (400 MHz, CDCl_3): δ 7.66 (8H, d, $J=6.5$, ArH), 7.45-7.33 (12H, m, ArH), 3.57 (4H, m), 3.42 (2H, m), 1.75-1.61 (4H, m), 1.19, 1.18, 1.14, 1.12 (3H each, all s, 2 x $\text{C}(\text{CH}_3)_2$), 0.95, 0.92 (3H each, both d, $J=6.7$, 2 x H_3 -17), $^{13}\text{C-NMR}$ (100 MHz, CDCl_3): δ 135.6, 134.0, 129.5, 127.6, 79.1, 78.7, 73.1, 68.9, 68.5, 35.7, 35.6, 30.4, 30.3, 29.07, 29.02, 26.9, 26.49, 26.45, 23.17, 23.15, 19.3, 17.1, 16.8; HRMS (ESI) m/z calcd for $\text{C}_{25}\text{H}_{38}\text{NaO}_3\text{Si}$ $[\text{M}+\text{Na}]^+$ 437.2488, found 437.2473.

To a stirred solution of diol **34** (4.83 g, 11.6 mmol) in acetone/water 5:1 (57 mL) at 0°C , sodium periodate (4.98 g, 23.2 mmol) was added. After a few minutes a large amount of a white solid precipitated. After 4 h the reaction mixture was filtrated under vacuum and the precipitate was carefully washed with acetone. The solvent was evaporated in vacuo and the aqueous suspension was extracted with EtOAc (3 x 30 mL). The organic layer was dried and concentrated in vacuo to give aldehyde **10** as a colourless oil (4.34 g) that was applied to the next step without further purification. $^1\text{H-NMR}$ (400 MHz, CDCl_3): δ 9.74 (1H, s, CHO), 7.66 4H, d, $J=7.1$, ArH), 7.46-7.34 (6H, m, ArH), 3.50 (2H, m, H_2 -15), 2.47-2.31 (2H, m, H_2 -19), 1.87-1.75 (1H, m), 1.75-1.61 (1H, m), 1.55-1.43 (1H, m), 1.06 (9H, s, $\text{C}(\text{CH}_3)_3$), 0.92 (3H, d, $J=6.7$, H_3 -17).

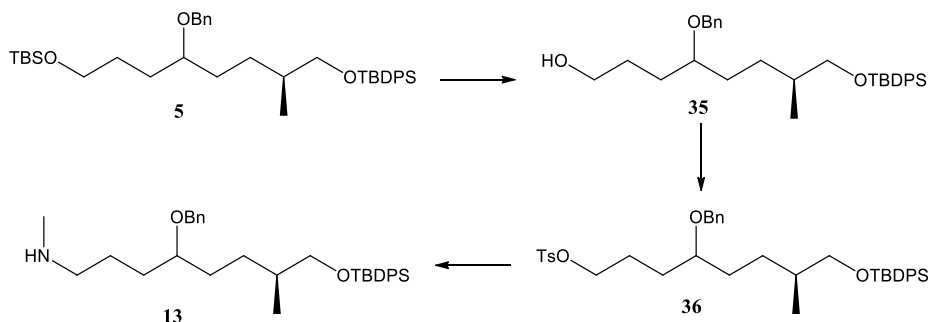
Alcohol 12

To a suspension of magnesium turnings (583 mg, 24.0 mmol) in anhydrous THF (30 mL) a catalytic amount of iodine was added. After 10 min (3-bromopropoxy)-tert-butyldimethylsilane (4.56 g, 4.17 mL, 18.0 mmol) in THF (20 mL) was slowly added at rt, under argon. During the addition, the temperature was maintained at 30-35 °C. After the addition was completed, the reaction mixture was stirred at 40°C for 1h. To the above solution, crude aldehyde **10** (4.34 g, 12.2 mmol) in THF (10 mL) was dropwise added. After the addition was completed, the reaction mixture was stirred for 1h at room temperature. Then, the reaction mixture was treated with a satd. aq. NH₄Cl solution (50 mL) and extracted with EtOAc. The organic phase was washed with brine, dried, concentrated in vacuo and purified by chromatography on silica gel (hexane-EtOAc, 95:5) to give alcohol **12** (4.83 g, 75 %) as a colourless oil. Mixture of two diastereomers, IR (neat) ν_{max} : 3420, 2954, 2930, 2858, 1472, 1464, 1428, 1389, 1256, 1111, 1007, 835, 777, 740, 702 cm⁻¹; ¹H-NMR: (400 MHz, CDCl₃): δ 7.70 (8H, d, J=7.0, ArH), 7.47-7.35 (12H, m, ArH), 3.69 (4H, bt, J=5.2), 3.63-3.53 (4H, m), 3.53-3.45 (2H, m, H-20), 2.45 (2H, bs, 2xOH), 1.77-1.54 (8H, m), 1.54-1.34 (8H, m), 1.34-1.13 (2H, m), 1.09, 0.94 (18H each, both s, 2 x C(CH₃)₃), 0.970 (3H, d, J=6.6, H₃-17), 0.965 (3H, d, J=6.6, H₃-17); ¹³C-NMR (100 MHz, CDCl₃): δ 135.6, 134.0, 129.4, 127.5, 71.73, 71.66, 68.8, 68.7, 63.5, 35.8, 34.8, 34.7, 34.6, 34.4, 29.2, 29.15, 29.09, 29.07, 26.8, 25.9, 19.3, 18.2, 16.9, -5.4; HRMS (ESI) m/z calcd for C₃₁H₅₃O₃Si₂ [M+H]⁺ 529.3528, found 529.3506.

Fully protected triol 5

To a stirred solution of alcohol **12** (1.93 g, 3.66 mmol) in anhydrous THF (40 mL), under argon, sodium hydride (60% dispersion in mineral oil, 292.8 mg, 7.32 mmol) was added. After stirring at reflux for 5 min, benzyl bromide (0.790 mL, 6.59 mmol) was added, followed by TBAI (20 mol%, 271 mg, 0.732 mmol). The reaction was stirred at 50 °C for 24 h. After cooling to room temperature, the reaction mixture was diluted with EtOAc (50 mL) and quenched by careful addition of a satd. aq. NaHCO₃ solution (50 mL). Phases were separated and the aqueous layer was extracted with EtOAc (2 x 50 mL). The combined organic phases were washed with water (50 mL) and brine (50 mL), dried, and concentrated in vacuo. Purification by column chromatography on silica gel (hexane-EtOAc, 95:5) gave fully protected triol **5** (2.05 g, 91%) as a colourless oil. Mixture of two diastereomers, IR (neat) ν_{max} : 2955, 2929, 2858, 1472, 1473, 1463, 1428, 1388, 1255, 1112, 1095, 835, 776, 738, 701 cm⁻¹; ¹H-NMR: (400 MHz, CDCl₃): δ 7.67 (8H, d, $J=7.3$, ArH), 7.45-7.28 (22H, m, ArH), 4.48 (4H, d, $J = 3.3$, OCH₂Ph), 3.60 (4H, bt, $J= 6.0, 2 \times H_2-24$), 3.52 (2H, m, 2 x H_{a-15}), 3.45 (2H, m, 2 x H_{b-15}), 3.36 (2H, m, 2 x H-20), 1.71-1.10 (18H, overlapped m's), 1.05 (18H, s, 2 x C(CH₃)₃), 0.93 (6H, bd, $J=6.6$, 2 x H₃₋₁₇), 0.05 (12H, s, 2 x Si(CH₃)₂); ¹³C-NMR (100 MHz, CDCl₃): δ 139.0, 135.6, 134.0, 129.5, 128.3, 127.7, 127.5, 127.3, 79.1, 70.73, 70.68, 68.8, 63.3, 35.95, 35.91, 31.3, 31.2, 30.0, 29.9, 28.82, 28.80, 28.61, 28.56, 26.9, 26.0, 19.3, 18.3, 16.9, -5.3; HRMS (ESI) m/z calcd for C₃₈H₅₈NaO₃Si₂ [M+Na]⁺ 641.3822, found 641.3804.

Amine 13



To a flask containing compound **5** (2.05 g, 3.32 mmol) at rt, a premixed solution of AcOH/THF/H₂O (3:1:1, 34 mL) was added. After 4 h the reaction was quenched with a satd. aq. NaHCO₃ solution (20 mL) and extracted with EtOAc. The organic phase was washed with water, dried, filtered and concentrated in vacuo. Purification by column chromatography over silica gel (hexane-EtOAc, 9:1) afforded alcohol **35** (1.52 g, 91%) as a colourless oil. Mixture of two diastereomers, IR (neat) ν_{\max} : 3400, 2930, 2857, 1455, 1428, 1389, 1112, 1066, 824, 739, 701 cm⁻¹; ¹H-NMR: (400 MHz, CDCl₃), δ 7.67 (8H, d, J=6.8, ArH), 7.44-7.30 (12H, m, ArH), 7.32 (10H, m, ArH), 4.51 (2H, m, OCH₂Ph), 4.47 (2H, m, OCH₂Ph), 3.62 (4H, t, J=5.2, OCH₂), 3.55-3.43 (4H, m), 3.43-3.36 (2H, m, 2 x H-20), 1.90 (2H, bs, 2 x OH), 1.70-1.40 (16H, overlapped m's, 8 x CH₂), 1.28-1.09 (2H, m), 1.06, (18H each, s, 2 x C(CH₃)₃), 0.93 (6H, bd, J=6.6, 2 x H₃-17); ¹³C-NMR (100 MHz, CDCl₃): δ 138.6, 135.6, 134.0, 129.5, 128.3, 127.8, 127.6, 79.11, 79.06, 70.86, 70.82, 68.78, 68.74, 63.1, 35.9, 35.8, 30.9, 30.7, 30.25, 30.16, 28.7, 28.5; 26.9, 19.3, 16.88, 16.83; HRMS (ESI) m/z calcd for C₃₂H₄₄NaO₃Si [M+Na]⁺ 527.2957, found 527.2953.

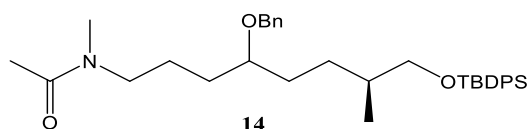
To a stirred solution of alcohol **35** (763 mg, 1.51 mmol) in dry CH₂Cl₂ (12 mL) at 0 °C DMAP (111 mg, 0.906 mmol), *p*-toluensulfonyl chloride (345 mg, 1.81 mmol) and triethylamine (230.8 mg, 0.318 mL, 1.51 mmol) were added in sequence. After 4.5 h the suspension was diluted with Et₂O (30 mL) and stirred for 30 min. Then

the precipitate was removed by filtration. The organic phase was washed with a 10% CuSO₄ solution (2 x 100 mL), a 10% NaHCO₃ solution (2 x 100 mL) and brine (100 mL). The combined organic phases were dried, filtered and concentrated in vacuo to give tosylate **36** (946 mg) as a colourless oil. An analytically pure sample of this compound was obtained by chromatography over silica gel (hexane/EtOAc, 7:3) for characterization. Mixture of two diastereomers, IR (neat) ν_{\max} : 2960, 2929, 2857, 1455, 1428, 1361, 1261, 1176, 1111, 1028, 814, 740, 702, 664 cm⁻¹; ¹H-NMR: (400 MHz, CDCl₃): δ 7.83 (4H, d, J = 7.9, ArH), 7.74 (8H, d, J = 7.9, ArH), 7.50-7.39, 7.39-7.27 (overall 26H, m's, ArH), 4.52 (2H, A part of an apparent AB system further coupled, dd, J = 11.5, 3.7, OCH₂Ph), 4.43 (2H, B part of an apparent AB system further coupled, bd, J = 11.5), 4.08 (4H, bd, J = 5.9), 3.56 (4H, m), 3.37 (2H, bs, 2 x H-20), 2.45 (6H, s, 2 x CH₃PhSO₃-), 1.90-1.10 (18H, overlapped m's), 1.13 (18H, s, 2 x C(CH₃)₃), 0.99 (6H, d, J = 6.7, 2 x H₃-17); ¹³C-NMR (100 MHz, CDCl₃): δ 144.7, 138.8, 135.7, 134.0, 133.3, 129.9, 129.6, 128.4, 127.9, 127.76, 127.70, 78.3, 77.5, 70.92, 70.90, 70.86, 70.82, 68.8, 36.00, 35.9, 31.1, 31.0, 29.7, 29.6, 28.7, 28.6, 27.0, 24.92, 24.88, 21.6, 19.4, 17.0; HRMS (ESI) m/z calcd for C₃₉H₅₀NaO₅SSi [M+Na]⁺ 681.3046, found 681.3037.

To a solution of tosylate **36** (946 mg, 1.43 mmol) in CHCl₃ (22.8 mL) methylamine (40% solution in water, 22.8 mL) was added. The mixture was vigorously stirred for 2 days at room temperature and then poured into a separatory funnel. The organic phase was separated and the water phase was extracted with CHCl₃ (2 x 50 mL). The combined organic phases were dried and concentrated in vacuo. Purification by silica gel chromatography (CHCl₃/CH₃OH, 8:2) gave amine **13** (562 mg, 72% over two steps) as a colourless oil. Mixture of two diastereomers, IR (neat) ν_{\max} : 2959, 2928, 2855, 1456, 1428, 1261, 1112, 800, 740, 702, 667 cm⁻¹; ¹H-NMR

(400 MHz, CDCl₃): δ 7.68 (8H, d, J =7.8, ArH), 7.45-7.35 (12H, m, ArH), 7.33 (10H, m, ArH), 4.51 (2H, apparent dd, J=11.5, 4.7, OCH₂Ph), 4.49 (2H, apparent dd, J=11.5, 1.9, OCH₂Ph), 3.56-3.43 (4H, m, OCH₂TBDPS), 3.37 (2H, bs, 2 x H-20), 2.58 (4H, bs, 2 x H₂-24), 2.43 (6H, s, 2 x H₃-27), 1.71-1.08 (18H, overlapped m's), 1.07 (18H, s, 2 x C(CH₃)₃), 0.94 (6H, d, J=6.5, 2 x H₃-17); ¹³C-NMR (100 MHz, CDCl₃): δ 138.9, 135.5, 134.0, 129.4, 128.2, 127.7, 127.5, 127.3, 79.0, 70.8, 70.7, 68.8, 52.1, 36.3, 35.9, 35.8, 31.45, 31.36, 31.1, 31.0, 28.7, 28.6, 26.8, 25.6, 25.5, 19.2, 16.8; HRMS (ESI) *m/z* calcd for C₃₃H₄₈NO₂Si [M+H]⁺ 518.3449, found 518.3434.

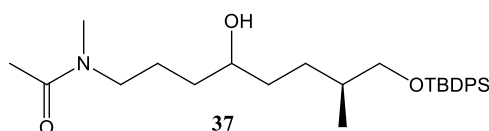
Amide 14



To a stirred solution of amine **13** (526 mg, 1.02 mmol) in CH₂Cl₂ (3.5 mL) at 0 °C, excess Et₃N (0.720 mL, 5.15 mmol) was added, followed by dropwise addition of acetyl chloride (160 mg, 0.15 mL, 2.04 mmol). After 30 min the reaction mixture was diluted with CH₂Cl₂ and a few drops of water were added. The reaction mixture was washed with a satd. aq. NaHCO₃ solution and brine. The combined organic phases were dried and concentrated in vacuo to give amide **14** (511.7 mg, 90 %) as a colourless oil. An analytically pure sample of this compound was obtained by chromatography over silica gel (CHCl₃/CH₃OH, 95:5) for characterization. Mixture of two diastereomers, IR (neat) ν_{\max} 2955, 2925, 2858, 1632, 1465, 1455, 1261, 1112, 803, 739, 701 cm⁻¹; ¹H-NMR (400 MHz, CDCl₃, mixture of rotamers): δ 7.67 (8H, d, J=7.1, ArH), 7.46-7.23 (12H, m, ArH), 4.58-4.39 (4H, m, OCH₂Ph), 3.57-3.43 (m), 3.42-3.32 (m), 3.23 (2H, t, J=7.1, H₂-24), 2.93 (1.5 H, s, H₃-27), 2.89 (1.5

H, s, H₃-27), 2.06 (1.5 H, s, H₃-26), 2.05 (1.5 H, s, H₃-26), 1.74-0.98 (18H, overlapped m's), 1.07 (18H, s, 2 x C(CH₃)₃), 0.94 (6H, bd, J=6.4, 2 x H₃-17); ¹³C-NMR (100 MHz, CDCl₃): δ 170.3, 138.9, 138.6, 135.5, 133.93, 133.88, 129.45, 129.41, 128.3, 128.2, 127.6, 127.5, 127.3, 78.89, 78.87, 78.68, 78.62, 70.92, 70.86, 70.82, 68.73, 68.67, 68.65, 50.8, 47.3, 35.87, 35.85, 35.81, 35.77, 33.0, 31.2, 31.1, 31.0, 30.9, 30.81, 30.78, 30.69, 28.70, 28.66, 28.58, 28.56, 26.8, 24.15, 24.11, 23.0, 22.9, 21.8, 21.2, 19.2, 16.8; HRMS (ESI) *m/z* calcd for C₃₅H₄₉NNaO₃Si [M+Na]⁺ 582.3379, found 582.3369.

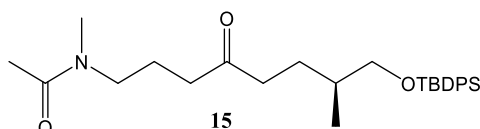
Alcohol 37



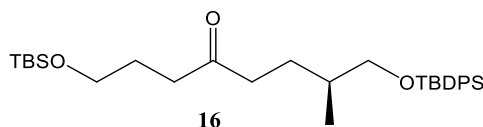
Amide **14** (511 mg, 0.91 mmol) and Pd(OH)₂/C (274 mg 20% w/w) were suspended in EtOH (14 mL). The mixture was hydrogenated at atmospheric pressure for 2 days. Then, the reaction mixture was filtered over celite and the filtrate was dried under reduced pressure to give alcohol **37** (371 mg, 87%) a colourless oil. An analytically pure sample of this compound was obtained by chromatography over silica gel (CHCl₃/CH₃OH, 98:2) for characterization. Mixture of two diastereomers, IR (neat) ν_{max} : 3416, 2931, 2858, 1631, 1472, 1456, 1428, 1261, 1112, 824, 741, 703 cm⁻¹; ¹H-NMR (400 MHz, CDCl₃, mixture of rotamers): δ 7.66 (8H, d, J=6.9, ArH), 7.46-7.31 (12H, m, ArH), 3.59-3.39 (6H, m, 2x H-20 and 2 x H₂-15), 3.25 (4H, bt, J=7.6, 2 x H₂-24), 2.95 (1.5H, s, H₃-27), 2.89 (1.5H, s, H₃-27), 2.07 (1.5H, s, H₃-26), 2.04 (1.5H, s, H₃-26), 1.80-1.08 (18H, overlapped multiplets, 8 x CH₂ and 2 x CH), 1.05 (18H, s, 2 x C(CH₃)₃), 0.92 (3H, d, J=6.4, H₃-16), 0.91 (3H, d, J = 6.4, H₃-17); ¹³C-NMR (100 MHz, CDCl₃): δ 170.6, 170.4, 135.5, 133.95, 133.90,

129.5, 129.4, 127.5, 71.7, 71.6, 71.5, 68.8, 68.7, 68.6, 50.8, 47.4, 36.0, 35.73, 35.68, 35.6, 35.0, 34.1, 33.9, 33.8, 33.1, 29.07, 29.02, 26.8, 24.55, 24.50, 23.46, 23.43, 21.8, 21.2, 19.2, 16.85, 16.79, 16.76; HRMS (ESI) m/z calcd for $C_{28}H_{44}NO_3Si$ $[M+H]^+$ 470.3085, found 470.3067.

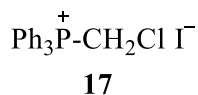
Ketone 15



To a stirred solution of alcohol **37** (368 mg, 0.79 mmol) in CH_2Cl_2 (55 mL), *N*-methylmorpholine-*N*-oxide (138 mg, 1.18 mmol) and powdered 4Å molecular sieves (392 mg) were added under argon. After 10 min TPAP (13.8 mg, 0.039 mmol, 5 mol %) was added. After 2.5 h, the reaction mixture was filtered through a short silica gel plug ($CHCl_3/EtOAc$, 8:2) and the filtrate was concentrated under reduced pressure. Purification by column chromatography over silica gel (hexane- $EtOAc$, 6:4) afforded ketone **15** (335 mg, 91%) as a colourless oil. $[\alpha]_D^{20} = +2.7$ ($c=1.0$, $CHCl_3$); IR (neat) ν_{max} : 2958, 2924, 2854, 1715, 1651, 1462, 1367, 1261, 1111, 800, 704 cm^{-1} ; 1H -NMR (400 MHz, $CDCl_3$, mixture of rotamers): δ 7.65 (8H, d, $J=7.2$, ArH), 7.46-7.33 (12H, m, ArH), 3.52-3.40 (4H, m, 2 x H_2 -15), 3.34 (0.6 H, t, $J=7.1$, H_2 -24), 3.24 (0.4 H, t, $J=7.4$, H_2 -24), 2.96 (1.8 H, s, H_3 -27), 2.90 (1.2 H, s, H_3 -27), 2.48-2.28 (8H, m, H_2 -22 and H_2 -19), 2.08 (1.2 H, s, H_3 -26), 2.05 (1.8 H, s, H_3 -26), 1.86-1.20 (18H, overlapped multiplets, 8 x CH_2 and 2 x CH), 1.05 (18H, s, 2 x $C(CH_3)_3$), 0.90 (6H, bd, $J=6.5$, 2 x H_3 -17); ^{13}C -NMR (100 MHz, $CDCl_3$): δ 210.5, 209.7, 170.6, 170.4, 135.5, 133.8, 129.51, 129.48, 127.5, 68.43, 68.39, 49.8, 46.6, 40.5, 40.4, 39.5, 38.6, 35.8, 35.2, 33.0, 27.1, 27.0, 26.8, 21.9, 21.7, 21.1, 19.2, 16.6. HRMS (ESI) m/z calcd for $C_{28}H_{42}NO_3Si$ $[M+H]^+$ 468.2928, found 468.2913.

Ketone 16

To a stirred solution of alcohol **12** (102.3 mg, 0.194 mmol) in CH₂Cl₂ (0.5 mL) *N*-methylmorpholine-*N*-oxide (34 mg, 0.291 mmol) and powdered 4 Å molecular sieves (94 mg) were added under argon. After 10 min stirring, TPAP (3.4 mg, 0.0097 mmol, 5 mol %) was added. After 2.5 hours, the reaction mixture was filtered through a short silica gel plug eluting with CH₂Cl₂/EtOAc (8:2) and concentrated in vacuo. Purification by preparative TLC (hexane-EtOAc, 8:2) afforded ketone **16** (91.8 mg, 90%) as a colourless oil. $[\alpha]_D^{20} = -1.8$ (c=1.0, CHCl₃); IR (neat) ν_{\max} : 2957, 2930, 2858, 1717, 1472, 1464, 1428, 1389, 1257, 1112, 836, 777, 740, 702 cm⁻¹; ¹H-NMR (400 MHz, CDCl₃): δ 7.68 (8H, d, J=6.6, ArH), 7.47-7.36 (12H, m, ArH), 3.63 (4H, bt, J=6.3), 3.51 (4H, m), 2.47 (2H, t, J=7.3), 2.41 (2H, m), 1.08 (9H, s, C(CH₃)₃), 0.94 (3H, d, J=6.7, H₃-17), 0.91 (9H, s, C(CH₃)₃), 0.06 (6H, s, Si(CH₃)₂); ¹³C-NMR (100 MHz, CDCl₃): δ 211.0, 135.6, 133.8, 129.5, 127.6, 68.5, 62.2, 40.5, 38.9, 35.3, 27.2, 26.86, 26.82, 25.9, 19.3, 18.3, 16.7, -5.4; HRMS (ESI) m/z calcd for C₃₁H₅₁O₃Si₂ [M+H]⁺ 527.3371, found 527.3379.

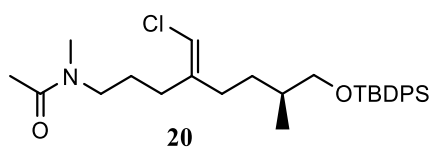
Phosponium salt 17

(Chloromethyl)triphenylphosponium iodide **17** was prepared by a modification of the reported procedure,²¹ starting from triphenylphosphine (31.44 g, 120 mmol) and chloriodomethane (25 g, 10.3 mL, 142 mmol). In particular, the Widmer condenser was replaced by a double jacketed condenser. After 4h the process was stopped by

Wittig reaction on model ketone **16** using *tert*-BuOK as the base

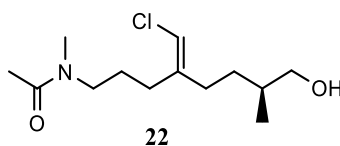
To a stirred suspension of (chloromethyl)triphenylphosphonium iodide (137 mg, 0.31 mmol) in THF (3.5 mL), at 0°C, under argon, *tert*-BuOK (0.314 mL, 0.314 mmol, 1.0 M sol. in THF) was added dropwise.²¹ The solution became immediately yellow. After 30 min at 0°C, a solution of ketone **16** (82.8 mg, 0.157 mmol) in dry THF (1.0 mL plus 0.2 mL rinse) was added and the mixture was allowed to reach room temperature. After 4h, the reaction was quenched with a satd. aq. NH₄Cl solution (10 mL) and extracted with Et₂O (3 x 15 mL). The organic phase was washed with brine, dried and evaporated under reduced pressure. Purification by preparative TLC (hexane/EtOAc, 8:2) gave compounds **18** (66.5 mg, 76%, 1.8:1 mixture of diastereomers, ¹H-NMR analysis), as a colourless oil. ¹H-NMR (400 MHz, CDCl₃): mixture of two diastereomers, δ 7.72 -7.27 (ArH), 5.78, 5.74 (both s, vinyl proton), 3.63 -3.55, 3.52-3.45 (both m, 2 x OCH₂), 2.29-2.04 (m, H₂-19 and H₂-22), 1.71-1.51 (m), 1.06, 0.89 (both s, 2 x C(CH₃)₃), 0.041 (m, (CH₃)₂Si); HRMS (ESI) *m/z* calcd for 559.3189 [M+H]⁺, found 559.3178.

Chlorovinyl derivative **20**

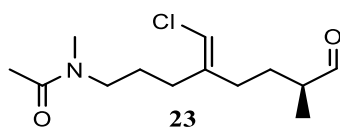


To a stirred suspension of (chloromethyl)triphenylphosphonium iodide (128 mg, 0.292 mmol) in THF (5 mL), at 0°C, under argon, *tert*-BuOK (0.281 mL, 0.7281 mmol, 1.0 M sol. in THF) was added dropwise.²¹ The solution became immediately yellow. After 30 min at 0°C, a solution of ketone **15** (45.5 mg, 0.097 mmol) in dry THF (1.0 mL plus 1.0 mL rinse) was added and the mixture was allowed to reach room temperature. After 4h, the reaction was quenched with a satd. aq. NH₄Cl solution (10 mL) and extracted with Et₂O (3 x 20 mL). The organic phase was

washed with brine, dried and evaporated under reduced pressure. Separation by column chromatography over silica gel (hexane-EtOAc, 8:2) gave compounds **20** (19.6 mg, 40.4%) and **21** (20.5 mg, 42.3%) as colourless oils. Compound **20**. $[\alpha]_D^{20} = -1.6$ ($c = 0.23$, CHCl_3); IR (neat) ν_{max} : 2955, 2930, 2858, 1652, 1428, 1112, 824, 798, 741, 703 cm^{-1} ; $^1\text{H-NMR}$: (400 MHz, CDCl_3 , mixture of rotamers): δ 7.65 (4H, d, $J = 6.9$, ArH), 7.45-7.34 (6H, m, ArH), 5.81 (0.5H, s, vinyl proton), 5.75 (0.5H, s, vinyl proton), 3.48 (2H, bt, $J = 5.6$, H_2 -15), 3.37, 3.25 (1H each, both t, $J = 7.6$, H_2 -24), 2.97 (1.5H, s, H_3 -27), 2.90 (1.5H, s, H_3 -27), 2.24-2.13 (2H, m), 2.13-1.95 (5H, overlapped signals including a singlet at 2.07 for H_3 -26), 1.77-1.53 (4H, m), 1.34-1.13 (1H, m), 1.06 (9H, s, $\text{C}(\text{CH}_3)_3$), 0.91 (3H, d, $J = 6.6$, H_3 -17); $^{13}\text{C-NMR}$ (100 MHz, CDCl_3): δ 170.4, 170.3, 142.1, 141.4, 135.6, 133.89, 133.81, 129.59, 129.54, 127.6, 113.0, 112.3, 68.5, 68.4, 50.5, 47.1, 36.0, 35.2, 33.1, 32.25, 32.22, 31.05, 30.99, 27.5, 27.3, 26.9, 25.8, 24.7, 21.9, 21.2, 19.3, 16.6; HRMS (ESI) m/z calcd for $\text{C}_{29}\text{H}_{42}\text{ClNNaO}_2\text{Si}$ $[\text{M}+\text{Na}]^+$ 522.2566, found 522.2541. Compound **21**. $[\alpha]_D^{20} = -1.4$ ($c = 0.6$, CHCl_3); IR (neat) ν_{max} : 2958, 2931, 2858, 1627, 1428, 1112, 823, 802, 742, 703 cm^{-1} ; $^1\text{H-NMR}$ (400 MHz, CDCl_3): mixture of rotamers, δ 7.66 (4H, d, $J = 7.5$, ArH), 7.45-7.34 (6H, m, ArH), 5.80 (1H, s, vinyl proton), 3.50 (2H, m, H_2 -15), 3.32 (0.6 H, t, $J = 7.7$, H_2 -24), 3.21 (0.4 H, t, $J = 7.7$, H_2 -24), 2.94 (1.8 H, s, H_3 -27), 2.89 (1.2 H, s, H_3 -27), 2.21 (2H, m), 2.10-2.02 (5H, overlapped signals including a singlet at 2.06 for H_3 -26), 1.77-1.56 (4H, m), 1.31-1.15 (1H, m), 1.05 (9H, s, $\text{C}(\text{CH}_3)_3$), 0.95 (3H, d, $J = 6.6$, H_3 -17); $^{13}\text{C-NMR}$ (100 MHz, CDCl_3): δ 170.4, 170.3, 142.05, 141.5, 135.6, 134.0, 133.9, 129.5, 127.6, 112.9, 112.3, 68.6, 68.5, 50.2, 47.2, 36.1, 35.7, 33.1, 32.0, 31.7, 30.3, 27.7, 27.5, 26.9, 26.2, 25.2, 21.9, 21.2, 19.3, 16.6; HRMS (ESI) m/z calcd for $\text{C}_{29}\text{H}_{42}\text{ClNNaO}_2\text{Si}$ $[\text{M}+\text{Na}]^+$ 522.2566, found 522.2562.

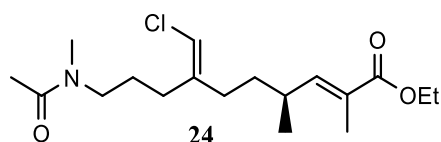
Alcohol 22

To a solution of **20** (47.2 mg, 0.094 mmol) in THF (6.7 mL), TBAF (0.142 mL, 0.142 mmol, 1.0 M solution in THF) was added dropwise, at 0°C. The reaction mixture was allowed to reach room temperature and stirred for 1h. Then, the reaction was quenched with a satd. aq. solution of NH₄Cl (2 mL). The phases were separated and the aqueous layer was extracted with EtOAc (3 x 20 mL). The combined organic phases were dried and evaporated in vacuo. Purification by column chromatography over silica gel (CHCl₃/CH₃OH, 99:1) gave alcohol **22** (21.4 mg, 87%) as colourless oil. $[\alpha]_D^{20} = -63.4$ (c=1.5, CHCl₃); IR (neat) ν_{\max} : 3410, 2953, 2927, 2858, 1634, 1489, 1456, 1404, 1046, 795 cm⁻¹; ¹H-NMR: (400 MHz, CDCl₃, mixture of rotamers): δ 5.86 (0.4H, s, vinyl proton), 5.82 (0.6H, s, vinyl proton), 3.46 (2H, t, J=5.3), 3.42-3.24 (2H, m's), 2.99 (1.8 H, s, H₃-27), 2.89 (1.2 H, s, H₃-27), 2.27-2.02 (7H, overlapped signals including two singlets at 2.09 and 2.07 for H₃-26), 1.78-1.52 (4H, m), 1.30-1.15 (1H, m), 0.93, 0.91 (overall 3H, overlapped d's, both J=6.0, H₃-17); ¹³C-NMR (100 MHz, CDCl₃): δ 170.6, 170.4, 142.0, 141.3, 113.2, 112.6, 67.8, 67.7, 50.5, 47.3, 36.1, 35.2, 33.2, 32.3, 32.2, 31.1, 31.0, 27.4, 27.3, 25.8, 24.6, 21.9, 21.2, 16.44, 16.38; HRMS (ESI) m/z calcd for C₁₃H₂₅ClNO₂ [M+H]⁺ 262.1568, found 262.1564.

Aldehyde 23

To a stirred solution of alcohol **22** (16.2 mg, 0.062 mmol) in CH₂Cl₂ (0.3 mL) *N*-methylmorpholine-*N*-oxide (10.87 mg, 0.093 mmol) and powdered 4 Å molecular sieves (31 mg) were added under argon. After 10 min, TPAP (1.1 mg, 0.003 mmol, 5 mol %) was added. After 2 h the reaction mixture was filtrated through a short silica gel plug eluting with CHCl₃/EtOAc (8:2) and concentrated under reduced pressure to yield aldehyde **23** (13.7 mg) as a colourless oil, that was applied to the next step without further purification.

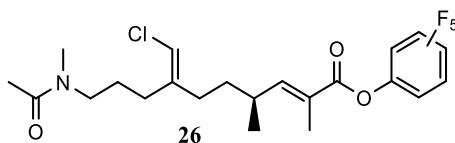
Ethyl ester **24**



To a stirred solution of the aldehyde **23** (13.7, 0.053 mmol) in anhydrous toluene (0.4 mL), at 80° C, under argon, (carboethoxyethylidene)triphenylphosphorane (40.8 mg, 0.106 mmol) was added all at once. After 6 h, the reaction mixture was concentrated under reduced pressure. Purification by column chromatography over silica gel (CHCl₃/CH₃OH, 95:5) afforded ethyl ester **24** (16.3 mg, 76% over two steps) as a colorless oil. $[\alpha]_D^{20} = +127.4$ (c=0.5, CHCl₃); IR (neat) ν_{max} : 2957, 2927, 2858, 1707, 1651, 1596, 1459, 1424, 1373, 1262, 1122 cm⁻¹; ¹H-NMR (400 MHz, CDCl₃, mixture of rotamers): δ 6.49 (1H, d, J=10.1, H-15), 5.82 (0.5H, s, vinyl proton), 5.76 (0.5H, s, vinyl proton), 4.18 (2H, q, J=7.0, OCH₂CH₃), 3.37, 3.27 (1H each, both t, J=7.6, H₂-24), 2.99 (1.5H, s, H₃-27), 2.91 (1.5H, s, H₃-27), 2.46 (1H, m, H-16), 2.18 (2H, m), 2.09 (1.5H, s, H₃-26), 2.08 (1.5H, s, H₃-26), 2.01 (2H, t, J=8.6), 1.83 (1.5H, d, J=1.2, H₃-14), 1.82 (1.5H, d, J=1.2, H₃-14), 1.30 (3H, t, J=7.0, OCH₂CH₃), 1.02 (1.5H, d, J=6.6, H₃-17), 1.00 (1.5H, d, J=6.6, H₃-17); ¹³C-NMR (100 MHz, CDCl₃) δ 170.5, 170.3, 168.3, 168.2, 146.9, 146.6, 141.6, 140.8, 132.1,

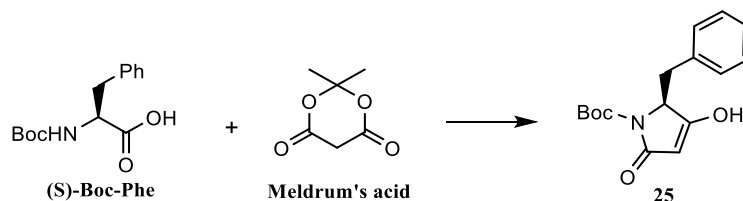
132.0, 131.94, 131.91, 128.5, 128.4, 127.2, 127.0, 113.4, 112.7, 60.6, 60.5, 50.4, 47.1, 36.0, 34.7, 34.6, 33.1, 32.7, 27.4, 27.3, 25.7, 24.6, 21.9, 21.3, 20.01, 19.98, 14.3, 12.63, 12.61; HRMS (ESI) m/z calcd for $C_{18}H_{30}ClNNaO_3$ $[M+Na]^+$ 366.1812, found 366.1802.

Pentafluorophenyl ester **26**.



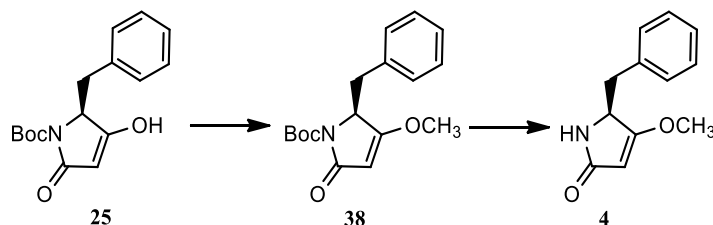
To a solution of **3** (4.5 mg, 0.014 mmol) in EtOAc (0.130 mL), at 0°C, pentafluorophenol (4.0 mg, 0.022 mmol) and DCC (4.5 mg, 0.22 mmol) were added. The reaction mixture was stirred for 1 hour at 0°C and 3h at rt, and evaporated under reduced pressure. Purification by preparative TLC ($CHCl_3/CH_3OH$, 95:5) gave pentafluorophenyl ester **26** (5.5 mg, 82%) as a colourless oil. IR (neat) ν_{max} : 2962, 2917, 2949, 1683, 1626, 1521, 1261, 1096, 1022, 801, 760 cm^{-1} ; 1H -NMR: (400 MHz, $CDCl_3$, mixture of rotamers): δ 6.85 (1H, d, $J=10.1$, H-15), 5.86 (0.5H, s, vinyl proton), 5.80 (0.5H, s, vinyl proton), 3.39, 3.29 (1H each, both t, $J=7.7$, H₂-24), 3.00 (1.5H, s, H₃-27), 2.92 (1.5H, s, H₃-27), 2.58 (1H, m, H-16), 2.20 (2H, m), 2.09 (1.5H, s, H₃-26), 2.08 (1.5H, s, H₃-26), 2.07 (2H, t, $J=8.5$), 1.97 (1.5H, d, $J=1.2$, H₃-14), 1.96 (1.5H, d, $J=1.2$, H₃-14), 1.10 (1.5H, d, $J=6.8$, H₃-17), 1.08 (1.5H, d, $J=6.8$, H₃-17); ^{13}C -NMR (100 MHz, $CDCl_3$): δ 152.4, 152.0, 141.3, 140.6, 124.4, 124.2, 113.7, 113.0, 50.4, 49.1, 47.1, 36.0, 34.5, 34.4, 33.9, 33.3, 33.1, 32.74, 32.68, 27.31, 27.29, 25.8, 25.6, 24.9, 24.6, 21.9, 21.3, 19.67, 19.64, 12.7; HRMS (ESI) m/z calcd for $C_{22}H_{26}ClF_5NO_3$ $[M+H]^+$ 482.1516, found 482.1499.

Pyrrolinone **25**



To a stirred solution of Meldrum's acid (1.60 g, 11.1 mmol) and DMAP (1.57 g, 12.9 mmol) in CH_2Cl_2 (60 mL), at 0°C , Boc-(L)-Phe-OH (2.44 g, 9.21 mmol) was added followed by EDC·HCl (1.76 g, 11.1 mmol). The yellow mixture was stirred overnight at rt, then poured into EtOAc (200 mL) and sequentially washed with brine (2 x 100 mL), 5% citric acid solution (3 x 300 mL) and again brine (1 x 300 mL). The organic phase was refluxed for 1 h. and evaporated under reduced pressure to give compound **25** (2.69 g) that was applied to the next step without further purification.

Pyrrolinone **4**

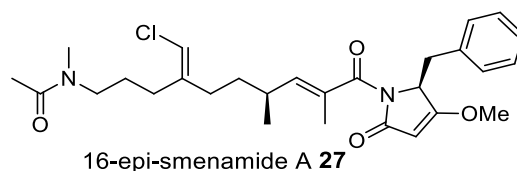


To a stirred solution of pyrrolinone **25** (1.0 g, 3.46 mmol) and triphenylphosphine (1.36 g, 5.19 mmol) in CH_2Cl_2 (20 mL), at 0°C , under argon, CH_3OH (0.21 mL, 5.19 mmol) and DIAD (1.0 mL, 5.19 mmol) were added. The reaction mixture was allowed to warm to rt and after 6 h concentrated in vacuo. Purification by column chromatography over silica gel (hexane/EtOAc, 6:4) gave Boc-protected pyrrolinone **38** (621 mg, 57% over three steps) as a colourless oil. $[\alpha]_{\text{D}}^{20} = +203.3$ ($c=1.0$, CH_3OH); IR (neat) ν_{max} : 2980, 2940, 1779, 1733, 1705, 1634, 1456, 1319, 1246, 1152, 1094, 1073, 981, 848, 808, 757, 701, 667 cm^{-1} ; $^1\text{H-NMR}$: (400 MHz,

CDCl₃): δ 7.11-7.00 (3H, m, ArH), 6.87 (2H, d, $J=7.1$, ArH), 4.66 (1H, s, H-10), 4.52 (1H, bdd, $J=5.0, 3.0$, H-8), 3.62 (3H, s, OCH₃), 3.31 (1H, dd, $J=13.8, 5.1$, H_a-7), 2.98 (1H, dd, $J=13.8, 3.0$, H_b-7), 1.48 (9H, s, C(CH₃)₃); ¹³C-NMR (100 MHz, CDCl₃) δ 175.6, 168.0, 148.8, 133.5, 128.9, 127.6, 126.4, 94.5, 81.8, 59.5, 57.7, 34.7, 27.6. HRMS (ESI) m/z calcd for C₁₇H₂₂NO₄ [M+H]⁺ 304.1543, found 304.1532.

To a stirred solution of **38** (212 mg, 0.66 mmol) in CH₂Cl₂ (2.5 mL) TFA (2.5 mL) was added. After 30 min the reaction mixture was evaporated in vacuo. Residual TFA was removed by evaporation with toluene (3 x 1.5 mL) to give pyrrolinone **4** (144 mg, quant.) as a white waxy solid. Mp 84-85 (EtOAc/hexane) [lit. 103-104³]; $[\alpha]_D^{20} = -62.3$ ($c=1.0$, CHCl₃) [lit. -63.0 ($c=1.0$, CHCl₃)²⁶]; IR (neat) ν_{\max} : 3238, 3030, 2939, 2848, 1683, 1623, 1497, 1455, 1365, 1344, 1232, 989, 806, 700 cm⁻¹; ¹H-NMR: (400 MHz, CDCl₃): δ 7.32-7.20 (3H, m, ArH), 7.14 (2H, d, $J=7.1$, ArH), 5.6 (br s, NH), 5.04 (1H, s, H-10), 4.33 (1H, m, H-8), 3.83 (3H, s, OCH₃), 3.17 (1H, dd, $J=13.7, 3.4$, H_a-7), 2.78 (1H, dd, $J=13.7, 7.6$, H_b-7); ¹³C-NMR (100 MHz, CDCl₃) δ 177.2, 173.7, 136.3, 129.1, 128.4, 126.8, 94.0, 58.4, 58.1, 38.3. HRMS (ESI) m/z calcd for C₁₂H₁₄NO₂ [M+H]⁺ 204.1019, found 204.1011.

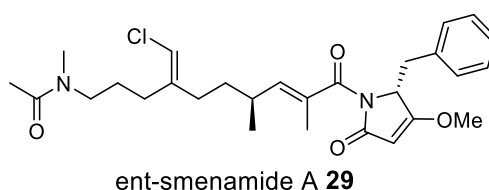
16-*epi*-smenamamide **27**



To a stirred solution of pyrrolinone **4** (9.9 mg, 0.049 mmol) in THF (0.1 mL) at -78°C, *n*BuLi (0.020 mL, 0.033 mmol, 1.6 M sol. in hexane) was added dropwise. After 15 min, a solution of pentafluorophenyl ester **26** (1.5 mg, 0.0031 mmol) in THF (0.1 mL) was added via syringe. After 2h, the reaction was quenched with a

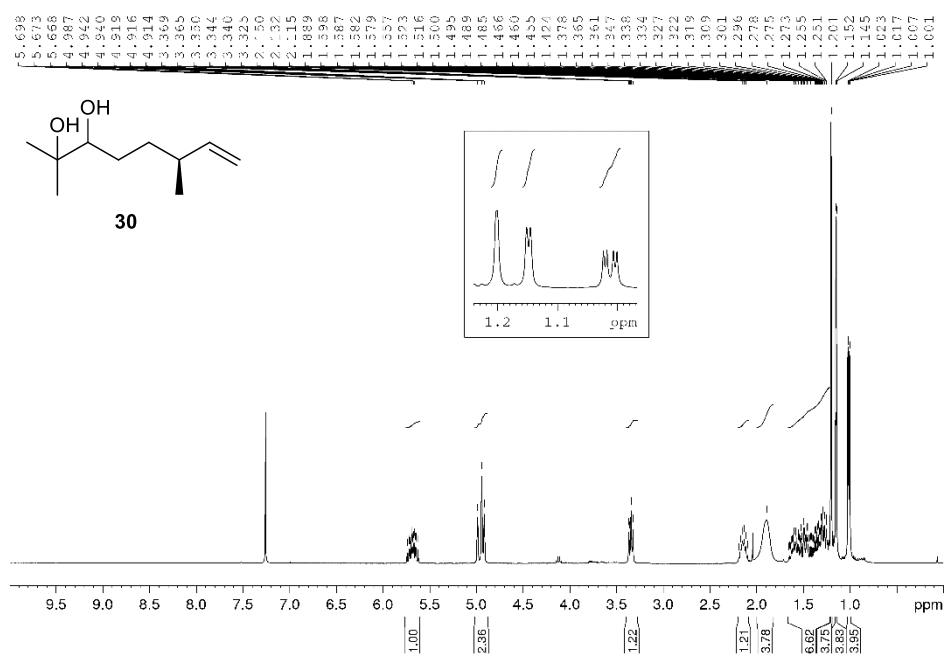
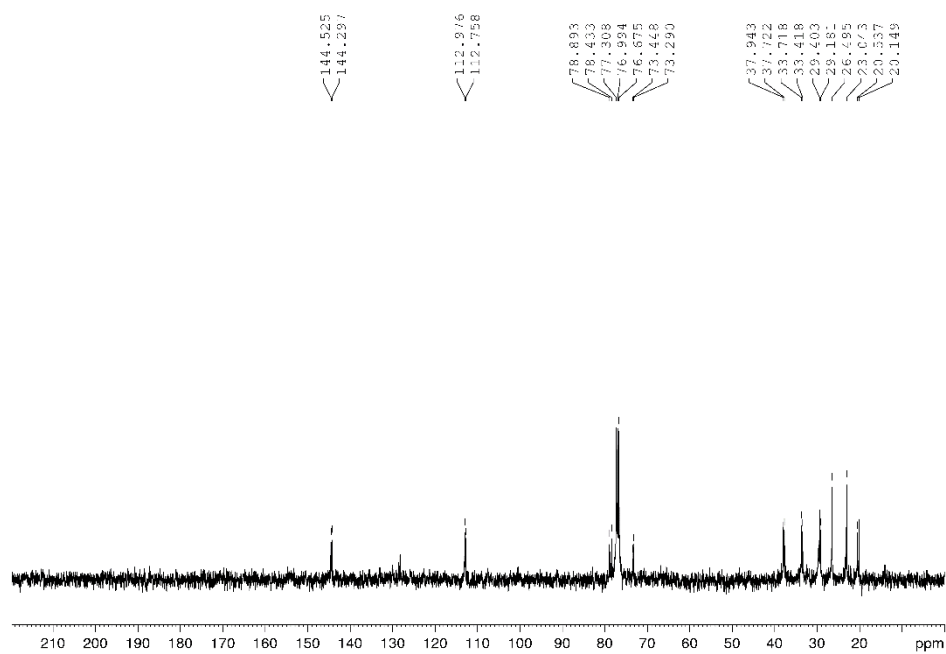
satd. aq. NH₄Cl solution (1 mL) and extracted with EtOAc (3 x 10 mL). The organic phase was washed with water (6 mL) and brine (6 mL), dried and concentrated in vacuo. The crude was subjected to reversed-phase HPLC separation [column Luna (Phenomenex) C18, 250 × 4.6 mm, 5 μm; eluent A: H₂O; eluent B: CH₃CN; gradient: 50→100% B, over 35 min, flow rate 1 mL min⁻¹], to give 16-*epi*-smenamide A (*t_R*=17.5 min, 1.3 mg, 84%) as a colourless oil. [α]_D²⁰ = 86.9 (c=0.1, CHCl₃); IR (neat) ν_{max} : 2958, 2928, 2857, 1731, 1631, 1455, 1308, 1245, 1197, 1024, 965, 807, 753, 708 cm⁻¹; ¹H-NMR: (400 MHz, CD₃OD, mixture of rotamers): δ 7.26-7.20 (3H, m, H-3, H-4, H-5), 6.99 (2H, m, H-2, H-6), 6.00 (0.5H, s, H-21), 5.97 (0.5H, s, H-21), 5.41 (1H, bdd, J=10.0, 1.5, H-15), 5.40 (1H, bdd, J=10.0, 1.5, H-15), 5.03 (0.5H, s, H-10), 5.02 (0.5H, s, H-10), 5.00 (1H, m, H-8), 3.96 (3H, s, OCH₃), 3.46-3.33 (3H, overlapped m's), 3.19 (1H, dd, J=14.0, 2.4), 3.03 (1.5H, s, H₃-27), 2.89 (1.5H, s, H₃-27), 2.44 (1H, m), 2.32-2.13 (3H, overlapped m's), 2.13-2.02 (4H, overlapped signals including a singlet at 2.07 for H₃-26), 1.81-1.60 (5H, overlapped signals including two doublets for H₃-14 at 1.714 and 1.708, both J=1.3), 1.60-1.50 (1H, m), 1.39-1.27 (1H, m), 0.99 (1.5H, d, J=7.1, H₃-17), 0.98 (1.5H, d, J=7.1, H₃-17); ¹³C NMR (126 MHz, CD₃OD) δ 180.0, 143.2, 143.0, 142.6, 142.2, 135.6, 133.2, 130.9, 129.2, 128.2, 114.2, 114.0, 95.4, 60.6, 59.5, 51.5, 36.6, 36.2, 36.1, 34.7, 33.6, 33.4, 33.22, 33.17, 28.2, 28.0, 26.6, 25.7, 21.7, 21.1, 20.3, 20.2, 14.3, 14.2; HRMS (ESI) *m/z* calcd for C₂₈H₃₈ClN₂O₄ [M+H]⁺ 501.2515, found 501.2493.

***ent*-smenamide 29**



To a stirred solution of pyrrolinone **28** (9.9 mg, 0.049 mmol) in THF (0.1 mL) at -78°C, *n*BuLi (0.20 mL, 0.033 mmol, 1.6 M sol. in hexane) was added dropwise. After 15 min, a solution of pentafluorophenyl ester **26** (1.5 mg, 0.0031 mmol) in THF (0.1 mL) was added via syringe. After 2h, the reaction was quenched with a satd. aq. NH₄Cl solution (1 mL) and extracted with EtOAc (3 x 10 mL). The organic phase was washed with water (6 mL) and brine (6 mL), dried and concentrated in vacuo. The crude was subjected to reversed-phase HPLC separation [column Luna (Phenomenex) C18, 250 × 4.6 mm, 5 μm; eluent A: H₂O; eluent B: CH₃CN; gradient: 50→100% B, over 35 min, flow rate 1 mL min⁻¹], to give ent-smenamide **A 29** (*t*_R = 18.5 min, 1.4 mg, 88%) as a colourless oil. $[\alpha]_{\text{D}}^{20} = -9.8$ (c=0.1, CHCl₃); IR (neat) ν_{max} : 2958, 2923, 2853, 1729, 1631, 1455, 1306, 1205, 1132, 1026, 802 cm⁻¹; ¹H- and ¹³C-NMR see Table 1. HRMS (ESI) *m/z* calcd for C₂₈H₃₈ClN₂O₄ [M+H]⁺ 501.2515, found 501.2495.

2.8 Supplementary spectroscopic data

Figure 2.22. ¹H NMR spectrum of compound 30 (CDCl₃, 400 MHz)Figure 2.23. ¹³C NMR spectrum of compound 30 (CDCl₃, 100 MHz)

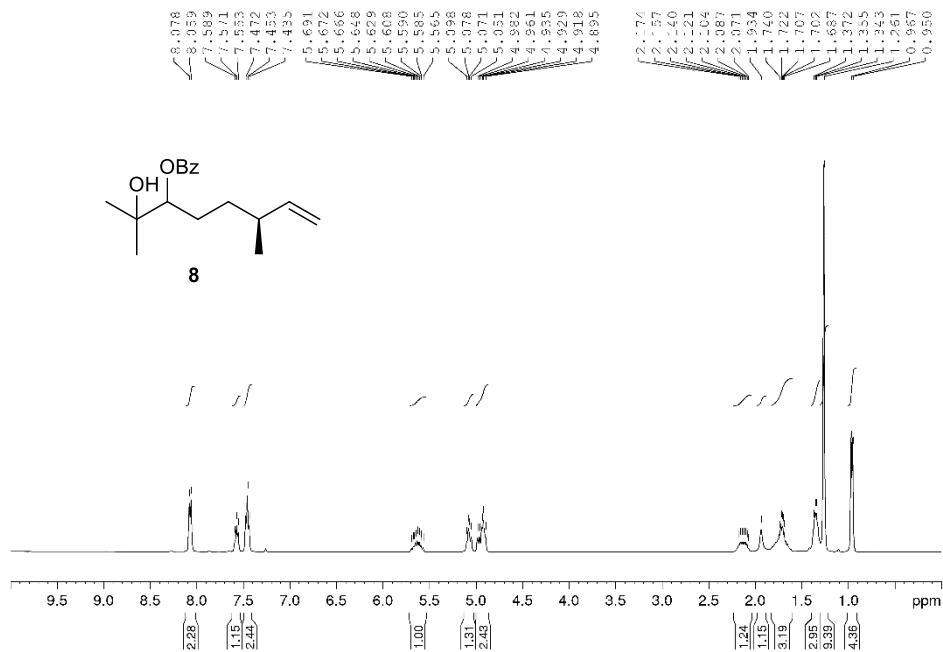


Figure 2.24. ¹H NMR spectrum of compound **8** (CDCl₃, 400 MHz)

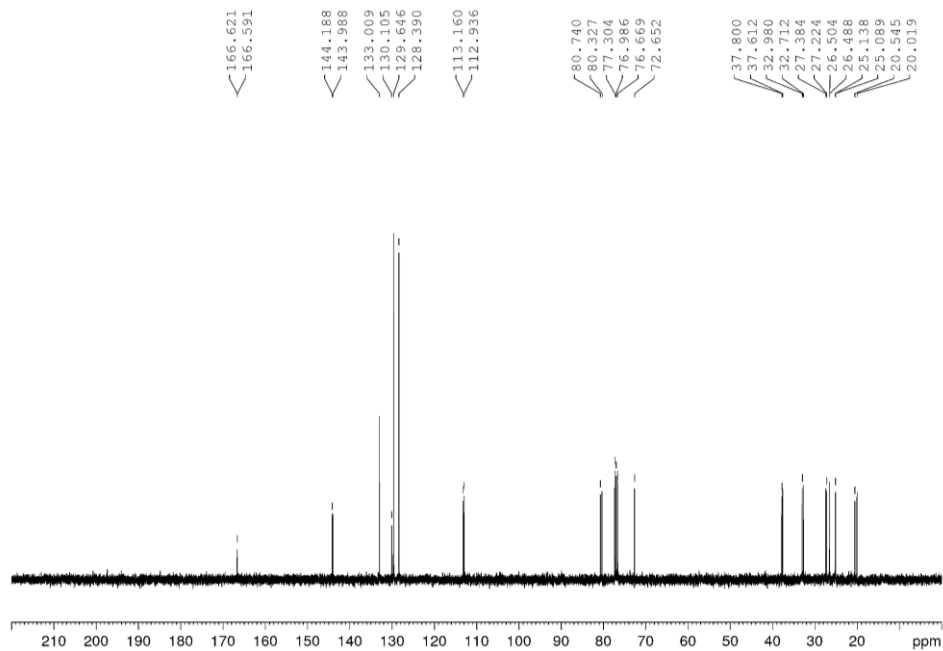


Figure 2.25. ¹³C NMR spectrum of compound **8** (CDCl₃, 100 MHz)

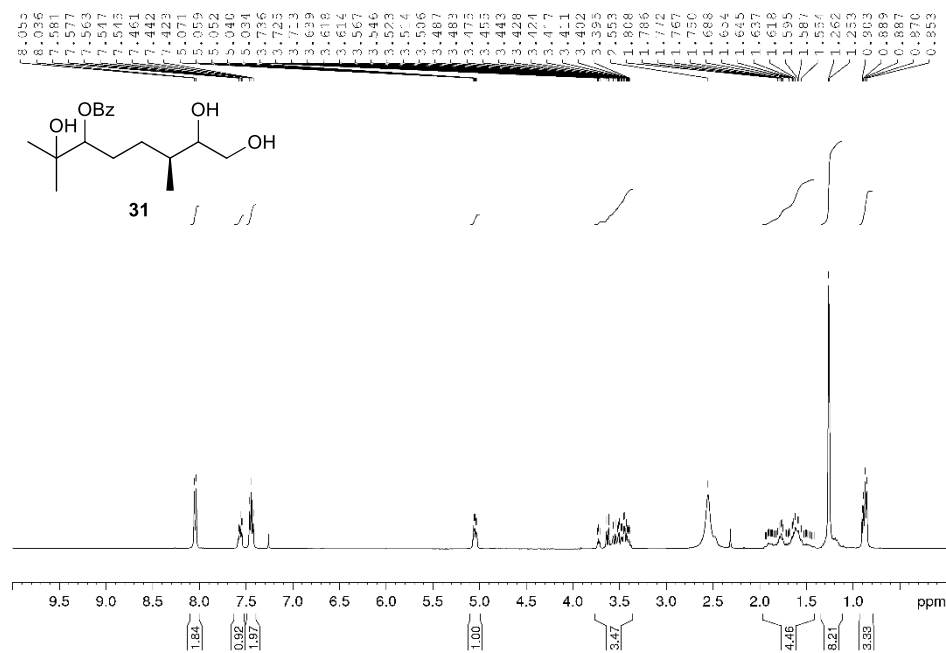


Figure 2.26. ¹H NMR spectrum of compound 31 (CDCl₃, 400 MHz)

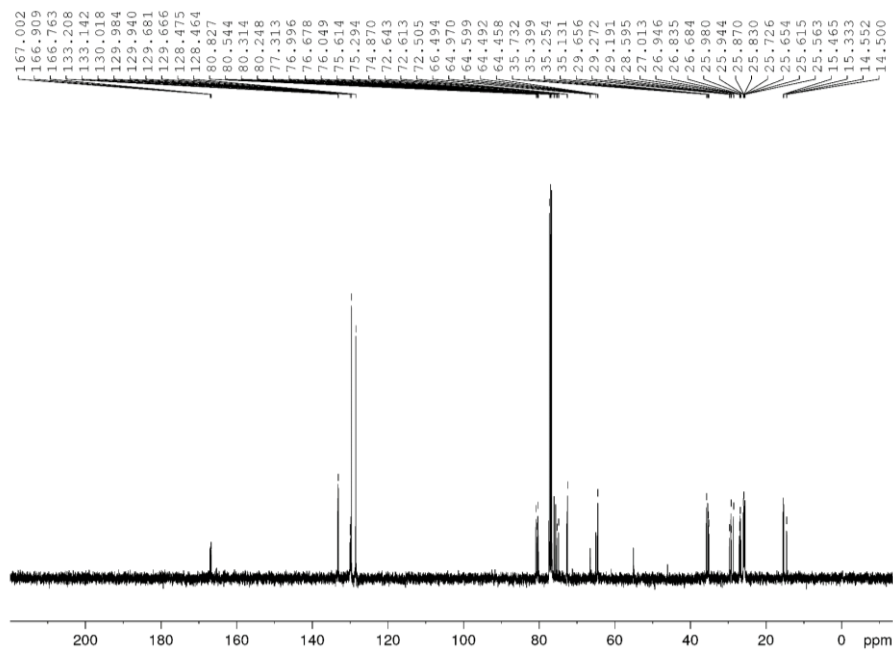


Figure 2.27. ¹³C NMR spectrum of compound 31 (CDCl₃, 100 MHz)

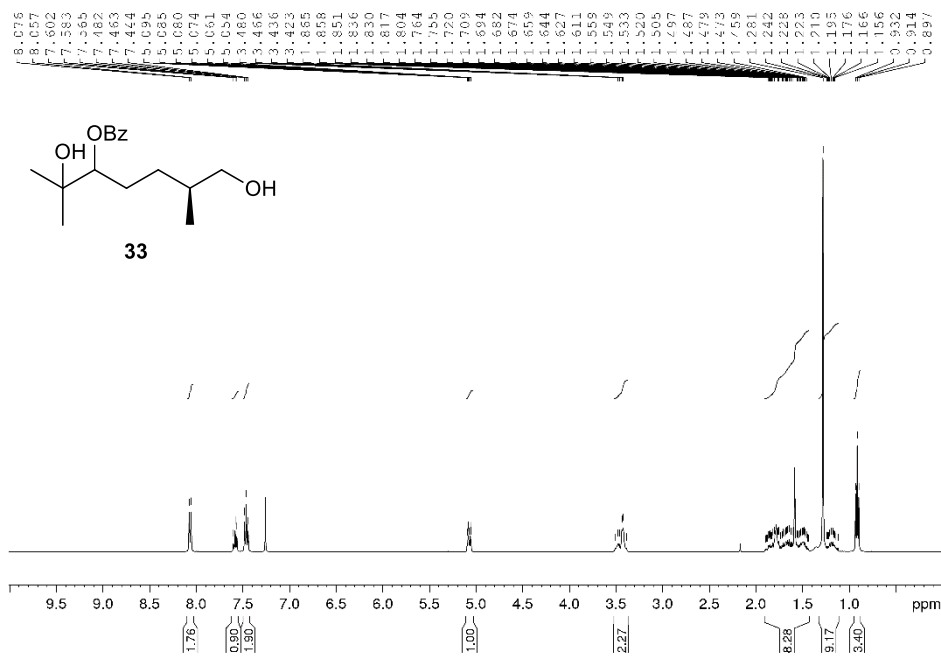


Figure 2.28. ¹H NMR spectrum of compound **33** (CDCl₃, 400 MHz)

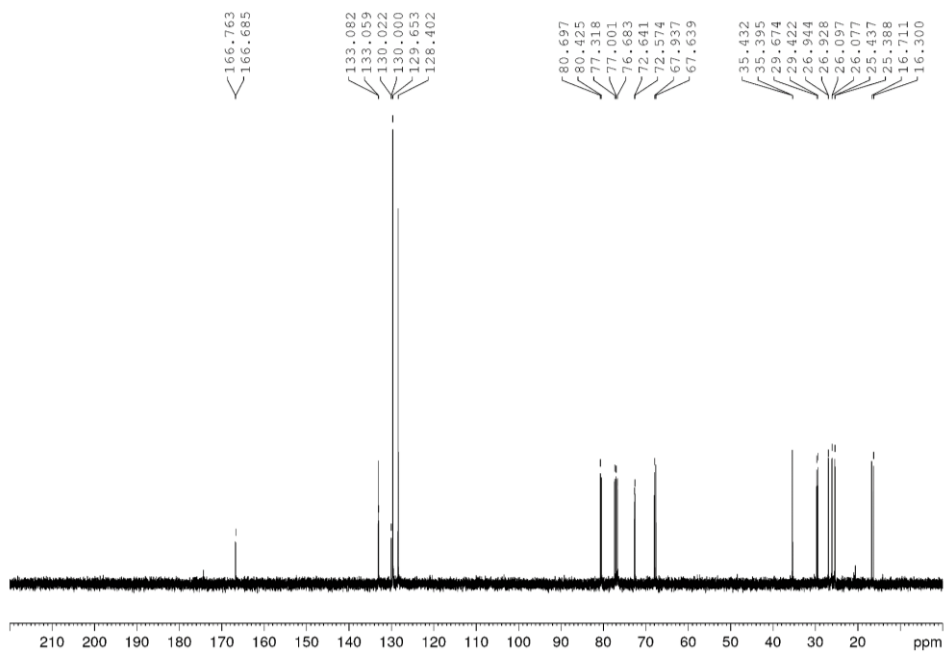


Figure 2.29. ¹³C NMR spectrum of compound **33** (CDCl₃, 100 MHz)

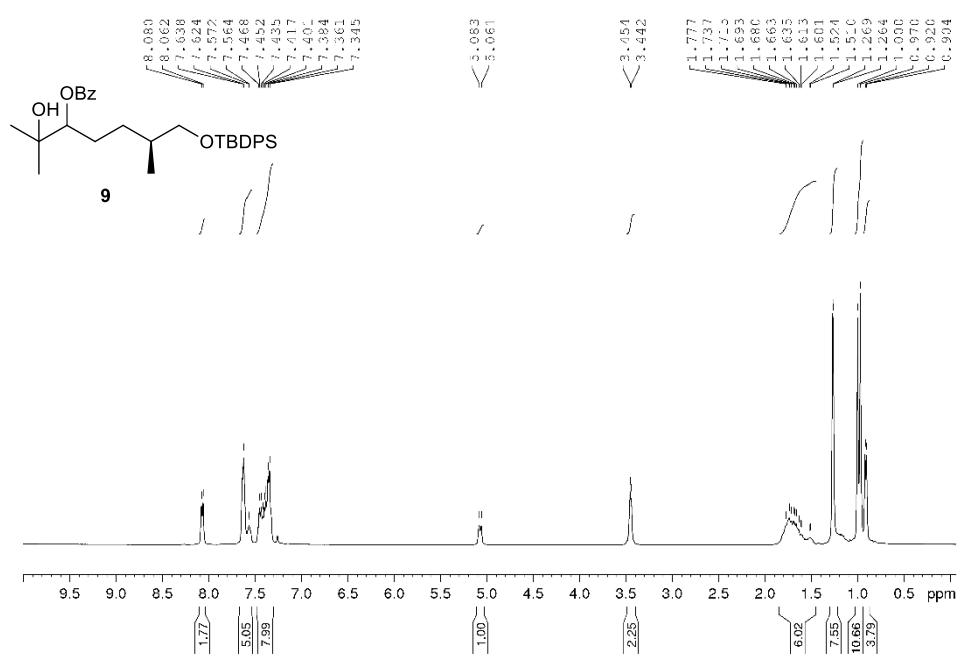


Figure 2.30. ¹H NMR spectrum of compound 9 (CDCl₃, 400 MHz)

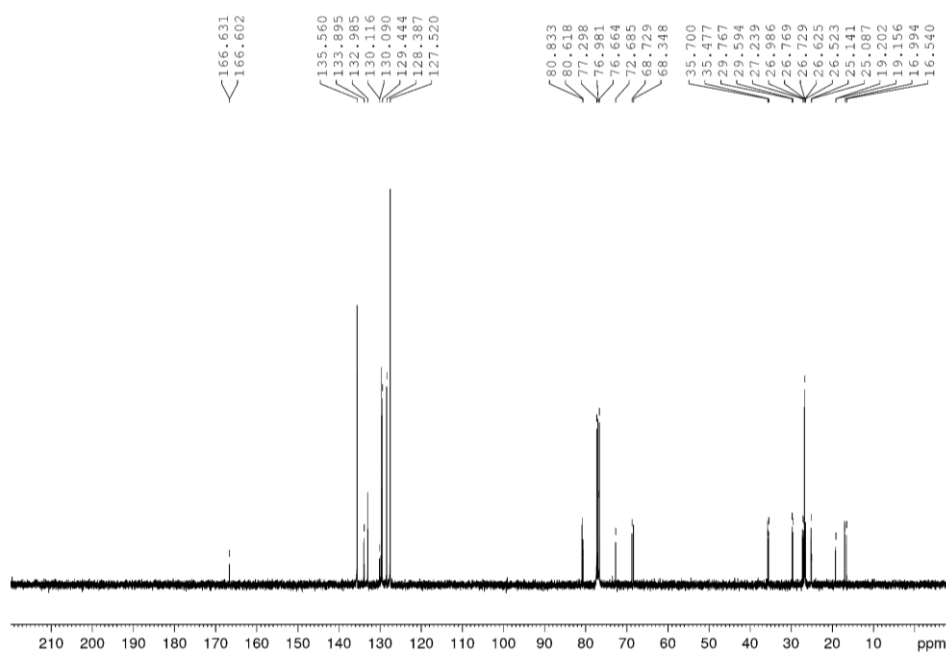


Figure 2.31. ¹³C NMR spectrum of compound 9 (CDCl₃, 100 MHz)

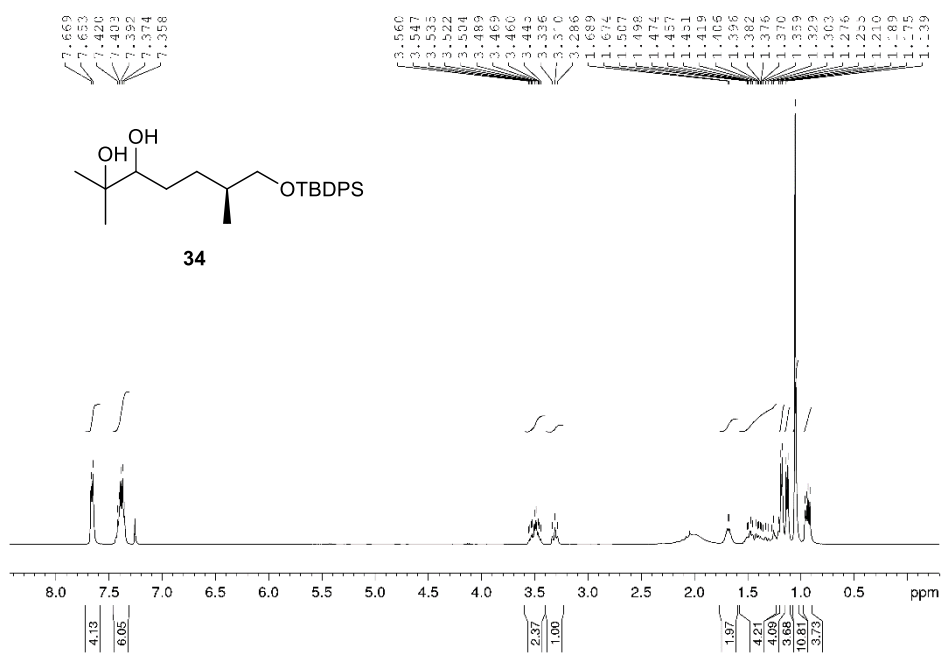


Figure 2.32. ^1H NMR spectrum of compound 34 (CDCl_3 , 400 MHz)

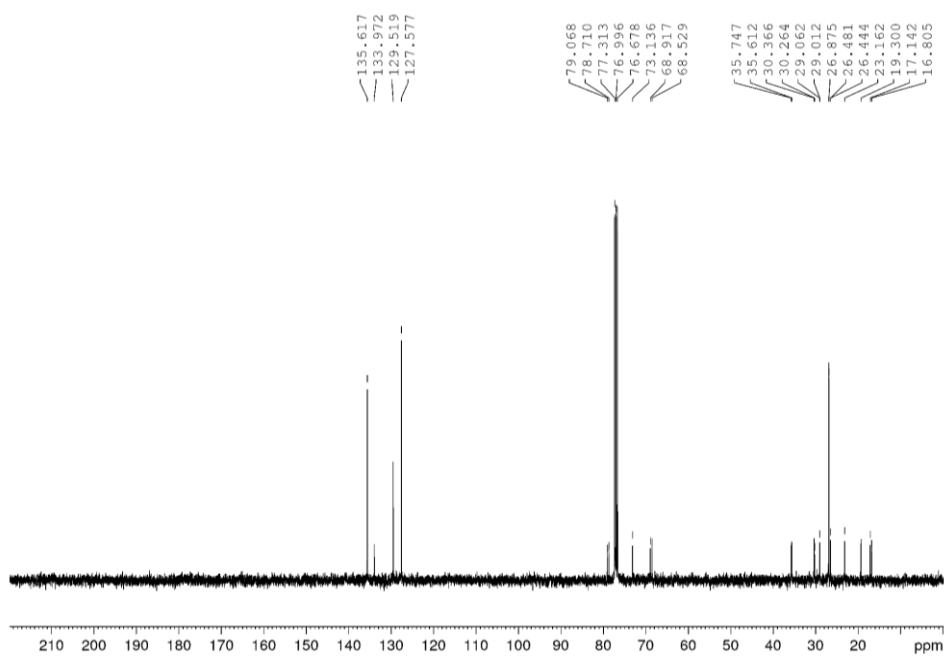


Figure 2.33. ^{13}C NMR spectrum of compound 34 (CDCl_3 , 100 MHz)

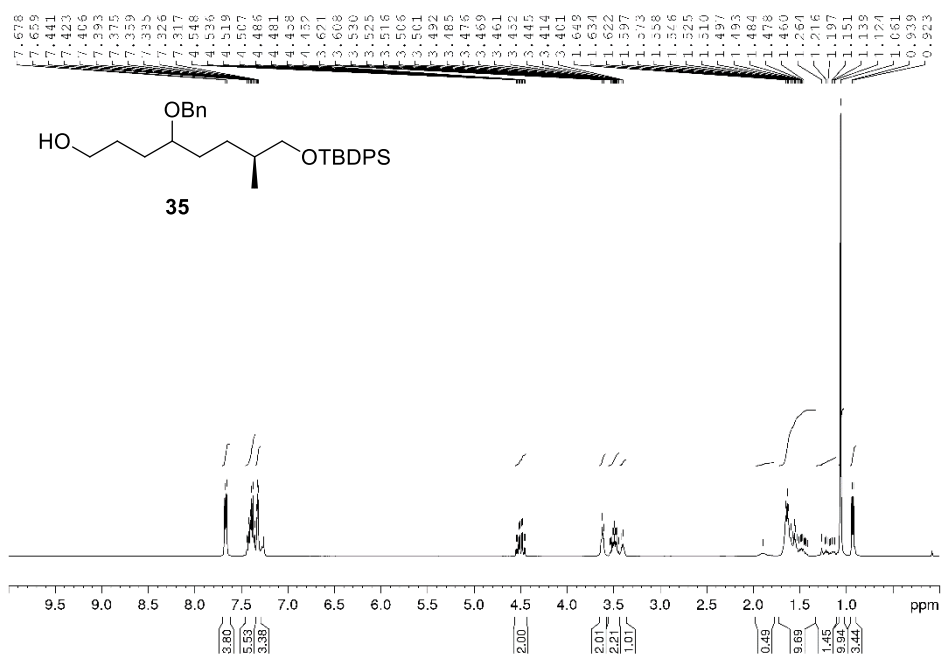


Figure 2.39. ¹H NMR spectrum of compound **35** (CDCl₃, 400 MHz)

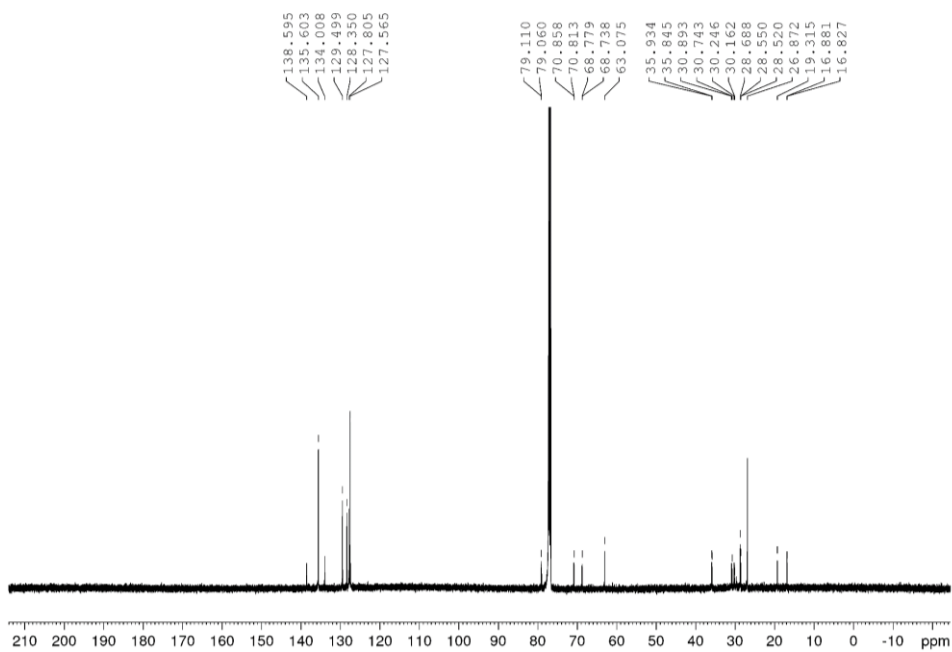


Figure 2.40. ¹³C NMR spectrum of compound **35** (CDCl₃, 100 MHz)

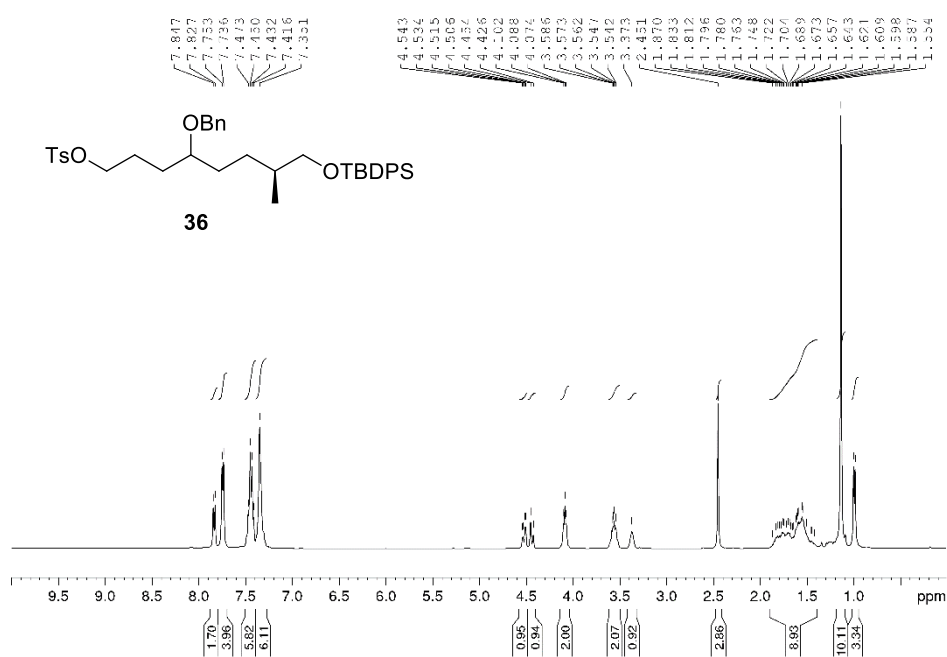


Figure 2.41. ¹H NMR spectrum of compound **36** (CDCl₃, 400 MHz)

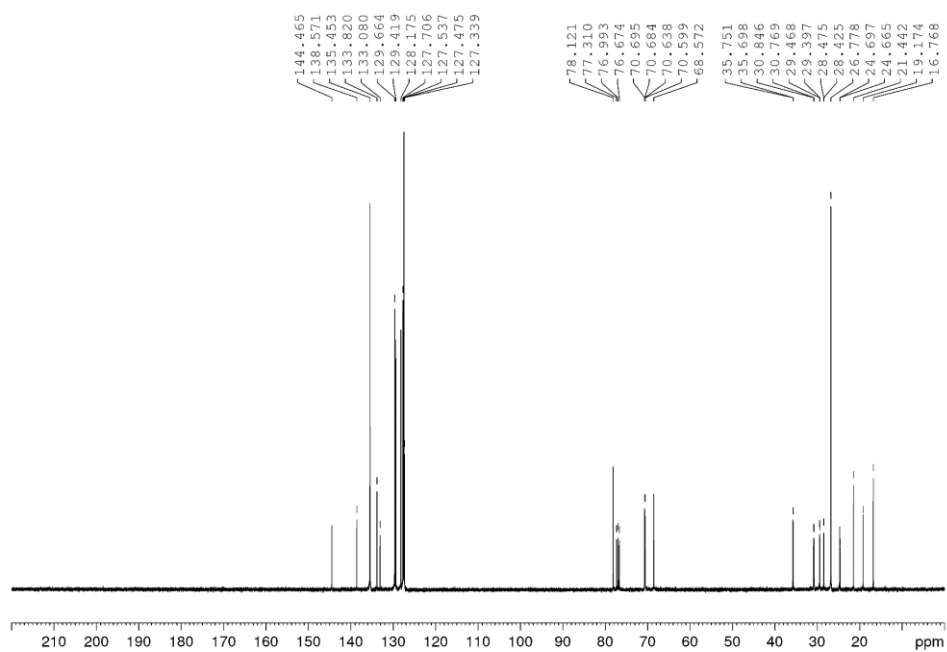


Figure 2.42. ¹³C NMR spectrum of compound **36** (CDCl₃, 100 MHz)

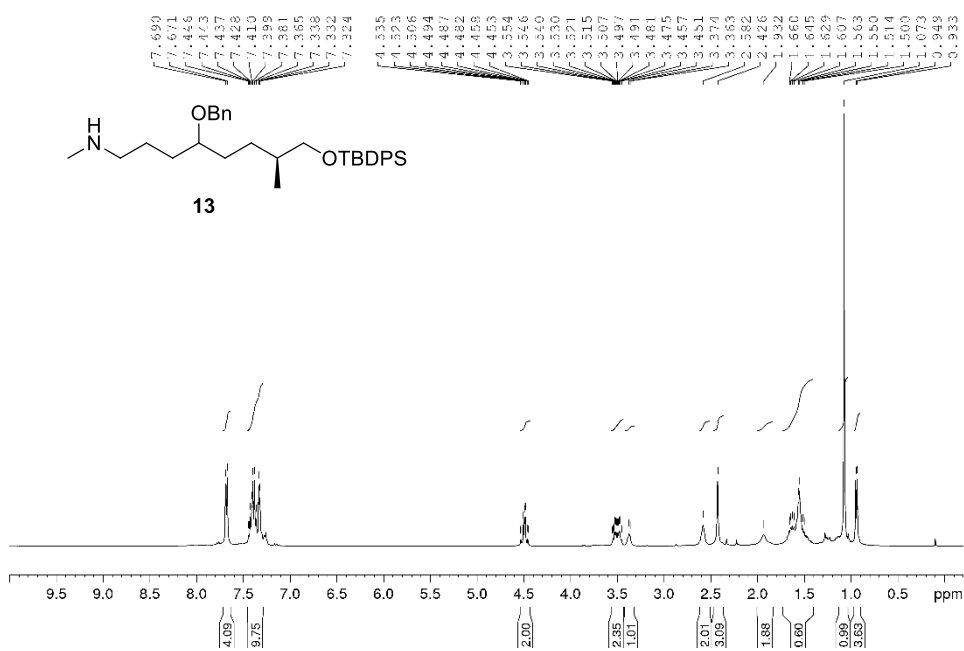


Figure 2.43. ^1H NMR spectrum of compound 13 (CDCl_3 , 400 MHz)

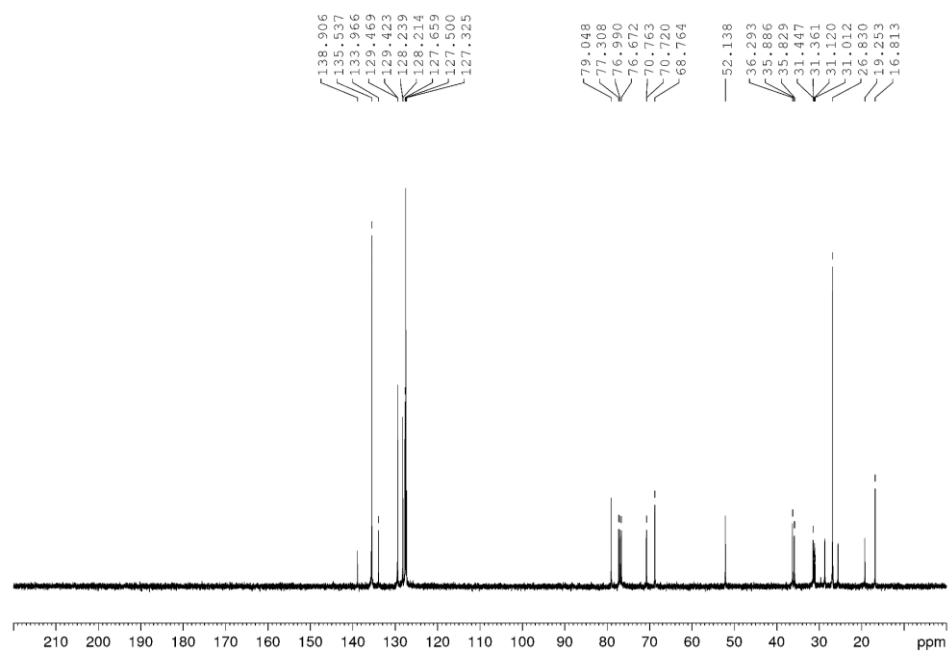


Figure 2.44. ^{13}C NMR spectrum of compound 13 (CDCl_3 , 100 MHz)

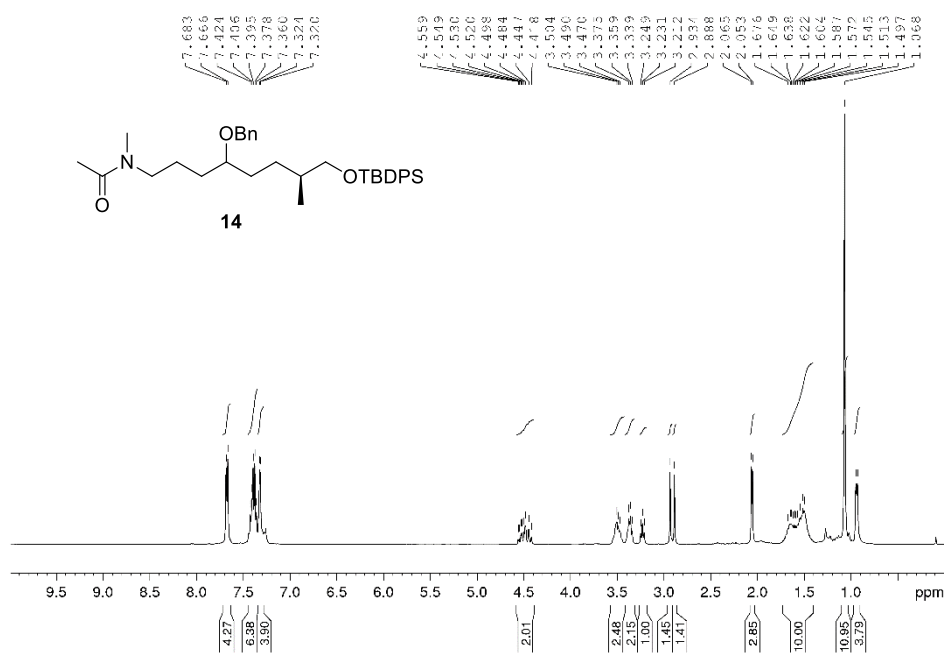


Figure 2.45. ^1H NMR spectrum of compound **14** (CDCl₃, 400 MHz)

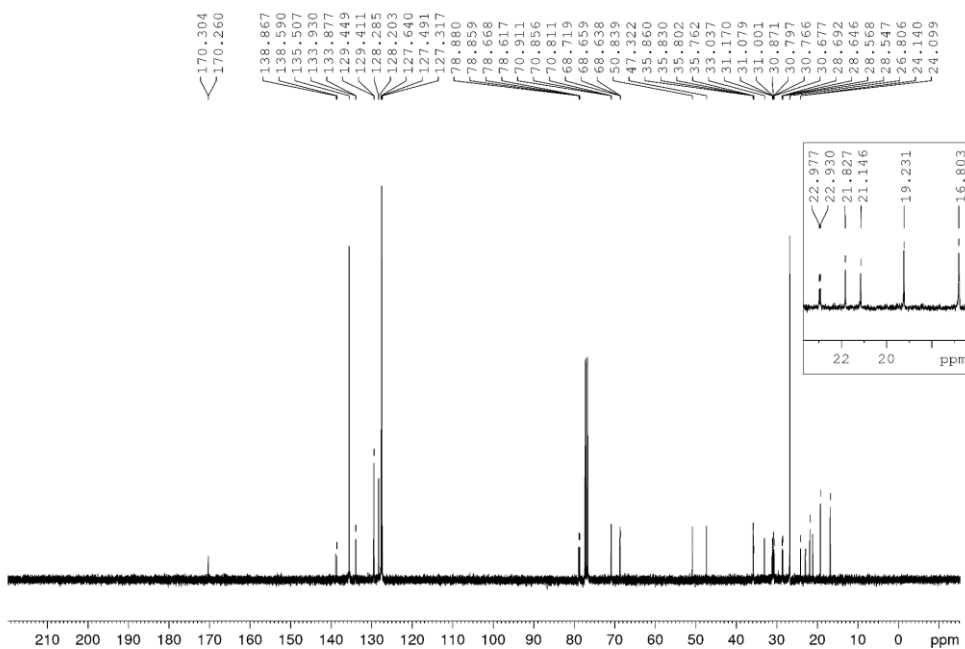


Figure 2.46. ^{13}C NMR spectrum of compound **14** (CDCl₃, 100 MHz)

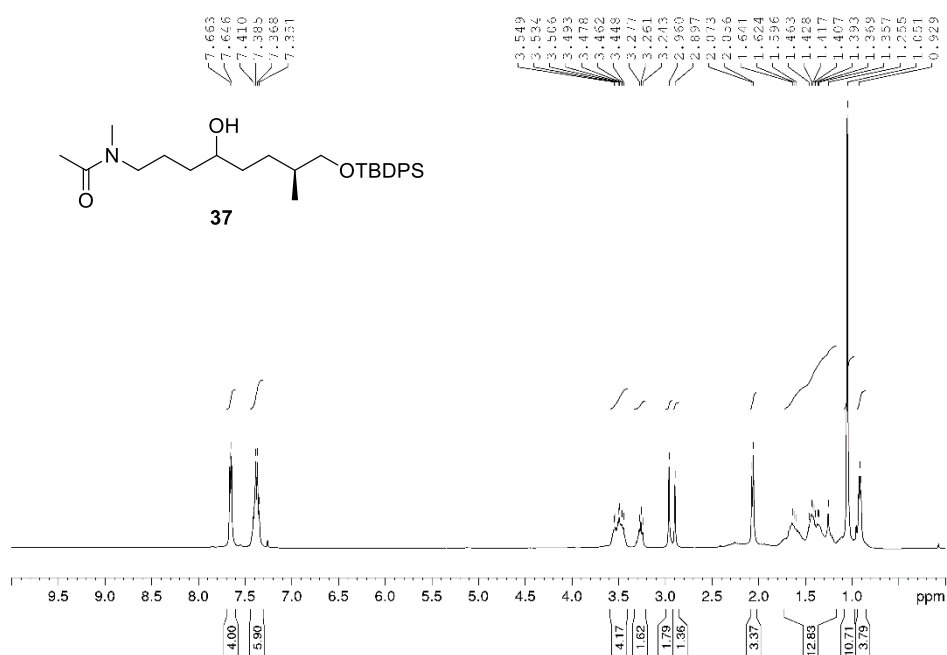


Figure 2.47. ¹H NMR spectrum of compound 37 (CDCl₃, 400 MHz)

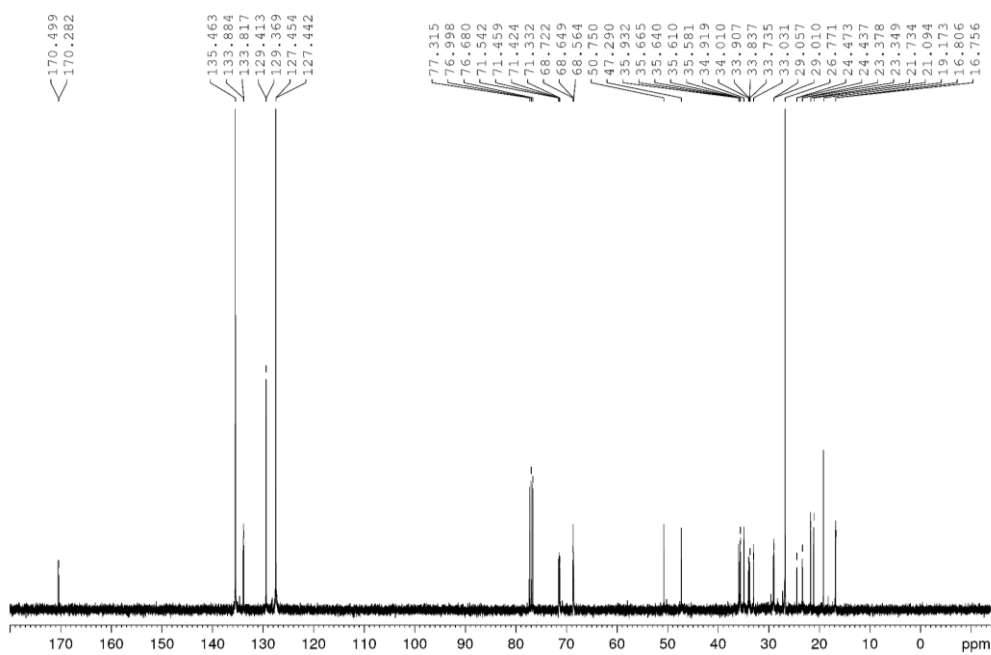


Figure 2.48. ¹³C NMR spectrum of compound 37 (CDCl₃, 100 MHz)

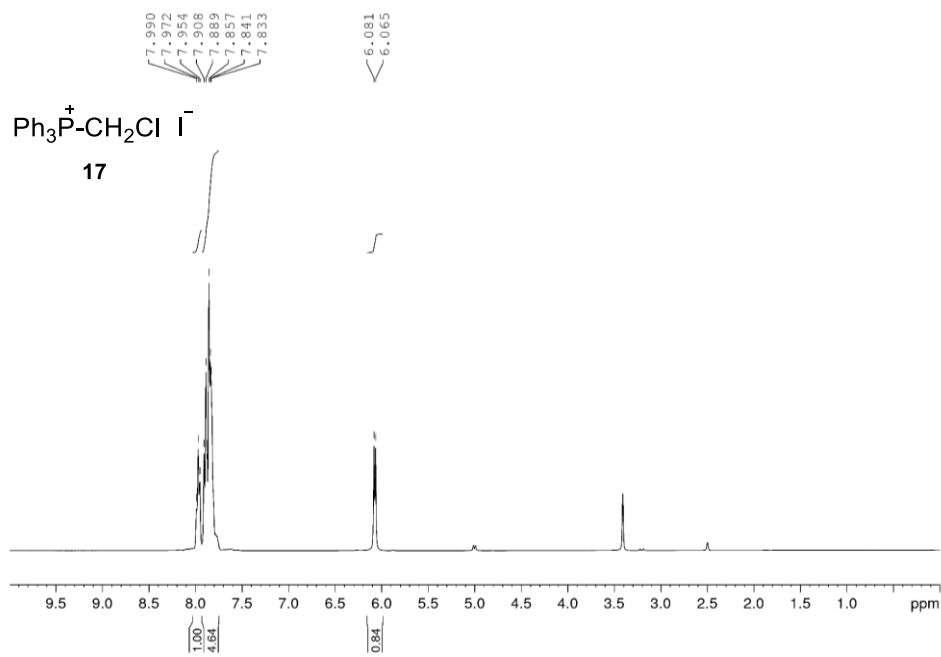


Figure 2.53. ^1H NMR spectrum of compound 17 (DMSO, 400 MHz)

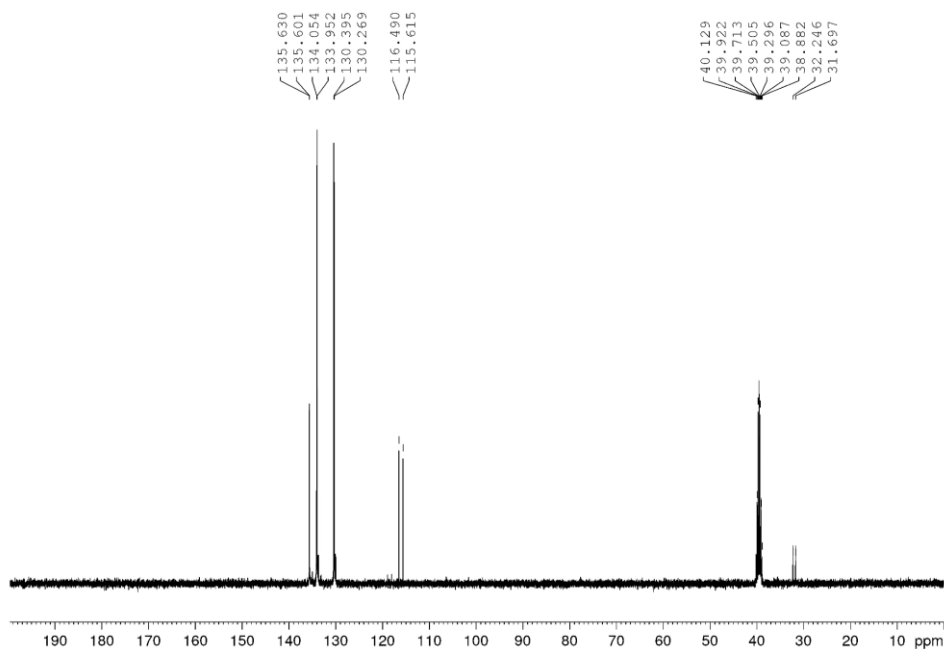


Figure 2.54. ^{13}C NMR spectrum of compound 17 (DMSO, 100 MHz)

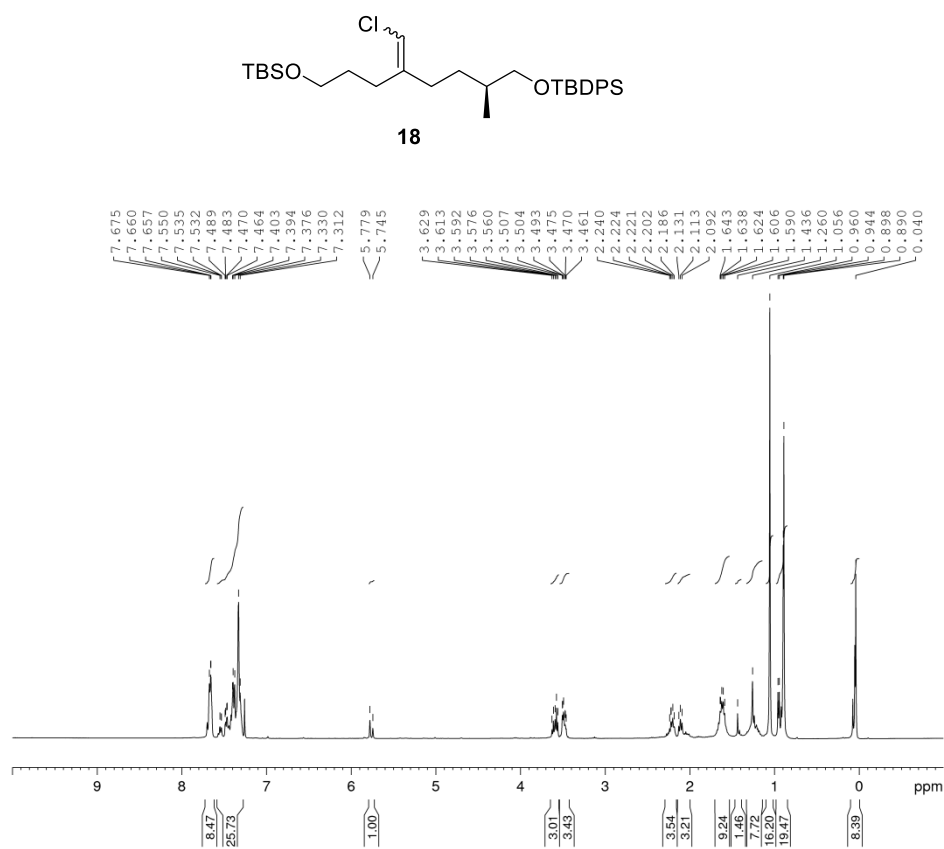


Figure 2.55. ¹H NMR spectrum of compounds **18** (CDCl₃, 400 MHz)

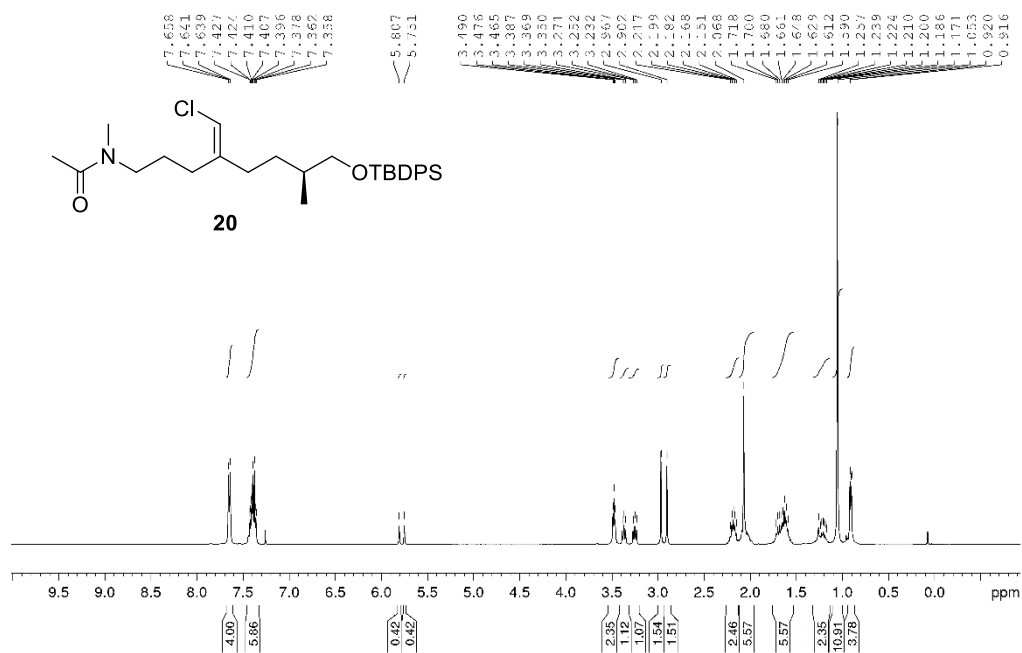


Figure 2.56. ^1H NMR spectrum of compound **20** (CDCl_3 , 400 MHz)

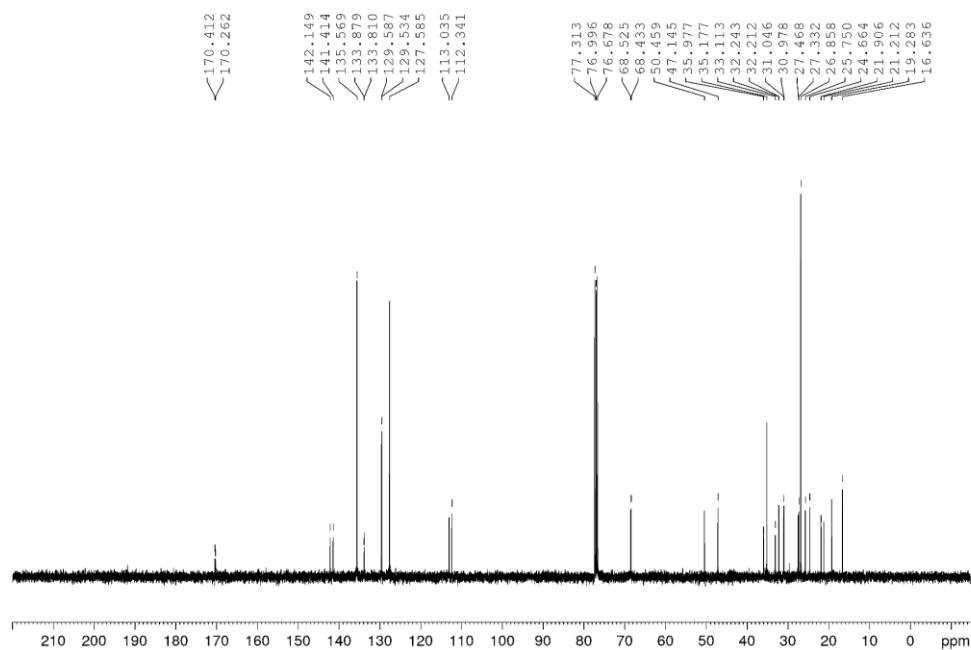


Figure 2.57. ^{13}C NMR spectrum of compound **20** (CDCl_3 , 100 MHz)

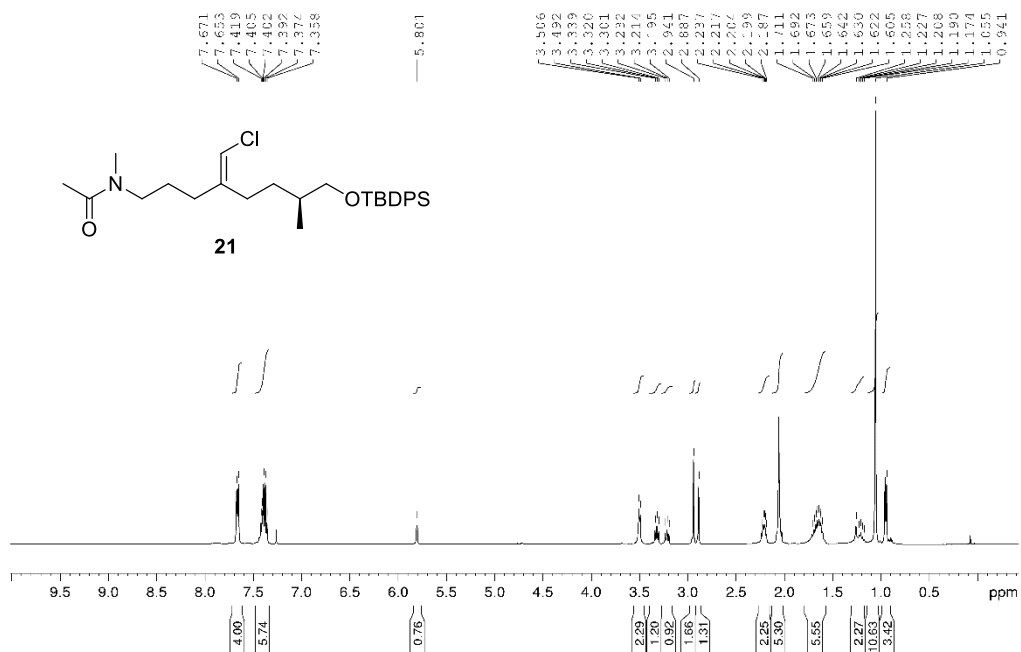


Figure 2.58. ^1H NMR spectrum of compound **21** (CDCl_3 , 400 MHz)

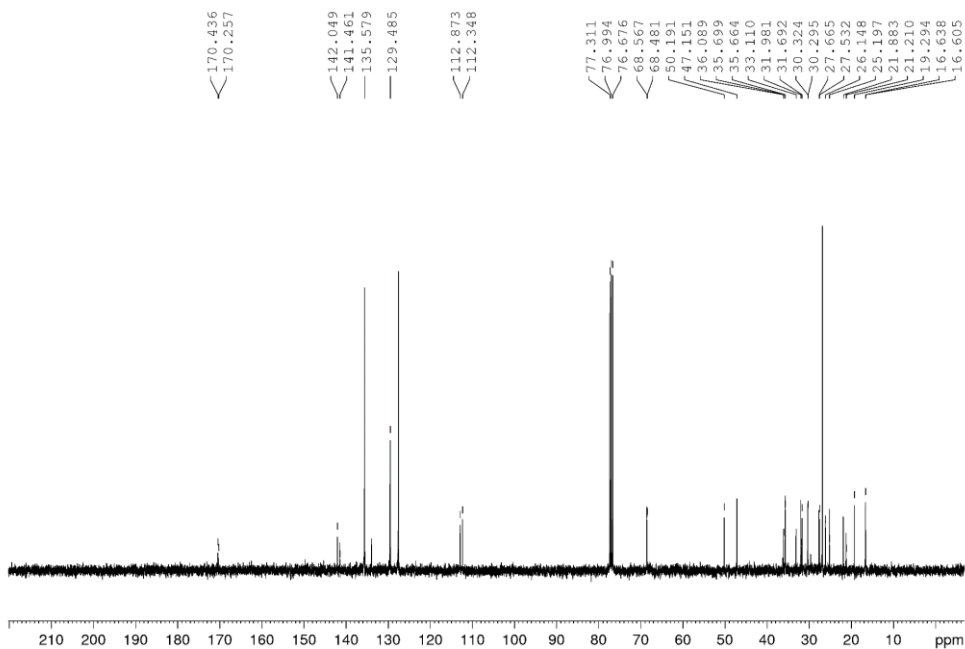


Figure 2.59. ^{13}C NMR spectrum of compound **21** (CDCl_3 , 100 MHz)

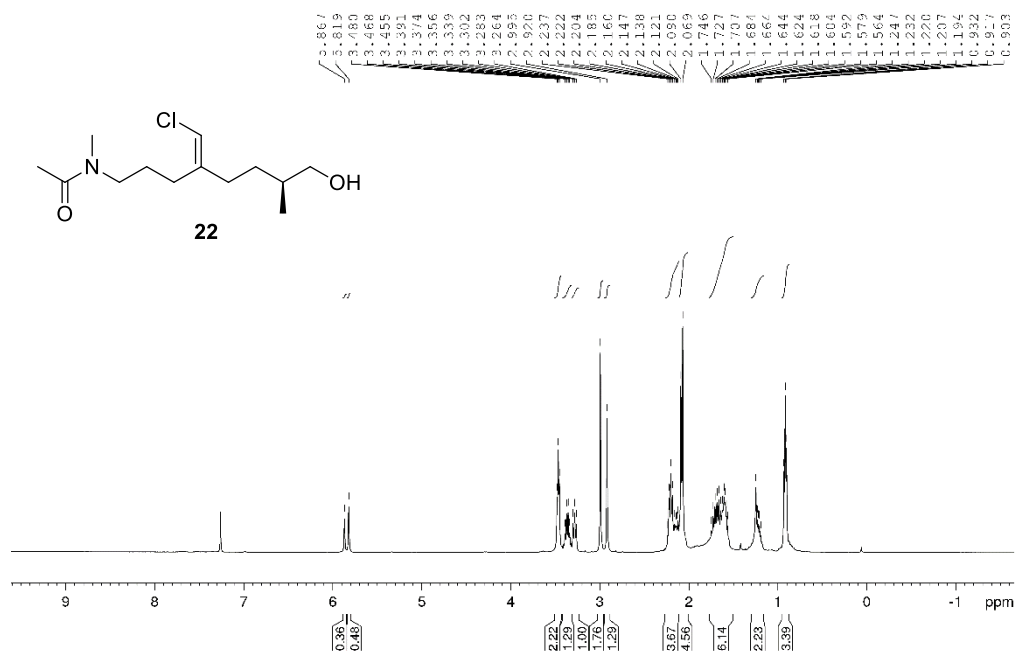


Figure 2.60. ¹H NMR spectrum of compound 22 (CDCl₃, 400 MHz)

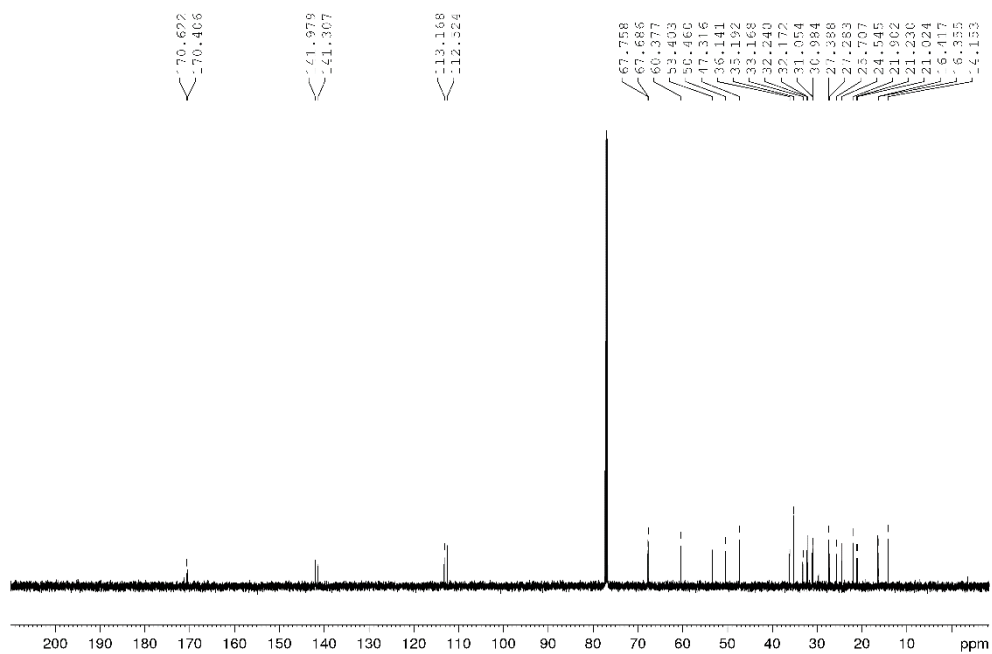


Figure 2.61. ¹³C NMR spectrum of compound 22 (CDCl₃, 100 MHz)

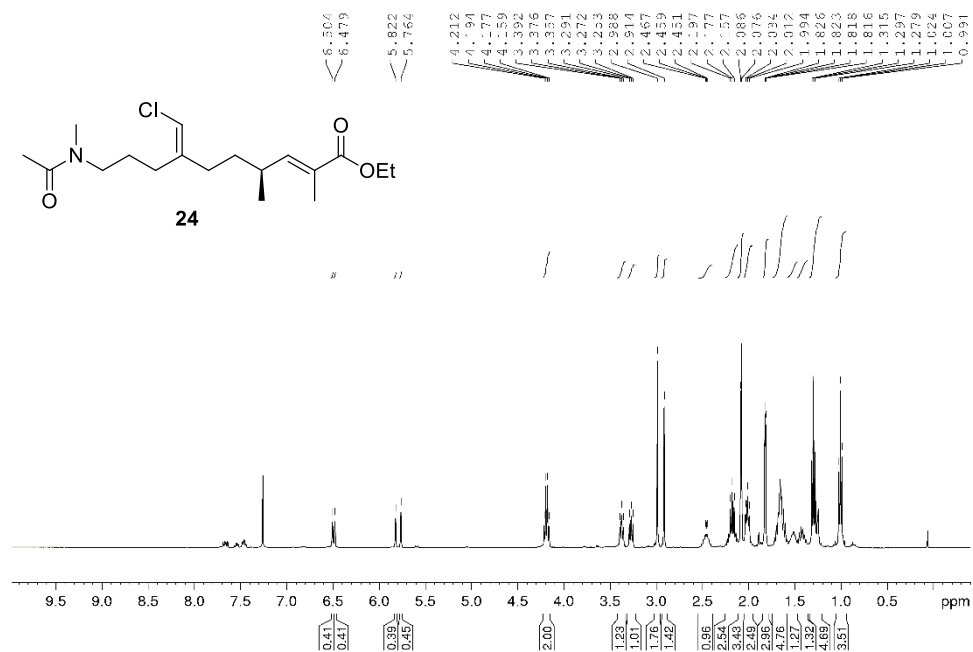


Figure 2.62. ^1H NMR spectrum of compound **24** (CDCl_3 , 400 MHz)

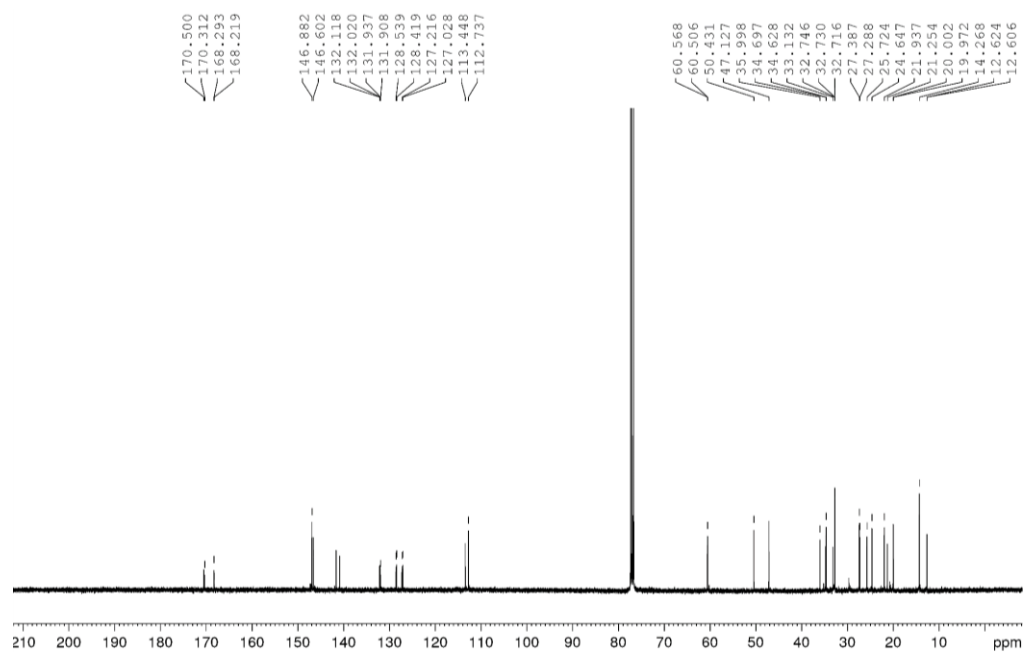


Figure 2.63. ^{13}C NMR spectrum of compound **24** (CDCl_3 , 100 MHz)

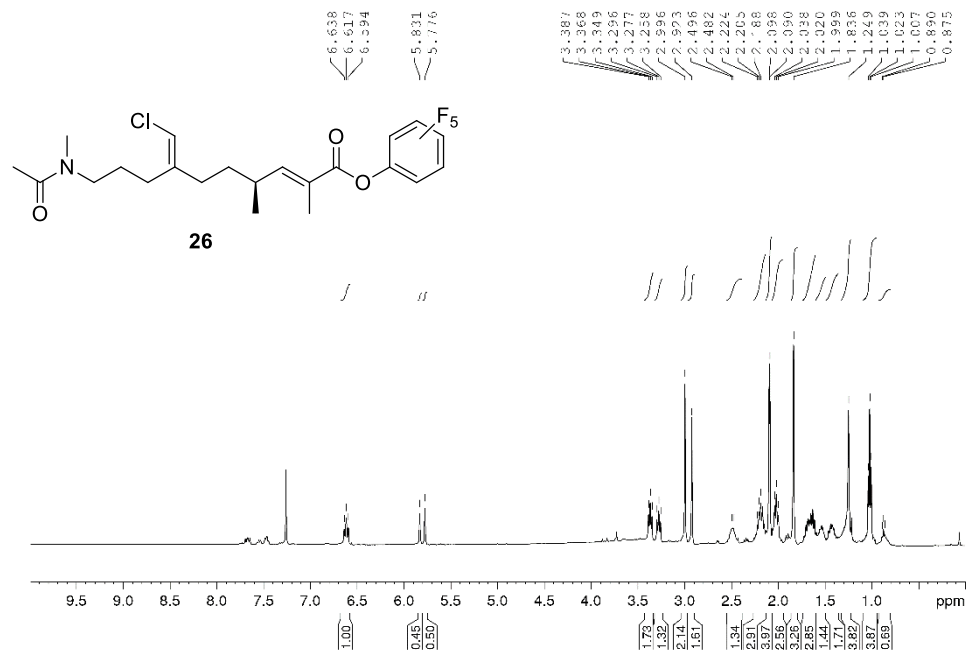


Figure 2.64. ^1H NMR spectrum of compound **26** (CDCl_3 , 400 MHz)

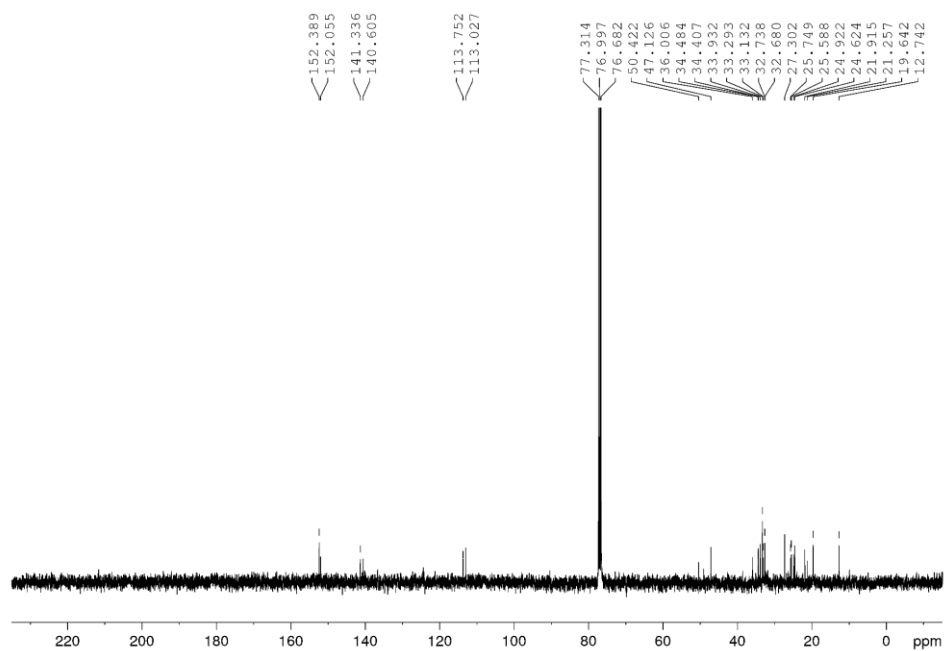


Figure 2.65. ^{13}C NMR spectrum of compound **26** (CDCl_3 , 400 MHz)

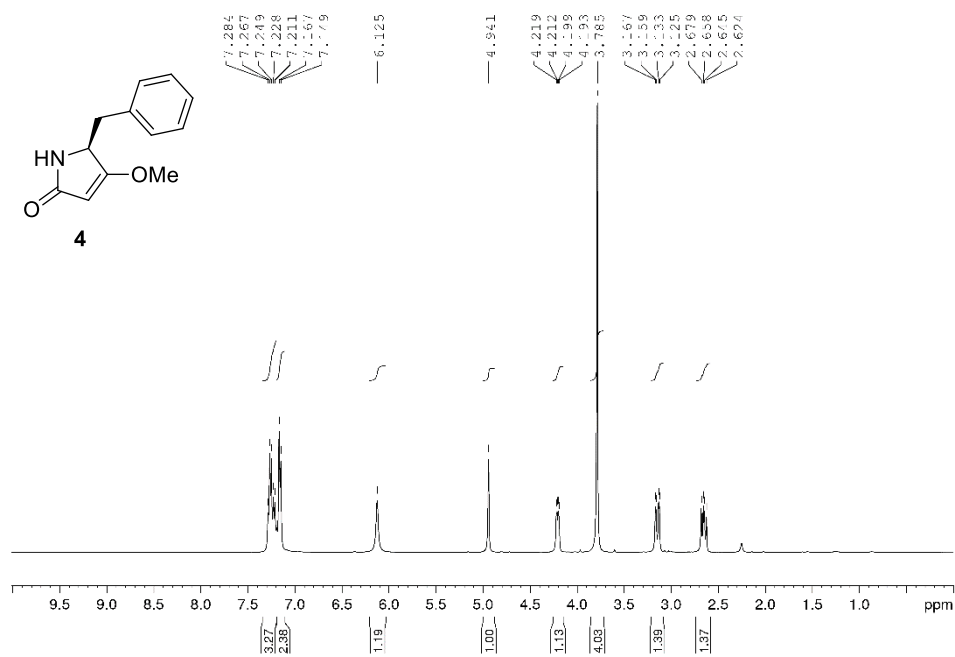


Figure 2.66. ¹H NMR spectrum of compound 4 (CDCl₃, 400 MHz)

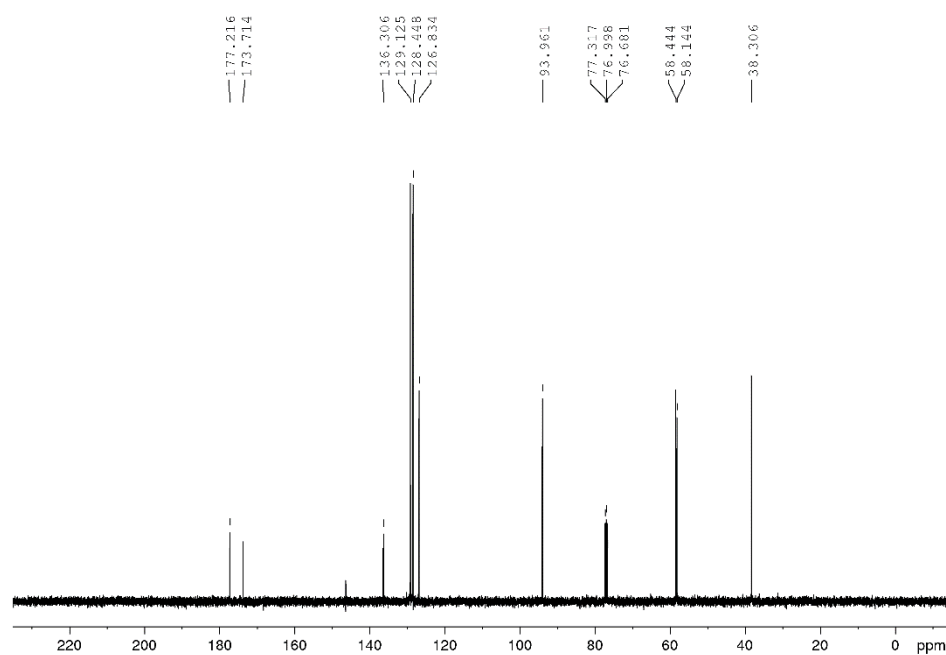


Figure 2.67. ¹³C NMR spectrum of compound 4 (CDCl₃, 100 MHz)

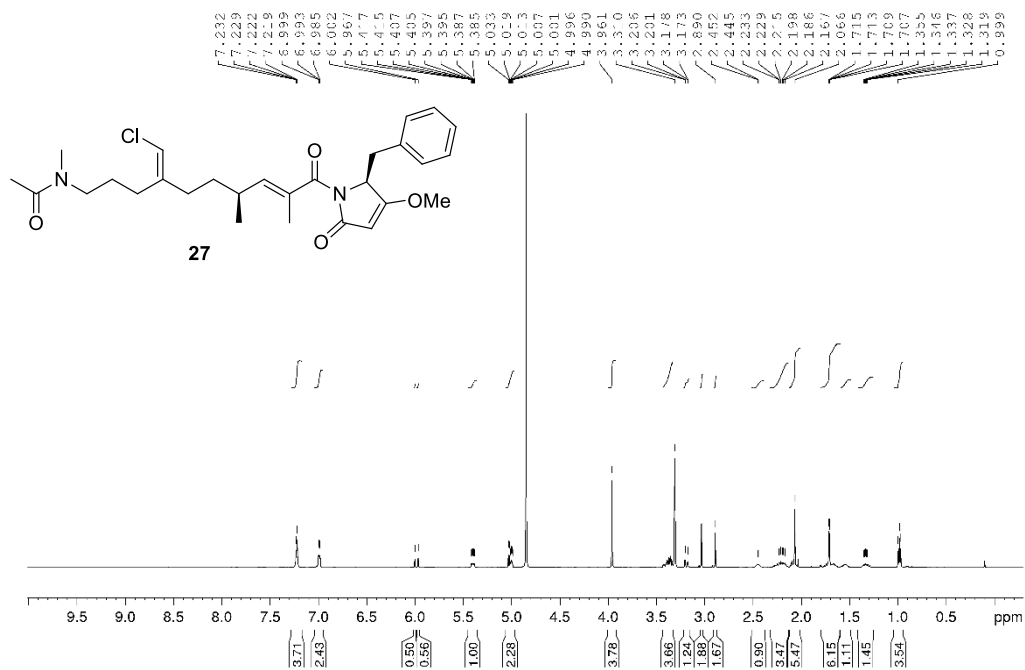


Figure 2.68. ¹H NMR spectrum of compound 27 (CD₃OD, 500 MHz)

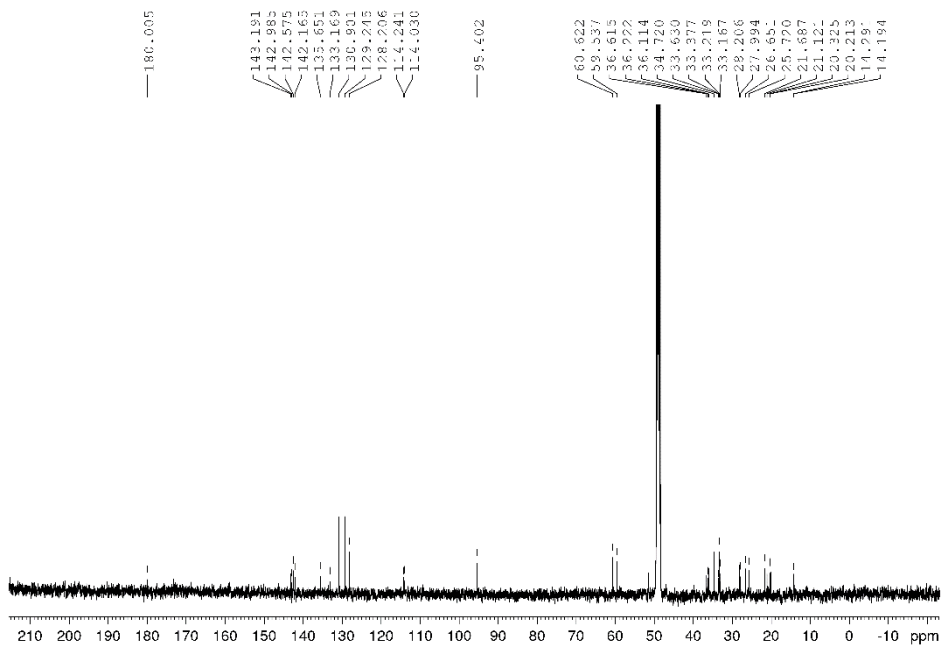


Figure 2.69. ¹³C NMR spectrum of compound 27 (CD₃OD, 125 MHz)

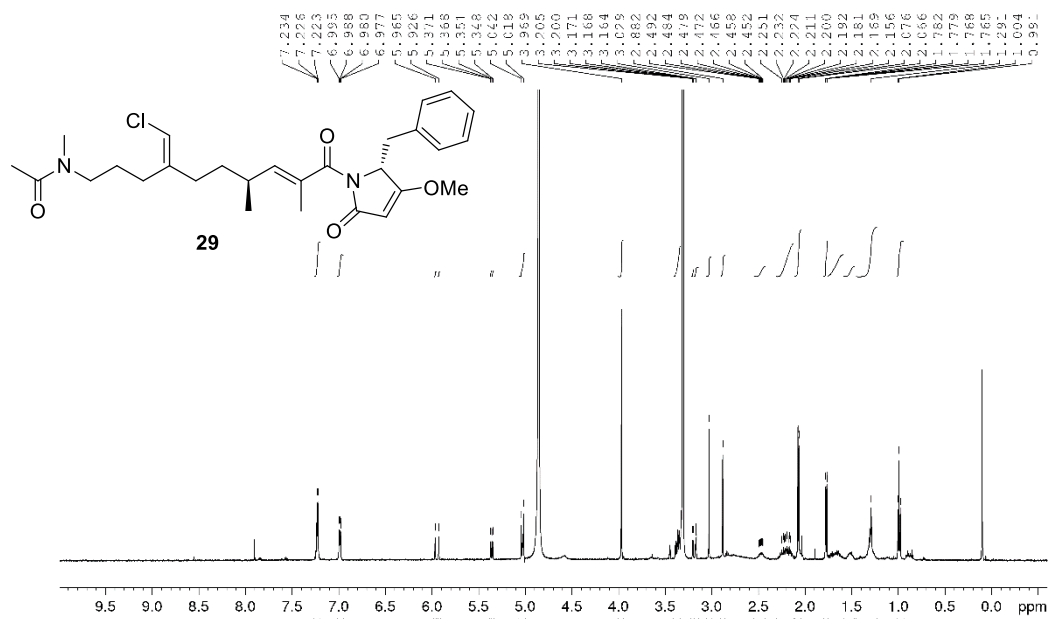


Figure 2.70. ¹H NMR spectrum of compound 29 (CD₃OD, 700 MHz)

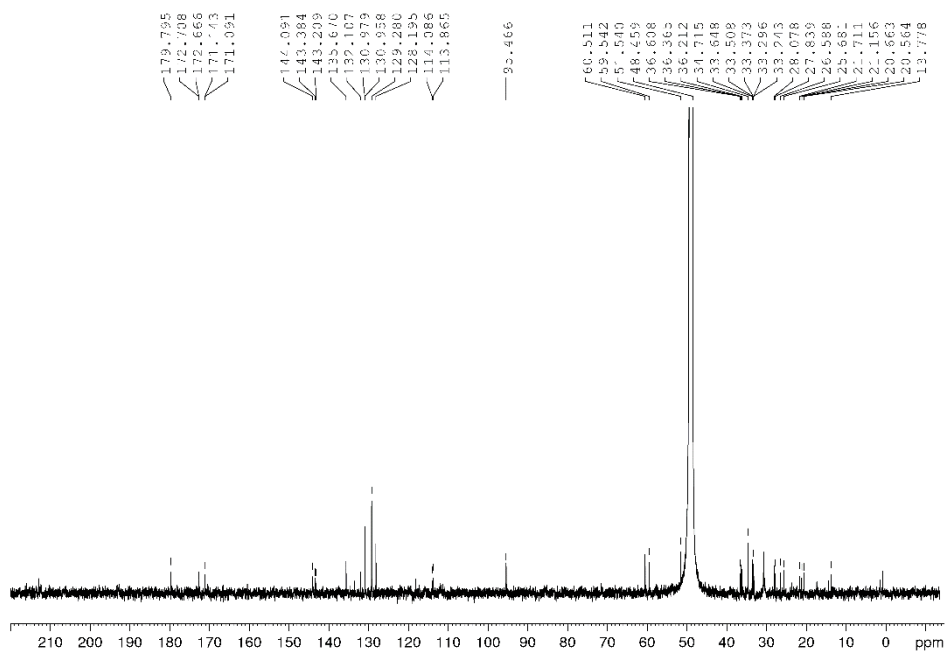


Figure 2.71. ¹³C NMR spectrum of compound 29 (CD₃OD, 175 MHz)

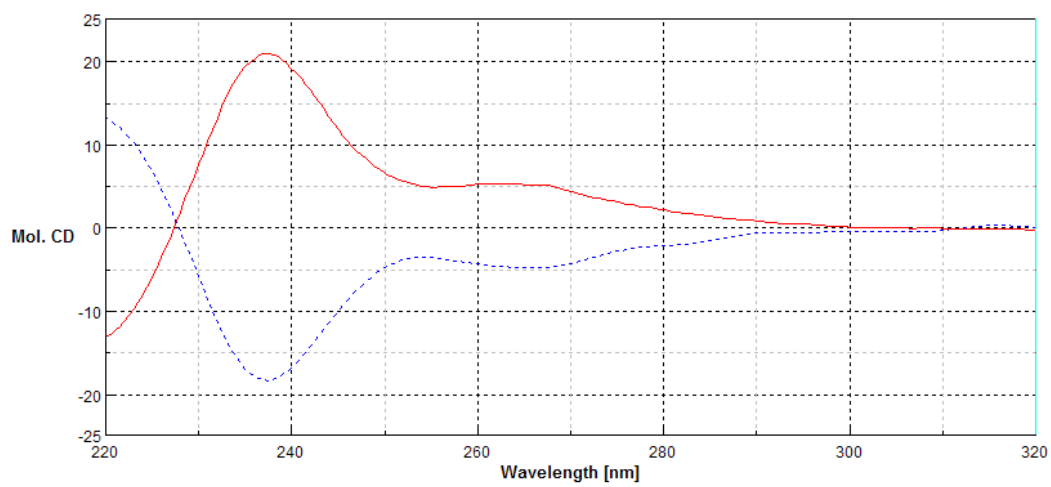


Figure 2.72. ECD spectra of natural smenamamide A (solid red line) and *ent*-smenamamide A (**29**) (dashed blue line).

Table 1. NMR data of natural smenamamide A (1) and *ent*-smenamamide A (29) (700 MHz, CD₃OD).

		smenamamide A						<i>ent</i> -smenamamide A					
		Z-Conformer			E-Conformer			Z-Conformer			E-Conformer		
Position	δ_H [Mult., J (Hz)]	δ_C [Mult.]	δ_H [Mult., J (Hz)]	δ_C [Mult.]	Position	δ_H [Mult., J (Hz)]	δ_C [Mult.]	δ_H [Mult., J (Hz)]	δ_C [Mult.]	Position	δ_H [Mult., J (Hz)]	δ_C [Mult.]	δ_C [Mult.]
1	–	135.6 (C)	–	135.6 (C)	1	–	135.7 (C)	–	135.7 (C)	–	–	–	135.7 (C)
2/6	6.99 (m)	130.8 (CH)	6.99 (m)	130.8 (CH)	2/6	6.90 (m)	130.9 (CH)	6.90 (m)	130.9 (CH)	6.90 (m)	6.90 (m)	130.9 (CH)	130.9 (CH)
3/5	7.23 (ovl)	129.4 (CH)	7.23 (ovl)	129.4 (CH)	3/5	7.23 (ovl)	129.3 (CH)	7.23 (ovl)	129.3 (CH)	7.23 (ovl)	7.23 (ovl)	129.3 (CH)	129.3 (CH)
4	7.23 (ovl)	128.3 (CH)	7.23 (ovl)	128.3 (CH)	4	7.23 (ovl)	128.3 (CH)	7.23 (ovl)	128.2 (CH)	7.23 (ovl)	7.23 (ovl)	128.2 (CH)	128.2 (CH)
7	a 3.37 (ovl)	34.8 (CH ₂)	3.37 (ovl)	34.8 (CH ₂)	7	a 3.36 (ovl)	34.8 (CH ₂)	3.36 (ovl)	34.7 (CH ₂)	7	a 3.36 (ovl)	34.7 (CH ₂)	34.7 (CH ₂)
	b 3.19 (m)		3.19 (m)			b 3.20 (m)		3.20 (m)			3.20 (m)		
8	5.02 (ovl)	60.5 (CH)	5.02 (ovl)	60.5 (CH)	8	5.02 (ovl)	60.5 (CH)	5.02 (ovl)	60.5 (CH)	8	5.02 (ovl)	60.5 (CH)	60.5 (CH)
9	–	179.5 (C)	–	179.5 (C)	9	–	179.8 (C)	–	179.8 (C)	9	–	179.8 (C)	179.8 (C)
10	5.04 (br. s)	95.5 (CH)	5.02 (br. s)	95.5 (CH)	10	5.04 (br. s)	95.5 (CH)	5.04 (br. s)	95.5 (CH)	10	5.04 (br. s)	95.5 (CH)	95.5 (CH)
11	–	170.7 (C)	–	170.7 (C)	11	–	171.1 (C)	–	171.1 (C)	11	–	171.1 (C)	171.1 (C)
12	–	172.3 (C)	–	172.2 (C)	12	–	172.7 (C)	–	172.7 (C)	12	–	172.7 (C)	172.7 (C)
13	–	132.1 (C)	–	132.1 (C)	13	–	132.1 (C)	–	132.1 (C)	13	–	132.1 (C)	132.1 (C)
14	1.77 (d, 1.5)	13.7 (CH ₃)	1.78 (d, 1.5)	13.7 (CH ₃)	14	1.77 (d, 1.4)	13.7 (CH ₃)	1.77 (d, 1.4)	13.7 (CH ₃)	14	1.78 (d, 1.4)	13.7 (CH ₃)	13.7 (CH ₃)
15	5.36 (br. d, 10.2)	144.1 (CH)	5.36 (br. d, 10.2)	144.1 (CH)	15	5.36 (br. d, 10.1)	144.1 (CH)	5.36 (br. d, 10.1)	144.1 (CH)	15	5.36 (br. d, 10.1)	144.1 (CH)	144.1 (CH)
16	2.45 (m)	33.4 (CH)	2.48 (m)	33.4 (CH)	16	2.45 (m)	33.4 (CH)	2.45 (m)	33.4 (CH)	16	2.48 (m)	33.5 (CH)	33.5 (CH)
17	0.98 (d, 6.5)	20.4 (CH ₃)	1.00 (d, 6.5)	20.6 (CH ₃)	17	0.98 (d, 6.5)	20.6 (CH ₃)	0.98 (d, 6.5)	20.6 (CH ₃)	17	1.00 (d, 6.5)	20.7 (CH ₃)	20.7 (CH ₃)
18	a 1.51 (ovl)	36.1 (CH ₂)	1.52 (ovl)	35.9 (CH ₂)	18	a 1.51 (ovl)	36.4 (CH ₂)	1.51 (ovl)	36.4 (CH ₂)	18	a 1.51 (ovl)	36.2 (CH ₂)	36.2 (CH ₂)
	b 1.28 (ovl)		1.30 (ovl)			b 1.29 (ovl)		1.29 (ovl)			b 1.29 (ovl)		
19	a 2.19 (ovl)	33.2 (CH ₂)	2.23 (ovl)	33.2 (CH ₂)	19	a 2.19 (ovl)	33.2 (CH ₂)	2.19 (ovl)	33.2 (CH ₂)	19	a 2.23 (ovl)	33.3 (CH ₂)	33.3 (CH ₂)
	b 2.06 (ovl)		2.05 (ovl)			b 2.05 (ovl)		2.05 (ovl)			b 2.05 (ovl)		
20	–	143.1 (C)	–	142.8 (C)	20	–	143.4 (C)	–	143.4 (C)	20	–	143.4 (C)	143.2 (C)
21	5.93 (br. s)	113.9 (CH)	5.97 (br. s)	114.1 (CH)	21	5.97 (br. s)	113.9 (CH)	5.92 (br. s)	113.9 (CH)	21	5.96 (br. s)	114.1 (CH)	114.1 (CH)
22	a 2.22 (m)	28.1 (CH ₂)	2.26 (m)	28.0 (CH ₂)	22	a 2.22 (m)	28.1 (CH ₂)	2.22 (m)	28.1 (CH ₂)	22	a 2.26 (m)	27.9 (CH ₂)	27.9 (CH ₂)
	b 2.15 (m)		2.18 (m)			b 2.15 (m)		2.15 (m)			b 2.18 (m)		
23	1.64 (m)	25.9 (CH ₂)	1.70 (m)	26.6 (CH ₂)	23	1.65 (m)	25.7 (CH ₂)	1.65 (m)	25.7 (CH ₂)	23	1.70 (m)	26.6 (CH ₂)	26.6 (CH ₂)
24	3.36 (ovl)	48.6 (CH ₂)	3.33 (ovl)	51.5 (CH ₂)	24	3.36 (ovl)	48.4 (CH ₂)	3.36 (ovl)	48.4 (CH ₂)	24	3.34 (ovl)	51.6 (CH ₂)	51.6 (CH ₂)
25	–	172.9 (C)	–	172.7 (C)	25	–	172.7 (C)	–	172.7 (C)	25	–	172.7 (C)	172.7 (C)
26	2.08 (s)	21.7 (CH ₃)	2.07 (s)	21.1 (CH ₃)	26	2.08 (s)	21.7 (CH ₃)	2.08 (s)	21.7 (CH ₃)	26	2.07 (s)	21.0 (CH ₃)	21.0 (CH ₃)
27	3.03 (s)	36.6 (CH ₃)	2.88 (s)	33.7 (CH ₃)	27	3.03 (s)	36.6 (CH ₃)	3.03 (s)	36.6 (CH ₃)	27	2.88 (s)	33.7 (CH ₃)	33.7 (CH ₃)
OMe	3.97 (s)	59.7 (CH ₃)	3.97 (s)	59.7 (CH ₃)	OMe	3.97 (s)	59.7 (CH ₃)	3.95 (s)	59.6 (CH ₃)	OMe	3.95 (s)	59.6 (CH ₃)	59.6 (CH ₃)

Table 2.1. NMR data of natural smenamamide A and *ent*-smenamamide A.

References

-
- ¹ Anand, P.; Kunnumakara, A.B.; Sundaram, C.; Harikumar, K.B.; Tharakan, S.T.; Lai, O. S.; Sung, B.; Aggarwal, Bharat B. *Pharm. Res.* **2008**, *25*, 2097-2116.
- ² Kravchenko, J.; Akushevich, I.; Manton, K.G.; *Cancer mortality and morbidity patterns in the U. S. population: an interdisciplinary approach* Berlin, Springer, **2009**.
- ³ Moudi, M.; Go, R.; Yong Seok Yien, C.; Nazre, M. *Int. J. Prev. Med.* **2013**, *4(11)*, 1231-1235.
- ⁴ Wani, M.C.; Taylor, H.L.; Wall, M.E. et al. *J Am Chem Soc* **1971**; *93*: 2325-7.
- ⁵ Newman, D.J.; Cragg, G.M. *Mar. Drugs* **2014**, *12*, 255-278.
- ⁶ Newman, D.J.; Giddings, L.A. *Phytochem. Rev.* **2013**, *12*, 293-304.
- ⁷ R. Teta, E. Irollo, G. Della Sala, G. Pirozzi, A. Mangoni, V. Costantino, *Marine Drugs*, **2013**, *11* (11), 4451-4463.
- ⁸ Esposito G., Teta R., Miceli R., Ceccarelli L., Della Sala G., Camerlingo R., Irollo E., Mangoni A., Pirozzi G., Costantino V., *Mar. Drugs* **2015**, *13*, 444-459.
- ⁹ G. Esposito, G. Della Sala, R. Teta, A. Caso, M.L. Bouguet-Kondracki, J.R. Pawlik, A. Mangoni, V. Costantino, *Eur. J. Org. Chem.* **2016**, *16*, 2871–2875.
- ¹⁰ A. Caso, A. Mangoni, G. Piccialli, V. Costantino, V. Piccialli, *ACS Omega*, **2017**, *2*, 1477–1488.
- ¹¹ A. Caso, I. Laurenzana, D. Lamorte, S. Trino, G. Esposito, V. Piccialli, and V. Costantino, *Mar. Drugs*, **2018**, accepted.
- ¹² Pettit, G. R.; Kamano, Y.; Dufresne, C.; Cerny, R. L.; Herald, C. L.; Schmidt, J. M. *J. Org. Chem.* **1989**, *54*, 6005–6006.
- ¹³ Edwards, D. J.; Marquez, B. L.; Nogle, L. M.; McPhail, K.; Goeger, D. E.; Roberts, M. A.; Gerwick, W. H. *Chem. Biol.* **2004**, *11*, 817–833.
- ¹⁴ Marfey, P. *Carlsberg Res. Commun.* **1984**, *49*, 591-596.
- ¹⁵ Hosseini, M.; Kringelum, H.; Murray, A.; Tønder, J. E. *Org. Lett.* **2006**, *8*, 2103-2106. (b) Conroy, T.; Guo, J. T.; Linington, R. G.; Hunt, N. H.; Payne, R. J. *Chem. Eur. J.* **2011**, *17*, 13544-13552.
- ¹⁶ Hosseini, M.; Tanner, D.; Murray, A.; Tønder, J. E. *Org. Biomol. Chem.* **2007**, *5*, 3486-3494.
- ¹⁷ a) Sharpless, K. B.; Ojima, I. *VCH publishers.* **1993**. b) Kolb, H.C.; VanNienwenhze, M. S.; Sharpless, K. B. *Chem. Rev.* **1994**, *94*, 2483-2557.

-
- ¹⁸ Kocienski, P. J. *Ed. G. Thieme*. **1994**, 38.
- ¹⁹ Yi, C. S.; Martinelli, L. C.; DeWitt Blanton, C. Jr. *J. Org. Chem.* **1978**, 43, 405-409.
- ²⁰ (a) Ley, S. V.; Norman, J.; Griffith, W. P.; Marsden, S. P. *Synthesis*. **1994**, 639-666. (b) Piccialli, V. *Molecules*. **2014**, 19, 6534-6582.
- ²¹ (a) Miyano, S.; Izumi, Y.; Fujii, K.; Ohno, Y.; Hashimoto, H. *Bull. Chem. Soc. Jpn.* **1979**, 52, 1197-1202. (b) Kahnberg, P.; Sterner, O. *Tetrahedron*, **2001**, 57, 7181-7184. (c) Kahnberg, P.; Lee, C. W.; Grubbs, R. H.; Sterner, O. *Tetrahedron*, **2002**, 58, 5203-5208. (d) Chen, J.; Shi, Z.-F.; Zhou, L.; Xie, A.-L.; Cao, X.-P. *Tetrahedron*, **2010**, 66, 3499-3507. (e) Zhang, J.-T.; Qi, X.-L.; Chen, J.; Li, B.-S.; Zhou, Y.-B.; Cao, X.-P. *J. Org. Chem.* **2011**, 76, 3946-3959. (f) Esmieu, W. R.; Worden, S. M.; Catterick, D.; Wilson, C.; Hayes, C. J. *Org. Lett.* **2008**, 10, 3045-3048.
- ²² Graf, K. M.; Tabor, M. G.; Brown, M. L.; Paige, M. *Org. Lett.* **2009**, 11, 5382-5385.
- ²³ Mitchell, T. N.; Killing, H.; Dicke, R.; Wickenkamp, R. *Chem. Commun.* **1985**, 354-355.
- ²⁴ (a) Erver, F.; Hilt, G. *J. Org. Chem.* **2012**, 77, 5215-5219. (b) Kigoshi, H.; Kita, M.; Ogawa, S.; Itoh, M.; Uemura, D. *Org. Lett.* **2003**, 5, 957-960.
- ²⁵ Mitsunobu, O.; Yamada, M.; Mukaiyama, T. *Bull. Chem. Soc. Jpn.* **1967**, 40, 10, 2380-2382.
- ²⁶ Lan, H.-Q.; Ye, J.-L.; Wang, A.-E.; Ruan, Y.-P.; Huang, P.-Q. *Chem. Eur. J.* **2011**, 17, 958-968.
- ²⁷ (a) Andrus, M. B.; Li, W.; Keyes, R. F. *J. Org. Chem.* **1997**, 62, 5542-5549. (b) Andrus, M. B.; Li, W.; Keyes, R. F. *Tetrahedron Lett.* **1998**, 39, 5465-5468.
- ²⁸ Mori, K. *Tetrahedron* **2008**, 64, 4060-4071.

Chapter 3

Synthesis and biological activity of eight smenamide A-functional analogues

As part of a broad research project focused on the study of the chemistry of marine natural products and their synthetic or semi-synthetic derivatives, a flexible synthetic route, aimed to the synthesis of new bioactive compounds, was planned. Smenamide A is a hybrid peptide/polyketide (PKS/NRPS) compound possessing a promising cytotoxic activity against the Calu-1 lung cancer cell line.¹ Recently, two synthetic derivatives of the natural compound, namely 16-*epi*- and *ent*-smenamide A, were synthesised starting from the commercially available *S*-citronellene.² With the aim of gaining a better insight into the cytotoxic activity of smenamides family, eight shorter-chain synthetic analogues of the 16-*epi*- series have been designed and prepared.³

3.1 Synthesis of eight smenamide A-analogues of the 16-*epi*- series and their biological activity

Smenamides are small but highly functionalised organic molecules, the structure of which contains a *N*-methylacetamido western function, a chlorovinyl moiety and a pyrrolinone eastern terminal. In order to investigate the role of the three main functionalities of the molecules in the biological activity, eight shorter-chain (**8-15**) analogues of 16-*epi*-smenamide A were designed and prepared (Figure 3.1).

Although they are simplified analogues, they retain the main structural features of the natural lead compound **1**. They were indeed thought as "functional-analogues".

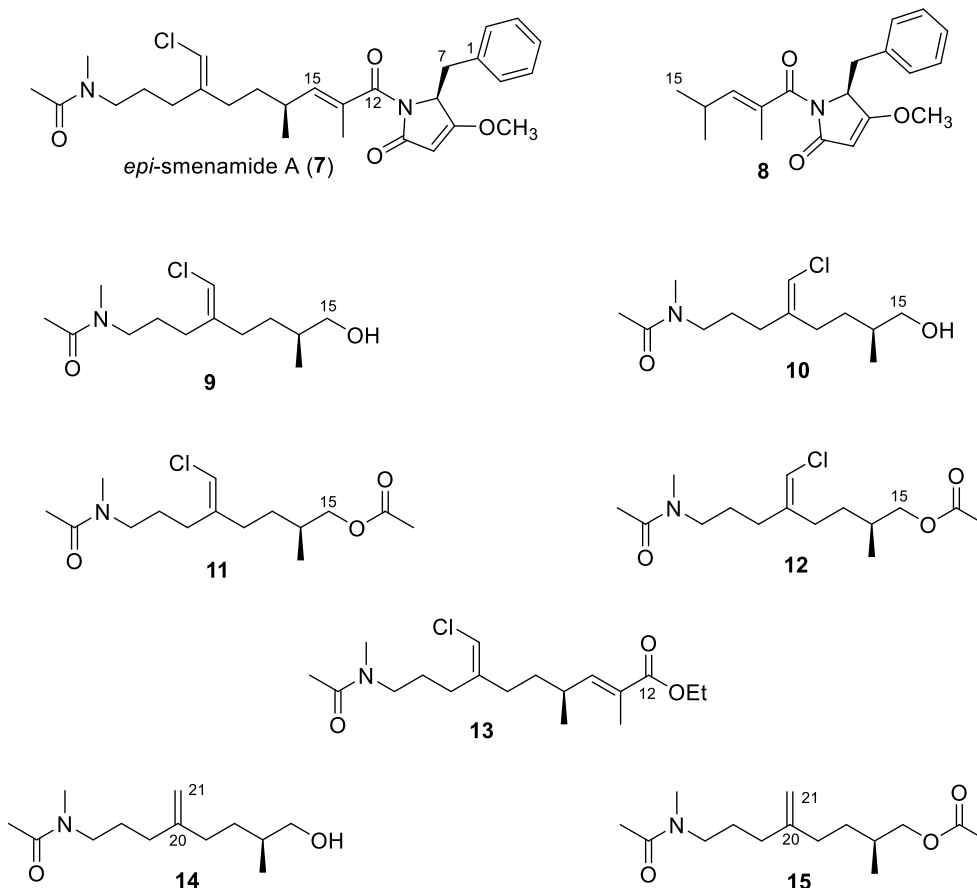


Figure 3.1. Structures of compounds 7-15.

Compound **8**, truncated in position 18, consists essentially of the dolapyrrolidinone subunit. It was prepared in order to probe the role of the pyrrolinone moiety, whereas compounds **9-15** were prepared to simulate the polyketide portion, and, more precisely, the role of the chlorine atom and the stereochemistry of C 20-21 double bond. Thanks to the flexible synthetic approach, all eight functional analogues were easily prepared. The activation of 2,4-dimethyl-2-pentenoic acid as pentafluorophenyl ester (**16**) and its subsequent coupling with the

dolapyrrolidinone subunit (**17**), previously synthesized² afforded derivative **8** (Figure 3.2) in high yield (85 %).

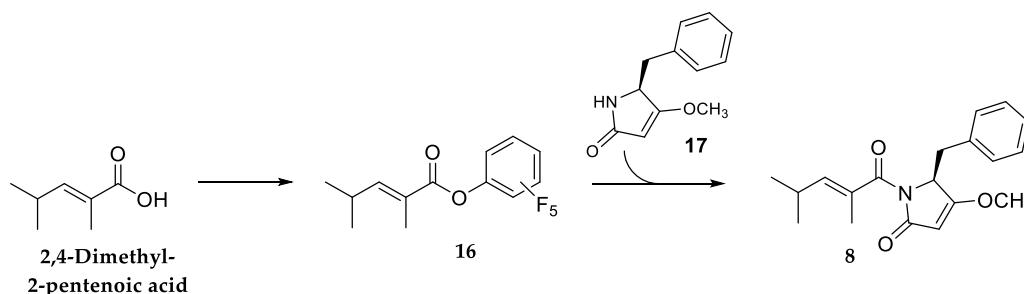


Figure 3.2. Preparation of dolapyrrolidinone derivative **8**.

As for compounds **9-15** they have been prepared according to the reported procedure,² starting from the chiral *S*-citronellene, commercially available. *S*-citronellene, properly oxidised and degraded, provided the carbon backbone of C15-C20 aldehyde, which was further manipulated affording ketone **18**. The latter is a versatile intermediate, the modification of which allowed the introduction of the desired functionalities: the chlorovinyl and the methylene moieties, and the α,β -unsaturated ethyl ester function (Figure 3.3).

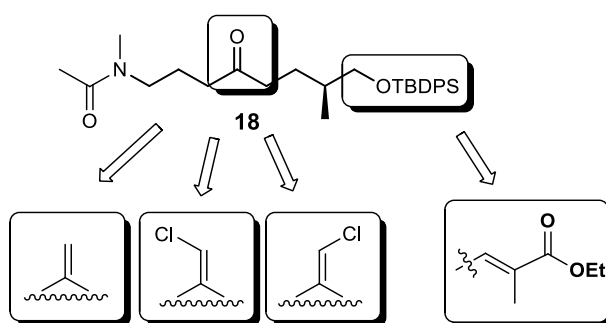


Figure 3.3. Ketone **18** as a versatile intermediate.

Compounds **9-13** were prepared as depicted in Figure 3.4. For the installation of the chlorovinyl function, we took advantage of one of the most useful C-C formation reactions: the Wittig reaction. Ketone **18** was reacted with the proper phosphonium

salt, (chloromethyl)triphenylphosphonium iodide, previously synthesized,² to get the chlorovinyl derivatives **9** and **10**, possessing the opposite configuration of the double bond. Since an unstabilised ylide was used, the process afforded both stereoisomers *Z* and *E* in ratio 3:2, respectively. **9** and **10** were then acetylated in classic conditions ($\text{Ac}_2\text{O}/\text{Pyr}$) to give the corresponding acetyl derivatives **11** and **12**. Moreover, a further modification of **9** through an oxidation under Ley's conditions ($\text{TPAP}_{(\text{cat})}/\text{NMO}$) afforded the corresponding aldehyde **21**, which was used in the subsequent Wittig reaction with the stabilized ylide, (carboethoxyethylidene)triphenylphosphorane, commercially available. The last reaction led to the synthesis of the α,β -unsaturated ethyl ester **13**, bearing the same C 13-15 double bond configuration of the natural smenamide A (**1**).

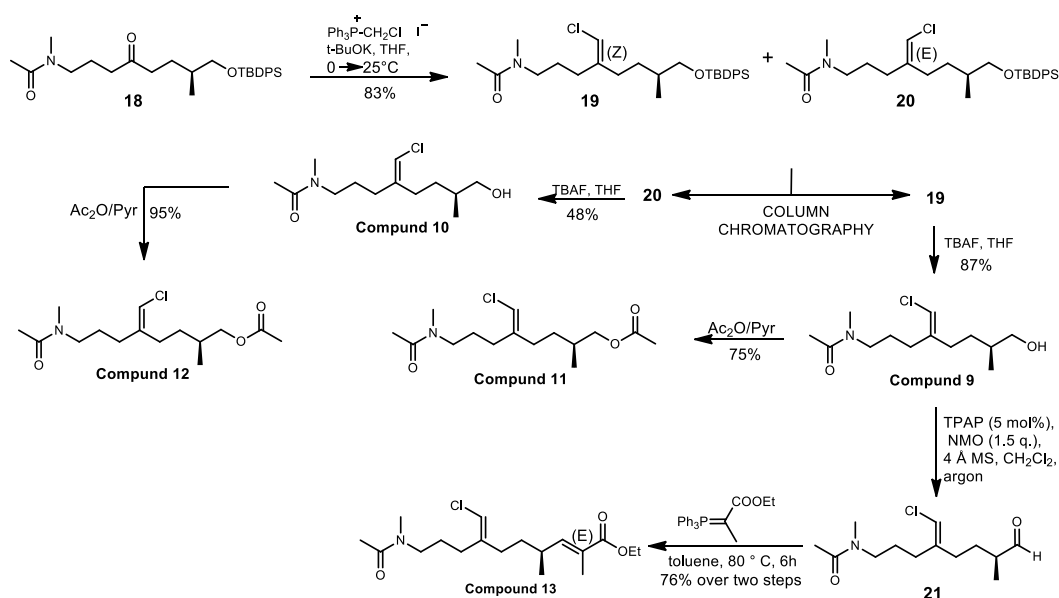


Figure 3.4. Preparation of compounds **9-13**.

Finally, methylene derivative **14** was prepared by using the same procedure described above for compounds **9** and **10**, using the proper phosphonium salt (Figure 3.5). Ketone **18** was let to react with methylenetriphenylphosphane,

commercially available, to give compound **22**, which was deprotected with TBAF affording compound **14**. Finally, acetylation of **14** with Ac₂O/Pyr afforded compound **15** (Figure 3.5).

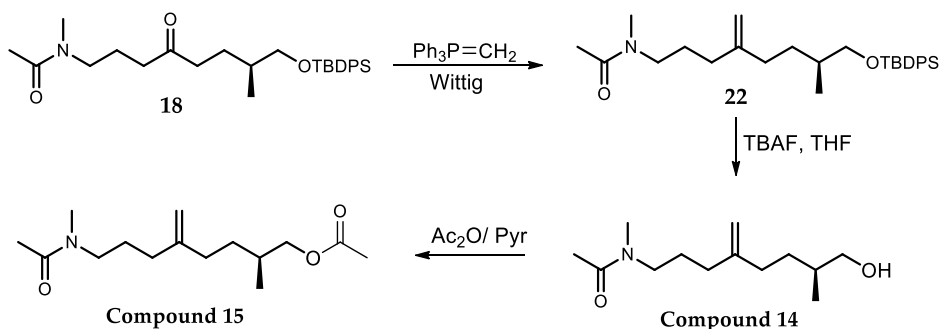


Figure 3.5. Preparation of compounds **14** and **15**.

3.2. In vitro evaluation of the antiproliferative activity

Smenamide A was shown to have a cytotoxic activity against the Calu-1 lung cancer cell line, blocking the proliferation of the cancer cells through a clear pro-apoptotic mechanism.¹ Therefore, the antiproliferative activity of 16-*epi*-smenamide A, together with its analogues (**8-15**), will be evaluated in collaboration with the IRCCS CROB (Scientific Institute of Hospitalization and Care- Basilicata Oncological Center) of Rionero in Vulture (PZ)³ by MTS cell viability assays on SKM-M1 and RPMI-8226 (multiple myeloma) cell lines.

3.3 Conclusions

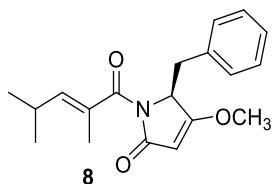
Eight shorter-chain synthetic analogues (**8-15**) of 16-*epi*-smenamide A have been prepared in order to expand the knowledge on the antiproliferative activity of smenamides family. The evaluation of their antiproliferative activity is in progress.

3.4. Experimental section

3.4.1 Generals

All reagents and anhydrous solvents were purchased (Aldrich and Fluka) at the highest commercial quality and used without further purification. Where necessary, flame-dried and argon-charged glassware was used. The reactions were monitored using thinlayer chromatography (TLC) carried out on precoated silica gel plates (Merck 60, F254, 0.25 mm thick). Merck silica gel (Kieselgel 40, particle size 0.063–0.200 mm) was used for the column chromatography. MgSO₄ was used as a drying agent for aqueous workup. Nuclear magnetic resonance (NMR) experiments were performed using Varian Unity Inova spectrometers at 400, 500, and 700 MHz in CDCl₃. Proton chemical shifts were referenced to the residual CHCl₃ signal (7.26 ppm). ¹³C NMR chemical shifts were referenced to the solvent (77.0 ppm). Abbreviations for signal coupling are as follows: s = singlet, d = doublet, t = triplet, q = quartet, m = multiplet, and b = broad. Optical rotations were measured using a JASCO P-2000 polarimeter at the sodium D line. HRMS spectra were recorded by infusion on a Thermo LTQ Orbitrap XL mass spectrometer equipped with an electrospray source in the positive mode using MeOH as the solvent.

3.4.2 Experimental procedures

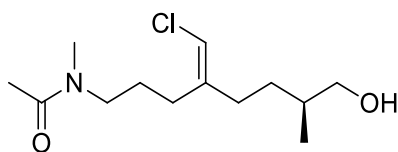


Compound 8. To a solution of 2,4-dimethyl-2-pentenoic acid (114 mg, 0.889 mmol) in EtOAc (4.0 mL), pentafluorophenol (188.2 mg, 1.02 mmol) and DCC (210.5 mg, 1.02 mmol) were added at 0 °C. The reaction mixture was stirred for 1

h at 0 °C and 3 h at rt and evaporated under reduced pressure to give **16** (185,9 mg, 0.632 mmol) that was used in the next step without further purification. ¹H-NMR: (400 MHz, CDCl₃): δ 6.90 (1H, d, J=9.75), 2.8-2.6 (1H, m), 1.95 (3H, s), 1.07 (6H, d, J=6.6).

To a stirred solution of pyrrolinone **17** (126.6 mg, 0.624 mmol)⁵ in THF (5.0 mL), nBuLi (0.390 mL, 0.632 mmol, 1.6 M soln in hexane) was added dropwise at -78 °C. After 15 min, a solution of pentafluorophenyl ester **16** (183.45 mg, 0.624 mmol) in THF (0.1 mL) was added *via* syringe. After 2 h, the reaction was quenched with a saturated aqueous NH₄Cl solution (5 mL) and extracted with EtOAc (3 × 15 mL). The organic phase was washed with water (15 mL) and brine (15 mL), dried, and concentrated in vacuo. The crude was purified by preparative TLC (CHCl₃/CH₃OH, 98:2) to give **8** (166.2 mg, 0.530 mmol, 85%) as a colourless oil. [α]_D²⁰ = -63.4 (c=1.5, CHCl₃); ¹H-NMR: (400 MHz, CDCl₃): δ 7.23-7.17 (3H, m, ArH), 7.0-6.9 (2H, m, ArH), 5.62 (1H, d, J=9.47), 5.01-4.96 (1H, m), 4.84 (1H, s), 3.87 (3H, s, OCH₃), 3.39 (1H, dd, J=14.1, 5.4, H_a-7), 3.15 (1H, dd, J=14.1, 2.0, H_b-7), 2.68-2.54 (1H, m), 1.8 (3H, s), 0.99 (6H, d, J=6.5); ¹³C-NMR (100 MHz, CDCl₃): δ 177.2, 171.3, 168.8, 145.2, 134.4, 129.8, 129.4, 128.1, 127.0, 94.8, 59.1, 58.3, 33.9, 27.4, 21.9, 21.5, 13.3; HRMS (ESI) *m/z* calcd for C₁₃H₂₅ClNO₂ [M+H]⁺ 262.1568, found 262.1566.

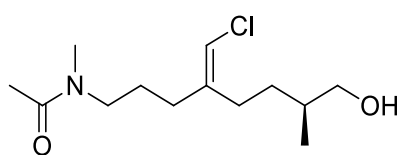
Compound 9



A mixture of compounds **19** and **20** was prepared as previously described [4]. Pure **19** and **20** were obtained by silica gel chromatography (hexane-EtOAc, 1:2).

Deprotection of **19**, as reported [5] afforded alcohol **9** as a colourless oil. $[\alpha]_D^{20} = -63.4$ ($c=1.5$, CHCl_3); $^1\text{H-NMR}$: (400 MHz, CDCl_3 , mixture of rotamers): δ 5.86 (0.4H, s, vinyl proton), 5.82 (0.6H, s, vinyl proton), 3.46 (2H, t, $J=5.3$), 3.42-3.24 (2H, m's), 2.99 (1.8 H, s, H_3 -27), 2.89 (1.2 H, s, H_3 -27), 2.27-2.02 (7H, overlapped signals including two singlets at 2.09 and 2.07 for H_3 -26), 1.78-1.52 (4H, m), 1.30-1.15 (1H, m), 0.93, 0.91 (overall 3H, overlapped d's, both $J=6.0$, H_3 -17); $^{13}\text{C-NMR}$ (100 MHz, CDCl_3): δ 170.6, 170.4, 142.0, 141.3, 113.2, 112.6, 67.8, 67.7, 50.5, 47.3, 36.1, 35.2, 33.2, 32.3, 32.2, 31.1, 31.0, 27.4, 27.3, 25.8, 24.6, 21.9, 21.2, 16.44, 16.38; HRMS (ESI) m/z calcd for $\text{C}_{13}\text{H}_{25}\text{ClNO}_2$ $[\text{M}+\text{H}]^+$ 262.1568, found 262.1566.

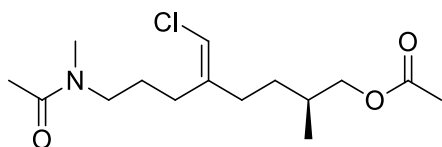
Compound 10



To a solution of **20** (3.9 mg, 0.008 mmol) in THF (0.6 mL), TBAF (0.012 mL, 0.012 mmol, 1.0 M solution in THF) was added dropwise at 0 °C. The reaction mixture was allowed to reach RT and stirred for 1 h. Then, the reaction was quenched with a saturated aqueous solution of NH_4Cl (0.5 mL). The phases were separated, and the aqueous layer was extracted using EtOAc (3×3 mL). The combined organic phases were dried and evaporated in vacuo. The crude was subjected to HPLC separation [column Ascentis (Supelco) Si, 25 cm \times 4.6 mm, 5 μm ; eluent: n-hexane/isopropanol 7:3, flow rate 1 mL min^{-1}] to give alcohol **10** ($t_R=14.5$ min, 1.0 mg, x %) as a colorless oil. $[\alpha]_D^{20} = +12.13$ ($c = 0.13$; CHCl_3); $^1\text{H NMR}$ (400 MHz, CDCl_3 , mixture of rotamers): δ 5.83 (0.4H, s, vinyl proton), 5.81 (0.6H, s, vinyl proton), 3.50 (2H, bt, $J=5.7$), 3.34, 3.26 (1H each, both t, uno dei due non è proprio

un tripletto, $J=7.49$, H₂-24), 2.98 (1.8H, s, H₃-27), 2.91 (1.2H, s, H₃-27), 2.31-2.17 (2H, m), 2.11-2.05 (-H, overlapped signals including a singlet at 2.08 for H₃-26); 1.75-1.53 (-H, questo segnale a circa 1.57 è l'acqua??); 1.29-1.19 (1H, m), 0.98, 0.96 (overall 3H, overlapped doublets, both $J=6.10$, H₃-17); ¹³C NMR (100 MHz, CDCl₃): δ 170.7, 170.5, 142.0, 141.4, 113.0, 112.5, 67.9, 50.2, 47.4, 35.7, 35.6, 33.2, 32.2, 31.7, 30.33, 30.28, 27.6, 27.5, 26.2, 25.2, 21.9, 16.4; HRMS (ESI) m/z calcd for C₁₃H₂₅ClNO₂ [M + H]⁺ 262.1568; found 262.1566.

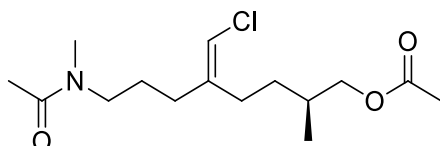
Compound 11



To a stirred solution of alcohol **9** (1.4 mg, 0.005 mmol) in pyridine (0.6 mL), excess acetic anhydride (0.4 mL) was added at rt. After 2h the reaction mixture was evaporated under reduced pressure. The crude was subjected to HPLC separation [column Ascentis Si (Supelco), 25 cm x 4.6 mm, 5 μ m; eluent: *n*-hexane/isopropanol 75:25, flow rate 1 mLmin⁻¹] to give acetyl derivative **11** as a colourless oil (1.5 mg, 0.0047 mmol, 95%). $[\alpha]_D^{20} = + 5.1$ (c = 0.12, CHCl₃); ¹H-NMR: (400 MHz, CDCl₃, mixture of rotamers): δ 5.87 (0.4H, s, vinyl proton), 5.82 (0.6H, s, vinyl proton), 3.98-3.85 (2H, m), 3.39 (1.2 H, t, $J=6.7$, H₂-24), 3.29 (0.8 H, t, $J=6.7$, H₂-24), 3.00 (1.8 H, s, H₃-27), 2.93 (1.2H, s, H₃-27), 2.27-2.03 (10H, overlapped signals including singlets at 2.10, 2.09 and 2.07 for acetates), 1.80-1.54 (4H, m), 1.57-1.47 (1H, m), 1.31-1.21 (1H, m), 0.95, 0.93 (overall 3H, overlapped d's, both $J=6.0$, H₃-17); ¹³C-NMR (100 MHz, CDCl₃): δ 141.9, 141.7, 141.3, 141.0, 113.5, 112.7, 68.92, 68.83, 50.5, 47.2, 36.0, 33.2, 32.12, 32.11, 32.09, 32.08, 31.31,

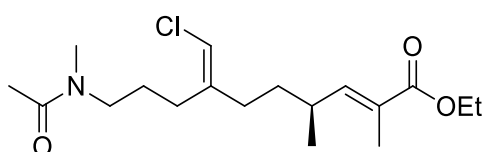
31.29, 31.27, 31.26, 27.45, 27.40, 27.38, 25.8, 24.7, 21.2, 20.9, 16.7; HRMS (ESI) m/z calcd for $C_{15}H_{27}ClNO_3$ $[M+H]^+$ 304.1674, found 304.1669.

Compound 12



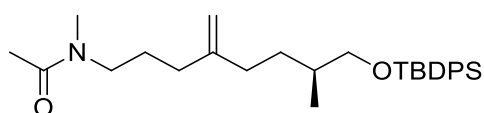
To a stirred solution of alcohol **10** (1.2 mg, 0.004 mmol) in pyridine (0.5 mL), excess acetic anhydride (0.4 mL) was added at rt. After 2h the reaction mixture was evaporated under reduced pressure. The crude was subjected to HPLC separation [column Ascentis Si (Supelco), 25 cm x 4.6 mm, 5 μ m; eluent: *n*-hexane/isopropanol 75:25, flow rate 1 mLmin⁻¹] to give acetyl derivative **12** as a colourless oil (1.0 mg, 0.003 mmol, 75%). $[\alpha]_D^{20} = +12.88$ ($c = 0.06$; $CHCl_3$); ¹H-NMR: (500 MHz, $CDCl_3$, mixture of rotamers): δ 5.83 (0.4H, s, vinyl proton), 5.82 (0.6H, s, vinyl proton), 3.99-3.88 (2H, m), 3.34 (1.2 H, t, $J=7.6$, H_2-24), 3.26 (0.8 H, t, $J=7.6$, H_2-24), 2.98 (1.8 H, s, H_3-27), 2.91 (1.2 H, s, H_3-27), 2.27-2.20 (3H, m), 2.10-2.03 (7H, overlapped signals including singlets at 2.08, 2.07 and 2.06 for acetates), 1.85-1.45 (5H, m), 1.32-1.23 (1H, m), 0.99, 0.98 (overall 3H, overlapped d's, both $J=6.0$, H_3-17); ¹³C-NMR (100 MHz, $CDCl_3$): δ 171.4, 171.3, 170.6, 141.7, 141.0, 113.24, 112.7, 112.6, 69.0, 68.9, 50.2, 47.2, 36.2, 33.2, 32.44, 32.40, 31.7, 30.5, 27.5, 27.4, 26.1, 25.2, 22.0, 21.1 16.7; HRMS (ESI) m/z calcd for $C_{15}H_{27}ClNO_3$ $[M + H]^+$ 304.1674; found 304.1671.

Compound 13



Compound **13** was prepared from alcohol **9** as previously described [4]. $[\alpha]_{\text{D}}^{20} = +127.4$ ($c = 0.5$, CHCl_3); IR (neat) ν_{max} : 2957, 2927, 2858, 1707, 1651, 1596, 1459, 1424, 1373, 1262, 1122 cm^{-1} ; ^1H NMR (400 MHz, CDCl_3 , mixture of rotamers): δ 6.49 (1H, d, $J = 10.1$, H-15), 5.82 (0.5H, s, vinyl proton), 5.76 (0.5H, s, vinyl proton), 4.18 (2H, q, $J = 7.0$, OCH_2CH_3), 3.37, 3.27 (1H each, both t, $J = 7.6$, H_2 -24), 2.99 (1.5H, s, H_3 -27), 2.91 (1.5H, s, H_3 -27), 2.46 (1H, m, H-16), 2.18 (2H, m), 2.09 (1.5H, s, H_3 -26), 2.08 (1.5H, s, H_3 -26), 2.01 (2H, t, $J = 8.6$), 1.83 (1.5H, d, $J = 1.2$, H_3 -14), 1.82 (1.5H, d, $J = 1.2$, H_3 -14), 1.30 (3H, t, $J = 7.0$, OCH_2CH_3), 1.02 (1.5H, d, $J = 6.6$, H_3 -17), 1.00 (1.5H, d, $J = 6.6$, H_3 -17); ^{13}C NMR (100 MHz, CDCl_3) δ 170.5, 170.3, 168.3, 168.2, 146.9, 146.6, 141.6, 140.8, 132.1, 132.0, 131.94, 131.91, 128.5, 128.4, 127.2, 127.0, 113.4, 112.7, 60.6, 60.5, 50.4, 47.1, 36.0, 34.7, 34.6, 33.1, 32.7, 27.4, 27.3, 25.7, 24.6, 21.9, 21.3, 20.01, 19.98, 14.3, 12.63, 12.61; HRMS (ESI) m/z calcd for $\text{C}_{18}\text{H}_{30}\text{ClNNaO}_3$ $[\text{M} + \text{Na}]^+$ 366.1812; found 366.1802.

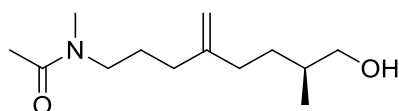
Compound 22



To a stirred suspension of methylenetriphenylphosphorane (6.6 mg, 0.024 mmol) in THF (0.5 mL), $n\text{BuLi}$ (0.015 mL, 0.024 mmol, 1.6 M sol. in hexane) was added dropwise at $0\text{ }^\circ\text{C}$ under argon. After 30 min at $0\text{ }^\circ\text{C}$, a solution of ketone **18** (5.5 mg, 0.012 mmol) in dry THF (0.3 + 0.3 mL rinse) was added, and the mixture was allowed to reach rt. After 4 h, the reaction was quenched with a saturated aqueous NH_4Cl solution (2 mL) and extracted using Et_2O (3×5 mL). The organic phase was washed with brine, dried, and evaporated under reduced pressure. The crude was

purified by preparative TLC (chloroform/methanol 95:5) affording compounds **22** as a colourless oil. $^1\text{H NMR}$: δ 7.66 (4H, $J=6.9$, ArH), 7.44-7.35 (6H, m, ArH), 4.76 (0.5H, s, methylene proton), 4.72 (0.5H, s, methylene proton), 4.71 (1H, s, methylene protons), 3.53-3.44 (2H, m), 3.34, 3.23 (1H each, both t, $J=7.6$, H₂-24), 2.96 (1.5H, s, H₃-27), 2.90 (1.5H, s, H₃-27), 2.07 (3H, s, H₃-26), 2.05-1.92 (4H, m), 1.74-1.56 (4H, m), 1.32-1.17 (1H, m), 1.05 (9H, s, C(CH₃)₃), 0.93 (3H, d, $J=6.5$, H₃-17); $^{13}\text{C NMR}$ (100 MHz, CDCl₃): δ 170.4, 149.2, 148.4, 135.6, 134.0, 133.9, 129.52, 129.48, 109.5, 108.9, 68.8, 68.7, 50.5, 47.4, 36.1, 35.4, 33.45, 33.38, 33.2, 32.8, 31.2, 29.7, 26.9, 26.1, 25.3, 21.9, 21.2, 19.3, 16.7; HRMS (ESI) m/z calcd for C₂₉H₄₃NO₂Si [M + H]⁺ 466.3136; found 466.3124.

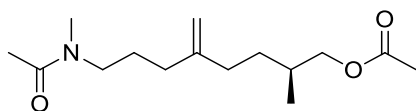
Compound 14



To a solution of **22** (5.4 mg, 0.012 mmol) in THF (0.8 mL), TBAF (0.017 mL, 0.017 mmol, 1.0 M solution in THF) was added at 0 °C. The reaction mixture was allowed to reach rt and stirred for 1 h. Then, the reaction was quenched with a satd. aq. solution of NH₄Cl (1 mL). The phases were separated, and the aqueous layer was extracted with EtOAc (3 x 5 mL). The combined organic phases were dried and evaporated in vacuo. The crude was subjected to HPLC separation [column Ascentis Si (Supelco), 25 cm x 4.6 mm, 5 μm ; eluent: ethyl acetate/isopropanol 9:1, flow rate 1 mLmin⁻¹] to give alcohol **14** (1.9 mg, 0.008 mmol, 70%) as a colourless oil. $[\alpha]_{\text{D}}^{20} = + 7.24$ ($c = 0.07$; CHCl₃); $^1\text{H NMR}$ (400 MHz, CDCl₃, mixture of rotamers): δ 4.79 (0.5 H, s, methylene proton), 4.75 (1.5H, bs, methylene protons), 3.54-3.43 (2H, m), 3.41-3.30 (1H, m, H₂-24), 3.27 (1H, t, $J=7.4$, H₂-24), 2.99 (1.5H,

s, H₃-27), 2.92 (1.5H, s, H₃-27), 2.12-1.98 (overall 7H, including singlets at 2.09 and 2.07 for H₃-26), 1.75-1.50 (4H, m), 1.32-1.19 (1H, m), 0.95, 0.93 (overall 3H, overlapped d's, J=6.5, H₃-17); ¹³C NMR (100 MHz, CDCl₃): δ 170.6, 150.8???, 148.8, 148.3, 109.6, 109.2, 68.14, 68.10, 50.4, 47.5, 36.3, 35.4, 33.4, 33.2, 33.1, 33.0, 32.1, 31.08, 31.03, 29.7, 26.0, 25.1, 21.3, 16.6, 16.5; HRMS (ESI) *m/z* calcd for C₁₃H₂₆NO₂ [M + H]⁺ 228.1958; found 228.1956.

Compound 15



To a stirred solution of alcohol **14** (1.5 mg, 0.006 mmol) in pyridine (0.2 mL), excess acetic anhydride (0.2 mL) was added at rt. After 2h the reaction mixture was evaporated under reduced pressure. The crude was subjected to HPLC separation [column Ascentis Si (Supelco), 25 cm x 4.6 mm, 5 μm; eluent: *n*-hexane/isopropanol 75:25, flow rate 1 mLmin⁻¹] to give acetyl derivative **15** as a colourless oil (1.0 mg, 0.004 mmol, 62%). [α]_D²⁰ = + 13.63 (c = 0.07 ; CHCl₃); ¹H NMR (400 MHz, CDCl₃, mixture of rotamers): δ 4.78 (0.5H, s, methylene proton), 4.75 (0.5H, s, methylene proton), 4.74 (1H, s, methylene protons), 3.99-3.84 (2H, m), 3.36, 3.26 (1H each, both t, J=7.6, H₂-24), 2.98 (1.5H, s, H₃-27), 2.92 (1.5H, s, H₃-27), 2.12-1.96 (10H, overlapped signals including singlets at 2.09, 2.08 and 2.06 for acetates) 1.82-1.60 (4H, m), 1.34-1.22 (1H, m), 0.95, 0.94 (overall 3H, overlapped d's, J=6.5, H₃-17); ¹³C NMR (175 MHz, CDCl₃): δ 170.42, 171.36, 170.6, 141.7, 141.05, 113.24, 112.6, 112.65, 69.0, 68.9, 50.2, 47.1, 36.2, 33.2, 32.42, 32.40, 31.9, 31.7, 30.5, 27.45, 27.39, 26.1, 25.2, 22.0, 21.4, 21.0, 16.7; HRMS (ESI) *m/z* calcd for C₁₅H₂₇NO₃ [M + H]⁺ 270.2063; found 270.2061.

3.6 Supplementary spectroscopic data

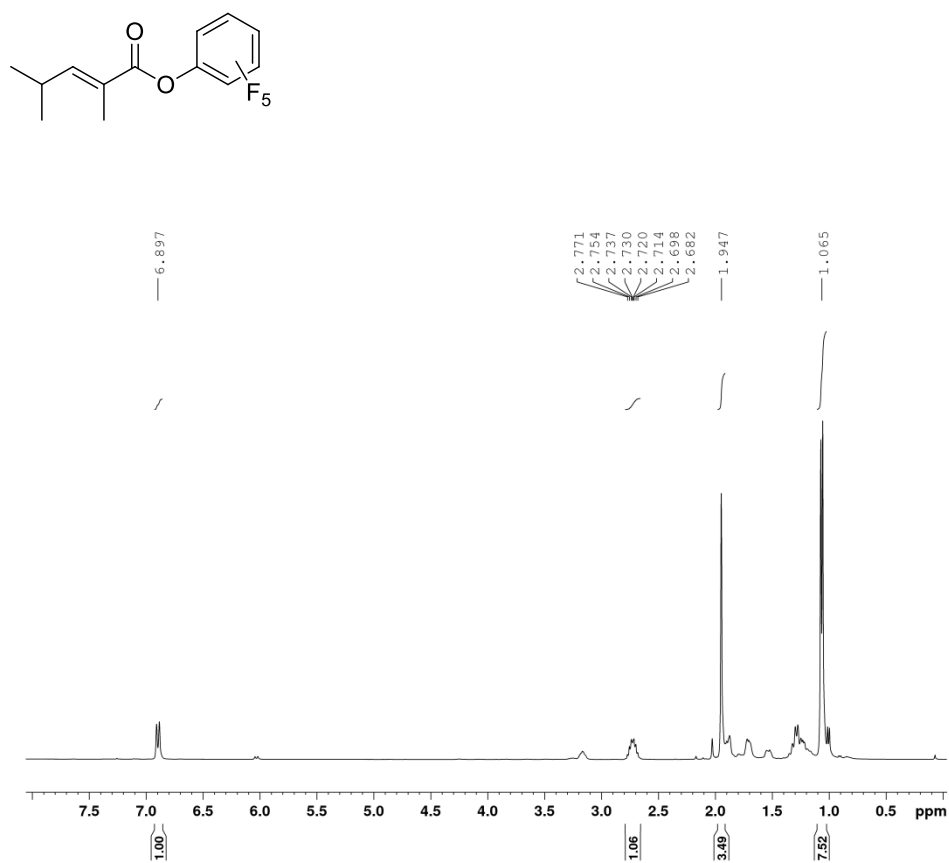


Figure 3.6. ¹H NMR spectrum of compound 16 (CDCl₃, 400 MHz).

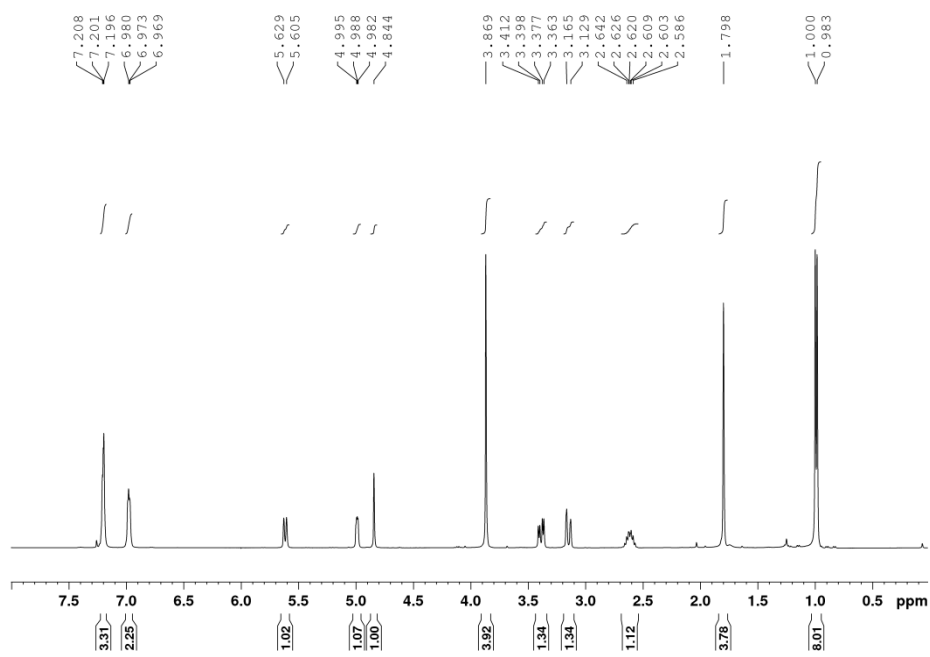


Figure 3.7. ^1H NMR spectrum of compound **8** (CDCl_3 , 400 MHz).

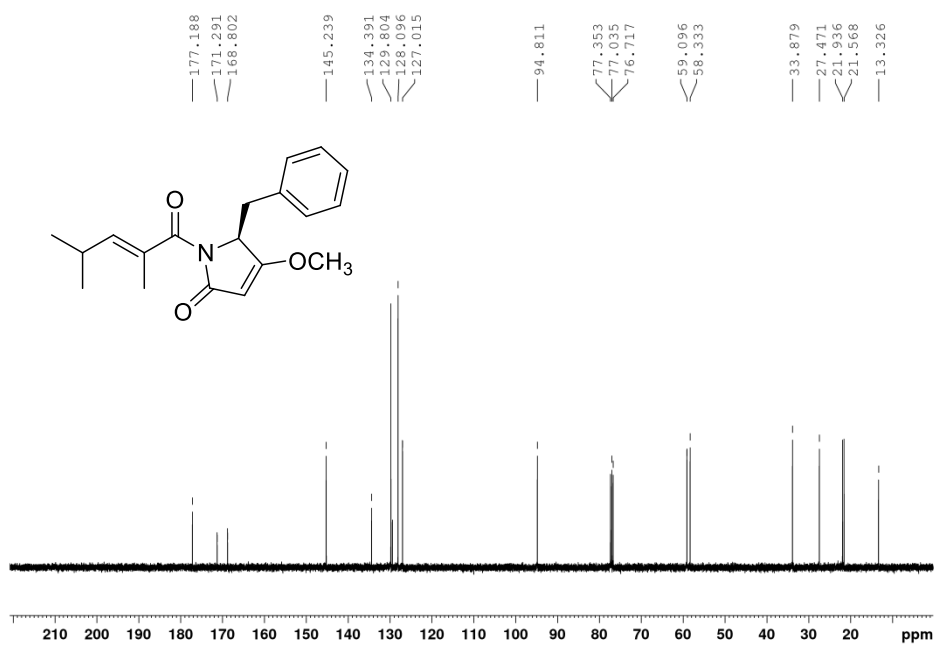


Figure 3.8. ^{13}C NMR spectrum of compound **8** (CDCl_3 , 100 MHz).

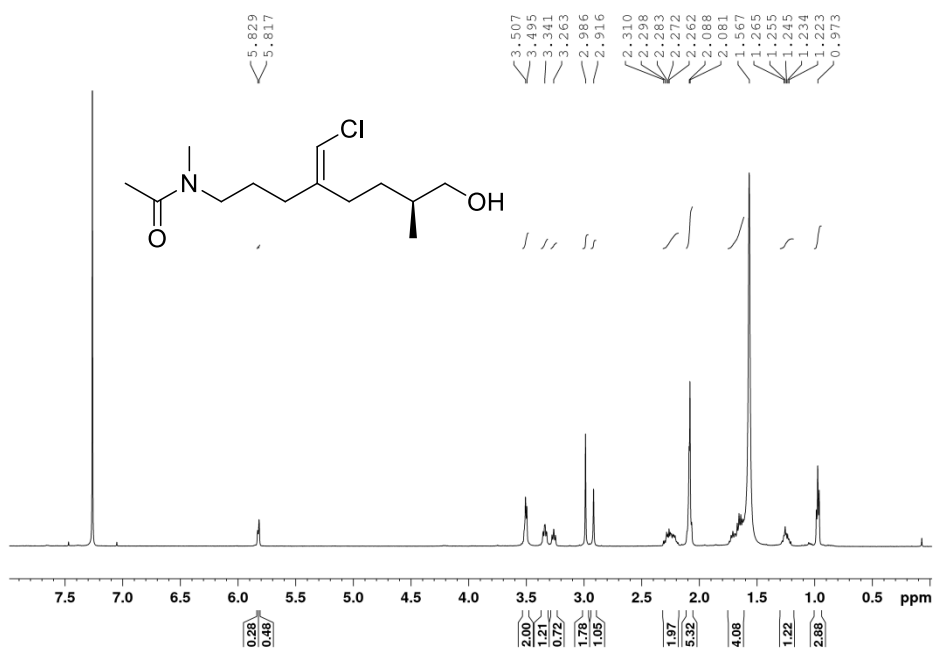


Figure 3.9. ¹H NMR spectrum of compound 10 (CDCl₃, 400 MHz).

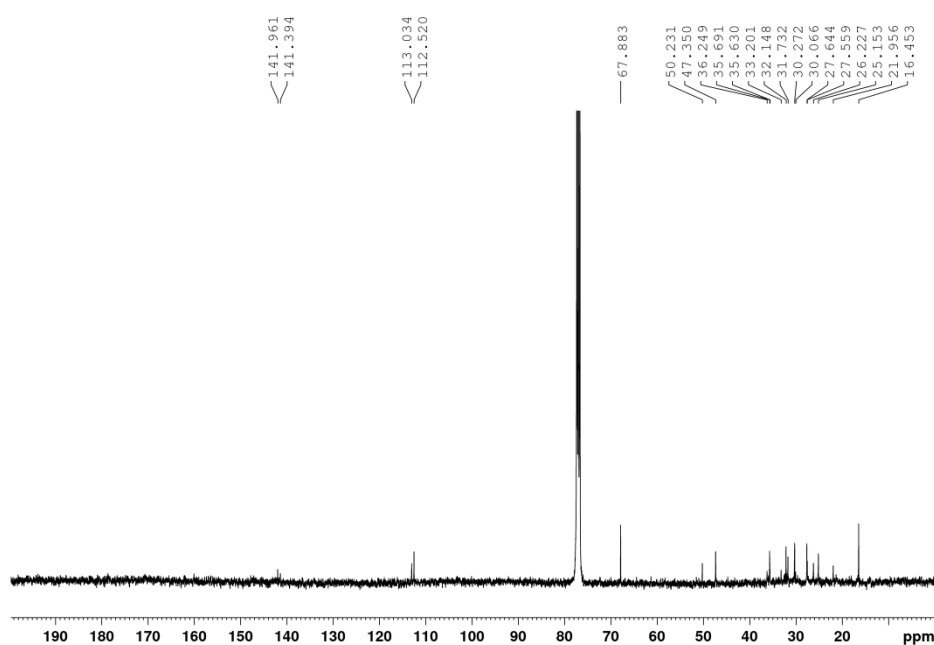


Figure 3.10. ¹³C NMR spectrum of compound 10 (CDCl₃, 100 MHz).

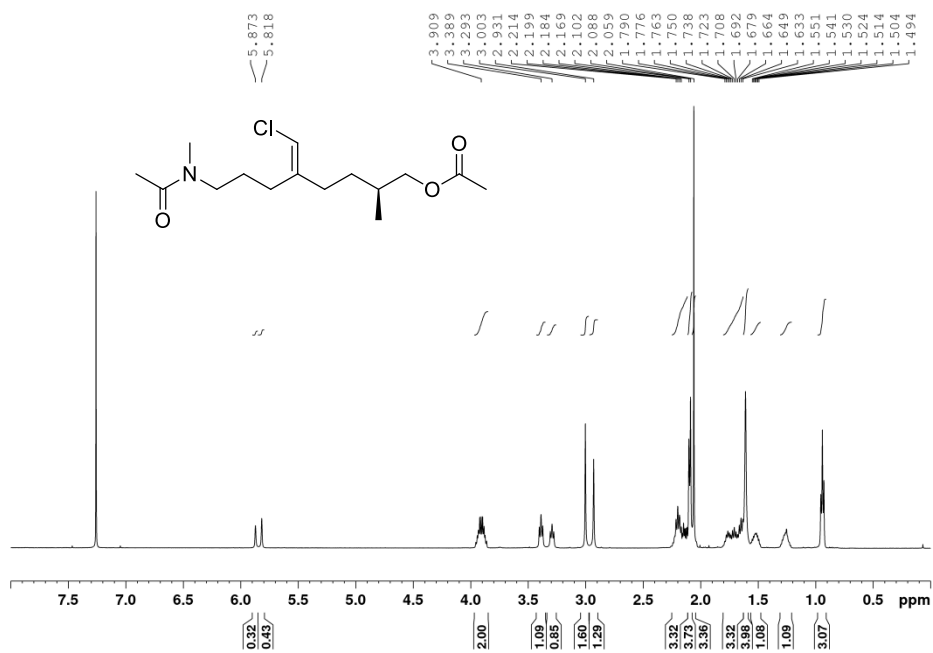


Figure 3.11. ¹H NMR spectrum of compound 11 (CDCl₃, 400 MHz).

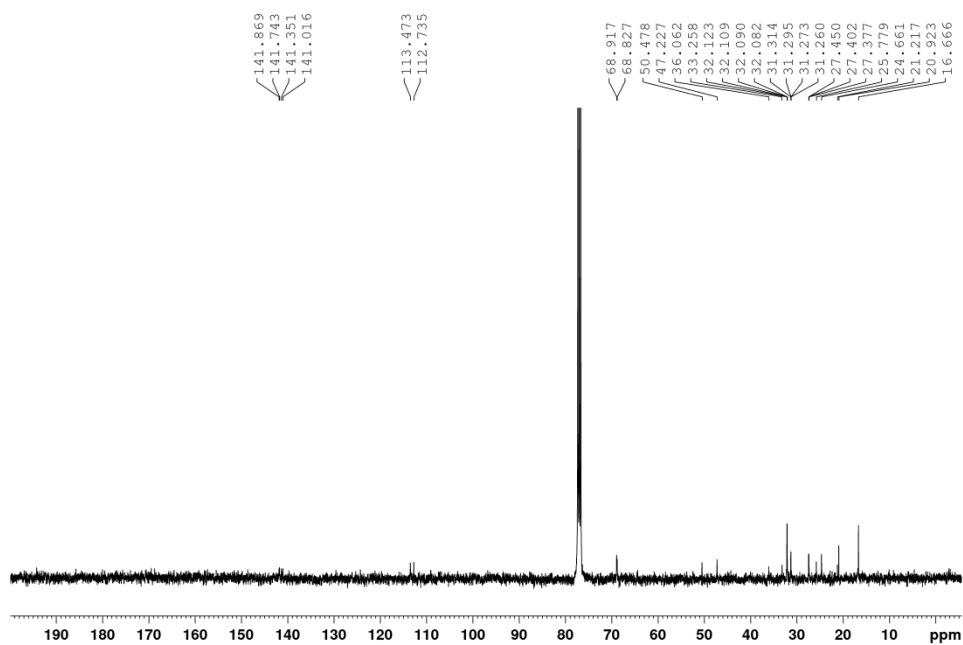


Figure 3.12. ¹³C NMR spectrum of compound 11 (CDCl₃, 100 MHz).

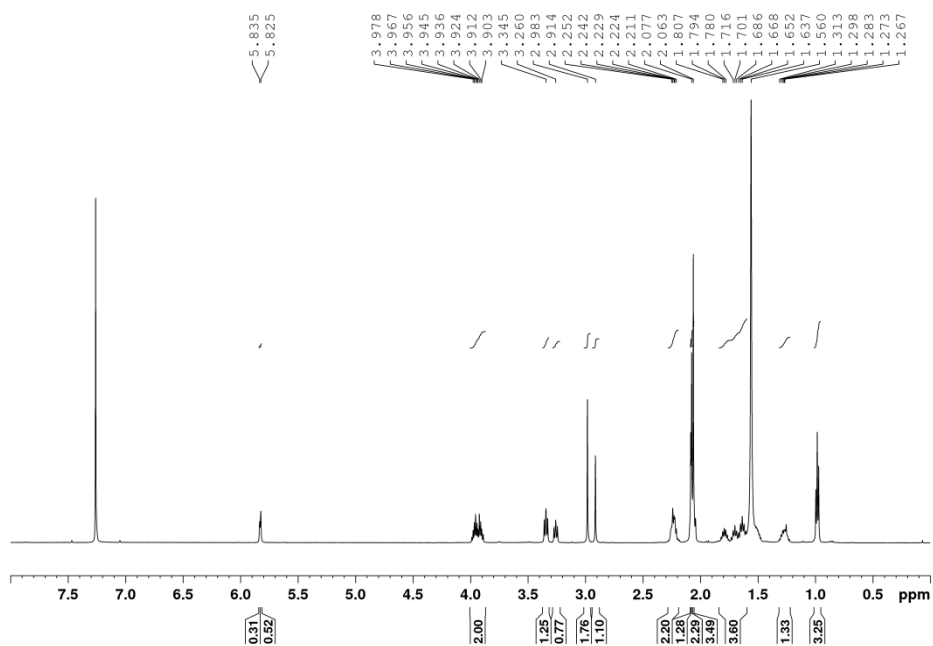


Figure 3.13. ^1H NMR spectrum of compound **12** (CDCl_3 , 400 MHz)

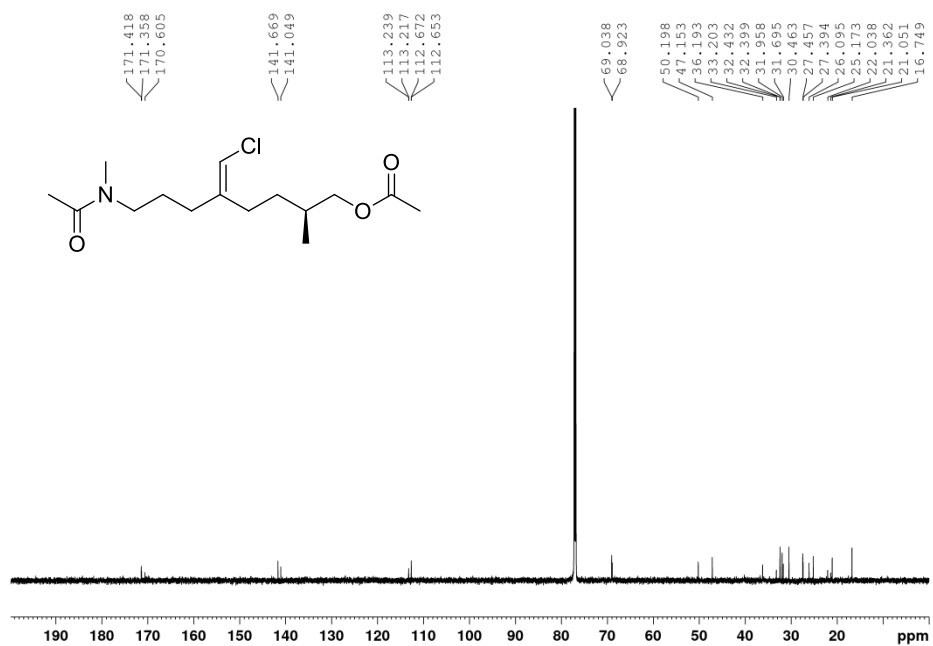


Figure 3.14. ^{13}C NMR spectrum of compound **12** (CDCl_3 , 100 MHz)

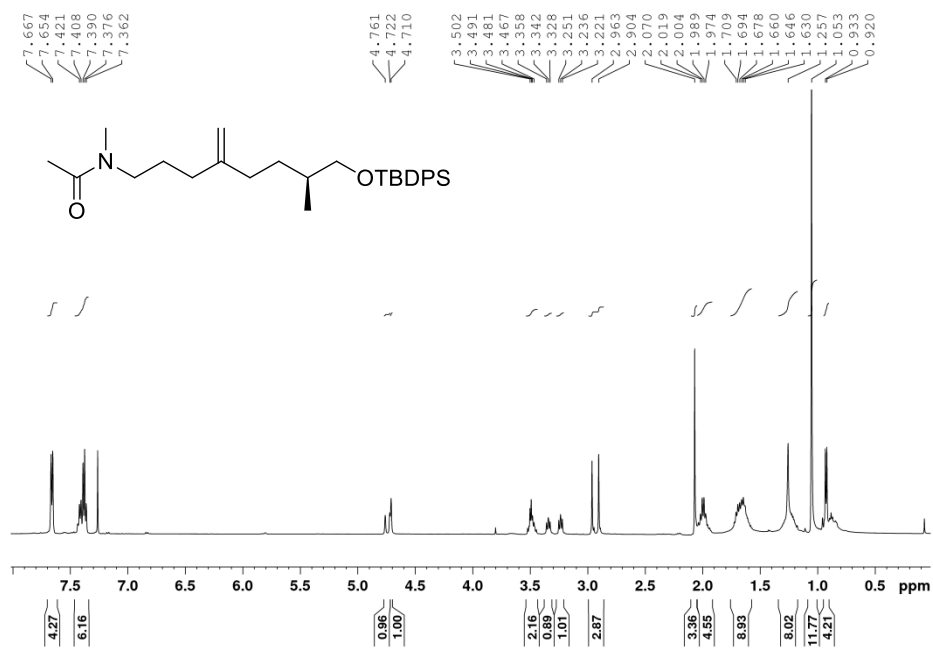


Figure 3.15. ¹H NMR spectrum of compound 22 (CDCl₃, 400 MHz).

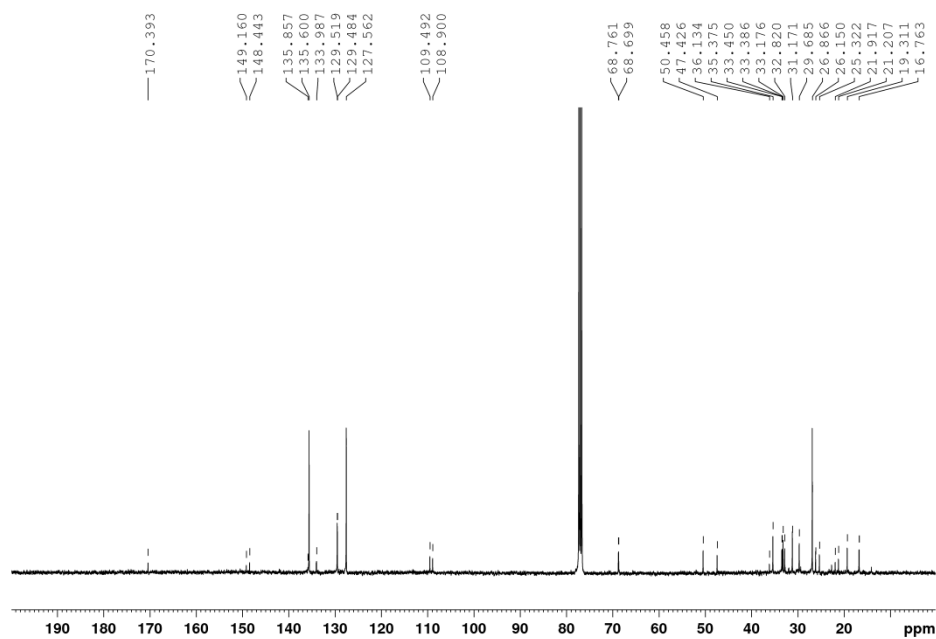


Figure 3.16. ¹³C NMR spectrum of compound 22 (CDCl₃, 100 MHz).

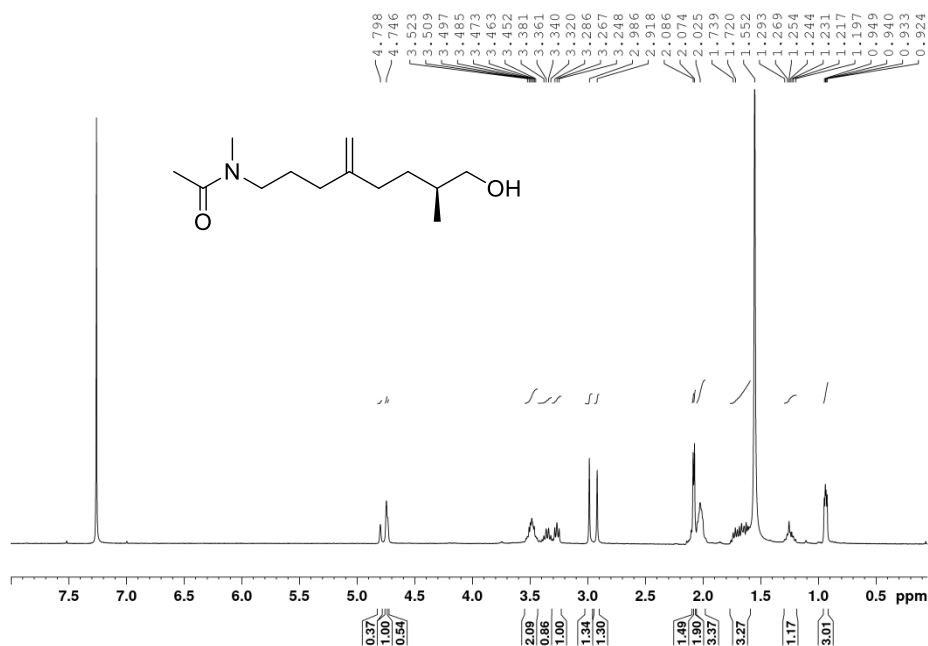


Figure 3.17. ¹H NMR spectrum of compound 14 (CDCl₃, 400 MHz).

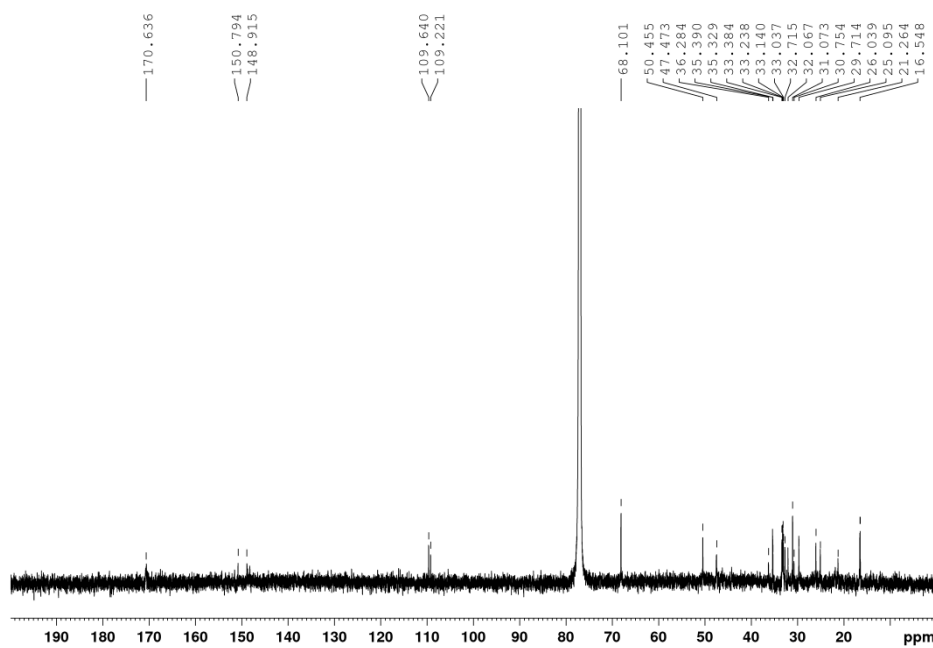


Figure 3.18. ¹³C NMR spectrum of compound 14 (CDCl₃, 100 MHz).

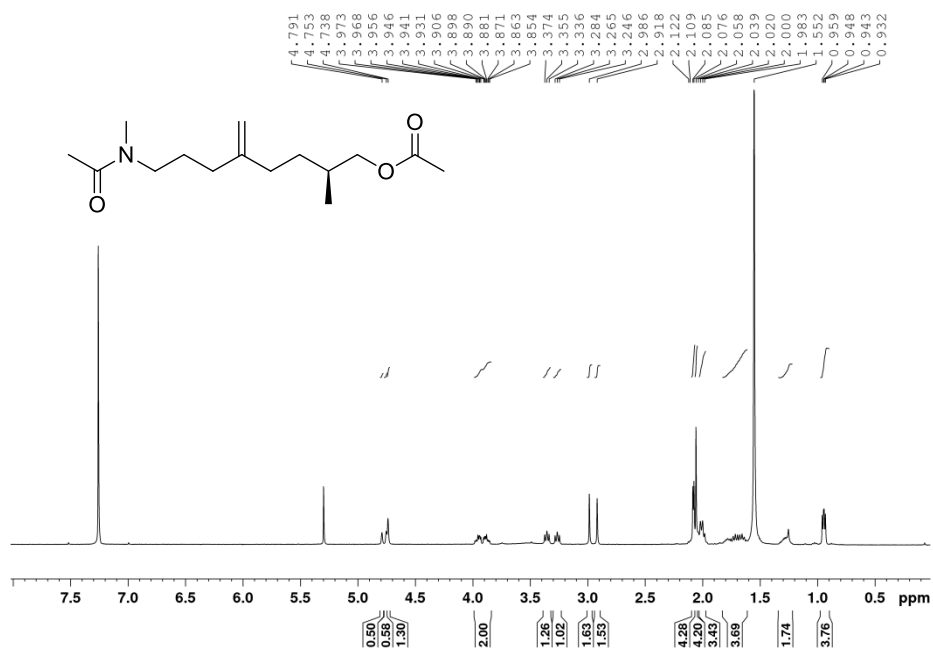


Figure 3.19. ¹H NMR spectrum of compound 15 (CDCl₃, 400 MHz).

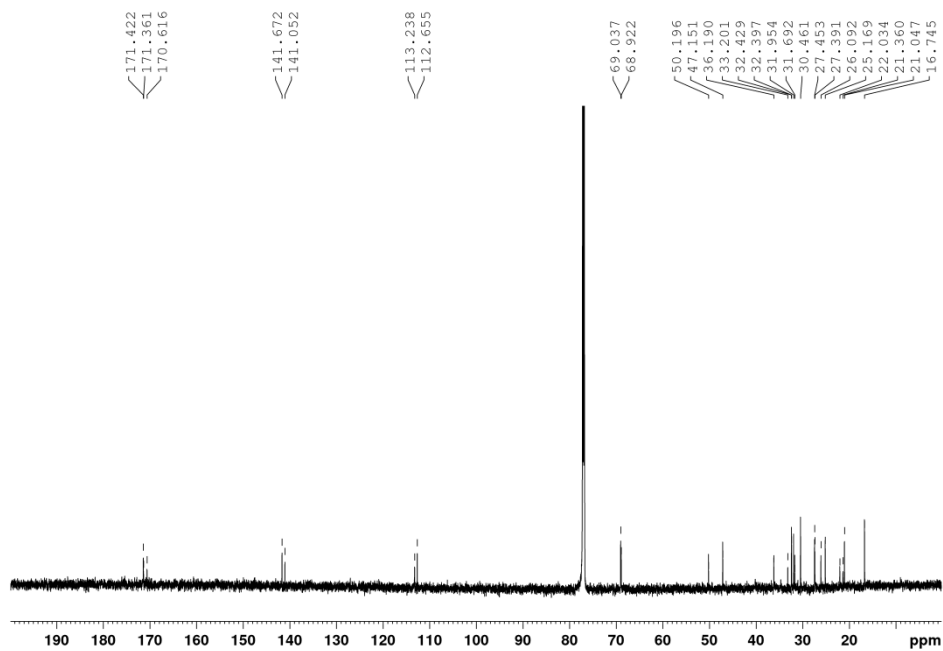


Figure 3.20. ¹³C NMR spectrum of compound 15 (CDCl₃, 100 MHz).

References

-
- ¹ R. Teta, E. Irollo, G. Della Sala, G. Pirozzi, A. Mangoni, V. Costantino, *Marine Drugs*, **2013**, 11 (11), 4451-4463.
- ² A. Caso, A. Mangoni, G. Piccialli, V. Costantino, V. Piccialli, *ACS Omega*, **2017**, 2, 1477–1488.
- ³ A. Caso, I. Laurenzana, D. Lamorte, S. Trino, G. Esposito, V. Piccialli, and V. Costantino, *Mar. Drugs*, **2018**, accepted.

PART 2

Isolation and structural determination of new bioactive metabolites from marine sources

Chapter 4

Conulothiazoles A and B, two chlorinated peptide/polyketide metabolites from the marine sponge *Smenospongia conulosa*

In an attempt to identify new bioactive metabolites to be used as lead compounds in the anticancer drug discovery, the study of the chemical composition of the Caribbean sponges of *Smenospongia* genus (Demospongiae, Dictyoceratida, Thorectidae), in particular *S. aurea* and *conulosa*, was carried out.



Figure 4.1. *Smenospongia aurea* and *conulosa* sponges, respectively.

The chemical analysis of the organic extract of *S. aurea* led to the isolation of four chlorinated PKS/NRPS compounds, namely smenamide A (1) and B (2), and smenothiazole A (3) and B (4), the structure of which is depicted in Figure 4.2.

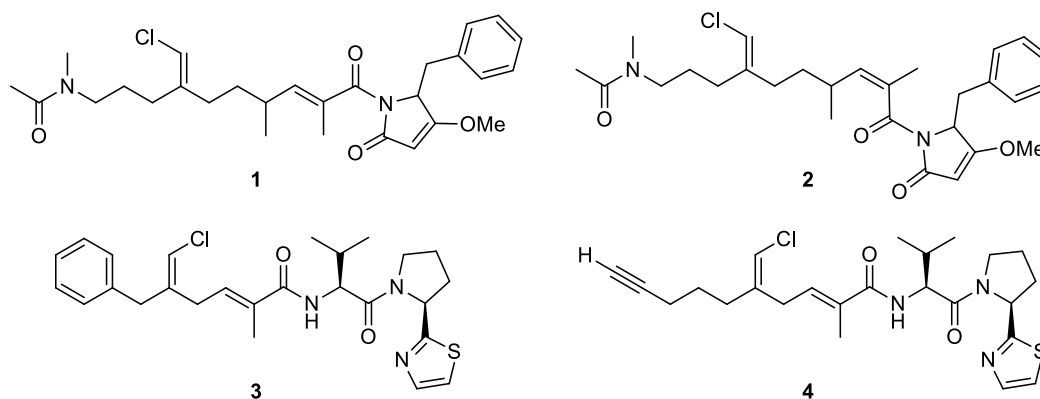


Figure 4.2. Structures of smenamide A (1) and B (2), and smenothiazole A (3) and B (4).

Both smenamides and smenothiazoles showed an interesting cytotoxic activity at nanomolar concentrations. More precisely, smenamides were shown to exert their cytotoxic activity against Calu-1 lung cancer cells,¹ whereas smenothiazoles have shown a certain selectivity against ovarian cancer cells.²

In lights of the captivating chemical content of *S. aurea*, its congeneric species, *S. conulosa*, was studied. The in-depth analysis revealed the presence in the organic extract of two additional chlorinated NRP/PK derivatives (Figure 4.3): conulothiazoles A (5) and B (6).³

4.1 Isolation of conulothiazoles A and B

A specimen of the sponge *S. conulosa* was collected by Scuba along the coasts of Little Inagua (Bahamas) in 2013, during one of Prof. J. Pawlik expeditions. After collection, it was immediately frozen and stored at $-20\text{ }^{\circ}\text{C}$ until it arrived to the Department of Pharmacy, in the laboratory of Prof. Costantino. The sample, properly homogenized, was subjected to several extractions using CH_3OH , mixtures of $\text{CH}_3\text{OH} / \text{CHCl}_3$ and CHCl_3 . The methanol extract was partitioned between water and butanol with the aim of separating the lipophilic metabolites,

including compounds **5** and **6**, from hydrophilic molecules such as proteins, carbohydrates and nucleic acids, which instead split up into the aqueous phase. The butanol phase was combined with the chloroform extracts and concentrated under vacuum obtaining a crude extract, then subjected to reverse phase chromatography on silica gel RP-18. Fraction A5 (MeOH/H₂O 9:1) of the column chromatography was shown to be the fraction of interest, containing compounds **5** and **6**. Due to the high content in known alkaloids, fraction A5 undergone an acid partition between chloroform, methanol and acidic water (1% v/v of acetic acid), in order to remove the alkaloids from the organic phase. The latter was hence subjected to two subsequent reverse phase HPLC separations, affording **5** (225 µg) and **6** (47 µg) as pure compounds (Figure 4.3).

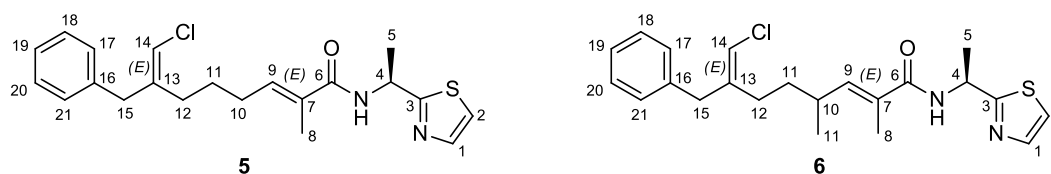


Figure 4.3. Structures of conulothiazoles A (**5**) and B (**6**).

4.2 Structural determination of compound **5** and **6**

The structural elucidation of natural compounds, which are often isolated and purified in exiguous amounts, is undoubtedly the most fascinating aspect of the work of natural products chemists. The interest towards natural products increased in parallel with the technological progress and the development of new powerful analytical tools. The combined use of the most modern spectroscopic (NMR, IR, UV) and spectrometric (MS) techniques led to the isolation of conulothiazoles A (**5**) and B (**6**). Despite the small amount of the compounds isolated from the sponge, it was possible to record a complete series of two-dimensional homonuclear and

heteronuclear NMR spectra (COSY, HSQC, HMBC), which allowed the complete assignment of its structure. All ^{13}C chemical shifts were assigned using the 2D NMR spectra, therefore one-dimensional NMR ^{13}C spectra were not recorded.

The positive ion mode high-resolution ESI mass spectrum of conulothiazole A (Figure 4.4) showed the presence of a $[\text{M} + \text{Na}]^+$ pseudomolecular ion peak at m/z 411.1270 and a M+2 isotopic peak, whose intensity (38%) suggested the presence in the structure of the molecule of both a chlorine (^{37}Cl , 32%) and a sulfur atom (^{34}S , 4%). These data are in perfect agreement with the molecular formula, which was determined as $\text{C}_{21}\text{H}_{25}\text{ClN}_2\text{OS}$.

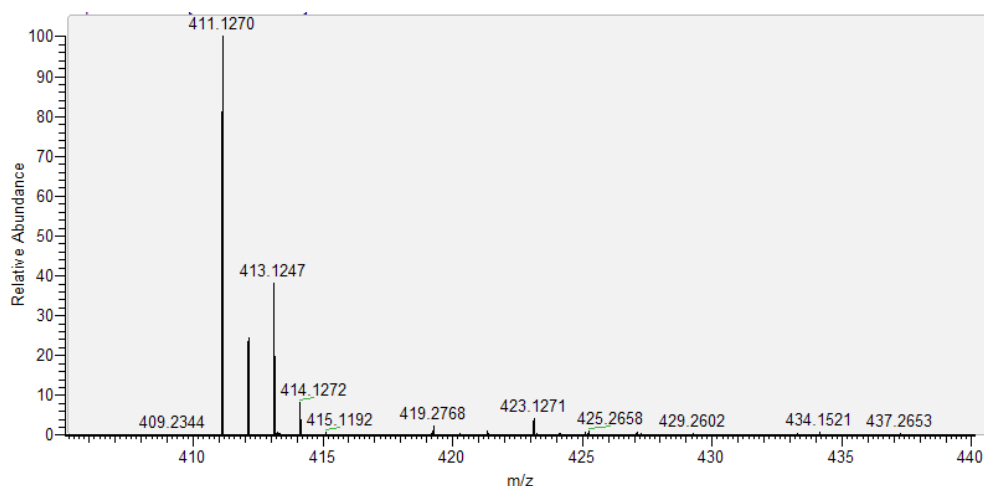


Figure 4.4. Positive ion mode high-resolution ESI MS spectrum of compound **5**.

From the molecular formula it was possible to establish the number of unsaturations, which is equal to 10.

The analysis of the ^1H NMR spectrum (Figure 4.5) of **5**, evidenced a certain similarity of this compound with the smenothiazole A (**3**, Figure 4.2). Both compounds share indeed a benzyl-vinyl chloride function and a thiazole ring.

These data were confirmed by the analysis of ^{13}C NMR spectrum and by the main correlation peaks provided by the homonuclear and heteronuclear 2D-NMR spectra (Table 4.1 and Figure 4.6).

The elucidation of central portion of the molecule could not be determined by the comparison with known compounds, and instead required a detailed analysis of one- and two-dimensional NMR spectra.

The presence of an α -methyl, α,β -unsaturated amide function was demonstrated by the analysis of the HMBC spectrum (Figure 4.14), in which three correlations peaks of the methyl singlet ($\text{H}_3\text{-8}$) at δ 1.83 with the carbonyl carbon at δ 172.3 (C-6) and with the two olefinic carbons at δ 132.5 (C-7) and 137.7 (C-9) are present. This function is directly linked to a carbon chain constituted by three methylene groups, as confirmed by the vicinal couplings in the COSY spectrum (Figure 4.11). The allylic coupling of protons at δ 2.20 ($\text{H}_2\text{-12}$) with the proton H-14 at (δ 6.02) allowed to demonstrate that the chlorovinyl function is linked to the three methylene-chain.

The correlations peaks of the methyl protons at δ 1.63 ($\text{H}_3\text{-5}$) with the proton at δ 5.39 (H-4) in the COSY spectrum suggested the presence of a single α -amino acid CH, deriving from an alanine residue [$\delta_{\text{H}}5.39$ (H-4) and $\delta_{\text{C}}48.9$ (C-4)]. The presence in the HMBC spectrum of two correlation peaks of proton H-4 at δ 5.39 with both carbon C-3 at δ 176.7 of the thiazole ring and the carbonyl carbon at δ 172.3 (C-6), allowed to understand that the thiazole ring was directly linked to the alanine-derived residue.

At that point, the only possible connection between the polyketide and the peptide moiety of the molecule was an amide bond between the carbonyl carbon C-6 (δ 172.3) and the amino group at δ 48.9 (C-4).

These data completed the determination of planar structure of conulothiazole A (**5**, Figure 4.3).

Pos.	δH [mult., J (Hz)]	δC (mult.)	COSY	HMBC
1	7.71 (d, 3.4)	142.9 (CH)	2	
2	7.48 (d, 3.3)	120.5 (CH)	1	1, 3
3	-	176.7 (C)		
4	5.39 (quartet, 7.1)	48.9 (CH)	5	3, 5, 6
5	1.63 (d, 7.1)	20.9 (CH ₃)	4	3, 4
6	-	172.3 (C)		
7	-	132.5 (C)		
8	1.83 (br. s)	12.8 (CH ₃)	9, 10	6, 7, 9
9	6.34 (t of quartets, 7.4, 1.4)	137.7 (CH)	8, 10	6, 8
10	2.16 (quartet, 7.5)	29.1 (CH ₂)	8, 9, 11	7, 9, 11, 12
11	1.55 (quintet, 7.7)	27.2 (CH ₂)	12	9, 10, 12, 13
12	2.20 (br. t, 7.9)	30.5 (CH ₂)	11, 14	10, 11, 13, 14, 15
13	-	143.5 (C)		
14	6.02 (br. s)	115.4 (CH)	12, 15	12, 13, 15
15	3.42 (br. s)	42.0 (CH ₂)	14, 17/21	12, 13, 14, 16, 17/21
16	-	139.9 (C)		
17/21	7.19 (br. d, 7.8)	130.1 (CH)	15, 18/20	15, 19, 21/17
18/20	7.28 (br. t, 7.8)	129.7 (CH)	17/21, 19	16, 20/18
19	7.20 (br. t, 7.8)	127.7 (CH)	18/20	17/21

Table 4.1. NMR data of conulothiazole A (**5**) (700 MHz, CD₃OD).

The molecular formula C₂₂H₂₇ClN₂OS of compound **6** was established by the analysis of the high resolution ESI mass spectrum (Figure 4.5), in which a [M+Na]⁺ pseudomolecular ion peak at *m/z* 425.1426. In comparison with conulothiazole A (**5**) (Figure 4.3), the molecular formula of **6** accounts for 14 additional amu. This suggested the presence in compound **6** of an additional methyl group, which was indeed confirmed by the analysis of ¹H NMR spectrum of compound **6** (Figure 4.15 and table 4.2).

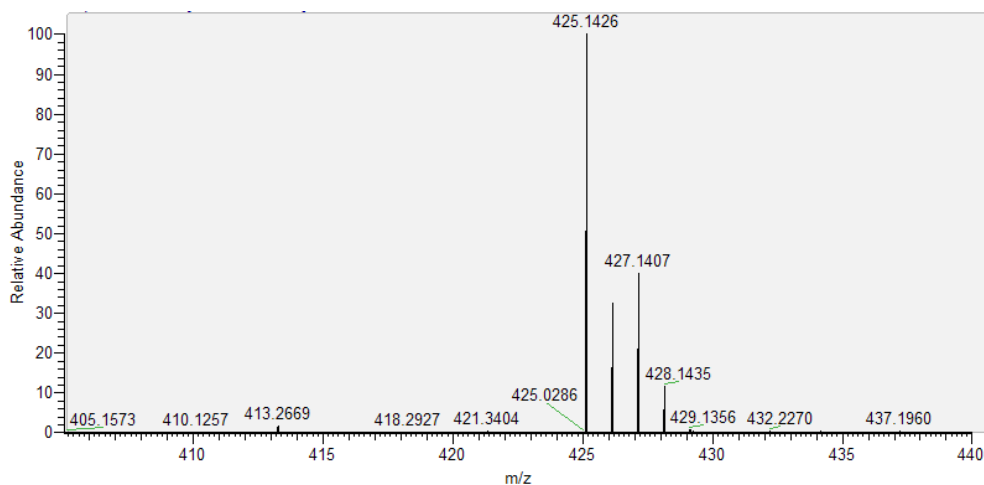


Figure 4.5. Positive ion mode high-resolution ESI MS spectrum of compound **6**.

As for conulothiazole A (**5**), a full set of homonuclear and heteronuclear two-dimensional NMR spectra were recorded to elucidate the planar structure of compound **6**. The only difference, from the spectroscopic point of view, between compounds **5** and **6** resides in the presence in the COSY spectrum (Figure 4.16) of a correlation between methyl protons H₃-22 (δ 1.01) with the allylic methine proton H-10 (δ 2.47), and the absence of the allylic methylene proton signal at δ 2.16 (H₂-10), which allowed to understand that the additional methyl group is located in position 10. These data confirmed the structure of conulothiazole B (**6**).

Pos.	δH [mult., J (Hz)]	δC (mult.)	COSY	HMBC
1	7.71 (d, 3.4)	145.3 (CH)	2	
2	7.48 (d, 3.3)	120.5 (CH)	1	1, 3
3	-	176.8 (C)		
4	5.40 (quartet, 7.1)	49.3 (CH)	5	3, 5, 6
5	1.64 (d, 7.2)	21.7 (CH ₃)	4	3, 4
6	-	172.3 (C)		
7	-	131.6 (C)		
8	1.84 (d, 1.4)	13.6 (CH ₃)	9	6, 7, 9
9	6.14 (dq, 9.8, 1.4)	144.2 (CH)	8, 10	8
10	2.47 (dddq, 9.8, 7.9, 5.9, 6.7)	34.4 (CH ₂)	9, 11a, 11b, 22	
11	a 1.48 (dddd, 13.2, 10.7, 5.9, 5.9)	35.5 (CH ₂)	10, 11b, 12a, 12b	13
	b 1.38 (dddd, 13.2, 10.7, 7.9, 5.5)		10, 11a, 12a, 12b	10, 12, 13
12	a 2.15 (ddd, 13.2, 10.7, 5.9)	29.8 (CH ₂)	11a, 11b, 12b, 14	11, 13, 14, 15
	b 2.10 (ddd, 13.2, 10.7, 5.5)		11a, 11b, 12a, 14	10, 13, 14, 15
13	-	143.8 (C)		
14	5.99 (br. s)	115.5 (CH)	12a, 12b, 15	12, 13, 15
15	3.40 (br. s)	42.5 (CH ₂)	14, 17/21, 18/20	12, 13, 14, 16, 17/21
16	-	140.3 (C)		
17/21	7.17 (br. d, 7.8)	130.5 (CH)	15, 18/20	15, 19, 21/17
18/20	7.27 (br. t, 7.2)	129.9 (CH)	15, 17/21, 19	16, 20/18
19	7.20 (br. t, 7.0)	127.7 (CH)	17/21, 18/20	
22	1.01 (d, 6.7)	20.4 (CH ₃)	10	9, 10, 11

Table 4.2. NMR data of conulothiazole B (**6**) (700 MHz, CD₃OD).

4.3 Stereostructural determination of the two double bonds of conulothiazole

A and B

The correlations peaks present in the NOESY spectrum (Figure 4.12) allowed the assignment of the configuration of the two double bonds of compound **5** and **6**. The configuration of both double bonds in conulothiazole A was determined as *E*, thanks to the presence in the NOESY spectrum of the correlation peaks between the

proton H-14 (δ 6.02) and the protons H₂-15 (δ 3.42) and between protons H₃-8 (δ 1.83) and the protons H₂-10 (δ 2.16).

Conulothiazole B (**6**) possess the same configuration at both double bonds of conulothiazole A (**5**). The configurations were determined as *E* through the analysis of ROESY spectrum (Figure 4.6 and Figure 4.17).

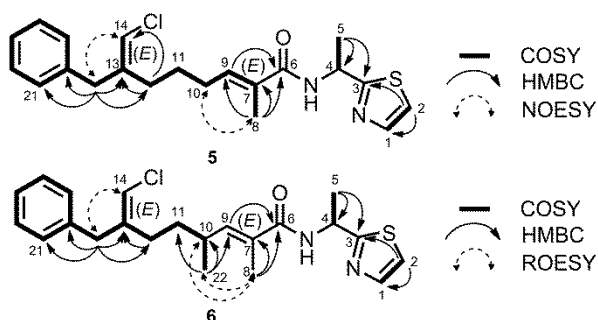


Figure 4.6. The most significant correlations provided by the COSY, HMBC, and NOESY/ROESY 2D NMR spectra of conulothiazoles A (**5**) and B (**6**).

4.4 Determination of the absolute configuration of the amino acid residues of conulothiazoles A and B

As for smenamide A (chapter 1, paragraph 2.4), the absolute configuration of the amino acid residues of both compound **5** and **6** was determined by using a modified procedure of Marfey's method. The sample was subjected to ozonolysis prior to hydrolysis with HCl to prevent racemisation which is reported to occur during hydrolysis at the carbon in α position to a thiazole ring (Figure 4.7).

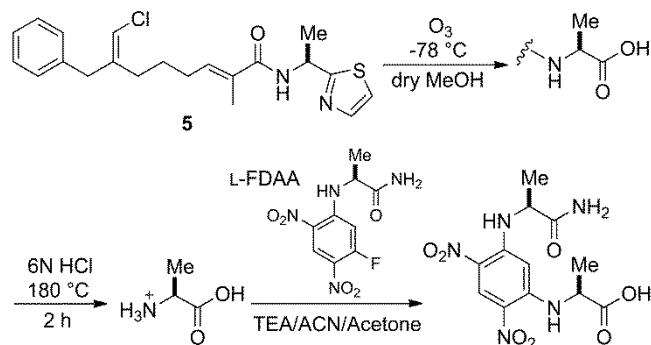


Figure 4.7. Ozonolysis, hydrolysis and derivatization of conulothiazole A (**5**) with L-enantiomer of Marfey's reagent.

The absolute configuration of the alanine residue of conulothiazole A (**5**) and B (**6**) was determined as *S* for both compounds, on the basis of the retention times of their respective Marfey's derivatives (Figure 4.8).

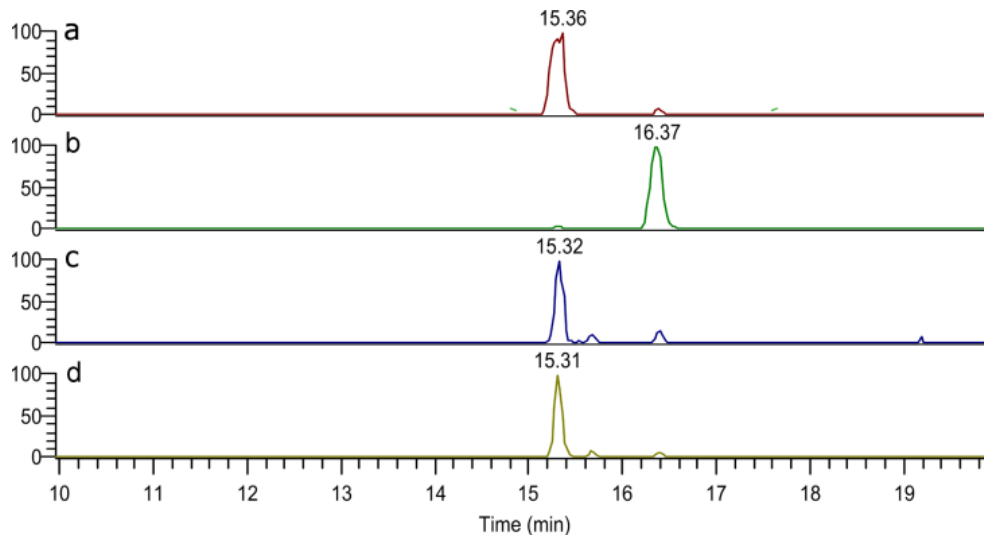


Figure 4.8. HR-ESI-MS-HPLC analysis of Marfey's derivatives from conulothiazole A (**5**) and B (**6**). Extracted-ion chromatograms at m/z 342.1044 of (a) authentic L-1-fluoro-2-4-dinitrophenyl-5-alanine amide L-alanine (L-FDAA-L-Ala); (b) authentic D-FDAA-L-Ala; (c) L-FDAA-Ala from **5**; and (d) L-FDAA-Ala from **6**.

4.5 Biogenetic studies

The biogenetic studies on these new metabolites were carried out in collaboration with the research group of Prof. Alfonso Mangoni. Since I was not directly involved in this part of the project, I will only discuss the most significant results.

Although smenamides, smenothiazoles and conulothiazoles do not have analogues in the field of natural products, they share some structural features with different known molecules, belonging to the class of hybrid peptides/polyketides compounds (Figure 4.9).

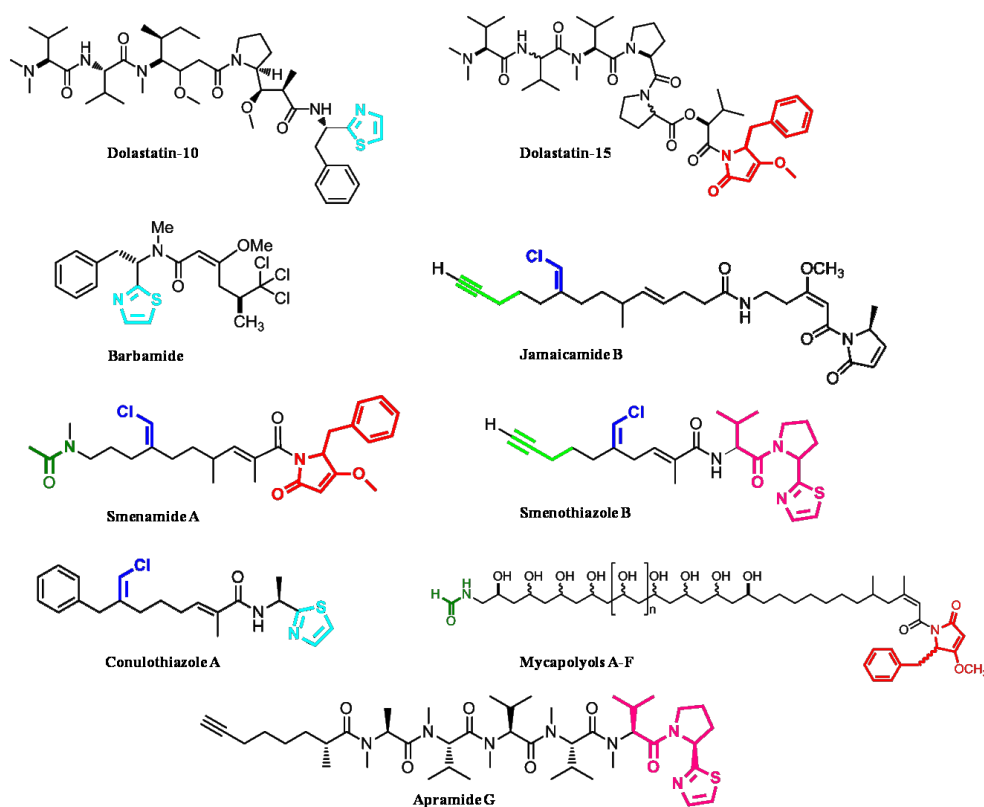


Figure 4.9. Structural analogies of *Smenospongia* metabolites with cyanobacteria metabolites.

The dolapyrrolidinone eastern terminus of smenamides is also present in dolastatin-15 (a depsipeptide of probable cyanobacterial origin isolated for the first time from the sea hare *Dolabella auricularia*) and in other cyanobacterial metabolites, known as mycapolyols A–F.⁴ The chlorovinyl function, present in the structure of all the

three smenamides, smenothiazoles and conulothiazoles, is an intriguing structural feature shared with jamaicamides, isolated from the cyanobacterium *Lyngbia majuscula*⁵ (recently renamed as *Moorea producens*).⁶ Moreover, the peptide moiety of both smenothiazole A and B (**3** and **4**, respectively, Figure 4.2) is very similar to the eastern part of apramide G.⁷

The secondary metabolites isolated from sponges can be either produced through the secondary metabolism of the sponge itself or through the symbiotic relationship of the sponge with microorganisms, such as bacteria or cyanobacteria. Although it has not yet been possible to establish whether compounds **1-6** (Figure 4.2 and 4.3), isolated from *Smenospongia aurea* and *conulosa*, are produced in one or the other way, comparable amounts of smenamides (**1** and **2**, Figure 4.2) were found in three samples of *S. aurea* collected in different moments and in different geographical areas. This observation, strengthened by the structural similarity of the smenamides with products of the metabolism of cyanobacteria, suggests their probable cyanobacterial origin.

Recently, biogenetic studies were performed in order to detect the presence in the metagenome of *S. aurea* of cyanobacterial sequences.³ PCR experiments were performed by using the metagenome of the sponge as a template, while specific primers were used to reveal the presence of 16S rRNA cyanobacterial sequences. The production of clear bands of the expected length of 670 bp, confirmed the presence of cyanobacteria in *S. aurea*. Therefore, a gene library of the 16S rRNA sequences was build up from amplicons and 24 clones were sequenced. Except for three sequences not related to cyanobacteria, all the sequences match at 99% and were assigned to the *Candidatus Synechococcus spongiarum*, a "sponge-specific" line of unicellular symbiont cyanobacteria. The latter are considered the most

prevalent and widespread symbiotic cyanobacteria in tropical and temperate reef sponges.⁸

Despite the presence of *Ca. Synechococcus spongiarum* in *S. aurea* was confirmed, this is not a sufficient condition to affirm that this cyanobacterium is the real producer of compounds **1-4** (Figure 4.2). The isolation of metagenomic DNA from a complex and heterogeneous matrix, including marine sponges tissues, is a delicate procedure which involves the risk of overlooking underrepresented microbial taxa present among the symbiont microorganisms of the sponge. Moreover, the genome of *Ca. Synechococcus spongiarum* from the sponge *Carteriospongia foliascens* was recently sequenced,⁹ providing no clue with the presence of NRPS or PKS pathways.¹⁰ This evidence further weakened the hypothesis according to which *Synechococcus spongiarum* may be the real producer of smenamides (**1, 2**) and smenothiazoles (**3, 4**).

Envisioning different approaches to metagenomic screening in order to detect the microbial source of these compounds, cell separation has emerged as a valid alternative approach.^{11,12,13} The latter was shown to be valuable technique used for the identification of symbiont microorganism producing secondary metabolites and the isolation of the relevant biosynthetic gene clusters.

Therefore, a cell separation, using density gradient centrifugation (to prepare fractions enriched with bacteria of different cell densities), was performed on a freshly collected sample of *S. conulosa*, in order to gain a preliminary idea of the cellular distribution of the chlorinated peptide/polyketide hybrids of interest.

The cell fractions were analysed by high resolution LC-MS revealing that these metabolites are mainly localised in two high-density fractions. In addition, the microscopically examination of these fractions showed that they are principally

constituted by a highly enriched population of large filamentous and branched green microorganisms, which could represent the producers of our compounds.

Moreover, the unicellular cyanobacterium *Synechococcus spongiarum* is mostly localized in low-density cell fractions. The latter evidence allows the exclusion of this bacterium as the producer of the chlorinated compounds from *Smenospongia* spp.

Further studies are in progress to gain a better insight in the biogenesis of these metabolites, using the metagenomic DNA from the filamentous cell fractions, and to identify and isolate their biosynthetic gene clusters, with the future perspective of heterologous expression.

4.6 Conclusions

The analysis of the lipophilic extract of the Caribbean sponge *Smenospongia conulosa* led to the isolation of two new hybrid peptide/polyketide compounds, conulothiazoles A (**5**) and B (**6**). Despite the scarce amount of these compounds isolated from the marine source, a full set of one- and two-dimensional NMR spectra were recorded, which allowed the structural elucidation of the molecule. The absolute configuration of the amino acidic α carbon of the alanine residue of both molecules was established by using Marfey's method. Recent biogenetic studies on the metagenome of *S. aurea* showed the presence of *Ca Synechococcus spongiarum* as symbiont bacterium of the sponge. Unfortunately, further studies demonstrated that this microorganism is not the real producer of the chlorinated compounds isolated from *S. aurea*. Due to the little amount of these metabolites isolated from the sponge, the evaluation of their cytotoxic activity was not carried

out in order to avoid the massive collection of the sponge preserving the marine ecosystem.

4.7 Experimental section

4.7.1 Collection

A sample (615 g wet weight) from the sponge *Smenospongia conulosa* (Order Dictyoceratida, Family Thorectidae) was collected on 10 July 2013 at 15 m depth by Scuba-diving along the coast of Little Inagua Island, Bahamas (GPS coordinates 21°27.041' N 73°03.483' W) during a ship-board research expedition. The sample (a relatively small portion of a much larger sponge) was excised with a sharp scalpel to minimally affect the remaining sponge tissue and allow recovery and regrowth. After collection, the sample was unambiguously identified onboard using a web-based photographic and taxonomic key, The Sponge Guide (www.spongeguide.org), with subsequent confirmation by sponge taxonomist Dr. Sven Zea. The sample was frozen immediately after collection and stored at $-20\text{ }^{\circ}\text{C}$ until extraction. A voucher specimen of the organism is stored at Dipartimento di Farmacia, Università degli Studi di Napoli “Federico II” with the reference number 24713.

4.7.2 Extraction and Isolation

The sponge (615 g wet weight) was homogenized and extracted with MeOH (4×4 L), MeOH and CHCl_3 in different ratios (2:1, 1:1, 1:2) and then with CHCl_3 (2×4 L). The MeOH extracts were partitioned between H_2O and n-BuOH; the BuOH layer was combined with the CHCl_3 extracts and concentrated in vacuo. The total organic extract (15.31 g) was chromatographed on a column packed with RP-18

silica gel. The fraction eluted with MeOH/H₂O (9:1, 293.5 mg) was partitioned into a two-phase system composed of H₂O (160 mL), MeOH (260 mL), CHCl₃ (140 mL), and AcOH (5 mL); (see chapter 4) the organic layer, containing conulothiazoles, was subjected to reversed-phase HPLC separation [column 250 × 10 mm, 10 μm, Luna (Phenomenex) C18; eluent A: H₂O; eluent B: MeOH; gradient: 55→100% B, over 60 min, flow rate 5 mL min⁻¹], thus affording a fraction (t_R = 31 min) containing conulothiazole A and a fraction (t_R = 33 min) containing the conulothiazole B. The two fractions were each separated on reversed-phase HPLC [C18, 5 μm, 250 × 4.6 mm; eluent A: H₂O; eluent B: ACN; gradient: 50→100% B, over 35 min, flow rate 1 mL min⁻¹], which gave 36 μg of pure conulothiazole A (t_R = 20 min) and 41 μg of pure conulothiazole B (t_R = 22 min). The weights were determined using an NMR quantitation method (QSCS)¹⁴ based on integration of solvent ¹³C satellite peaks. A solution of pyridine in CD₃OD (1.47 mg/600 μL) was used as external calibration.

4.7.3 Conulothiazole A (5)

Colorless amorphous solid, UV (MeOH): λ_{max} (ε) 244 nm (15900) 216 nm (50900); HRESIMS (positive ion mode, MeOH) *m/z* 411.1270 [M+Na]⁺ (calcd. for C₂₁H₂₅ClN₂NaOS⁺ 411.1268); MS isotope pattern: M (100%), M + 1 (24%, calcd. 22.7%), M + 2 (39%, calcd. 38.0%), M + 3 (8.3%, calcd. 8.3%); ¹H and ¹³C NMR: see Table 5.1.

4.7.4 Conulothiazole B (6)

Colorless amorphous solid, UV (MeOH): λ_{max} (ε): 244 nm (15600), 215 nm (48200); HRESIMS (positive ion mode, MeOH) *m/z* 425.1426 [M+Na]⁺ (calcd. for

$C_{22}H_{27}ClN_2NaOS^+$ 425.1425); MS isotope pattern: M (100%), M+1 (24%, calcd. 23.8%), M+2 (38%, calcd. 39.2%), M+3 (11%, calcd. 8.7%); 1H and ^{13}C NMR: see Table 5.2.

4.7.5 Ozonolysis and Hydrolysis

A small amount of compound **5** (4 μ g) or **6** (4 μ g) was separately suspended in ozone-saturated MeOH (300 μ L) at -78 $^{\circ}C$ for 5 min. The samples were dried under a N_2 stream to remove ozone, then treated with 6 N HCl and heated in a sealed glass tube at 180 $^{\circ}C$ for 2 h. The residual HCl fumes were removed in vacuo.

4.7.6 Marfey's Derivatization with D- and L-FDAA

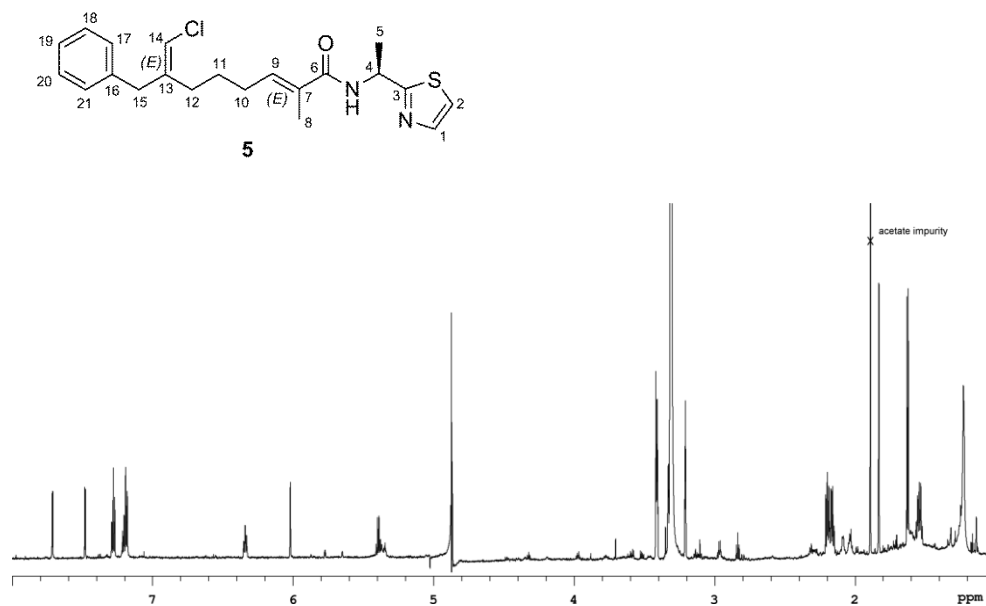
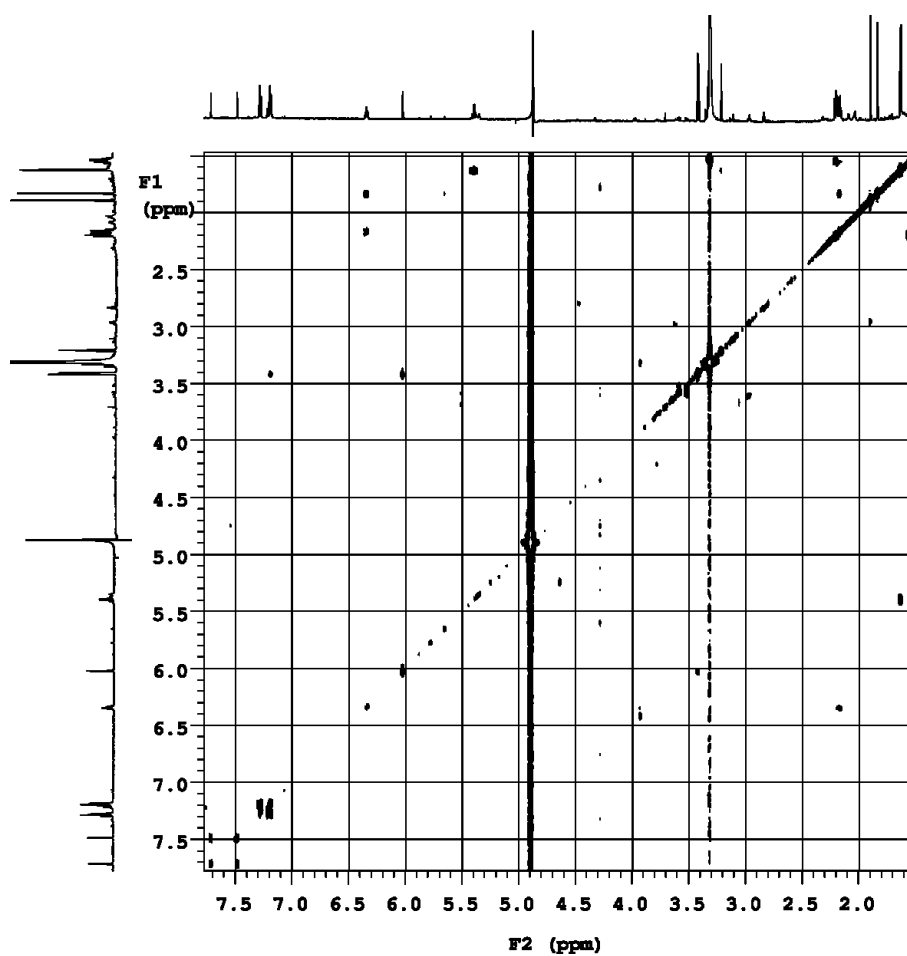
The hydrolysate of **5** or **6** was dissolved in TEA/acetone (2:3, 100 μ L) and the solution was treated with 100 μ L of 1% 1-fluoro-2,4-dinitrophenyl-5-l-alaninamide (L-FDAA) in ACN/acetone (1:2). The vial was heated at 50 $^{\circ}C$ for 1 h. The mixture was dried, and the resulting L-FDAA-Ala derivatives were redissolved in ACN/ H_2O (5:95, 500 μ L) for LC-MS analysis. An authentic L-Ala standard was treated with L-FDAA and D-FDAA as described above and yielded, respectively, the L-FDAA-L-Ala and D-FDAA-L-Ala standards used in the subsequent LC-MS analysis.

4.7.7 High-resolution LC-MS Analysis of Marfey's derivatives

Marfey's derivatives were analyzed by LC-HRESIMS. A 5 μ m Kinetex C18 column (50 \times 2.10 mm), maintained at 25 $^{\circ}C$ was eluted at 200 μ L min^{-1} with H_2O and CH_3CN , using a gradient elution. The gradient program was as follows: 5% CH_3CN 3 min, 5–60% MeOH over 20 min, 90% CH_3CN 5 min. Mass spectra were

acquired in positive ion detection mode and the data were analyzed using the suite of programs Xcalibur. The retention times of L-FDAA-L-Ala and D-FDAA-L-Ala standards were determined as 15.36 and 16.37 min, respectively, on the basis of the extracted-ion chromatograms at m/z 342.1044. The retention times measured in the same way for the L-FDAA-Ala samples obtained from compounds **5** and **6** were, respectively, 15.32 min and 15.31 min, and were indicative of the L configuration of Ala in both compounds.

4.8 Supplementary spectroscopic data

Figure 4.10. ¹H NMR spectrum of conulothiazole A (5) (CD₃OD, 700MHz).Figure 4.11. COSY spectrum of conulothiazole A (5) (CD₃OD, 700MHz).

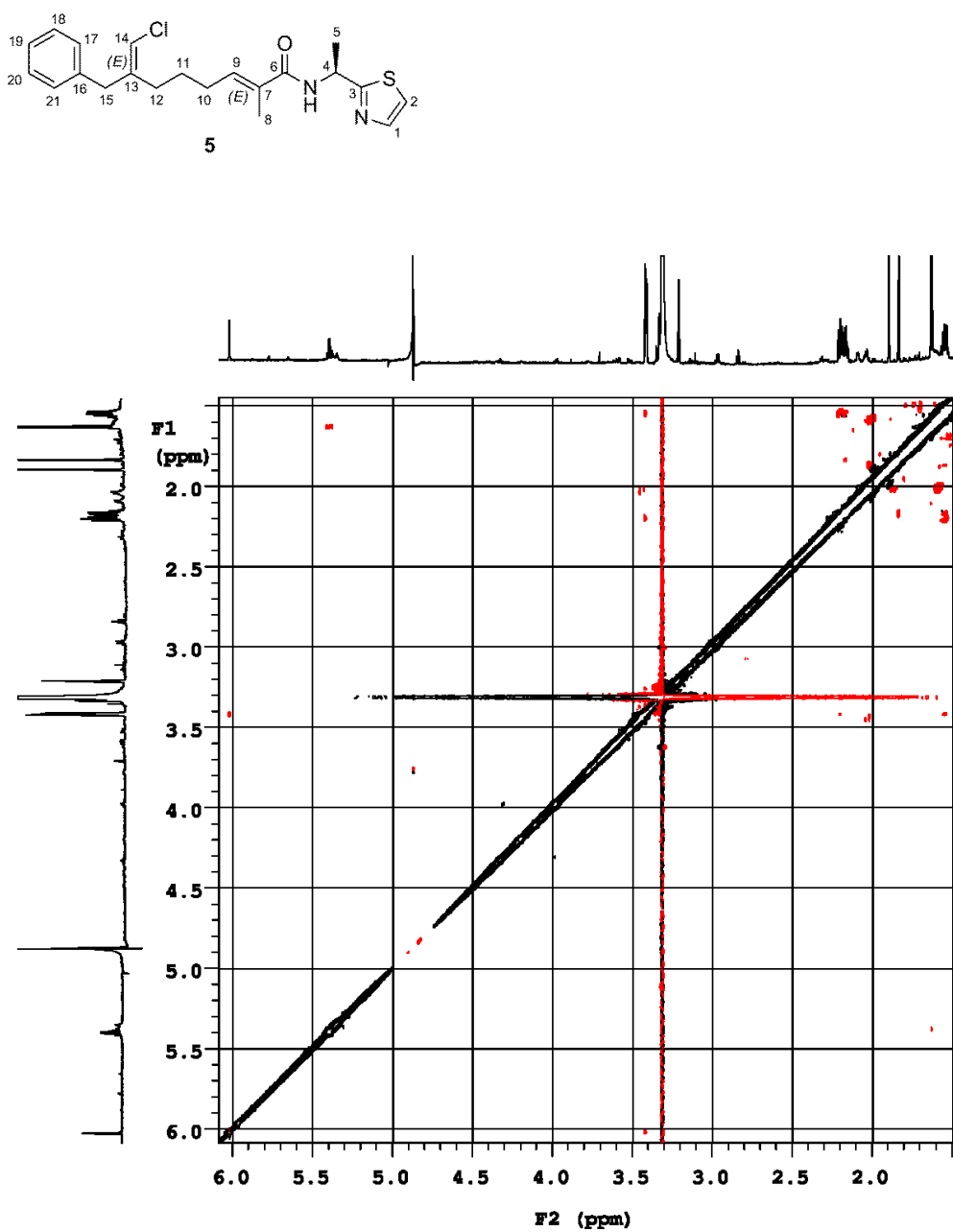


Figure 4.12. NOESY spectrum of conulothiazole A (5) (CD₃OD, 700MHz).

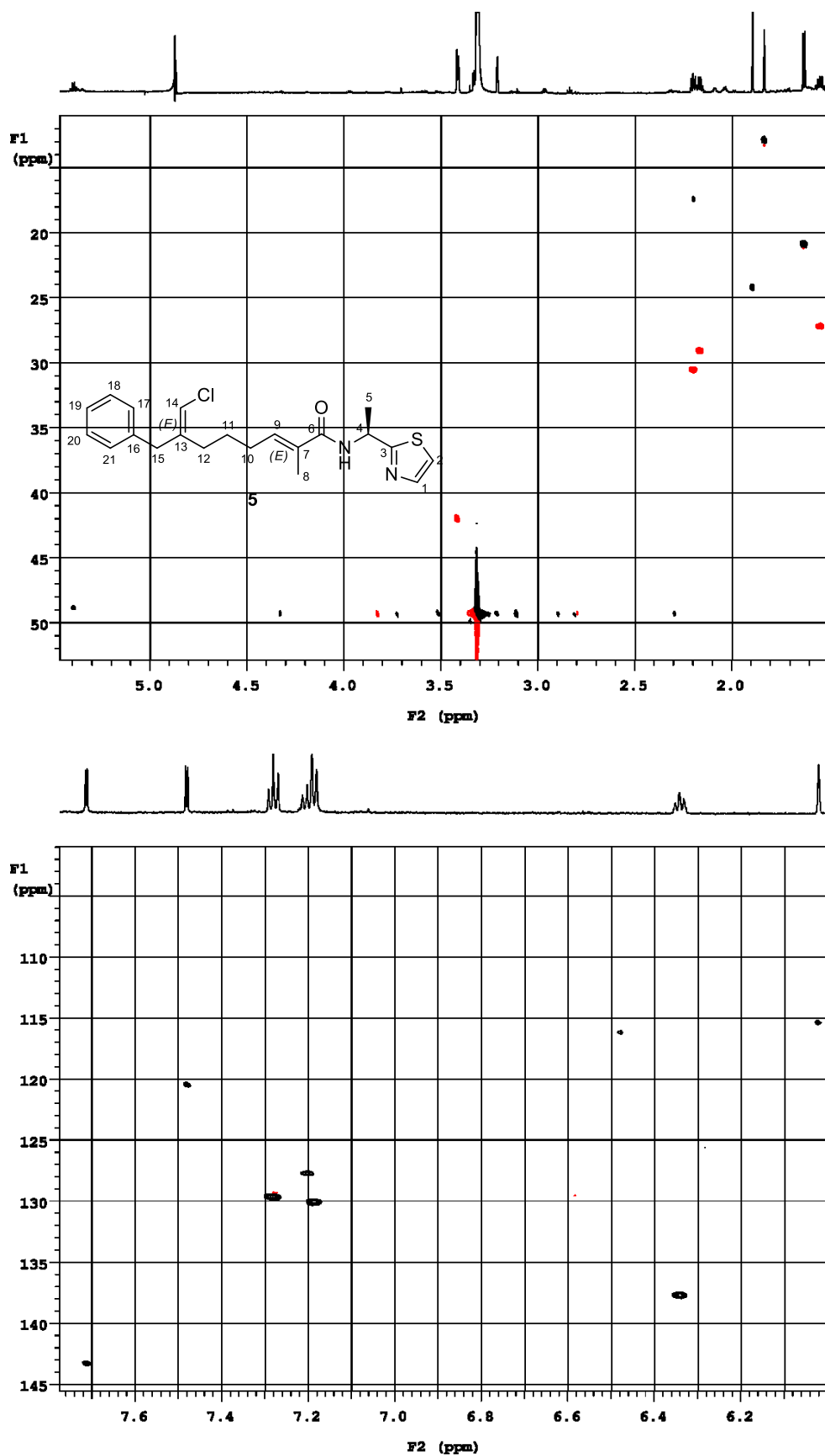


Figure 4.13. HSQC spectrum of conulothiazole A (5) (CD₃OD, 700MHz).

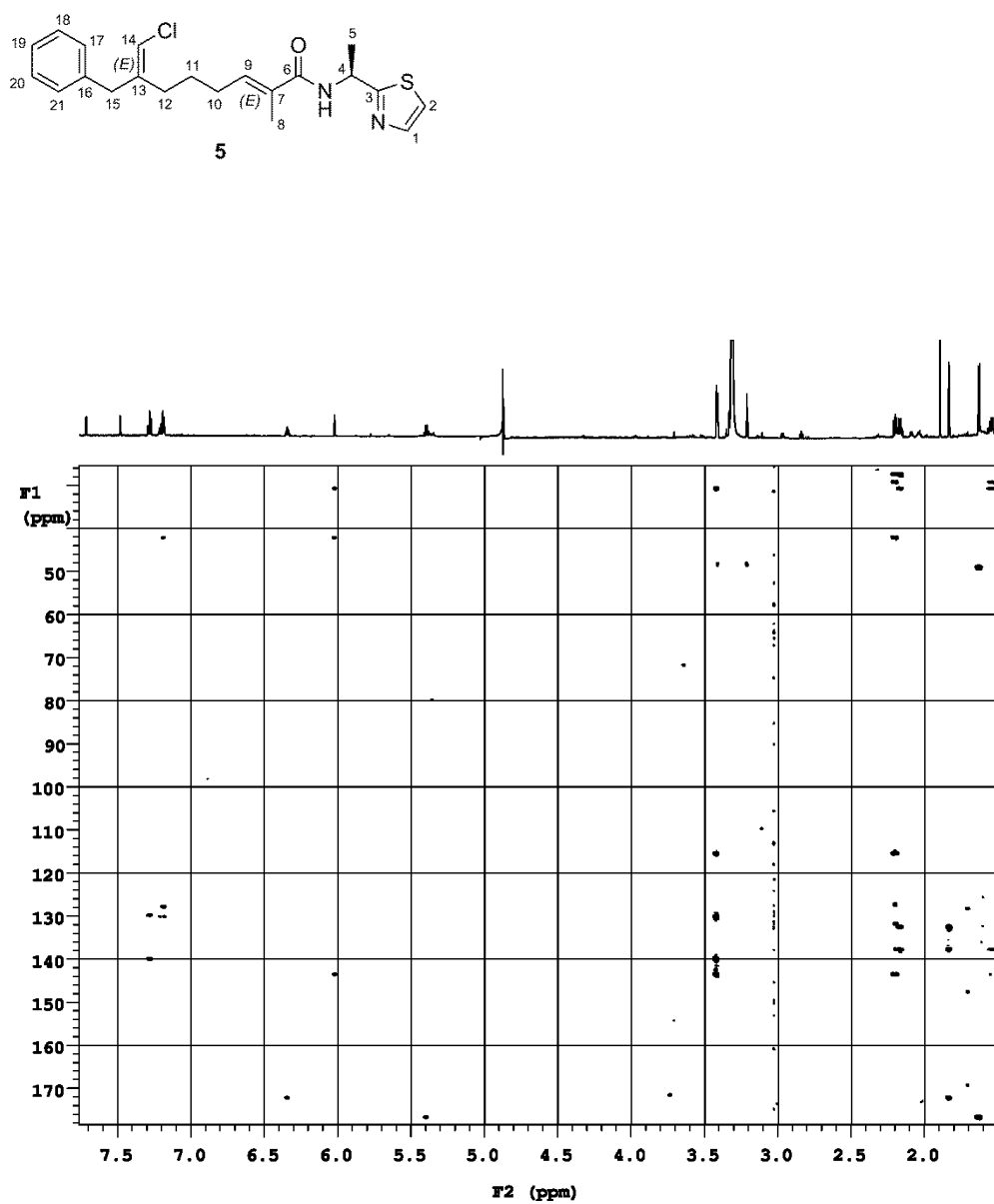


Figure 4.14. HMBC spectrum of conulothiazole A (5) (CD₃OD, 700MHz).

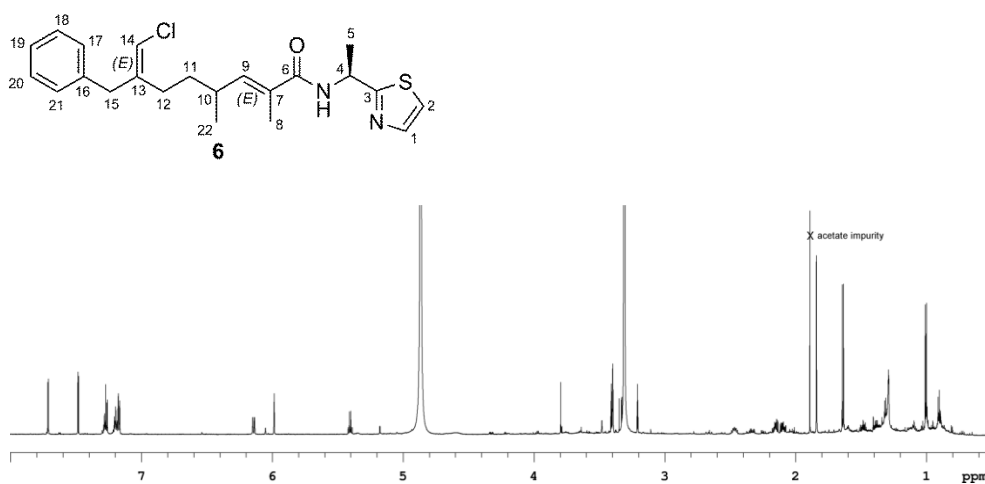


Figure 4.15. ¹H NMR spectrum of conulothiazole B (6) (CD₃OD, 700MHz).

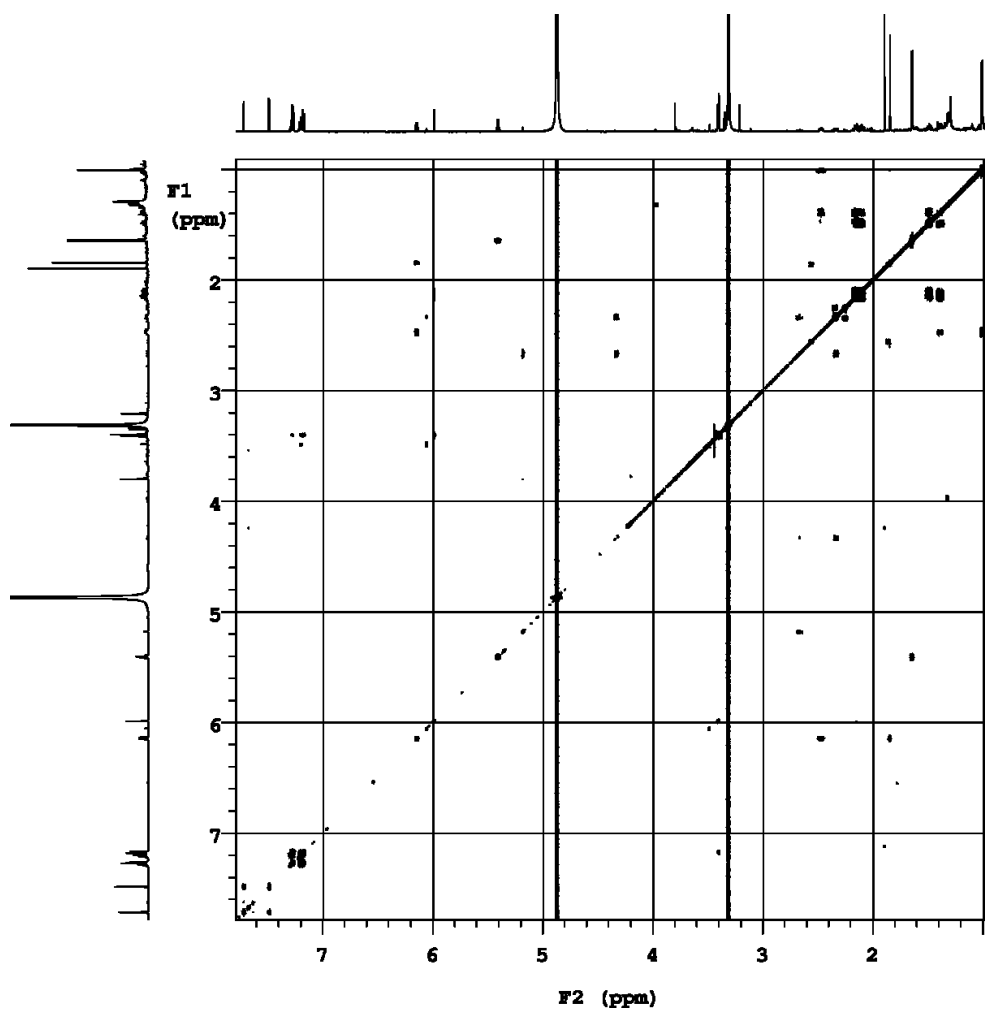


Figure 4.16. COSY spectrum of conulothiazole B (6) (CD₃OD, 700MHz).

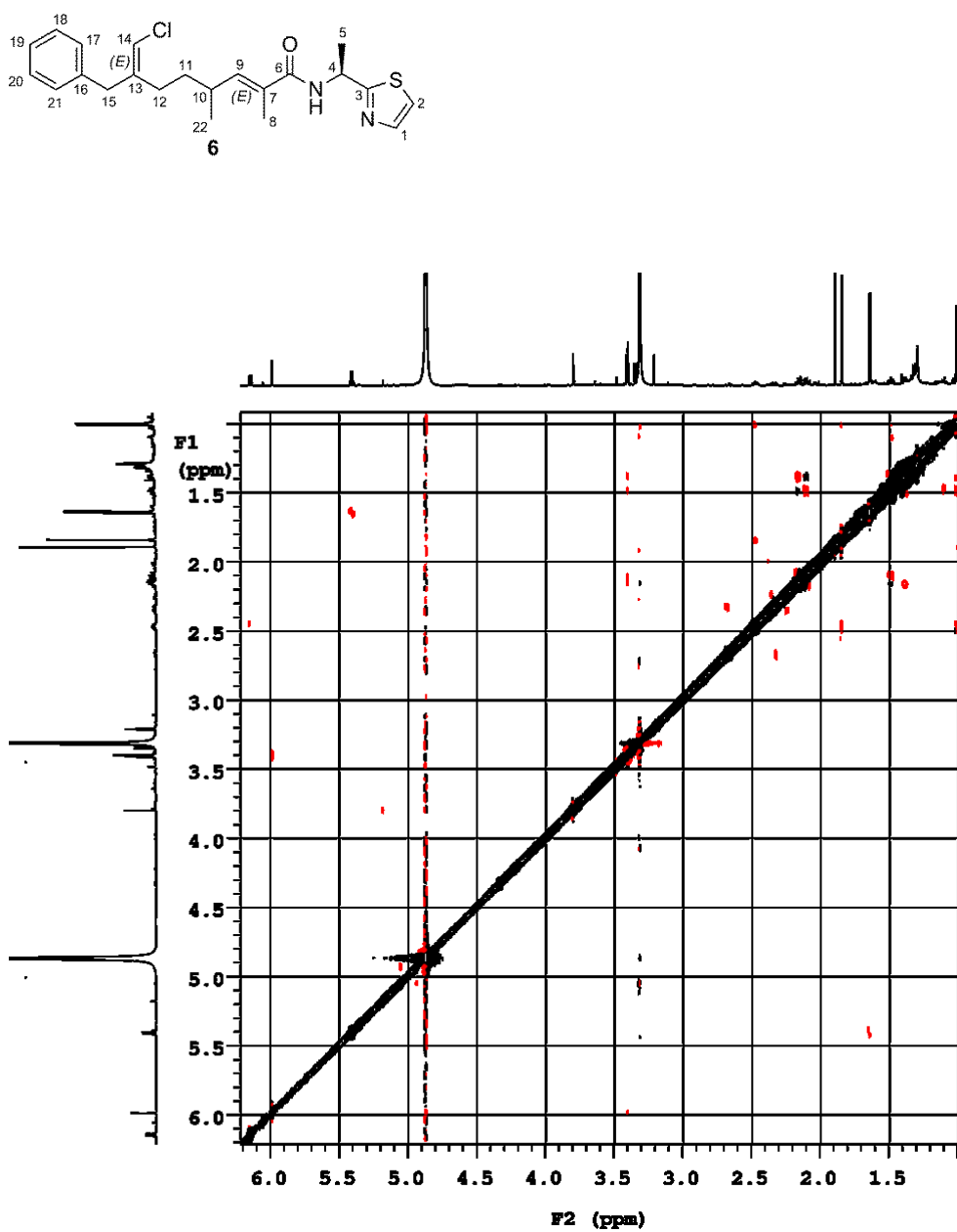


Figure 4.17. ROESY spectrum of conulothiazole B (6) (CD₃OD, 700MHz).

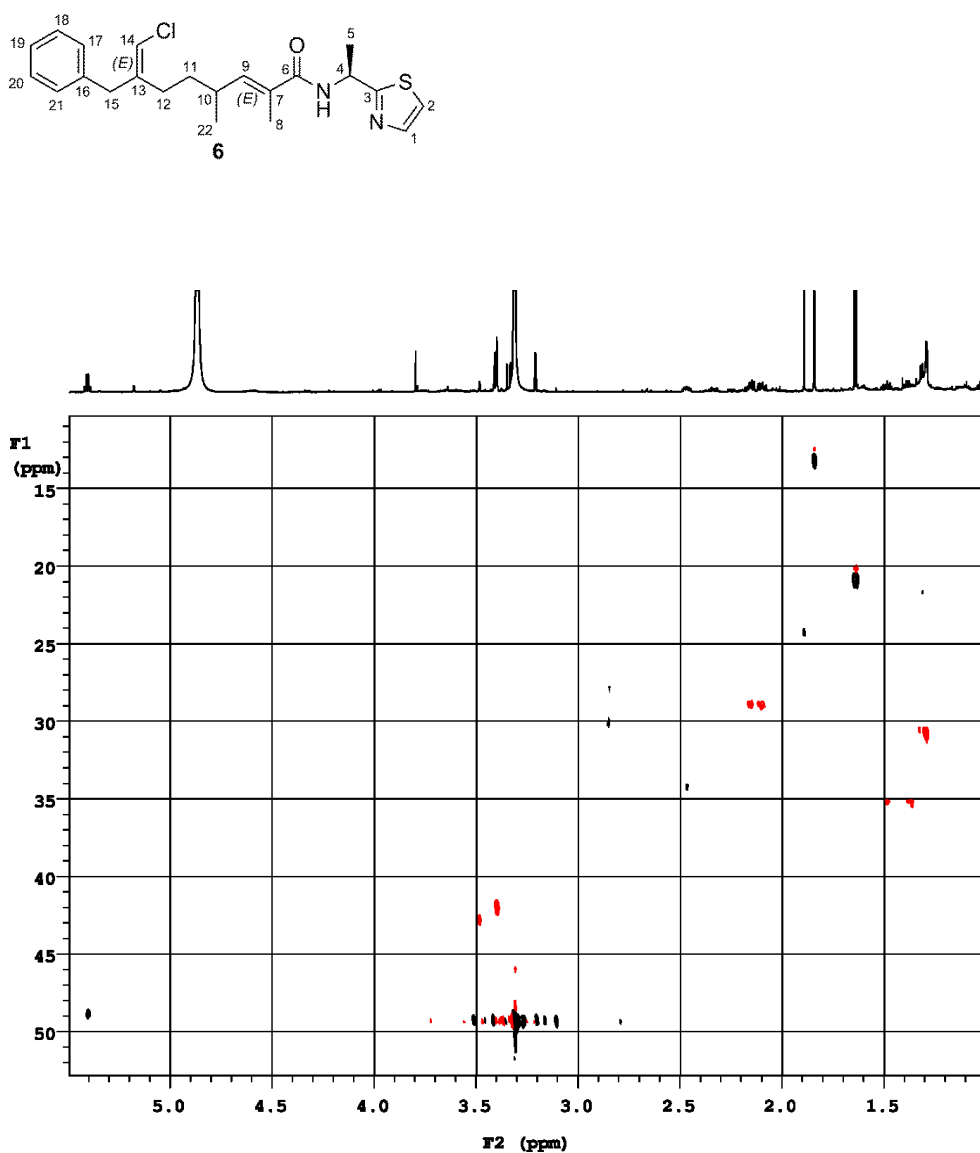


Figure 4.18. HSQC spectrum of conulothiazole B (6) (CD₃OD, 700MHz).

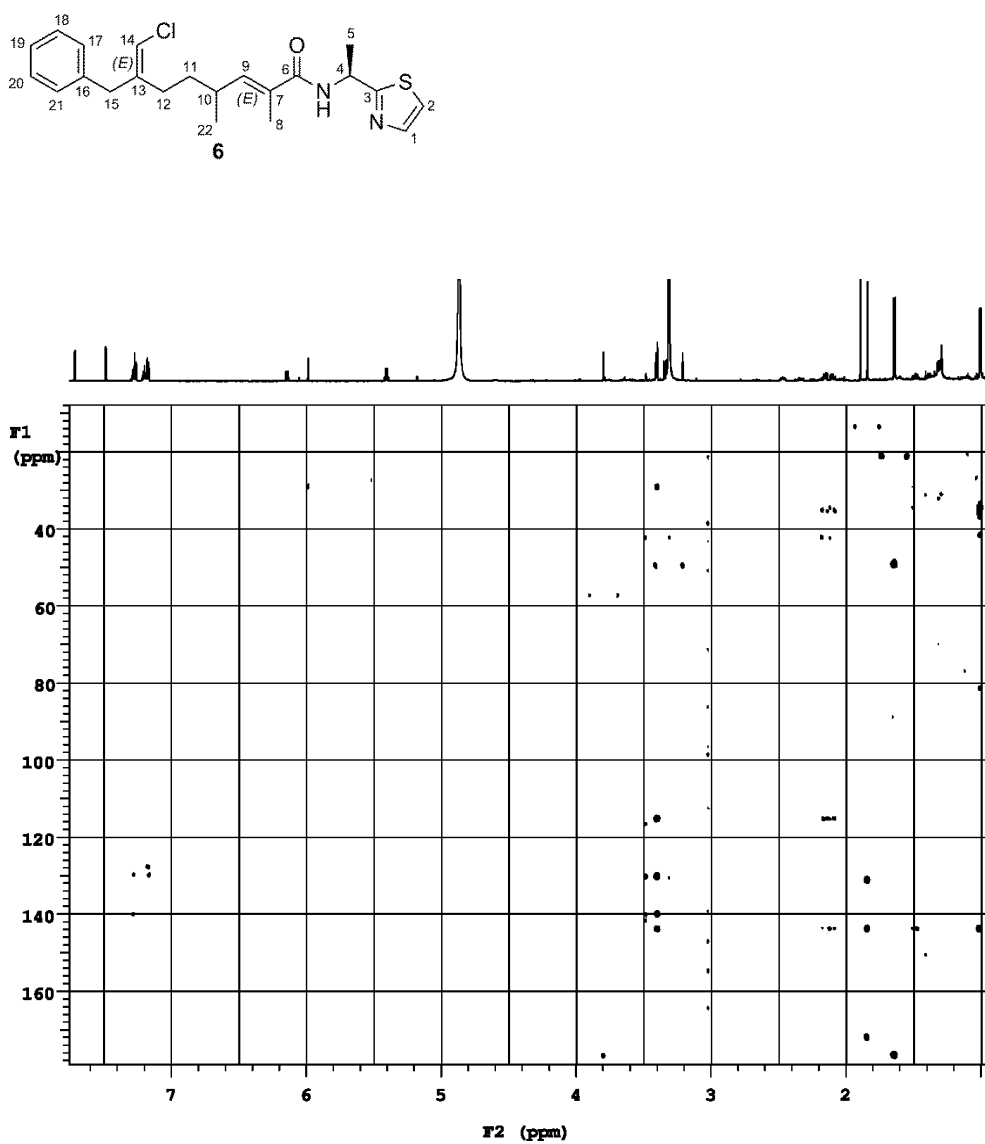


Figure 4.19. HMBC spectrum of conulothiazole B (6) (CD₃OD, 700MHz).

References

-
- ¹ R. Teta, E. Irollo, G. Della Sala, G. Pirozzi, A. Mangoni, V. Costantino, *Marine Drugs*, **2013**, 11 (11), 4451-4463.
- ² Esposito G., Teta R., Miceli R., Ceccarelli L., Della Sala G., Camerlingo R., Irollo E., Mangoni A., Pirozzi G., Costantino V., *Mar. Drugs* **2015**, 13, 444-459.
- ³ G. Esposito, G. Della Sala, R. Teta, A. Caso, M.L. Bouguet-Kondracki, J.R. Pawlik, A. Mangoni, V. Costantino, *Eur. J. Org. Chem.* **2016**, 16, 2871–2875.
- ⁴ Phuwapraisirisan, P.; Matsunaga, S.; Fusetani, N. *Organic Lett.* **2005**, 7, 2233-2236.
- ⁵ Edwards, D.J.; Marquez, B.L.; Nogle, L.M.; McPhail, K.; Goeger, D.E.; Roberts, M.A.; Gerwick, W.H. *Chem. Biol.* **2004**, 11, 817–833.
- ⁶ Engene, N.; Rottacker, E.C.; Kastovsky, J.; Byrum, T.; Choi, H.; Ellismanm, M.H.; Komàrek, J.; Gerwick, W.H. *Int. J. Syst. Evol. Microbiol.* **2012**, 62, 1171.
- ⁷ Luesch, H.; Yoshida, W.Y.; Moore, R.E.; Paul, V.J. *J. Nat. Prod.* **2000**, 63, 1106–1112.
- ⁸ Erwin, P.M.; Thacker, R.W. *Mol. Ecol.* **2008**, 17, 2937-2947.
- ⁹ Gao, Z. M.; Wang, Y.; Tian, R. M.; Wong, Y. H.; Batang, Z. B.; Al-Suwailem, A. M.; Bajic, V. B.; Qian, P. Y. *MBio* **2014**, 5.
- ¹⁰ Shih, P. M.; Wu, D.; Latifi, A.; Axen, S. D.; Fewer, D. P.; Talla, E.; Calteau, A.; Cai, F.; Tandeau de Marsac N.; Rippka, R.; Herdman, M; Sivonen, K.; Coursin, T.; Laurent, T.; Goodwin, L.; Nolan, M.; Davenport, K. W.; Han, C. S.; Rubin, E. M.; Eisen, J. A.; Woyke, T.; Gugger, M.; Kerfeld, C. A. *Proc Natl Acad Sci U S A.* **2013**, 110, 1053-1058.
- ¹¹ Schirmer, A.; Gadkari, R.; Reeves, C. D.; Ibrahim, F.; DeLong, E. F.; Hutchinson, C. R. *Appl. Environ. Microbiol.* **2005**, 71, 4840–4849.
- ¹² Bewley, C. A.; Holland, N. D.; Faulkner, D. J. *Experientia* **1996**, 52, 716–722.
- ¹³ Laroche, M.; Imperatore, C.; Grozdanov, L.; Costantino, V.; Mangoni, A.; Hentschel, U.; Fattorusso, E. *Mar. Biol.* **2007**, 151, 1365–1373.
- ¹⁴ D. S. Dalisay, T. F. Molinski, *J. Nat. Prod.* **2009**, 72, 739-744.

Chapter 5

Evaluation of the antiproliferative activity of the organic extract of *Geodia cydonium*

It is well known that marine sponges are one of the most prolific sources of bioactive compounds, with about 4851 metabolites identified to date which correspond to nearly 30% of MNPs so far discovered.¹ Currently, several studies have been conducted on most of the marine sponges, except for the Mediterranean sponge *Geodia cydonium* (*Demospongiae*, *Astrophorida*, *Geodidae*), for which only studies leading to the isolation of steroidal ketones have been reported.²



Figure 5.1. A specimen of the Mediterranean sponge *Geodia cydonium*.

A recent study³ on *G. cydonium* showed the anti-inflammatory effect of its methanol extract on human breast cancer MCF-7 cell line. Since inflammatory processes are often involved in the development, progression and metastasis of malignant tumours, the present study aimed to the evaluation of the anticancer

activity of the organic extract of *G. cydonium*.⁴ Since this was a multidisciplinary project, it was carried out in collaboration with the Istituto Nazionale per lo Studio e la cura dei Tumori “Fondazione G. Pascale”, the “Stazione Zoologica Anton Dohrn”, the Department of Biology of University of Naples Federico II, and the Institute of Biomolecular Chemistry-CNR. As for my contribution to this project, I was involved in the analysis of the chemical content of the methanol extract of the sponge and its purification, as well as in the dereplication strategy. More precisely, the methanol extract of the sponge was subjected to chromatography and the three most abundant fractions obtained were tested on MCF-7, MDA-MB231 and MDA-MB468 human breast cancer cell lines. Fraction 3 (Figure 5.3) was shown to have an antiproliferative activity on all of three cell lines, without interfering with the cell proliferation of the MCF-10A normal breast cell line, used as a control. Cellular studies were then carried out to understand whether the fraction is able to induce apoptosis and/or to block the cell cycle. Moreover, metabolomic studies have been performed on the cells treated with the fraction 3 in order to identify the metabolic pathways modulated by this fraction, whereas the increasing/decreasing of cytokines levels were analysed to evaluate the role of the active fraction in anti- or pro-inflammatory processes. Finally, the combined use of high resolution LC-MS, tandem mass spectrometry (MS/MS) and the molecular networking technique allowed to identify the known as well as the new metabolites present in the fraction of interest.

5.1 Bioguided fractionation of *G. cydonium* extracts

A sample of the Mediterranean sponge *G. cydonium* was collected on July 2015 at 20 m depth by Scuba in the “Parco Sommerso di Baia” (Gulf of Naples, Italy). After

collection, the sponge was immediately frozen and stored at -20 °C until its arrival to the Department of Pharmacy. The sponge (509 g, wet weight) was properly homogenized and extracted with CH₃OH, mixtures of CH₃OH/CH₃Cl and CH₃Cl. The methanol extract was partitioned between water and butanol. The butanol phase was then combined with the chloroform extracts and concentrated under vacuum obtaining a crude extract (3.9 g). The latter was then subjected to Droplet CounterCurrent Chromatography (DCCC) using CH₃Cl/CH₃OH/H₂O (7:13:8) in the ascending mode. 6 mL fractions were collected and combined on the basis of their similar TLC profile. The most abundant fractions (fraction 1, 2 and 3) were tested on MCF-7, MDA-MB231 and MDA-MB468 human breast cancer cell lines and on MCF-10A normal breast cell line. Data showed that only fraction 3 has an antiproliferative activity on all the three cancer cell lines, while it has no effects on the healthy breast cell line.

5.2 Combined use of LC-HRMS, LC-HRMS/MS and molecular networking as a novel dereplication strategy

Molecular networking was recently introduced as a captivating dereplication strategy, allowing the identification of known metabolites as well as new compounds, which are present in an organic extract.⁵ The latter are analysed by LC-HRMS and LC-HRMS/MS and the data obtained are used to generate a molecular network using the Global Natural Product Social Molecular Network (GNPS).⁶ More precisely, the mass spectra obtained from one or more LC-HRMS/MS analyses are compared pairwise. Moreover, each spectrum is compared with MS/MS spectra of all of the natural compounds present in GNPS libraries. As a

result, a two-dimensional network is obtained, in which a node represents a single molecule, and each node is related to another through an edge.

The molecular network obtained from the active fraction 3 is depicted in Figure 5.2.

The network is characterized by six clusters, which are in turn constituted by two to thirteen nodes.

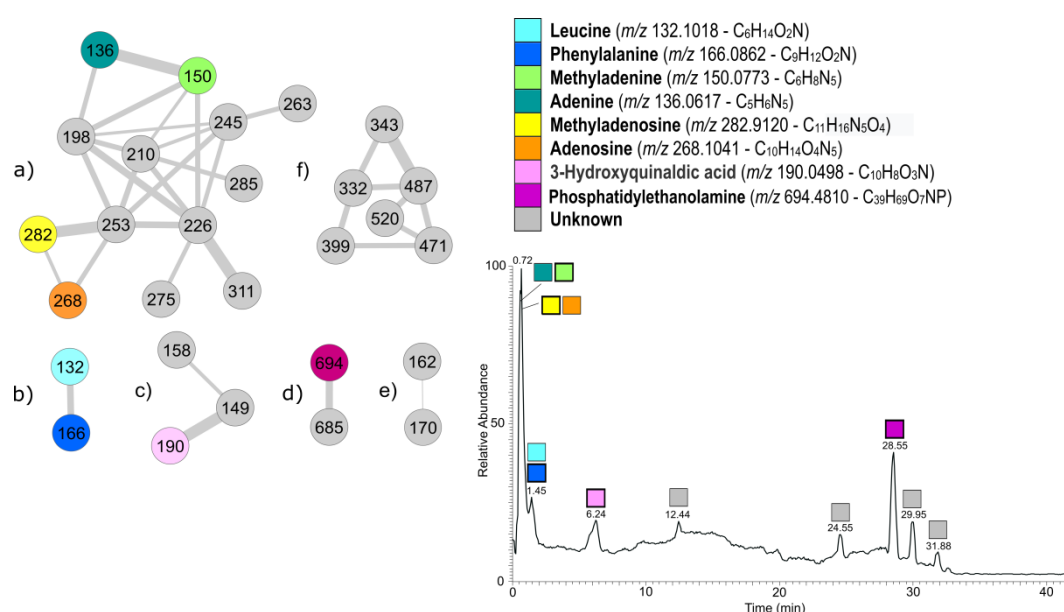


Figure 5.2. (Left) Two-dimensional molecular network of the active fraction from the sponge *Geodia cydonium*. In the clusters indicated with (a–f), nodes are labeled with parent m/z ratio $[M+H]^+$ ions; edge thickness is related to cosine similarity score; **(Right)** Liquid chromatography-high resolution mass spectrometry (LC-HRMS) profile of the active fraction; the most abundant ions are represented by colored bold contour squares.

Although molecular networking significantly reduces the dereplication efforts, a more traditional approach, based on the search against databases of marine natural compounds, is required when the molecular formula found does not match any compound name. A match within GNPS' libraries gives indeed valuable information on the structure of the molecule but sometimes does not allow immediately the identification of a compound. Moreover, even though the MS/MS

spectra libraries contain a large number of known natural compounds, this number is still limited.

Therefore, the results obtained from the molecular network of fraction 3 combined with the search of the traditional databases (Metlin at <https://metlin.scripps.edu/> and MarinLit at <http://pubs.rsc.org/marinlit/>) gave the following information. Cluster a), consisting of thirteen nodes (Figure 5.2), was shown to contain nucleosides and nucleobases. Data obtained show the presence in this cluster of methyladenosine (m/z 282) and methyladenine (m/z 150), which were in turn connected to two nodes (m/z 268 and m/z 136 respectively). Although these compounds were also recognized by GNPS as methyladenosine and methyladenine, they possess a mass difference of 14 amu (atomic mass unit) with the library compounds, which indicates a missing methyl group. To confirm the identity of these compounds the HRMS spectra were analysed. Their molecular formulas were determined as $C_{10}H_{13}O_4N_5$ and $C_5H_5N_5$, therefore confirming the identity of the compounds as adenosine and adenine, respectively. In addition, HRMS/MS spectra were recorded, confirming the characteristic fragmentation pattern of these nucleosides.⁷ More specifically, by cleavage of the glycosidic bonds, protonated bases (adenine and methyladenine) and a sugar moiety as the neutral fragment are obtained. According to LC-HRMS, the relative abundance of methyladenosine is 20-fold higher than adenosine, whereas methyladenine is double than adenine.

Cluster b) contained instead two nodes: one with m/z 166 corresponded to phenylalanine, as confirmed also by the molecular formula. The second node (m/z 132) was a compound related to pipercolinic acid ($C_6H_{11}O_2N$) but with 2 additional amu. The molecular formula $C_6H_{14}O_2N$ for the $[M+H]^+$ pseudomolecular ion peak was consistent with a molecule possessing two more hydrogens than pipercolinic

acid. This evidence suggested the presence in the compound of an open ring, corresponding therefore to a leucine. Both amino acids were found in comparable amounts in the active fraction, with Phe more abundant than Leu.

GNPS⁶ identified the node with m/z 190.0498 in cluster c) as 5-aminosalicylic acid (5-asa). The compound actually had 36 amu more than 5-asa, corresponding to an additional C₃ unit. The molecule containing 3 carbon atoms more as well as 3 additional unsaturations, could not be therefore 5-asa. The molecule was then identified as 3-hydroxyquinaldic acid (3-HQA) in Metlin. A further confirmation was provided by the analysis of the HRMS/MS spectrum of the molecule, in which the ions at m/z 172.0390 and 144.0440 were present, showing the loss of water and formic acid (HCOOH), but not the loss of ammonia as expected by 5-asa.

Finally, cluster d) included phosphatidylethanolamine (PE) and its analogues, while clusters e) and f) comprised unknown molecules, the structure of which could not be determined due to the small amount of the networked compounds.

Each of the molecules found in the active fraction 3 was shown to be involved in one or more biological functions. Nucleosides (methyladenine and methyladenosine) and nucleotides (adenine and adenosine), found in cluster a), are essential metabolites of the living cells and are involved in fundamental biological processes, such as the synthesis of nucleic acids. Moreover, it is well known the antiviral, anticancer, vasodilator, muscle relaxant, and hypertensive activity of many marine nucleosides, which makes them promising lead compounds in drug design.⁸ The amino acids, such as leucine and phenylalanine found in cluster b), are molecules that are frequently found in the organic extracts of marine organisms, occurring both in the free-state and as basic structural units of proteins and peptides. Many marine amino acids derivatives and peptides possess captivating biological

activities, including a high specificity against cancer cell lines.⁹ 3-HQA in cluster c) was identified as one of the two key chromophores (together with quinoxalinic acid) in many bisintercalator natural products of marine origin (such as thiocoraline, triostin, SW-163 and echinomycin/quinomycin),¹⁰ which are able to bind to duplex DNA by insertion between the bases allowing the proper placement of the peptidic core into the DNA minor groove.¹¹ As for phosphatidylethanolamine (PE), present to cluster d), it belongs to the family of phospholipids and glycolipids that are the main constituents of sponge cell membranes,^{12,13} and were shown to have immunomodulating and antitumor activity.^{14,15}

5.3 Biological studies

The biological studies on the three most abundant fractions obtained from the purification of the methanol extract of *G. cydonium* were performed in collaboration with the SC Farmacologia Sperimentale of Istituto Nazionale per lo Studio e la cura dei Tumori “Fondazione G. Pascale”, the Department of Biology and Evolution of Marine Organisms (Stazione Zoologica Anton Dohrn), the Department of Biology of University of Naples Federico II, and the Bio-Organic Chemistry Unit of the Institute of Biomolecular Chemistry-CNR. Here the main results of these activities are reported.

The antiproliferative activity of the three most abundant fractions obtained from the DCCC of the methanol extracts of *G. cydonium* was evaluated on three breast cancer (MCF-7, MDA-MB231, and MDA-MB468) cell lines through the sulforhodamine B (SRB) assay. After 24 and 48 hour of treatment, two of the three fractions (fraction 1 and 2) were not able to block cell proliferation in all three cancer cell lines. Fraction 3 blocked instead the cell proliferation in all three cancer

cell lines. The half minimal (50%) Inhibitory Concentration (IC_{50}) of fraction 3 were calculated for each cell line after 24 and 48 h:

- MCF-7 cells: 72 and 67 $\mu\text{g}/\text{mL}$ after 24 and 48 h, respectively (Figure 5.3a);
- MDA-MB231 cells: 73 and 44 $\mu\text{g}/\text{mL}$ after 24 and 48 h, respectively (Figure 5.3b);
- MDA-MB468 cells: 80 and 70 $\mu\text{g}/\text{mL}$ after 24 and 48 h, respectively (Figure 5.3c).

IC_{50} values are lower after 48 h than those observed after 24 h.

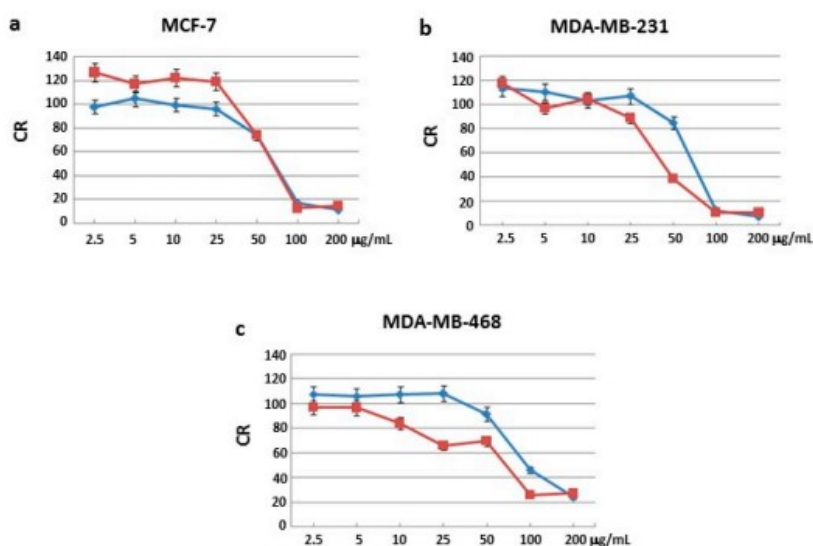


Figure 5.3. Cell proliferation. Cell viability rate (CR) related to breast cancer cells: (a) MCF-7; (b) MDA-MB231; and (c) MDA-MB468, after treatment with fraction 3 for 24 (blue line) and 48 (red line) hours.

On the basis of the results showed above, the Muse Annexin V and Dead Cell Assay was performed using the IC_{50} obtained after 48 h of treatment, in order to evaluate the pro-apoptotic mechanism of the active fraction 3. An increase in the number of apoptotic cells (51.2% for MCF-7, 63.1% for MDA-MB231 and 56.6% for MDA-MB468 cell line) respect to the control (untreated cells), as shown in Table 5.1.

	LIVE (%)	APOPTOSIS (%)	DEAD (%)
MCF-7 UNTREATED	94.8±2.4	3.8±2.6	1.4±0.8
MCF-7 TREATED	47.8±1.8	51.2±1.1	0.9±0.4
MDA-MB231 UNTREATED	97.7±3.2	2.1±2.3	0
MDA-MB231 TREATED	36.4±3.9	63.1±2.5	0
MDA-MB468 UNTREATED	96.3±2.4	3.5±2.3	0.30±0.05
MDA-MB468 TREATED	38.7±3.2	56.6±3.1	3.9±0.9

Table 5.1. Apoptosis. Percentage of live, apoptotic and dead cells expressed as mean \pm standard deviation by the Muse Annexin V and Dead Cell assay in MCF-7, MDA-MB231 and MDA-MB468 cells at IC50 concentration after 48h of treatment. Untreated cells were used as the control.

The difference in percentage of apoptotic cells revealed that the three cancer cell lines respond differently to the apoptosis assay. This phenomenon may be due to the different nature of cell lines. These differences in the percentage of apoptotic cells for the three breast cancer cell lines may be attributed to their different nature. MCF-7 cells are indeed estrogen-receptor-positive, while MDA-MB231 and MDA-MB468 cells are estrogen-receptor-negative. In addition, MCF-7 cell line possess the wild-type *tp53*, a gene that codes for the protein *p53*, which is a transcription factor that regulates the cell cycle acting as a tumour suppressor. The triple-negative human breast cancer cells, MDA-MB231 and MDA-MB468, have instead a mutated *p53* gene, expressing therefore a more malignant phenotype.^{16,17}

To gain a better insight in the cell death mechanism the mRNA expression of some genes involved in the intrinsic (*p53*, *Bax*, *p38* and *caspase-3*) and extrinsic (*caspase-3* and *caspase-8*) pathways involved in the apoptotic process was evaluated through the RT-qPCR analysis (Figure 5.4).

The expression of *p53*, *Bax*, *p38*, *caspase-3* and *caspase-8* increased significantly after 48 hour of treatment with fraction 3 in all the three breast cancer cell lines, indicating that both intrinsic and extrinsic pathways are involved in the apoptotic process.

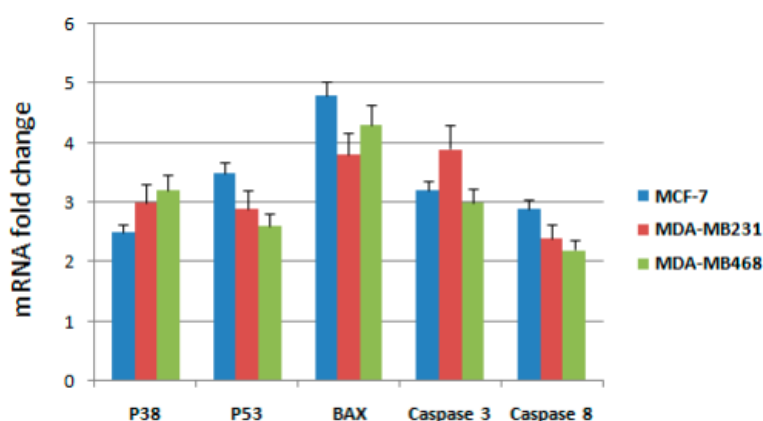


Figure 5.4. RT-qPCR analysis: mRNA fold changes were evaluated as ratios between the expression levels of five genes in three breast cancer cell lines, MCF-7, MDA-MB231 and MDA-MB468, after treatment with the active fraction compared to the control (untreated cells).

Cell cycle analysis was performed with the aim of understanding whether the active fraction was able to block the cell cycle. The effects of fraction 3 on the cell cycle were evaluated by treatment of the tumour cells with the IC_{50} obtained after 48 h. Negligible effects were observed for all the three cell lines (see Table 5.2), suggesting that the active fraction was able to induce apoptosis without interfering with the progression of the cell cycle.

	G0/G1	S	M
MCF7 UNTREATED	51.7±2.3	17.3±2.7	30.7±1.7
MCF7 TREATED	45.3±2.1	14.2±3.4	31.2±2.3
MDAMB231 UNTREATED	59.1±3.2	16.9±3.9	21.8±2.4
MDAMB231 TREATED	63.7±1.4	15.2±4.3	18.8±2.3
MDAMB468 UNTREATED	47.1±3.9	16.9±4.5	33.7±1.8
MDAMB468 TREATED	39.2±4.9	14.2±2.9	39.1±2.2

Table 5.2. Cell percentages in the different cell cycle phases (G0/G1, S, G2 and M) expressed as mean ± standard deviation after Muse Cell cycle assay in MCF-7, MDA-MB231 and MDA-MB468 cells at IC_{50} concentration after 48h of treatment. Untreated cells were used as the control.

Further studies were performed through ^1H NMR analysis of the polar extracts of MCF-7, MDA-MB231 and MDA-MB468 cells before and after treatment with fraction 3 in order to identify the metabolomic pathways modulated by the active fraction. The Orthogonal Projections to Latent Structures discriminant analysis (OPLS-DA) revealed that the spectra recorded for the three cell lines clustered in different groups (Figure 5.5a). As depicted in Figures 5.5b-d (variable importance in projection (VIP) score plots), each of the cell lines showed statistically different proton signals and metabolites after treatment respect to the control (untreated cells). Fraction 3 essentially modulated the metabolites involved in glycolysis and in the metabolism of lipids and amino acids. More precisely, the level of lactate increased after treatment in all three cell lines whereas the levels of alpha- and beta-glucose, choline, glycerophosphocholine, glutamine, glutamate and lipids decreased. A decreasing in the level of other metabolites differently decreased in the three cell lines: proline in MCF-7 cells, threonine in MDA-MB231 cells, asparagine and lysine in MDA-MB468 cells, while glycine in both MDA-MB231 and MDA-MB468 cell lines. It is well known the key role of the glucose as a bioenergetic support in the development of most tumours. Cancer cells are indeed characterised by a greater consumption of glucose through a different glycolysis pathway in comparison with normal cells, in which the pyruvate obtained by glycolysis is converted to lactate.¹⁸ The deprivation of glucose in cancer cells can therefore induce their death.^{19,20}

Fraction 3 was able to induce a decrease in glucose levels and an increase in lactate, that is turn due to the unbalanced conversion of glucose to lactate, in all three breast cancer cells. Since glutamine, glycine and glutamate originate from glycolysis intermediates, a decrease in their levels may be correlated to a decrease of glucose.

In addition, lower levels of choline were observed after treatment of the three cancer cell lines with the active sponge fraction. Choline is an essential molecule in the formation of cellular membrane, being the head group of 80% of phospholipids (phosphatidylcholine and sphingomyelin) in the extrarnal part of the membrane. The alteration of choline metabolism is considered a metabolic marker associated to oncogenesis and tumor progression.²¹ Choline levels decreased after treatment, suggesting that fraction 3 was able to block tumour progression.

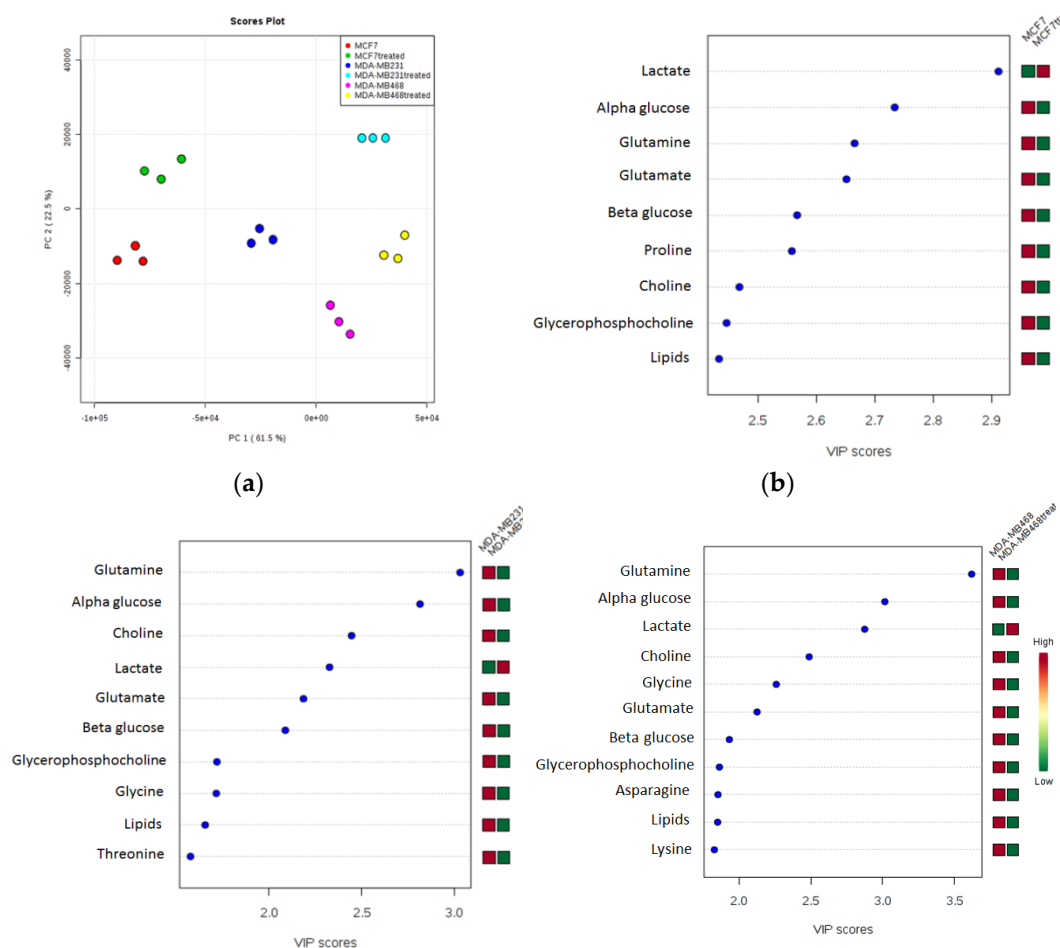


Figure 5.5. OPLS-DA plot. (a) OPLS-DA and variable importance in projection (VIP) analysis where the metabolites increased or decreased in the endo-metabolome of (b) MCF-7, (c) MDA-MB231 and (d) MDA-MB468 cells after treatment with the active fraction from the sponge *Geodia cydonium*, compared to untreated cells.

Oncogenesis and tumour progression are often related to inflammatory processes. The methanol extract of *G. cydonium*, from which fraction 3 was obtained, previously showed an anti-inflammatory activity on the human breast cancer MCF-7 cell line.³ Further studies were therefore carried out in order to establish whether fraction 3 was also able to modulate cytokines levels. After incubation of MCF-7, MDA-MB231 and MDA-MB468 cells with the IC₅₀ of the active fraction obtained after 48 h, the cytokines levels were evaluated in the cellular supernatants (Figure 5.6). Data showed that the levels of the pro-inflammatory cytokines VEGF, CXCL10, and IL-8 decreased. These three cytokines were shown to be related to tumours development.^{22,23,24} Moreover, a slight increase in levels of IL-4 and IL-10 was observed. IL-4 and IL-10 are anti-inflammatory cytokines which were proven to be involved in antitumor response.²⁵ These data are in agreement with the previous results showing that the methanol extract of the sponge induced decrease in pro-inflammatory cytokine levels in MCF-7 human breast cancer cell line.³

	MCF-7	MDA-MB-231	MDA-MB-468
CXCL10			
IL-4			
IL-8			
IL-10			
VEGF			

Figure 5.6. Cytokine levels in breast cancer cells. Scheme reporting the cytokines modulated by the active fraction obtained from the sponge *Geodia cydonium*. In particular, anti-inflammatory cytokines that are increased after treatment are reported in red and pro-inflammatory and pro-angiogenic cytokines that are decreased after treatment are reported in green.

5.4 Conclusions

The chromatographic purification of the methanol extract of the Mediterranean sponge *G. cydonium* yielded three most abundant fractions (fractions 1-3), which

were tested on three human breast cancer cell lines (MCF-7, MDA-MB231 and MDA-MB468). Among them, only fraction 3 was able to block the proliferation of the three cancer cell lines, but without interfering with the progression of the cell cycle. Moreover, this fraction showed any effect on the healthy MCF-10A breast cell line. The combined use of LC-HRMS, LC-HRMS/MS and molecular networking as a dereplication strategy allowed to identify most of the compounds contained in the active fraction. These metabolites were shown to be involved in pro- or anti-tumor processes, as confirmed by the analysis of the metabolomic profiling and cytokine levels observed in the three cancer cell lines after treatment with the active fraction. These results open up the possibility to use it for therapeutic purposes. Further studies are necessary to understand the mechanism of action of each compound present in fraction 3 and to evaluate the possible synergistic effect of a pool of compounds.

5.5 Experimental section

5.5.1 Collection, extraction, and separation

A sample of the sponge *Geodia cydonium* (Order [Tetractinellida](#), Family [Geodiidae](#)) was collected on July 2015 at 20 m depth by scuba diving in the “Parco Sommerso di Baia” (Gulf of Naples, Italy). After collection, the sample was immediately frozen and stored at $-20\text{ }^{\circ}\text{C}$ until extraction. The sponge (509 g wet weight) was homogenized and extracted with MeOH ($2 \times 2\text{ L}$), MeOH and CHCl_3 in different ratios (2:1, 1:1, 1:2) and then with CHCl_3 ($2 \times 2\text{ L}$). The MeOH extracts were partitioned between H_2O and *n*-BuOH; the BuOH layer was combined with the CHCl_3 extracts and concentrated *in vacuo*. The resulting organic extract (3.9 g) was chromatographed by DCCC using $\text{CHCl}_3/\text{CH}_3\text{OH}/\text{H}_2\text{O}$ (7:13:8) in the

ascending mode; 6 mL fractions were collected and combined in ten fractions on the basis of their similar TLC retention times. The most abundant fractions were tested to evaluate their antiproliferative activity on three human breast cancer cell lines, MDA-MB231, MDA-MB468 and MCF-7, and the normal human breast epithelial cell line MCF-10A.

5.5.2 LC-HRMS and LC-HRMS/MS and Molecular Networking Analyses

Experiments were performed using a Thermo LTQ Orbitrap XL high-resolution ESI mass spectrometer coupled to an Agilent model 1100 LC system, which included a solvent reservoir, in-line degasser, binary pump, and refrigerated autosampler. A 5 μm Kinetex C18 column (50×2.1 mm), maintained at 25 $^{\circ}\text{C}$, was operated using a gradient elution of H_2O and MeOH running at 200 $\mu\text{L}/\text{min}$. The gradient program was as follows: 10% MeOH for 5 min, 10%-100% MeOH over 25 min, 100% MeOH for 13 min. All the mass spectra were recorded in the positive-ion mode. MS parameters were a spray voltage of 4.8 kV, a capillary temperature of 285 $^{\circ}\text{C}$, a sheath gas rate of 32 units N_2 (ca. 320 mL/min), and an auxiliary gas rate of 15 units N_2 (ca. 150 mL/min). Data were collected in the data-dependent acquisition (DDA) mode, in which the first and second most intense ions of a full-scan mass spectrum were subjected to tandem mass spectrometry (MS/MS) analysis. MS/MS scans were obtained for selected ions with CID fragmentation, isolation width 2.0, normalized collision energy 36, Activation Q 0.250, and activation time 30 ms. Mass data were analyzed using the Thermo Xcalibur software.

A molecular network was created using the online workflow at GNPS. The data was then clustered with MS-Cluster with a parent mass tolerance of 2.0 Da and a MS/MS fragment ion tolerance of 0.5 Da to create consensus spectra. Further,

consensus spectra that contained less than 2 spectra were discarded. A network was then created where edges were filtered to have a cosine score above 0.6 and more than 6 matched peaks. Further edges between two nodes were kept in the network if and only if each of the nodes appeared in each other's respective top 10 most similar nodes. For dereplication purposes the spectra in the network were then searched against GNPS' spectral libraries. All matches kept between network spectra and library spectra were required to have a score above 0.6 and at least 6 matched peaks. Analog search was enabled against the library with a maximum mass shift of 100.0 Da. The data were then imported into Cytoscape 3.2.1 (<http://www.cytoscape.org/>) and displayed as a network of nodes and edges. The network was organized with the preferred layout plug-in.

5.5.3 Cell culture

Three human breast cancer cell lines, MDA-MB231, MDA-MB468 and MCF-7, all derived from adenocarcinoma metastasis and on normal human breast epithelial cells MCF-10A were used. In particular, MCF-7 and MCF-10A cells were expanded at 37°C in a humidified atmosphere of 5% CO₂ in culture medium DMEM (Dulbecco's Modified Eagle's Medium, Lonza), whereas MDA-MB-231 and MDA-MB-468 in RPMI 1640 (Lonza), supplemented with FBS (Invitrogen, Camarillo, CA, USA) at 10%, Penicillin/Streptomycin 100x (Euroclone, Devon, UK), Glutamax 100x (Invitrogen) non-essential amino acids 100x (Invitrogen). Moreover, in the case of MCF-10A the DMEM was supplemented also with human insulin 10µg /mL (Life Technologies Corporation, Carlsbad, CA, USA), human epidermal growth factor 20ng/mL (Life Technologies), and hydrocortisone 0.5µg/mL (Sigma-Aldrich) according to the procedure reported in Rothwell et al.

(2014), while for MDA-MB468 the medium was implanted with Ham's F-12 medium (1:1 mixture). Phosphate buffer (PBS phosphate buffered saline Ca²⁺ and Mg²⁺ free) and trypsin (Ca²⁺ and Mg²⁺ free) were supplied by Euroclone. Finally, the cells were kept in an incubator at a humidified atmosphere of 95% air and 5% CO₂ at 37°C.

5.5.4 Cell treatment and cell proliferation assay

Cell proliferation of cancer cells was assessed in the presence and absence of the methanol extract from *G. cydonium* by colorimetric assay with sulforhodamine B (SRB, Sigma Aldrich). This extract was first dissolved in dimethyl sulfoxide (DMSO 100mM, Sigma-Aldrich) at concentrations < 0.1%, so as not to induce toxic effects on cells. Thus, a stock solution (100 mg/mL) and its serial dilutions had a final concentration of DMSO of 0.05%.

Cancer cells were plated in 96 well tissue culture plates at a concentration of 15×10^3 cells per well and allowed to attach for 24h. Cells were then treated with different concentrations of the methanol extract (2.5 µg/mL, 5 µg/mL, 10 µg/mL, 25 µg/mL, 50 µg/mL, 100 µg/mL, 200 µg/mL) and incubated for 24h and 48h. These concentrations were selected on the basis of a recent paper.³ After 48h of treatment, cells were fixed with trichloroacetic acid (Sigma Aldrich, St. Louis, MO, USA) for 1h at 4°C. Subsequently they were stained for 30 min with 0.4% (wt/vol) sulforhodamine B (SRB, Sigma Aldrich) dissolved in 1% acetic acid. The number of viable cells was directly proportional to the amount of protein bound-dye which was then solubilized with 10mM Tris base solution (pH10.5) and measured at 540nm using the ELISA fluorometric assay (Bio-Rad, Hercules, CA, USA;

Microplate Reader). All experiments were performed in duplicate and repeated three times. The IC₅₀ was assessed from the dose-response curves.

5.5.5 Apoptosis evaluation

After counting, 3×10^5 cells were harvested and washed twice with ice-cold PBS. Cells were labeled with an Annexin V and Dead Cell Assay kit according to the manufacturer's instructions (Merck Millipore, Darmstadt, Germany). The kit detects the externalization of phosphatidylserine (PS) in apoptotic cells using fluorescently-labeled Annexin V in combination with the dead cell marker 7-aminoactinomycin D (7-AAD). We identified four populations of cells: (1) viable cells that did not undergo detectable apoptosis: Annexin V (-) and dead cell marker (-); (2) early apoptotic cells: Annexin V (+) and dead cell marker (-); (3) late apoptotic cells: Annexin V (+) and dead cell marker (+); and (4) cells that died via non-apoptotic pathways: Annexin V (-) and dead cell marker (+). Cells were counted using the Muse™ Cell Analyzer (Merck Millipore) and analyzed using a software provided by Merck Millipore.

5.5.6 Cell cycle assay

1×10^6 cells were counted for the Muse™ Cell Cycle Assay that consisted in the use of the nuclear DNA intercalating stain RNase A and propidium iodide (PI) in a proprietary formulation. The latter was used to discriminate cells in different phases of the cell cycle, based on differential DNA content in the presence of RNase to increase the specificity of DNA staining. After treatment with the active *G. cydonium* fraction, cells were washed with Phosphate buffered saline (PBS) and centrifuged. The supernatant was removed and 1mL of ice cold 70% ethanol was

added to the re-suspended cell pellet. Samples were capped and frozen at -20°C for at least 3h prior to staining. Ethanol-fixed cells were washed with PBS and incubated with 200 μL of Muse™ Cell Cycle Reagent for 30 min at room temperature, in the dark. After staining, cells were processed for cell cycle analysis.

5.5.7 Extraction of the polar fractions in untreated and treated cancer cells

All cancer cell lines were plated in cell culture flasks ($\sim 2 \times 10^6$ cells/flask) and treated with the active fraction at the IC_{50} concentration obtained after 48h treatment. After incubation time (48h), cellular supernatants were collected and stored at -80°C for further investigation. Cell pellets obtained by trypsin digestion were washed twice in Phosphate buffered saline and deuterated water (PBS- D_2O) and refrigerated at -80°C . Subsequently they were re-suspended in 170 μL of H_2O and 700 μL of methanol and were sonicated for 30 s. 350 μL of chloroform was added and cell pellets were shaken on ice in an orbital shaker for 10 min. H_2O /chloroform (350 μL , 1:1, v/v) was added to each cell suspension and centrifuged at 10,000 rpm for 10 min at 4°C . Thereafter, the aqueous (polar) and lipophilic (apolar) phases were collected separately and evaporated by SpeedVac system.

5.5.8 ^1H -NMR Metabolomic Analysis of the cellular polar fractions

A 600-MHz BrukerAvance DRX spectrometer with a TCI probe was used to acquire ^1H spectra on the cellular polar fractions. They were dissolved in 630 μL of PBS- D_2O with the pH adjusted to 7.20, and 70 μL of sodium salt of 3-(trimethylsilyl)-1-propanesulfonic acid (1% in D_2O) used as the internal standard.

All ^1H -NMR spectra were acquired at 300 K with the excitation sculpting pulse sequence to suppress water resonance. A double-pulsed field gradient echo was

used, with a soft square pulse of 4 ms at the water resonance frequency and with gradient pulses of 1 ms duration, adding 128 transients of 64 k complex points, with an acquisition time of 4 s/transient. Time domain data were all zero-filled to 256 k complex points and an exponential amplification of 0.6 Hz was applied prior to Fourier transformation.

5.5.9 Statistical and Pathway Analysis

The spectral 0.50–8.60 ppm region of ¹H-NMR spectra was integrated in buckets of 0.04 ppm by the AMIX package (Bruker, Biospin GmbH, Rheinstetten, Germany). The water resonance region (4.5–5.2 ppm) was excluded during the analysis and the bucketed region was normalized to the total spectrum area using Pareto scaling. Orthogonal Projections to Latent Structures discriminant analysis (OPLS-DA) was used to compare the spectra obtained on the polar phases from three breast cancer cell lines before and after treatment because OPLS-DA can more effectively cope with chemical shift variation in full-resolution ¹H NMR datasets²⁶ without requiring binning or alignment steps. Pathway analysis on the metabolites that were modulated after treatment was performed using Metabo Analyst tool.²⁷

5.5.10 Bio-Plex Assay

Several cytokines, chemokines, and growth factors levels were evaluated concurrently with the Bio-Plex assay that containing dyed microspheres conjugated with a monoclonal antibody highly specific for a target protein. The method was carried out according to the manufacturer's instructions (Bio-Plex Bio- Rad) to assess the cytokines levels. The Bio-Plex Pro Human Cytokine 27-Plex Immunoassay has been used on supernatants of the three lines of human breast

cancer after treatment with sponge extract concentrations. This panel consists of: IL-1 β , IL-1ra, IL-2, IL-4, IL-5, IL-6, IL-7, CCL2, CCL11, CXCL10, CXCL8, IFN- γ , IL-9, IL-10, IL-12 (p70), IL-13, IL-15, IL-17, basic FGF, G-CSF, GM-CSF, MIP-1 α , MIP-1 β , PDGF- $\beta\beta$, RANTES, TNF- α , and VEGF. Protein levels were determined using a Bio-Plex array reader (Luminex, Austin, TX, USA) that quantifies multiplex immunoassays in a 96-well format with very small fluid volumes. The analyte level was calculated using a standard curve, with software provided by the manufacturer (Bio-Plex Manager Software). A Bio-Plex array reader (Luminex, Austin, TX, USA) that quantifies multiplex immunoassays in a 96-well format with very small fluid volumes, has been used for protein level determination. The levels of the analytes were calculated using a standard curve, with the Bio-Plex Manager Software provided by the manufacturer.

References

-
- ¹ Mehbub, M.F.; Lei, J.; Franco, C.; Zhang, W. *Mar. Drugs* **2014**, *12*, 4539–4577.
- ² Migliuolo, A.; Piccialli, V.; Sica, D. *J. Nat. Prod.* **1990**, *53*, 1262–1266.
- ³ Costantini, S.; Romano, G.; Rusolo, F.; Capone, F.; Guerriero, E.; Colonna, G.; Ianora, A.; Ciliberto, G.; Costantini, M. *Mediators Inflamm.* **2015**, *2015*, 204975.
- ⁴ S. Costantini, E. Guerriero, R. Teta, F. Capone, A. Caso, A. Sorice, G. Romano, A. Ianora, N. Ruocco, A. Budillon, V. Costantino, M. Costantini, *Int J Mol Sci.*, **2017**, *18*(10). pii: E2112.
- ⁵ J. Y. Yang, L. M. Sanchez, C. M. Rath, X. Liu, P. D. Boudreau, N. Bruns, E. Glukhov, A. Wodtke, R. de Felicio, A. Fenner, W. Wong, R. G. Linington, L. Zhang, H. M. Deboni, W. H. Gerwick, and P. C. Dorrestein *J. Nat. Prod.*, **2013**, *76* (9), pp 1686–1699.
- ⁶ <https://gnps.ucsd.edu/ProteoSAFe/static/gnps-splash.jsp>.
- ⁷ Liu, R.; Ye, Y.; Qiang, L.; Liao, X.; Zhao, Y. *Life Sci J* **2008**, *5*, 37-37.
- ⁸ Huang, R.M.; Chen, Y.N.; Zeng, Z.; Gao, C.H.; Su, X.; Peng, Y. *Mar Drugs* **2014**, *12*, 5817-5838.
- ⁹ Negi, B.; Kumar, D.; Rawat, D.S. *Curr Protein Pept Sci* **2016**, *17*, 999 (Bentham Science Publishers, 2016).
- ¹⁰ Fernández, J.; Marín, L.; Alvarez-Alonso, R.; Redondo, S.; Carvajal, J.; Villamizar, G.; Villar, C.J.; Lombò, F. *Mar Drugs* **2014**, *12*, 2668-2699.
- ¹¹ Sheoran, A.; King, A.; Velasco, A.; Pero, J.M.; Garneau-Tsodikova, S. *Mol Biosyst* **2008**, *4*, 622-628.
- ¹² Costantino, V.; Fattorusso, E.; Imperatore, C.; Mangoni, A.; Teta, R. *Eur J Org Chem* **2008**, *2008*, 2130-2134.
- ¹³ Costantino, V.; Fattorusso, E.; Imperatore, C.; Mangoni, A.; Teta, R. *Eur J Org Chem* **2009**, *2009*, 2112–2119.
- ¹⁴ Noda, H.; Amano, H.; Arashima, K.; Nisizawa, K. *Hydrobiologia* **1990**, *204/205*, 577-584.
- ¹⁵ Natori, T.; Morita, M.; Akimoto, K.; Koezuka, Y. *Tetrahedron* **1994**, *50*, 2771-2784.
- ¹⁶ Bando, H.; Toi, M.; Kitada, K.; Koike, M. *Biomed Pharmacother* **2003**, *57*, 333-340.
- ¹⁷ Hui, L.; Zheng, Y.; Yan, Y.; Bargonetti, J.; Foster, D.A. *Oncogene* **2006**, *25*, 7305-7310.
- ¹⁸ Warburg, O.; Wind, F.; Negelein, E. *J Gen Physiol.* **1927**; *8*: 519-530.
- ¹⁹ Annibaldi A, Widmann C. *Curr Opin Clin Nutr Metab Care* **2010**, *13*, 466-470.

-
- ²⁰ Muñoz-Pinedo, C.; El Mjiyad, N.; Ricci, J.E. *Cell Death Dis* **2012**, *3*, 2489.
- ²¹ Glunde, K.; Bhujwalla, Z.M.; Ronen, S.M. *Nat Rev Cancer* **2011**, *11*, 835-848.
- ²² Luo, M.; Hou, L.; Li, J.; Shao, S.; Huang, S.; Meng, D.; Liu, L.; Feng, L.; Xia, P.; Qin, T.; Zhao, X. *Cancer Lett* **2016**, *373*, 1-11.
- ²³ Liu, M.; Guo, S.; Stiles, J.K. *Oncol Lett* **2011**, *2*, 583-589.
- ²⁴ Waugh, D.J.; Wilson, C. *Clin Cancer Res* **2008**, *14*, 6735-6741.
- ²⁵ Esquivel-Velázquez, M.; Ostoa-Saloma, P.; Palacios-Arreola, M.I.; Nava-Castro, K.E.; Castro, J.I.; Morales-Montor, J. *J Interferon Cytokine Res* **2015**, *35*, 1-16.
- ²⁶ Cloarec, O.; Dumas, M.E.; Trygg, J.; Craig, A.; Barton, R.H.; Lindon, J.C.; Nicholson, J.K.; Holmes, E. *Anal Chem* **2005**, *77*, 517-526.
- ²⁷ Xia, J.; Sinelnikov, I.; Han, B.; Wishart, D.S. *Nucl Acids Res* **2015**, *43*, 251-257.

Conclusion

Today the synthesis of new bioactive compounds is the key step of the biomedical research, enabling chemists and biologists to advance their researches to higher levels. During my PhD I pursued both the advanced synthesis of new compounds and the investigation of pharmacological properties of new metabolites isolated from marine sponges.

The asymmetric convergent total syntheses of 16-*epi*- and *ent*-smenamides A, two structural analogues of the cytotoxic smenamides A, were carried out in 23 steps with a 2.5% and 2.6% overall yield, respectively. Afterwards, eight shorter-chain “functional analogues” of 16-*epi*-smenamides A were designed and prepared using a flexible synthetic route in order to gain a better insight in the biological activity of smenamides family.

On the other hand, I was involved in the study of the chemical composition of two marine sponges, the Caribbean *Smenospongia conulosa* and the Mediterranean *Geodia cydonium*. Two new chlorinated compounds, namely conulothiazole A and B, were isolated from the organic extract of *S. conulosa*. At the same time, using a novel dereplication strategy, involving the use of LC-HRMS and LC-HRMS/MS coupled with a bioinformatic technique, e.g. Molecular Networking, an active subfraction of the organic extract of *G. cydonium* was identified. This fraction showed moderate antiproliferative activity on three human breast cancer cell lines (MCF-7, MDA-MB-231 and MDA-MB-468) and no toxicity on the healthy MCF-10A human breast cell line.

Although the study of the chemical composition of marine organisms is an intriguing research field, I was totally fascinated by the challenges posed by the total synthesis, “the endeavour of synthesizing the molecules of living nature in the laboratory”.¹

References

¹K. C. Nicolaou, *Proc. R. Soc.*, **2014**, A 470: 20130690.